UNIVERSITY OF LIVERPOOL

Molecular Characterisation of Interaction between Nurse-like cells and Chronic Lymphocytic Leukaemia cells

Thesis submitted in accordance with the requirements of the University of Liverpool for the degree of Doctor in Philosophy by

Ishaque Sayeed Mohammad

Monday, 25 January 2021

Abstract

Molecular Characterisation of Interaction between Nurse-like Cells and Chronic Lymphocytic Leukaemia Cells

Ishaque S. Mohammad

Department of Molecular and Clinical Cancer Medicine, University of Liverpool, Liverpool, UK

Chronic Lymphocytic Leukaemia (CLL) is a proliferative B cell malignancy characterised by an accumulation of mature B cells in the peripheral blood, lymph nodes and bone marrow. The disease is heterogenous in both clinical presentation and response to treatment. Despite the well-established immunochemotherapy and recently introduced molecularly targeted therapies such as ibrutinib and venetoclax, CLL is still incurable. One possible cause of relapse in patients is the involvement of the tissue microenvironment which supports CLL-cell survival and confers drug resistance. Nurse like cells (NLCs) are a major component of the CLL microenvironment. However, the exact molecular mechanisms mediating interactions between CLL cells and NLCs are still not fully understood. The aim of this study was to investigate how NLCs and CLL cells influence each other at the level of gene expression and to uncover molecules and pathways that are responsible for prolonging survival and conferring drug resistance of CLL cells. I therefore independently characterised the development of NLCs using fresh peripheral blood samples from CLL patients and applied a co-culture system where primary CLL cells were cultured with NLCs. I showed that the development of NLCs varies considerably between the individual CLL samples. Consequently, I developed an NLC scoring system to reflect the variable nature of the NLC development. I also confirmed the pro-survival effect of NLCs on CLL cells. To address the issue of variation in developing NLCs, I developed a cell-line model using human THP-1 monocytic leukemic cells to mimic NLCs. The cell line model closely resembled the morphology and phenotype of NLCs. Like NLCs, it also provided pro-survival signals to CLL cells when in co-culture, as THP-1 cell-derived macrophages protected CLL cells from spontaneous and fludarabine-induced apoptosis. Finally, I prepared mRNA samples from the co-cultured CLL cells and primary NLCs, together with their respective cells cultured alone as controls, and generated the comprehensive, global gene expression datasets using next generation sequencing technology (RNA-seq). Through the application of contemporary bioinformatics analysis techniques, I identified 326 out of 19,595 expressed genes that are significantly differentially expressed in co-cultured CLL cells. Gene set enrichment analysis revealed that gene expression profile of CLL cells co-cultured with NLCs resembled that of the tissue resident CLL cells from the lymph nodes, thus validating the use of the co-culture system in mimicking

the CLL microenvironment. Further analysis of differentially expressed genes led to identification of several signalling pathways that are critically involved in mediating the interaction between CLL cells and NLCs. These include some known pathways such as toll-like receptor and tumour necrosis factor, activation of which all lead to eventual activation of NF-κB, the master transcription factor of B cells. Furthermore, my analysis revealed other less well-known signalling pathways such as hypoxia-inducible factor that are also involved in cross-talk between CLL cells and NLCs. The novel observations from my study has thus provided a rational basis for future studies to investigate the molecular mechanisms responsible for the functions of these signalling pathways and associated molecules, which may lead to identification of potential targets for therapeutic intervention to overcome microenvironment-mediated drug resistance in CLL.

In the Name of God, the Most Gracious the Most Merciful

Narrated Abu Huraira:

The Prophet (may blessings and peace be upon him) said, "There is no disease that God has created, except that He also has created its treatment."

[Sahih al-Bukhari 5678]

"For indeed, with hardship [will be] ease. Indeed, with hardship [will be] ease"

- Quran (94:5-6)

Acknowledgments

First, I would like to acknowledge my PhD supervisors, Dr Jack Zhuang, Dr Ke Lin and Professor Andrew Pettitt, for taking care of me throughout my study. I thank them for being patient with me as they guided me throughout the research plan, practical work, result interpretation, manuscript writing and of course thesis writing.

In addition, I would like to thank all the members of the Haematology group in the Department of Molecular and Clinical Cancer Medicine for their support in my laboratory work. I extend the same thanks to members of other departments who had helped me at some point in my PhD. It is because of all of them, in their own way, that helped me survive my PhD journey; particularly Dr Umair Khan for his invaluable support, generosity and humour, Waad Almalki, Tahera Alnassfan and Chang Su for their support and useful discussions, Dr Lucy Ireland and Almudena Santos for uplifting my mood as I was working in the lab. My seniors Dr Omar Alishlash, Dr Imad, Dr Faris Tayeb and Dr Moses who provided me with great words of wisdom. I am particularly thankful to Dr Lakis Liloglou for his lectures and his advices, Dr Carlos Rubbi for teaching me how to use the immunofluorescent microscope. I thank Dr Gina Eagle, Dr Kathy Till, Prof Nagesh Kalakonda, Prof Joe Slupsky, Dr Shankar Varadarajan, Prof Michael Schmid, Prof Francesco Falciani and Dr Melanie Oates for their help as well. I thank the staff of the research technician team including Mohmmad Shuaib Choudry, Tim Dickinson, Natalie Coplin, John Stanbury and Gregor Govan. I thank Dr Mara Kozic for not only being one of the first friends I made when I arrived in Liverpool, but also for analysing my RNAseq data and taking time out to patiently help me understand the underlying rationale of the analysis.

I wish to extend my thanks to my family and friends who came to my aid when I needed it when my beloved father passed away. Thanks to members of the ISOC of The University of Liverpool for engaging in pleasant conversations and events, and my dear friend Sheikh Zane Abdo for a great deal of support and nurturing my curiosity. I thank my many friends at Dover Court who came and went and those who stayed in touch even during the pandemic, I cherish the memories of the friendship and my thoughts are with them all.

I thank my fiancé Fabia Miah and her family who not only have been so welcoming but has been patient with me and accompanying me via video calls as I work, giving a very peaceful and pleasant atmosphere. Her encompassing love, appreciation and generosity is a light that I needed during my dark days.

I dedicate this humble work to the departed soul of my beloved father Dr Mohammad Abu Sayeed Miah, who has supported me throughout my life and is still a shining example of a humble intellectual person, to my mother Dr Masuda Khatoon, who continuously proves her strength and is an inspiration to me, to my brother Dr Ismail Sayeed, who's determination to succeed in his work is also an inspiration. And finally, to all the struggling PhD students who come from various backgrounds and expectations in the hope of attaining their degrees and being accepted by their peers.

Declaration

With the exception of the RNA sequencing performed by Novogene plc. (Hong Kong, China) and some of the bioinformatics analysis of RNA sequencing data performed by Dr Mara Kozic under the supervision of Prof Francesco Falciani (Computational Biology Facility of University of Liverpool), all the work presented in this thesis is entirely my own.

Publications arising from this work

1. XVII International Workshop on CLL, New York, USA (May 2017) - Use of Differentiated THP-1 cells to mimic the pro-survival effect of Nurse-like cells on Chronic Lymphocytic leukaemia cells. *Leukemia & Lymphoma*, 2017, 58: 102-104.
2. Mohammad, Ishaque S; Lin, Ke; Oates, Melanie; Khan, Umair T; Burger, Jan; Pettitt, Andrew R; Zhuang, Jianguo, "Development of a cell-line model to mimic the pro-survival effect of nurse-like cells in chronic lymphocytic leukaemia". *Leukemia & Lymphoma*, 2020 Aug 28:1-13. doi: 10.1080/10428194.2020.1811274. Epub ahead of print.

Presentations arising from this work at University of Liverpool and International conferences

1. Presented a Poster of my work on use of differentiated THP-1 cell line to mimic NLCs prosurvival effect on CLL cells at the XVII International Workshop on CLL, New York, USA (May 2017)
2. Presented a Poster of my work on use of differentiated THP-1 cell line to mimic NLCs prosurvival effect on CLL cells at the ITM PG Research Day, in the University of Liverpool (Nov 2018)
3. Presented a Poster of my work on use of differentiated THP-1 cell line to mimic NLCs prosurvival effect on CLL cells at the Faculty of Health & Life Sciences Poster Day, in the University of Liverpool (June, 2018)
4. Gave an Oral Presentation on my PhD work on Primary and Cell line work on CLL and NLCs at the ITM PG Research Day, in the University of Liverpool (Nov 2018)
5. Won 1st place for the Photo Competition of the NWCR Symposium, held in the University of Liverpool (April, 2017)

Table of Contents

List of Figures

List of Tables

List of Equations

List of Abbreviations

Abbreviation	Full Description
ADCC	Antibody-dependent cellular cytotoxicity
ADP	Adenosine diphosphate
ALL	Acute lymphoblastic leukemia
AMC	Absolute monocyte count
AMP	Adenosine monophosphate
APAF	Apoptotic protease activating factors
APC	Antigen presenting cells
APRIL	A proliferating-inducing ligand
ATM	Ataxia telangiectasia mutated gene
ATP	Adenosine triphosphate
BAFF	B cell-activating factor
BAFFR	B cell-activating factor receptor
BCL-2	B cell lymphoma 2
BCMA	B cell maturation antigen
BCR	B cell receptor
BH	BCL2 homology
BIRC3	Baculoviral IAP Repeat-Containing Protein 3
BM	Bone Marrow
BMSC	Bone marrow stromal cells
BTK	Bruton's tyrosine kinase
CBC	Complete blood count
CCL	Chemokine (C-C motif) ligand
CCR	CC-chemokine receptor
CD	Cluster of differentiation
CIT	Chemoimmunotherapy
CLL	Chronic lymphocytic leukaemia
CML	Chronic myelogenous leukaemia
CMV	Cytomegalovirus
CSF	Colony-stimulating factor
DAG	Diacylglycerol
DAMP	Damage-associated molecular patterns

DAPI	4',6-Diamidino-2-Phenylindole, Dihydrochloride
DEA	Downstream Effector Analysis
DEG	Differentially expressed genes
DLBCL	Diffuse large B-Cell lymphoma
DMSO	Dimethyl sulfoxide
DNA	Deoxyribonucleic acid
ECACC	European Collection of Authenticated Cell Cultures
ECM	Extracellular matrix
EDTA	Ethylenediaminetetraacetic acid
ELISA	Enzyme-linked immunosorbent assay
FACS	Fluorescence-activated cell sorting
FBS	Fetal bovine serum
FCR	Fludarabine, cyclophosphamide and rituximab
FDC	Follicular dendritic cells
FDR	False Discovery Rate
FISH	Fluorescence in situ hybridization
FITC	Fluorescein isothiocyanate
GAPDH	Glyceraldehyde 3-phosphate dehydrogenase
GEP	Gene expression profile
GO	Gene Ontology
GSEA	Gene set Enrichment Analysis
HIF	Hypoxia-inducible transcription factor
HMGB1	High-mobility group protein B1
HSC	Hematopoietic stem cells
IF	Immunofluorescence
IFN-γ	Interferon gamma
IGHV	Immunoglobulin heavy chain variable region gene
IHC	Immunohistochemistry
IL	Interleukin
IPA	Ingenuity Pathway Analysis
ITAM	Immunoreceptor tyrosine-based activation motifs
LAM	Lymphoid-associated macrophages
LDH	Lactate dehydrogenase
LN	Lymph nodes

LPS	Lipopolysaccharide
MBL	Monoclonal B-lymphocytosis
MCL-1	Myeloid cell leukemia 1
MDS	Myelodysplastic syndrome
MFIR	Mean fluorescence intensity ratio
MGG	May Grünwald Giemsa
MM	Multiple myeloma
MSC	Mesenchymal stromal cells
NADPH	Reduced form of Nicotinamide adenine dinucleotide phosphate
NCBI	The National Center for Biotechnology Information
NGS	Next-generation sequencing
NK	Natural killer
NLC	Nurse-like cell
NO	Nitric oxide
OD	Optical density
OR	Overall response
OS	Overall survival
PP	Phosphatases
PBMC	Peripheral blood mononuclear cells
PBS	Phosphate-buffered saline
PCA	Principal Component Analysis
PCR	Polymerase chain reaction
PE	Phycoerythrin
PI	Propidium Iodide
PLL	Prolymphocytic leukaemia
PMA	Phorbol 12-myristate 13-acetate
RAGE	Receptor for Advanced Glycation End products
RIN	RNA integrity number
RNA	Ribonucleic acid
ROS	Reactive oxygen species
SD	Standard Deviation
SDF-1	Stromal derived factor-1
SEM	Standard Error of Mean
SF3B1	Splicing factor 3B subunit 1

SLL	Small lymphocytic lymphoma
SPP1	Secreted Phosphoprotein 1 (osteopontin)
TACI	Transmembrane activator and CAML interactor
TAM	Tumour associated macrophages
TCA	Tricarboxylic acid
TGF-β	Tumour growth factor beta
TLR	Toll-like receptor
TME	Tumour microenvironment
TNF	Tumour necrosis factor
TPA	12-O-tetradecanoylphorbol-13-acetate
UM	Unmutated
UV	Ultraviolet
VEGF	Vascular endothelial growth factor
WBC	White blood cell count
ZAP-70	Zeta-associated protein-70

1 General Introduction

1.1 Chronic Lymphocytic Leukaemia

Chronic Lymphocytic Leukaemia (CLL) is characterised by the clonal expansion and accumulation of mature, CD5+ B-cells in the blood, bone marrow and spleen (Fabbri & Dalla-Favera 2016). As of 2017, it is the most common type of adult leukemia in UK, which predrominantly affects males (Chronic lymphocytic leukaemia (CLL) statistics).

The treatment of CLL patients with fludarabine, cyclophosphamide, rituximab (FCR) and targeted therapy such as ibrutinib, idelalisib and venetoclax alone or in combination have improved the outcomes of CLL (Furstenau et al. 2019; Kipps et al. 2017). However, patients with 11q deletion and/or ATM mutations respond poorly to purine analogues (e.g. fludarabine) (Bosch & Dalla-Favera 2019). The deletion of 17p or TP53 mutation renders the chemotherapeutic drugs ineffective and thus patients with 17p deletion or TP53 mutations are treated with ibrutinib, a novel inhibitor of Bruton's tyrosine kinase (BTK), a kinase that is critically involved in B cell receptor (BCR) signalling (Hallek 2017; Kipps et al. 2017; Mir et al. 2019; Provan et al. 2015). Alternatively, venetoclax (ABT-199) can be offered to CLL patients who are not suitable for FCR (Hallek 2015, 2017).

Despite the development of the novel therapies, relapse of the disease still occurs (Kipps et al. 2017). One cause of relapsed disease is the existence of minimal residual disease (MRD) in CLL (Furstenau et al. 2019). Accumulating evidence suggests that CLL cells residing in the lymphoid tissues such as bone barrow, lymph nodes and spleen are the major source of MRD (Furstenau et al. 2019). MRD is defined as presence of CLL cells detected in the peripheral blood (PB) or bone marrow (BM) by flow cytometry following treatment (Furstenau et al. 2019). Undetectable MRD (defined as <1 CLL cells in 10,000 leukocytes) is a strong indicator for longer progression-free survival (Furstenau et al. 2019). Early studies in CLL have also shown that CLL cells survived prolonged period in vivo, but underwent apoptosis rapidly when cultured in vitro (Collins et al. 1989), which indicated that the survival of CLL cells depends on factors present in the tissue microenvironment including the bone marrow and lymph nodes. Therefore, better understantanding of how CLL cells interact with the microenvironment is vitally important. Below, I will provide an overview on the CLL biology and microenvironment based on the literature review.

1.2 Pathogenesis of CLL

1.2.1 Cell origins of CLL

In most patients of CLL, clonal expansion of B cells is arrested in the B-cell differentiation pathway, between pre-B cells and mature B Cells (Figure 1.1). Morphologically, they resemble mature lymphocytes (Hallek 2017; Mir et al. 2019; Zhang & Kipps 2014). It has been stated that mutations can occur anytime and contribute to the development of CLL cells. Mutations can even occur in hematopoietic stem cells (HSCs). During normal B cell development, the immature B cells leave the bone marrow and complete maturation where they differentiate, depending on micro environmental stimuli, into various B cell subtypes (Rickert 2013). CLL cells originating from B cells that have undergone Ig mutations lead to M-CLL (with mutated immunoglobulin heavy chain variable region gene (IGHV)), and those that have not are UM-CLL (with unmutated IGHV). Furthermore, it was shown that all CLL patients share a specific gene expression signature in their leukemic cells where it supported a model of CLL having a common cell of origin (Rosenwald et al. 2001). It was suggested that CLL cells are related to memory B cells more than to naïve B cells, based on their gene expression profile analysis. The involvement of genetic lesions, BCR stimulation and microenvironment interactions at later stages of B cell development contribute to CLL cell development (Zhang & Kipps 2014).

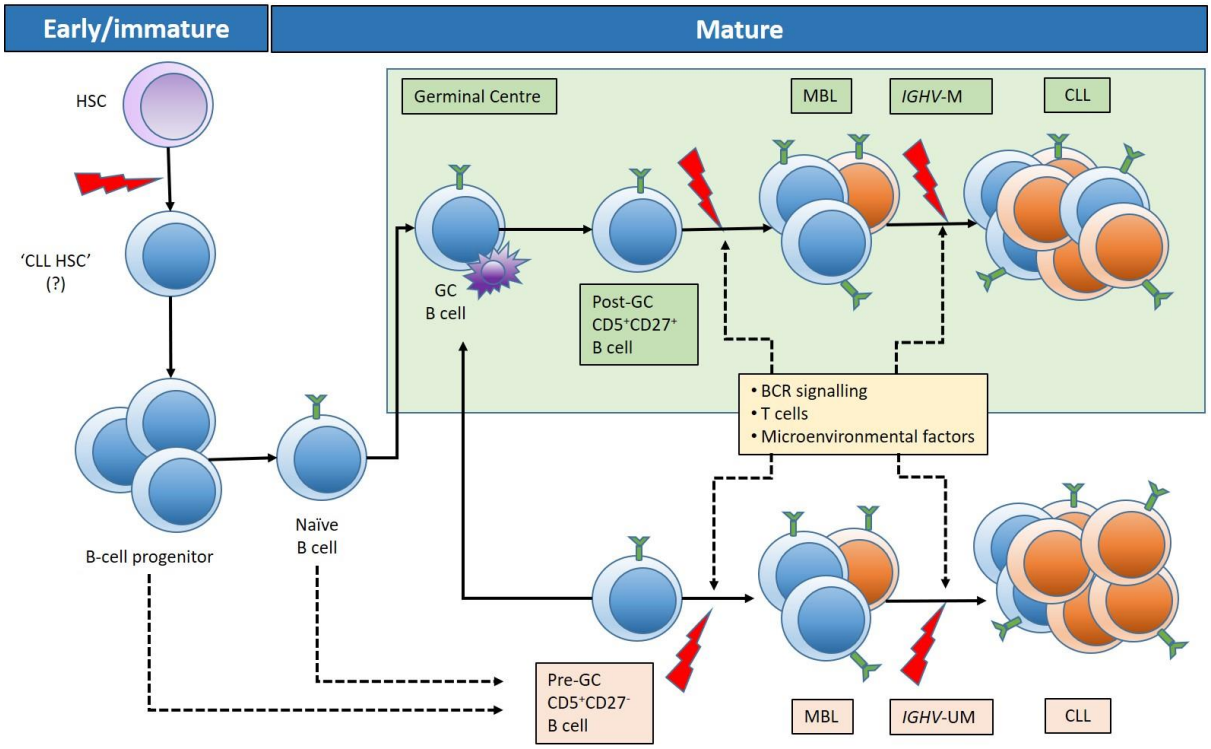

Figure 1.1 Cellular origin of CLL. Subsets of CLL based on IGHV mutation.

It has been suggested that in the hematopoietic stem cells (HSCs), that genetic events (lightning symbols) occur which lead to CLL. This could lead to the expansion of polyclonal B cells. Further stimulation may lead to clones and expansion of mature B cells. CLL cells with mutations in immunoglobulin heavy chain variable (IGHV-M) come from post-germinal centre (GC) B cells with $CD5^{+}CD27^{+}$. CLL cells with unmutated IGHV (IGHV-UM) are from pre-GC B cells with $CD5^{+}CD27^{-}$. The formation of germinal centre cells is T cell dependant and the formation of Pre-GC B cells is T cell independent. Monoclonal B lymphocytosis (MBL) and overt CLL is mandated by additional genetic and epigenetic lesions (indicated by lightning symbols), B cell receptor (BCR) stimulation, microenvironmental factors and T cells. Figure is modified from Bosch and Dalla-Favera (2019).

1.2.2 B-Cell Receptor Signalling

The B-cell receptor (BCR) complex is comprised of the membrane bound heavy and light chains of immunoglobulins (mIg) and CD79A and CD79B proteins (Geisberger, Lamers & Achatz 2006).

This complex is expressed on the surface of B lymphocytes from very early developmental stage till it becomes a plasma cell (Geisberger, Lamers & Achatz 2006). Before a B cell leaves the bone marrow, the mIg exists as the IgM isotype and subsequently starts to express a second isotype IgD when it enters into the peripheral lymphoid organs (Geisberger, Lamers & Achatz 2006). Contrast to normal naïve B cells, CLL-B cells express low levels of sIgM where in U-CLL the expression is down-modulated to a lesser extent than M-CLL (Packham & Stevenson 2010; Stevenson et al. 2011).

Upon binding to the antigen, the BCR is internalized (Geisberger, Lamers & Achatz 2006; Packham & Stevenson 2010). Activation results in the oligomerization of the BCR and the phosphorylation of immunoreceptor tyrosine-based activation motifs (ITAMs) CD79A and CD79B by LYN which also phosphorylates spleen tyrosine kinase (SYK) (Packham & Stevenson 2010; Stevenson et al. 2011). Through a 'trigger' event, the newly formed complex of kinases and scaffold proteins mentioned is called a 'signalosome' (Stevenson et al. 2011). Other motifs are involved and recruitment of PI3K is initiated after the formation of the signalosome (Stevenson et al. 2011). Subsequently, PI3K recruits AKT and Bruton's tyrosine kinase (BTK) to the membrane and eventually a further complex forms consisting of LYN, SYK, PI3K, BTK and PLC-γ2. This complex leads to downstream pathways such as NF-kB and RAS-ERK (Packham & Stevenson 2010; Zhang & Kipps 2014). The final phase of events involves downstream regulators, where modulation will mediate cell proliferation, survival and migration (Packham & Stevenson 2010; Stevenson et al. 2011).

Compared to normal naïve B cells, CLL cells express low level of CD79b and IgM proteins (Guo et al. 2016). There is a variable response to BCR stimulation in CLL cells (Packham & Stevenson 2010; Stevenson et al. 2011). There is an increased expression of LYN, SYK and ZAP70 in CLL where the levels of ZAP70 is used as a prognostic indicator for poor prognosis (Nabhan, Raca & Wang 2015; Packham & Stevenson 2010; Rassenti et al. 2008; Stevenson et al. 2011).

In summary, BCR signalling in CLL facilitates the prolonged survival and expansion of CLL cells. Thus, a wide range of proposed targets in BCR signalling of CLL cells were aimed to combat the CLL presence in the body.

1.2.3 Surface IgM and IgD

IgM and IgD receptor isotypes are co-expressed on mature B cells, and their function in B cell development and maturation is widely interchangeable (Ten Hacken et al. 2016). They bear the same antigenic specificity and differ only in terms of their H chains, with IgMs carrying mu (μ) chain and IgDs carrying delta (δ) chains, respectively (Ten Hacken et al. 2016). Most CLL cells express both IgMs and IgDs, and numerous studies have characterized the importance of IgM BCRs for CLL-cell survival, cell cycle entry and proliferation (Burger & Chiorazzi 2013; Ten Hacken et al. 2016). The function of IgD in CLL has been studied, although there have been some controversial results mostly related to effect of its stimulation on inducing cell survival (Zupo et al. 2000) or apoptosis (Tavolaro et al. 2013). In one study, it was shown that cross linking with IgD prolonged cell survival instead of apoptosis (Zupo et al. 2000). Yet, another study showed significant apoptosis was observed when cross-linked with IgD

(Tavolaro et al. 2013). This suggests that it is still not clear the exact role of IgD in CLL cell survival. The function of sIgD remains mysterious even in normal B cells (Packham & Stevenson 2010).

1.2.4 Evasion of apoptosis *in vivo*

CLL cells when cultured *in vitro* die rapidly from apoptosis (Collins et al. 1989), whereas they are long-lived *in vivo*. This strongly indicates that CLL cells rely on microenvironmental factors, from sites such as bone marrow and lymph nodes, to prolong their survival *in vivo*. The BCL-2 family of proteins are important in the regulation of apoptosis (Cang et al. 2015).

Within the family the anti-apoptotic proteins include BCL-2, BCL-XL, MCL1, BFL1/A1 and BCL-W. The pro-apoptotic proteins of BCL-2 family were further sub-divided into two groups: multi-BH domain proteins such as BCL-2-associated X protein (BAX) and BCL-2 antagonist/killer 1 (BAK) and BH3-only proteins. BH3 proteins such as BID, BCL-2-like 11 (BIM) and BCL-2 binding component 3 (PUMA) are also known as activators and BCL-2-associated agonist of cell death (BAD), BMF and NOXA are regarded as sensitizers (Buggins & Pepper 2010).

BCL-2 family of proteins regulates apoptosis, particularly the intrinsic pathway, by controlling the permeability of the outer mitochondrial membrane (Buggins & Pepper 2010; Cang et al. 2015). Since some of the proteins are anti-apoptotic and pro-apoptotic, when the balance of scales is more in favour of apoptosis (i.e. there are more pro-apoptotic proteins), this results in increased permeability of the outer mitochondrial membrane (Buggins & Pepper 2010; Cang et al. 2015). This causes the release of pro-apoptotic factors such as cytochrome-C from the inner mitochondrial membrane through the outer mitochondrial membrane into the cytoplasm (Buggins & Pepper 2010; Cang et al. 2015). The cytoplasmic cytochrome-c then forms a complex with apoptotic protease activating factors (APAF1), the complex is known as ‘apoptosome’, and this initiates caspase cascade by activating caspase-9 (Buggins & Pepper 2010; Cang et al. 2015). The resulting biological changes are apoptosis and cell death (Buggins & Pepper 2010; Cang et al. 2015).

In CLL, the anti-apoptotic protein, BCL-2 is over expressed (Buggins & Pepper 2010; Pekarsky, Balatti & Croce 2018). This high expression of BCL-2 is also observed in follicular lymphomas where there is chromosomal translocation t(14;18) (Kelly & Strasser 2011). High levels of BCL-2 were also detected in DLBCL and mantle cell lymphoma (Kelly & Strasser 2011).

The overexpression of BCL-2 is the result of loss or downregulation of *miR-15/16* in 13q of CLL cells (Kelly & Strasser 2011; Pekarsky, Balatti & Croce 2018). The expression of both *miR-15* and *miR-16* is linked with the level of BCL-2 expression in almost all CLL cases (Pekarsky, Balatti & Croce 2018). When

there is a high expression of *miR-15/16* it was seen that there is low expression of *BCL2* (Pekarsky, Balatti & Croce 2018). In CLL, there is deletion of 13q resulting in loss of *miR-15/16* and/or a mutation resulting in loss of function (Pekarsky, Balatti & Croce 2018). This in turn results in an overexpression of *BCL2* and the final outcome is a high level of BCL-2 anti-apoptotic protein which causes the CLL cells to evade apoptosis (Kelly & Strasser 2011; Pekarsky, Balatti & Croce 2018).

1.2.5 Tumour Microenvironment

The concept of the microenvironment and link with cancer was first described in the late 1960s by Stephen Paget who proposed the 'seed (tumor cells) and soil (microenvironment)' hypothesis (Bakker et al. 2016; Witz 2009). Cancer cells are surrounded by a complex milieu. This cancer cell niche is called the tumor microenvironment, and it contributes to the development and metastasis of tumors.

In CLL, the tumour microenvironment (summarised in Figure 1.2) comprises of the CLL cells, a mixture of cancer associated stromal cells (CAS)/ bone marrow stromal cells (BMSC), T cells via CD40 ligands, endothelial cells, follicular dendritic cells (FDC) and nurse-like cells (NLCs). It is presently recognised that CLL is a microenvironment-dependent disease (Burger 2011a; Caligaris-Cappio, Bertilaccio & Scielzo 2014; Ten Hacken & Burger 2016). The field of study in tumour microenvironment is currently intensive and expanding very fast and I will give a brief summary below into the areas relevant to CLL.

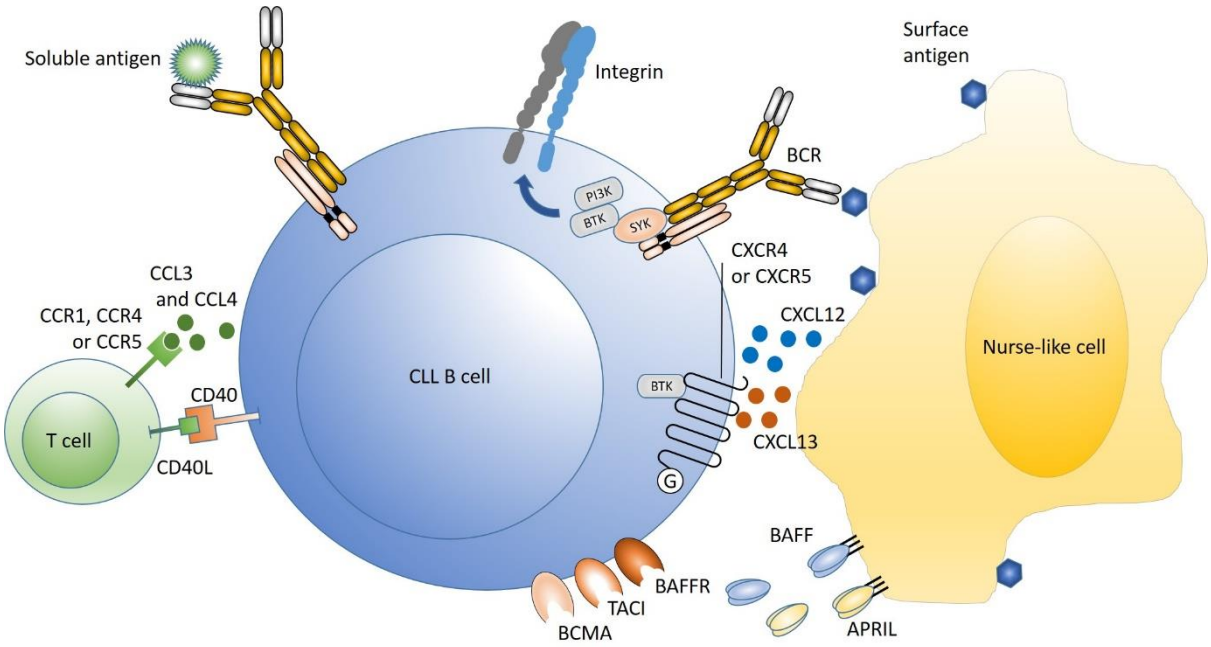

Figure 1.2 Schematic diagram of the CLL Microenvironment.

Schematic showing cross-talk between CLL cells and the microenvironment in secondary lymph nodes. CLL cells have B-cell receptor (BCRs) which respond to soluble antigen or cell surface antigens. This in turn activates BCR signalling which activates kinases such as spleen tyrosine kinase (SYK), Bruton tyrosine kinase (BTK) and PI3K. This signalling activates chemokine receptors such as CXC-chemokine receptor 4 (CXCR4) and CXCR5 and adhesion molecules (integrins). Activated T cells promote growth of CLL cells by CD40 ligand (CD40L)- CD40 receptor linkage. Nurse-like cells (NLCs) express B cell-activating factor (BAFF) and a proliferating-inducing ligand (APRIL) which activate receptors on the CLL cell. BAFFR, B cell-activating factor receptor; BCMA, B cell maturation antigen; CCR, CC-chemokine receptor; TACI, transmembrane activator. Schematic diagram adapted from a review by Burger and Wiestner (2018).

1.2.5.1 Hypoxia

In solid tumours, the vasculature becomes insufficient when its diameter grows more than 2mm, resulting in a local hypoxic (oxygen concentration <3%) and anoxic condition (oxygen concentration <0.1%) (Yang et al. 2015). Evidence has shown that 50-60% of tumours grow under hypoxic conditions (Yang et al. 2015). Metabolism is very high in areas of tumour growth and so the demand of oxygen would outweigh the supply of oxygen, thus causing hypoxia (Henze & Mazzone 2016; Petrova et al. 2018; Yang et al. 2015).

Hypoxia induces a wide range of biological changes, such as decreased cell proliferation, increased expression of drug-resistance genes, selection of apoptosis-resistant clones, facilitation of tumor invasion and metastasis, reduced expression of DNA repair genes and increased genomic instability (Kim et al. 2009). Preclinical evidence shows that hypoxia correlates with poor prognosis in solid tumors (Henze & Mazzone 2016; Kim et al. 2009).

The hypoxic response is to restore the oxygen availability and on the cellular level this is seen as induction of angiogenesis, metabolic reprogramming, proliferation, self-renewal and autophagy. However, all these processes are exploited to aid in tumor progression and metastatic dissemination. Oxygen deprivation contributes to a hostile microenvironment that selects for a more aggressive cancer phenotype (Henze & Mazzone 2016; Petrova et al. 2018). The hypoxic response is mediated by, among others, hypoxia-inducible transcription factors HIF1α and HIF2α (Henze & Mazzone 2016; Kim et al. 2009; Petrova et al. 2018; Serra et al. 2016). HIF activity switches the cell metabolism into glycolytic mode, increasing glucose consumption and pyruvate, lactate and H^+ production (Petrova et al. 2018), thus creating a more acidic pH environment.

The excessive release of angiogenic factors within the tumor microenvironment under hypoxic conditions results in a tortious vascular network that does not effectively restore the blood supply. In fact, an irregular vascular structure is formed and this further contributes to spatiotemporal changes in oxygen delivery. This leads to altering the phenotype of the tumors that may contribute to worse prognosis (Henze & Mazzone 2016).

Hypoxic conditions cause only the most aggressive cells to survive these hostile growth conditions and driving tumor growth. Oxygen shortage results in electron leakage and formation of reactive oxygen species (ROS), which can oxidize proteins and cause DNA damage. The net outcome of this is the hypoxic cells experience genomic instability, which might further influence parameters to then accelerate malignant progression (Henze & Mazzone 2016).

In CLL, high concentrations of ATP are present in the intracellular compartment, whereas low concentrations are typically available extracellularly (Serra et al. 2016). However, under conditions of increased cellular turnover and/or inflammation, such as those present in the tumor microenvironment, extracellular nucleotide levels can surge. ATP may then bind to specific receptors, which activate a signaling cascade, or it may be enzymatically converted to adenosine which is a potent immunosuppressant (Serra et al. 2016).

In vivo evidence confirms that hypoxia acts partly though the activation of A2A adenosine receptor (ADORA2A) signaling (Serra et al. 2016). Although circulating CLL cells express active HIF-1α, its role in regulating CLL survival and its mechanism of action remain incompletely understood (Serra et al. 2016).

HIF-1α was found to be intensely positive in CLL lymph nodes (LNs) in areas corresponding to proliferation centers (Serra et al. 2016). HIF-1α expression was highest in CLL cells recovered from LNs compared to Peripheral Blood (PB) and Bone Marrow (BM) (Serra et al. 2016).

At 1% O_2, purified cultured CLL cells didn't change their HIF-1α expression at the mRNA level, but an upregulation of the protein was apparent (Serra et al. 2016).

Expression of A2A adenosine receptor (ADORA2A) was markedly increased in hypoxic CLL cells. CLL cells adapt to hypoxia (Koczula et al. 2016; Serra et al. 2016) by upregulating HIF-1α signaling, in turn increasing nucleotide scavenging and activating adenosine signaling through the A2A receptor (Serra et al. 2016).

When deprived of oxygen, tumor cells quickly promote energy production through glycolysis. This metabolic adaptation is transcriptionally mediated by HIF-1α. Under normoxia, CLL cells predominantly obtain energy through oxidative phosphorylation. However, at 1% O_2, CLL cells markedly increased expression of genes involved in glycolysis (Koczula et al. 2016; Serra et al. 2016; Vander Heiden, Cantley & Thompson 2009).

In summary, hypoxic conditions brought on by tumor cells in the microenvironments creates an acidic, vasculature deprived environment where the metabolic demand of oxygen outweighs the supply. This initiates the expression of HIF proteins which aides in adapting the CLL cells to sustain energy productions through means of aerobic glycolysis "Warburg effect".

1.2.5.1.1 Warburg Effect

Briefly, aerobic glycolysis, also termed as Warburg effect, refers to the cells predominantly produce their energy through a high rate of glycolysis followed by lactic acid fermentation even in the presence of abundant oxygen (Vander Heiden, Cantley & Thompson 2009).

In 1924, Otto Warburg's observed cancer cells metabolize glucose in a manner that is distinct from that of cells in normal tissues (Vander Heiden, Cantley & Thompson 2009). He found that unlike most normal tissues, cancer cells tend to "ferment" glucose into lactate even in the presence of sufficient oxygen to support mitochondrial oxidative phosphorylation (Vander Heiden, Cantley & Thompson 2009). It was originally hypothesized by Warburg that cancer cells develop a defect in mitochondria that leads to impaired aerobic respiration and a subsequent reliance on glycolytic metabolism. However, subsequent work showed there was no impairment of mitochondrial function in most cancer cells (Vander Heiden, Cantley & Thompson 2009).

Cells that are deficient in ATP often undergo apoptosis. Normal proliferating cells can also undergo cell cycle arrest and reactivate catabolic metabolism when their ability to produce ATP from glucose is compromised, and signaling pathways exist to sense energy status (Vander Heiden, Cantley & Thompson 2009). During growth, glucose is used to generate biomass as well as produce ATP. One

glucose molecule can generate up to 36 ATPs, or 30 ATPs and 2 NADPHs (if diverted into the pentose phosphate shunt). The conversion of both glucose and glutamine to lactate involves the enzyme lactate dehydrogenase (LDH), where inhibiting this enzyme activity impairs cell proliferation. The excess generation of lactate that accompanies the Warburg effect would appear to be an inefficient use of cellular resources (Vander Heiden, Cantley & Thompson 2009).

Although tumor hypoxia is clearly important for other aspects of cancer biology, the available evidence suggests that it is a late-occurring event that may not be a major contributor in the switch to aerobic glycolysis by cancer cells (Vander Heiden, Cantley & Thompson 2009).

Although, when oxygen was available, the tricarboxylic acid (TCA) cycle appeared to be supported by glutaminolysis as evidenced by consumption of glutamine and O_2, associated with the production of glutamate, pyruvate, lactate and alanine. Hypoxia induced HIF-1α activity acts to sustain glycolysis, as CLL cells transit from oxygenated to hypoxic environments and that lactate production is largely mediated by the consumption of glucose (Koczula et al. 2016).

HIF-1α independently differentiates utilization of pyruvate in oxygenated and hypoxic conditions. When oxygenated, CLL cells exported pyruvate but as oxygen concentration dropped below 1%, CLL cells imported pyruvate. This pyruvate import is in response to hypoxia-associated oxidative stress rather than hypoxia *per se*, as CLL cells imported pyruvate when treated with H_2O_2 (which induced oxidative stress) under normoxic conditions (Koczula et al. 2016).

In summary, Warburg effect is observed in CLL cells by HIF-1α activity that permits glycolysis through multiple sources of energy when in hypoxic or anoxic conditions within the tumor microenvironment. This is also seen in other cancer conditions particularly solid tumors.

1.2.5.2 T cells

The interactions between CD40 from B cells and CD40 ligand (CD40L) on activated T cells, are important in the antigen presentation and initiating normal B-cell responses (Ten Hacken & Burger 2015; van Kooten & Banchereau 2000). In CLL, the T cells display impaired immunological synapses (Ramsay et al. 2012; Ramsay et al. 2008). This is viewed as an impaired T cell cytoskeletal rearrangement compared to that expected from non-CLL T cells and antigen presenting cells (APC) in order to proliferate and produce interleukin 2 (IL-2) (Ramsay et al. 2008). It is understood as chronic activation and 'exhaustion' of the T-cells is due to the CLL cells (Choi, Kashyap & Kumar 2016). It has been shown that activation of malignant B cells by CD40 ligation promotes survival of CLL cells (Kitada et al. 1999). CLL cells express high level of programmed cell death protein 1 ligand (PD-L1)

(McClanahan et al. 2015). Thus, interrupting the programmed cell death protein 1 (PD-1) and the PD-L1 axis can restore immune functions and inhibits CLL development in a mouse model of CLL (McClanahan et al. 2015). Taken altogether, these reports suggest that T cells have reduced activity, which may explain the evasion of CLL cells from immune-mediated cell death (Ten Hacken & Burger 2015).

Similar to T-cells, Natural killer cells (NK cells) have an immune dysfunction with defective actin polymerization and impaired immune synapse formation (Choi, Kashyap & Kumar 2016; Maki et al. 2008).

1.2.5.3 Stromal Cells

There are multiple cell types involved in forming the tumour stroma within the tumour microenvironment (Yang et al. 2015). Mesenchymal stromal cells (MSCs) such as bone marrow stromal cells (BMCs) are 'feeder' layers for hematopoietic progenitor cells and take part in normal bone marrow architecture (Yang et al. 2015). The BMCs have been shown to protect CLL cells from spontaneous and drug-induced apoptosis via direct contact (Kurtova et al. 2009; Lagneaux et al. 1998; Ten Hacken & Burger 2015). BMCs also secrete chemokines which regulate CLL cell trafficking and tissue homing and also provide additional signs that support their survival and encourage drug resistance (Burger et al. 2009a). BMCs were found to reduce the expression of CD20 on CLL cells which may implicate resistance to anti-CD20 antibody treatment (rituximab) (Marquez et al. 2015). Other studies have suggested promotion of cell survival and drug resistances by BMCs through the involvement of NOTCH signaling, protein kinase C beta II (PKCβII) expression and NF-κB pathway activation (Jitschin et al. 2015; Lutzny et al. 2013).

Ding et al. (2010) showed that CLL induces proliferation and induction of PI3K signaling by activating BMSC through platelet-derived growth factor (PDGF) receptor activation (Choi, Kashyap & Kumar 2016; Mangolini & Ringshausen 2020).

A cross-talk between CLL and stromal cells have also been suggested by the secretion of microvesicles by CLL that activate AKT pathway in BMCs (Choi, Kashyap & Kumar 2016; Ghosh et al. 2010).

It was seen that in CLL, the BMSCs take up the amino acid cystine which is then converted to cysteine and released into the microenvironment, which becomes available for the CLL cells (Zhang et al. 2012). This metabolic remodeling promotes CLL cells viability and drug resistance (Mangolini & Ringshausen 2020; Zhang et al. 2012).

1.2.5.4 Endothelial cells and follicular dendritic cells

Endothelial and follicular dendritic cells (FDCs) are essential for tissue homing and retention of CLL cells to tissues (Ten Hacken & Burger 2015). The adhesion to the endothelial cells promotes survival, activation and drug resistance of CLL cells (Badoux et al. 2011; Hamilton et al. 2012). CLL cells can bind to integrins and BAFF and APRIL that are expressed on the surface of endothelial cells (Cols et al. 2012). The endothelial cells help promote CLL-cell survival and resistance to drug-induced apoptosis (Ten Hacken & Burger 2015). It was also shown that *in vitro* FDCs delays spontaneous apoptosis of CLL cells by direct contact via CD44 ligation and upregulation of the myeloid cell leukemia 1 (MCL-1) protein which is a member of anti-apoptotic proteins of the BCL2 family (Pedersen et al. 2002).

It was seen that CD27 influences CLL binding to stroma, where its expression is correlated with ZAP-70 expression, elevated on BCR cross-linking and correlates with functional ability to adhere to stromal cells. Antibody blockade of CD27 was shown to impair binding of CLL cells to the stroma (Choi, Kashyap & Kumar 2016; Lafarge et al. 2015).

1.3 Nurse Like Cells: A history

As nurse like cells (NLCs) are essentially the macrophages derived from the circulating monocytes, I would like to introduce general biological aspects of macrophages first.

1.3.1 Macrophages: A spectrum

Macrophages can be of circulating monocyte origin, or originating from tissue resident monocytes. The blood monocyte is a motile cell that can migrate alone vessel walls and has the ability to adhere to surfaces. The monocytes respond to inflammation and chemotactic stimuli by diapedesis (movement through intact walls of capillaries) into inflammatory sites, where they mature into macrophages, with greater phagocytic ability and increased composition of hydrolytic enzymes (Lichtman et al. 2011a). Classic studies in the 1930s and 1940s showed that monocytes transform into macrophages *in vitro*. Macrophages can be produced from monocyte culture with cytokines such as granulocyte-macrophage colony-stimulating factor (GM-CSF) or macrophage-CSF (M-CSF) (Lichtman et al. 2011a). Macrophages are characterized by increased cell size and increase in the number of cytoplasmic granules, in heterogeneity of cell morphology and in the number of cytoplasmic clear vacuoles (Lichtman et al. 2011a).

Macrophages exist in either M0 (immediately differentiated from monocytes), M1 (tumoricidal) or M2 (tumorogenic) phenotype along the M1/M2 spectrum (Figure 1.3) (Italiani & Boraschi 2014; Murray

et al. 2014). Their position on the spectrum depends on the type of stimuli monocytes received and how they respond to the stimuli (Figure 1.3). On one end of the spectrum are the M1 macrophages and on the opposite end are the M2 macrophages. Therefore, a newly differentiated monocyte first appears to be in the middle of the macrophage spectrum (M0), displaying neither M1, nor M2 phenotypes. Upon further stimulation, the same macrophage moves towards either end on the spectrum. Process of the differentiation of a macrophage to the extreme ends is also known as polarisation.

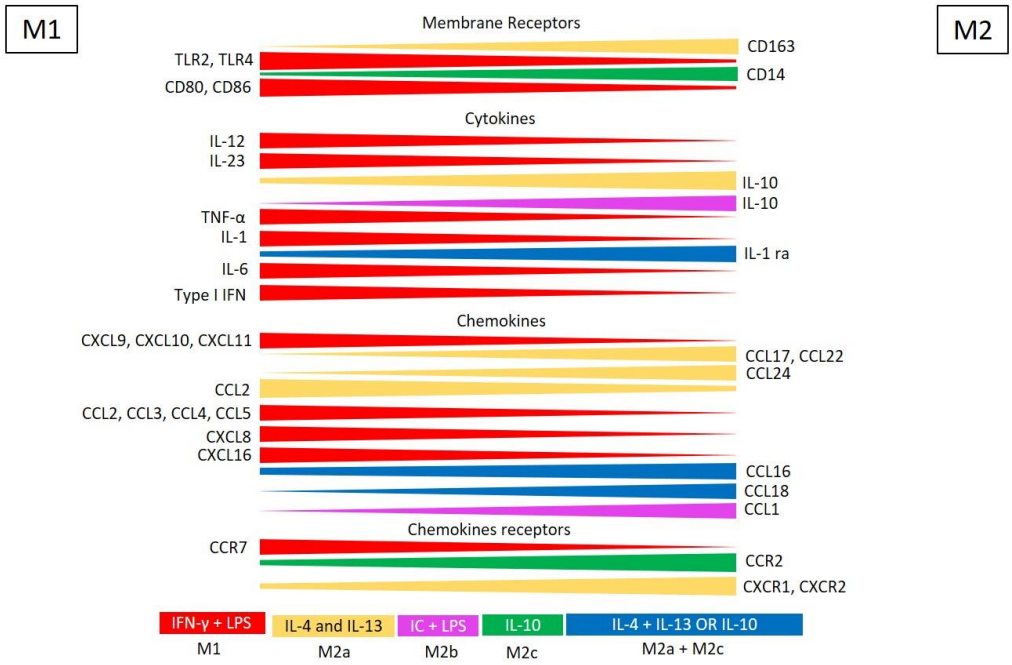

Figure 1.3 M1 and M2 macrophages

M1 and M2 macrophages: the extremes of a continuum. Macrophage activation is associated with changes in gene expression profiles where exposure to different stimuli induces distinct polarization profiles, associated with expression of selected molecules. Classical macrophage activation (M1 macrophage) is induced by exposure to IFN-γ and LPS (red). Alternative activation (M2 macrophage) can be induced by different stimuli such as IL-4 and IL-13 (induce M2a yellow), immune complexes (IC) + LPS (induce M2b magenta), and IL-10 (induce M2c green). IL-4 + IL-13 or IL-10 induce both M2a and M2c (blue). Abbreviations: IFN-γ, interferon gamma; IL-1 ra, IL-1 receptor antagonist; LPS, lipopolysaccharide; MR, mannose receptor; RNI, reactive nitrogen intermediates; ROI, reactive oxygen intermediates; TLR, Toll-like receptor. Image is modified from a review by Mantovani et al. (2004).

1.3.1.1 M1: The Classically Activated Macrophage

The major function of naive macrophages is clearance of apoptotic debris produced as part of the normal cellular process of homeostasis. In response to various endogenous signals, macrophages produce pro-inflammatory mediators and alter surface markers (Figure 1.3) (Tan et al. 2016). Classical

M1 activation is induced by intracellular pathogens, bacterial cell wall components such as lipopolysaccharide (LPS), Th1 (type 1 helper T cells) cytokines such as interferon gamma (IFN-γ) and tumour necrosis factor alpha (TNF-α) (Jablonski et al. 2015; Roszer 2015; Zhang et al. 2013). These polarized M1 macrophages harbour immune-stimulatory properties and cytotoxic function against tumour cells (Zhang et al. 2013).

M1 macrophages are characterized with inflammatory cytokine secretion and production of nitric oxide (NO), resulting in an effective pathogen elimination mechanism (Jablonski et al. 2015; Roszer 2015). Besides, M1 macrophage is associated with higher aerobic glycolysis and extracellular acidification rate; increase of HIF-1α further enhances IL-1β promoter activity, thus maintaining IL-1β production in M1 macrophages (Tan et al. 2016).M0-type macrophages are induced to polarize into M1 macrophages by LPS and IFN-γ, causing the cells to flatten to a round, pancake-like shape within 24h of stimulation (McWhorter et al. 2013).

As macrophage display a spectrum of phenotypes *in vivo*, it is not easy to distinguish macrophage phenotypes (Jablonski et al. 2015). Using expression profiling data, a study has found that as a result of different activation stimuli, M1 and M2 macrophages co-expressed many genes, referred to as shared signatures (Jablonski et al. 2015). Moreover, the same study also identified several distinct genes exclusively expressed in M1 macrophages, namely CD38, Gpr18 (G-protein coupled receptor 18) and Fpr2 (formyl peptide receptor 2) and established them as novel M1 markers (Jablonski et al. 2015).

1.3.1.2 M2: The Alternatively Activated Macrophage

Alternative M2 activation is induced by fungal cells, parasites, immune complexes, complement, apoptotic cells, macrophage colony stimulating factor (M-CSF), interleukin-4 (IL-4), IL-13, IL-10, tumour growth factor beta (TGF-β) and various other signals (Figure 1.3) (Jablonski et al. 2015; Roszer 2015).

Innate immune cells such as basophils and mast cells and other adaptive cells produce IL-4 and IL-13, priming M2 alternative phenotype (Tan et al. 2016). IL-4-induced M2 macrophages expressed high concentration of IL-10, decoy receptor IL-1R, IL-1R antagonist, chemokines CCL22 and CCL17, and intracellular enzyme arginase-1 (Figure 1.3) (Tan et al. 2016). All of these result in the recruitment and activation of Th2 immune response and immune-suppressive function of M2 macrophages. In addition to Th2 immune response, IL-4-induced macrophages stimulate arginase activity by converting arginine to polyamines and collagen precursors for tissue modelling and wound healing (Tan et al. 2016) . M2

macrophages also produce VEGFα, EGF, and IL-8 that are responsible for angiogenesis and lymph-angiogenesis (Tan et al. 2016) .

Apart from IL-4-induced phenotype, different schemes of M2 macrophages classification have been proposed due to the overlapping properties of alternatively activated macrophages. The activation of M2 macrophages stimulated by addition of either IL-4 and IL-13, TGFβ, immune complexes, glucocorticoids, or IL-10 may yield distinct activation profiles (Tan et al. 2016) . This gives a series of subtypes of M2 macrophages depending on how they were activated (Figure 1.3). The changes in shape of M0-type macrophages when induced to polarize into M2 macrophages with IL-4 and IL-13 was seen to be elongation of the cell (McWhorter et al. 2013).

M2 macrophages have high phagocytosis capacity, producing extracellular matrix (ECM) components, angiogenic and chemotactic factors and IL-10 (Jablonski et al. 2015; Roszer 2015). In addition to pathogen defence, they also clear apoptotic cells, mitigate inflammatory response, and promote wound healing (Jablonski et al. 2015; Roszer 2015). These anti-inflammatory features aid in growth of tumour tissues.

Cellular metabolism especially lipid metabolism also plays an important role in providing energy fuel for activation of alternative M2 macrophages. As opposed to M1 classical activation, M2-regulated gene transcription occurs in conditions favouring mitochondrial metabolism and oxidative glucose metabolism, in which the M2 phenotype tends to be switched towards anti-inflammatory state under low oxygen condition (Tan et al. 2016). This suggests that hypoxic conditions are favourable for M2 macrophages to thrive.

In a study analysing the expression profiling data, described earlier, authors also found several distinct genes highly expressed in M2 macrophages, including Egr2 (early growth response 2) and c-Myc and suggested that they can be used as novel M2 markers (Jablonski et al. 2015).

1.3.2 Tumour Associated Macrophages (TAM)

Macrophages represent up to 50% of the tumour mass (Solinas et al. 2009) and they have an important role to play. Tumour associated macrophages (TAMs) are macrophages expressing M2 phenotype and display mainly anti-inflammatory, pro-tumoral properties that promote tumour cell survival, proliferation and spread (Mantovani et al. 2002; Solinas et al. 2009).

The presence of TAMs is not always correlated with bad prognosis, but studies have shown a link between their abundance and the process of metastasis (Mantovani et al. 2017; Solinas et al. 2009). TAMs have been considered to originate from the cells in circulation, recruited by tumour and non-

tumour cells in the tumour microenvironment by the release of chemotactic signals (Mantovani et al. 2017). Monocyte differentiation is influenced by their position relative to the tumour mass by an IL-10 gradient, where this prevents formation into dendritic cells and is encouraged to differentiate into macrophages (Allavena et al. 1998). One hallmark of TAM is their tendency to accumulate into necrotic regions of tumours, characterized by low oxygen tension (Solinas et al. 2009). This preferential localization is regulated by tumor hypoxia, which induces the expression of hypoxia inducible factor 1 (HIF-1)-dependent molecules (vascular endothelial growth factor VEGF, C-X-C motif chemokine 12 CXCL12, and its receptor C-X-C chemokine receptor type 4 CXCR4) that modulate TAM migration in avascular regions (Solinas et al. 2009). TAMs also display immune suppressive activity by producing IL-10 and secretion of chemokines that attract naïve T cells in the microenvironment (Solinas et al. 2009).

TAMs have been shown to be present in solid tumour types, such as in breast, prostate, Ovary, cervix, stomach, lung, bladder, and glioma (Bingle, Brown & Lewis 2002a). In solid tumours they also provide pro-survival conditions to the tumour cells and allow their proliferation (Mantovani et al. 2017).

TAMs have also been isolated from the peripheral blood, spleen, and lymph nodes in CLL patients where they have shown to be essential for CLL cell survival in the tumor microenvironment (Edwards et al. 2018). Nurse-like cells (NLCs) or lymphoid-associated macrophages (LAMs) in CLL, share a similar gene expression profile to TAMs derived from other tumor types (Mantovani et al. 2017; Ysebaert & Fournie 2011). From this point onwards, TAMs and NLCs will be used interchangeably with NLC referring specifically to CLL.

1.3.3 Nurse-Like Cells: Origin

Nurse-like cells were first recognized in situ in the thymus, where they form characteristic complexes with immature T lymphocytes and play an important role in thymocyte maturation and differentiation, and the interaction is thus characterized by invasion into thymic nurse cells by thymocytes (emperipolesis) (Burger et al. 2000).

In CLL, leukemic B-cells were observed to crawl under these supporting cells but not become internalized. Therefore, this process is pseudo-emperipolesis, and the supporting cells are termed nurse-like cells (NLCs) with the initial characteristics of interacting physically with CLL cells and supporting the survival and activation of CLL cells (Burger et al. 2000).

1.3.4 Initial characterisations of NLCs

In the initial study, immunophenotyping of the NLCs was also performed, which showed that these cells express cell markers vimentin, STRO-1 (a mesenchymal stem cell marker) and CD68 (Burger et al. 2000). They do not express B-cell nor T-cell differentiating markers or CD83 (a marker for mature dendritic cells) (Burger et al. 2000). Strikingly, the morphology and immunophenotype of adherent cells derived from the peripheral blood of healthy donors were different to the adherent NLC from CLL blood samples (Burger et al. 2000).

Vimentin, encoded by *VIM* gene for intermediate filaments and mediating changes in cell shape, is involved in motility and adhesions, as well as cytoskeletal interactions (Mendez, Kojima & Goldman 2010; Stelzer G et al. 2016).

CD68 (a member of lysosome-associated membrane proteins) is highly expressed on monocytes and macrophages (Stelzer G et al. 2016), suggesting that the adherent NLC cells are from myelomonocytic lineage.

Also, the study investigated if trisomy 12 can be detected in the NLCs as some blood samples used in the study were obtained from patients whose CLL cells contained Trisomy 12. The study showed no observation of trisomy 12 in 'an overwhelming majority of NLCs from the same patient' (Burger et al. 2000). This suggests that NLC and CLL populations do not share the same chromosome defect, thus proving that NLC are not part of the CLL clone (Burger et al. 2000).

NLCs were found to express mRNA for stromal derived factor-1 (SDF-1), also known as C-X-C motif chemokine 12 (CXCL 12), which is a potent chemo-attractant for CLL B cells and mediator in their interaction with bone marrow stromal cells (Burger et al. 2000). Synthetic SDF-1 alone was also shown to be capable of rescuing CLL B cells from apoptosis (Burger et al. 2000).

A more in-depth study investigating distinctive features of these nurse-like cells in CLL was carried out later on. It was shown that one to two weeks after culturing blood mononuclear cells on plastic culture plates, NLCs formed a 'sparse monolayer of large, round, and sometimes bi-nucleate cells', where clusters of CLL B cells were attached around these NLCs (Nobuhiro Tsukada 2002).

It was also shown on flow cytometry analysis that NLCs typically had a larger forward and side scatter properties than CLL cells (indicating larger cell size of NLCs) (Tsukada et al. 2002). They expressed CD14, CD45 and HLA-DR but not CD3. This suggests that NLCs express surface markers of hematopoietic cells and surface antigens consistent with blood monocytes (Nobuhiro Tsukada 2002).

NLCs also expressed CD33 which has been known to be expressed on cells of myelomonocytic lineage that may facilitate cell-cell adhesion (Nobuhiro Tsukada 2002).

Collectively, the above findings show that NLCs are derived from blood monocytes, however, the expression levels of CD14 and CD33 in these cells are significantly lower than typical monotypes (Tsukada et al. 2002). Meanwhile, NLCs express higher levels of CD68 than blood monocytes, macrophages, or monocyte-derived dendritic cells (Nobuhiro Tsukada 2002).

To confirm that NLCs were derived from blood monocytes, the authors further showed that CLL PBMCs depleted of CD14+ cells (monocytes/macrophages) did not develop NLCs when cultured under the identical conditions (Tsukada et al. 2002). Also, PBMCs cultures depleted of CD2 (T cells/NK cells) developed NLCs of similar appearance to the unsorted PBMC culture (Nobuhiro Tsukada 2002). However, the exact duration and date of culture when comparisons were made was not provided.

A thorough antigen profile revealed that NLCs expressed significantly higher CD68 and lower CD33 than any other cells (Nobuhiro Tsukada 2002). Monocyte-derived dendritic cells expressed significantly higher levels of CD1a, CD40, CD80 and CD86 than NLCs (Nobuhiro Tsukada 2002).

Interestingly, it was shown in the study that CD14+ cells from PBMCs of healthy donors can also differentiate to NLCs (based on morphology, phenotype and function) when co-cultured with CLL cells (Nobuhiro Tsukada 2002). However, NLCs derived from PBMC of CLL patients expresses a greater level of CD68 than those from healthy donors.

Using a trans-well membrane separating CD14+ cells from CLLs, it was shown that NLCs were not developed (levels of expression of CD14 and CD33 were similar to CD14+ mononuclear cells cultured alone), suggesting that direct contact of CD14+ cells with CLL cells is needed to develop NLCs (Nobuhiro Tsukada 2002).

Finally, to test if NLCs exists *in vivo*, CD14+ splenocytes from CLL patients were examined and shown to display NLC morphological features and express higher levels of CD68 than CD14+ splenocytes obtained from patients without CLL (Nobuhiro Tsukada 2002).

Some studies reported a link between elevated peripheral blood monocyte count at the time of diagnosis in patients with CLL and poor clinical outcomes (Edwards et al. 2018; Friedman et al. 2016). It is thus speculated that high number of monocytes could lead to high number of NLCs, resulting in a more protective tumor microenvironment. However, the exact relationship between the number of peripheral blood monocytes and the number of NLCs is yet to be established.

1.3.5 Biological functions of NLCs

1.3.5.1 Protection of CLL cells against spontaneous and drug-induced apoptosis when in co-culture

In the early 2000s, *in-vitro* coculture with marrow stromal cells was found to have prolonged the viability of CLL cells when compared to CLL cells cultured alone (Burger et al. 2000). Adherent cells (nurse-like cells) were found to be present in such cultures after 3 days of culture and their numbers increased with time in culture (Burger et al. 2000). After separating the CLL cells from NLCs after 14 days, the CLL cells displayed decline in viability (Burger et al. 2000). The proof of apoptosis was the reduction in mitochondrial membrane potential (Burger et al. 2000). To further prove the effect of the NLCs, the CLL cells were re-plated onto them and their viability was stabilised over time compared to their counterparts cultured alone which continued a decline in viability (Burger et al. 2000). This phenomenon was confirmed in other studies (Burger et al. 2005; Nishio et al. 2005; Tsukada et al. 2002).

When cultured with NLCs, CLL cells were found to be less sensitive to dexamethasone and chlorambucil compared to CLL cells cultured alone (Filip, Cisel & Wasik-Szczepanek 2015). It was also shown that the NLCs protected CLL cells from spontaneous and drug-induced apoptosis by fludarabine, cladribine, methylprednisolone, bortezomib, valproic acid and flavopiridol (Burger et al. 2005; Fiorcari et al. 2016; Stamatopoulos et al. 2012). Therefore, there were clear evidence that NLCs can have cytoprotective effect on CLL cells when they were cultured together. However, how NLCs exert such effect on CLL cells is not well understood.

1.3.5.2 Effect of NLC on expression of IgM and IgD on CLL cells

Recently it was shown that NLCs cause a significant downregulation of surface expression of IgM and IgD on CLL cells when cultured together (Ten Hacken et al. 2016) . The expression of surface IgM and IgD recovered during 72hrs in culture in the absence of NLC, which resembles the recovery pattern of BCR in CLL cells when cultured *in vitro* in the absence of antigenic stimulation (Ten Hacken et al. 2016). It was postulated that NLC can present yet to be identified antigens that can trigger BCRs in CLL cells, resulting in down-modulation of both IgM and IgD. Although it was challenging to investigate BCR signaling responses with this coculture system, these data suggested that IgM and IgD may both be engaged and involved in activating BCR signaling in CLL cells when in coculture with NLC (Ten Hacken et al. 2016).

1.3.5.3 Effect of CLL on NLC

$CD14^{+}$ monocytes co-cultured with CLL cells developed large, adherent cells with cell morphology typical of NLCs (Nobuhiro Tsukada 2002). These cells also expressed higher level of cytoplasmic CD68,

when compared with $CD14^+$ monocytes cocultured with the $CD19^+$ cells of healthy donors (Tsukada et al. 2002). This indicates that CLL cells can also influence the differentiation of $CD14^+$ monocytes into NLCs *in vitro*.

The above finding has been confirmed by a separate study where $CD14^+$ monocytes co-cultured with CLL cells displayed more characteristic features of NLCs than their counterparts co-cultured with non-malignant B cells (Bhattacharya et al. 2011). Furthermore, CLL cells induced significant changes in expression of proteins involved in antigen presenting and immunity pathways in $CD14^+$ cells. It was shown that NLCs had reduced levels of lysosome activity and decreased expression of CD74 and HLA-DR *in-vitro* while expression of FCGR2B was increased (Bhattacharya et al. 2011). FCGR2B is an important inhibitory Fc-gamma receptor present on macrophages and immature dendritic cells that down-regulates the process of internalization (phagocytosis) (Bhattacharya et al. 2011). This *in-vitro* study suggests that CLL cells may specifically down-regulate genes in NLCs that are involved in immunocompetence (Bhattacharya et al. 2011).

1.3.5.4 Commonalities and differences of TAMs in CLL and in other cancers

Cancers that are not solid are generally grouped together as blood cancers and thus have differences in their disease presentation, pathology and progression. However, the tumor microenvironment within solid tumors provide the general protective function in a similar way to that in hematologic malignancies such as CLL disease (Petty & Yang 2019).

It is known that macrophages infiltrate solid tumors and studies have shown that in human malignancies such as hepatocellular, colon, breast and lung carcinoma, poor prognosis is associated with high level of macrophage infiltration (Mantovani et al. 2017; Minami et al. 2018). Tumor associated macrophage (TAM) markers such as CD68 and CD163 have been measured to predict patient outcomes after chemotherapy for cancers such as follicular lymphoma, Hodgkin lymphoma, colorectal cancer and pancreatic cancer (Mantovani et al. 2017). Some studies have investigated role of TAM in these cancers using cell lines such as HepG2 (hepatoma cells) or A549 (lung adenoma cells) (Genin et al. 2015).

In acute lymphocytic leukemia (ALL), it was seen that higher numbers of CD163 positive cells were correlated with poor prognosis (Petty & Yang 2019). Coculture with M2 macrophages *in vitro* induced cell proliferation of T-ALL cells (Petty & Yang 2019).

In acute myeloid leukemia (AML), it was seen that the number of M2-like TAMs that expressed CD163 CD206 was significantly increased in bone marrow (BM) compared to healthy donors (Petty & Yang

2019). The number of M2-like TAMs in spleen, but not in bone marrows, was correlated with poor prognosis in AML patients (Petty & Yang 2019).

In Hodgkin's lymphoma and non-Hodgkin's lymphoma, the presence of $CD68^+$ or $CD163^+$ TAM is also a strong predictor of poor clinical outcome (Petty & Yang 2019).

Therefore, there are many commonalities in the properties of TAM within tumor microenvironment between CLL and other cancers. As described in previous section 1.3.1, the research of NLCs in CLL is relatively new in comparison with research of TAMs in solid tumours. Even within the field of CLL research, other components of the CLL microenvironment (e.g. T cells and stromal cells) have been well characterized (Petty & Yang 2019). Therfeore, there are a need to inverstigate further the biology of NLCs in CLL, which will be the focus of this project.

1.4 Molecules mediating interaction between NLCs and CLL cells

1.4.1 CXCR4, CXCR5, CCL3, CCL4, CCL22

While the cytoprotective effect of NLCs on CLL cells have been reported, the mechanisms mediating interaction between NLCs and CLL cells were also being investigated. It was thus shown that circulating CLL cells expressed high levels of the chemokine receptor CXCR4 (CD184), which mediates chemotaxis, migration across vascular endothelium, actin polymerization and migration under bone marrow stromal cells (BMSCs) in response to CXCL12 (SDF-1) (Burger 2011b). CLL cells in the tissue express lower levels of CXCR4 (Burger 2011b). The signalling of CXCR4 can be inhibited by PI3K-δ, SYK and BTK inhibitors (Burger 2011b).

CXCR5 (CD185), the receptor for CXCL13, is also expressed on CLL cells, which regulates homing and positioning within lymphoid follicles. CXCL13 induces recruitment of naïve B cells into follicles and also induces activation via PI3K family of kinases. CXCL13 mRNA and protein are also expressed by NLC (Burger 2011b).

CLL cells have been shown to secrete CCL3, CCL4 and CCL22, which are chemo-attractants for T lymphocytes as well as monocytes (Hartmann et al. 2016; Sivina et al. 2011; Zucchetto et al. 2009). The CLL cells also secrete CCL3 and CCL4 in response to BCR stimulation and in co-culture with NLCs (Burger 2011b; Burger et al. 2009b; Hartmann et al. 2016).

1.4.2 BAFF and APRIL

CLL cells express B-lymphocyte stimulator (BLyS), otherwise known as B cell-Activating Factor of the tumor necrosis factor (TNF) Family (BAFF) (Kern et al. 2004; Nishio et al. 2005). BAFF is a type 2 transmembrane protein that exists as a membrane-bound or soluble form to promote B cell survival (Nishio et al. 2005). It was found in a mouse study that disruptive mutations of either BAFF or its receptor (BAFF-R) caused extensive loss of mature B-cells, suggesting that BAFF-BAFF-R interactions are important in the differentiation and/or survival of mature B cells. Other receptors were found to interact with BAFF, including B-cell maturation antigen (BCMA) and transmembrane activator and calcium modulator and cyclophilin ligand interactor (TACI) (Nishio et al. 2005).

BCMA and TACI also can bind to A Proliferating Inducing Ligand (APRIL), a factor which can also contribute for the survival of B-cell survival (Nishio et al. 2005). BAFF-R is specific to BAFF and cannot bind to APRIL. APRIL was initially observed in tumor cells which was secreted as soluble molecule through the action of furin proteases present in the Golgi (Nishio et al. 2005). It was shown that CLL cells also express surface APRIL (Cols et al. 2012; Kern et al. 2004; Nishio et al. 2005). It has been reported that NLCs expressed high levels of BAFF and APRIL (Nishio et al. 2005). Viability of CLL cells was enhanced when BAFF and APRIL were added to the culture medium (Nishio et al. 2005). However, the viability was still not as high as that seen when CLL cells were cultured with NLCs (Nishio et al. 2005). This suggests that there are other undiscovered factors at work in the CLL/NLC co-culture setting.

1.4.3 HMGB1

In a recent study, it was shown that damage-associated molecular patterns (DAMP) molecule HMGB1 (high-mobility group protein B1) was released from CLL cells and promoted the differentiation of NLCs (Li Jia 2014). HMGB1 is a DNA-binding protein and the HMGB1-DNA complex can trigger the immune response through the interaction with Receptor for Advanced Glycation End products (RAGE) and Toll-like receptor 9 (TLR9) (Al-Malti, Gribben & Jia 2012; Li Jia 2014).

In this study, HMGB1 was found in the nucleus as well as in the cytoplasm of CLL cells prior to its release. NLC differentiation *in vitro* was associated with HMGB1 release from CLL cells, whereas blockade of the HMGB1-RAGE/TLR9 signaling pathway prevented NLC differentiation (Li Jia 2014). Active release of HMGB1 was also observed in CLL lymph nodes where there was no necrotic cells detected (Li Jia 2014). Therefore, the authors concluded that the leukemic B cells were actively involved in modulating the CLL microenvironment by releasing HMGB1.

1.4.4 Nurse Like Cells and Hypoxia

In a study to investigate the role of hypoxia in shaping the CLL lymph node microenvironment, a comparative analysis of the expression of ATP-metabolizing enzymes in NLCs uncovered a significant increase in expression of CD73 under hypoxia (Serra et al. 2016). CD73 is an ecto-5'-nucleotidase (5'-NT), an enzyme which converts AMP to adenosine and is essential in generation of adenosine (Resta, Yamashita & Thompson 1998). Further analysis showed an increased adenosine accumulation in NLC cultures when exposed to extracellular AMP under hypoxia, which was not seen in their normoxic counterparts (Serra et al. 2016). Both mRNA and protein levels of adenosine A2A receptor were markedly increased in NLCs as well as in CLL cells under hypoxia condition. Increased adenosine production and signalling via the A2A receptor facilitated protection of CLL cells from drug-induced apoptosis and differentiation of monocytes from CLL PBMCs to M2 macrophages (Serra et al. 2016). In addition, a marked upregulation in CCL3 mRNA in NLCs was reported by the study, suggesting that differentiated macrophages upon hypoxia actively recruits myeloid cells. Also, optimal chemotaxis of normal monocytes toward conditioned media of NLCs cultured under hypoxia was observed. This chemotaxis was increased by A2A agonist and reduced by the antagonist (Serra et al. 2016). Finally, NLCs differentiated under hypoxia showed greater protection of CLL cells against cell death than those differentiated under normoxia (Serra et al. 2016). Therefore, the study showed that hypoxia can modulate the CLL microenvironment by activating adenosine signalling through the A2A receptor in both NLCs and CLL cells.

1.4.5 Changes in molecular interactions by Lenalidomide

Lenalidomide (Revlimid) is an immunomodulatory drug that has no direct cytotoxic effect on CLL cells (Chanan-Khan et al. 2011; Schulz et al. 2013). It was shown that levels of inflammatory cytokines were changed in patients treated with lenalidomide (Lee et al. 2011; Schulz et al. 2013). This drug was described to induce apoptosis in CLL cells indirectly via targeting components of the microenvironment (Schulz et al. 2013). A study was carried out to examine effect of lenalidomide on viability of CLL cells co-cultured with NLCs and reported that the mean survival rate of CLL was significantly reduced from 72% to 59.1% when lenalidomide was present (Schulz et al. 2013). However, the magnitude of response to this drug varied from patient to patient where some CLL samples even showed no reduction in viability of CLL cells when treated with lenalidomide (Schulz et al. 2013).

CCL2 (a chemokine that is involved in chemotactic activity for monocytes as well as differentiating to M2 type macrophages) is highly upregulated in monocytes after contact with CLL cells, was shown to be reduced after cultures were treated with lenalidomide (Schulz et al. 2013).

IL-10 (an immunosuppressive cytokine) levels were shown to be increased in cultures treated with lenalidomide. It was shown to induce apoptosis in CLL cells via activation of STAT1 pathway (Schulz et al. 2013). The study also found that lenalidomide had no or minimal effect on the viability of CLL cells cultured alone, or that of monocytes and NLCs in culture (Schulz et al. 2013). Lenalidomide was also been shown to reduce migration capability of CLL cells in this study (Schulz et al. 2013).

This suggests that some effects of lenalidomide extends to the monocytes via changes in levels of CCL2 and to CLL cells via changes in levels of IL-10 and migration ability (Schulz et al. 2013).

1.5 Prognostic factors in relation to the Microenvironment

A gold standard of prognostic marker is the mutational status of IGHV, which were first reported by by two independent groups (Hamblin et al. 1999; Damle et al. 1999). CLL cells with sequences in IGHV gene that are 2% or more non-homologous to that of the nearest germline are considered to have undergone somatic hypermutation (Ghia et al. 2006) (also known as M-CLL). Conversely, CLL cells having sequences of IGHV gene that are more than 98% homologous to that of the germline are considered to express un-mutated IGHV (also known as UM-CLL). Study conducted by Hamblin and colleagues showed that, regardless of clinical stage of the disease, the survival rate of patients with UM-CLL was significantly worse than those with M-CLL (Hamblin et al. 1999). In addition, work from Damle and colleagues showed that patients with UM-CLL had a higher percentage of $CD38^+$ B-CLL cells (>30%) than patients with M-CLL and that those patients with UM-CLL and also having >30% $CD38^+$ B-cells did not respond well to chemotherapy drugs and their survival was shorter (Damle et al. 1999). Through *in vitro* experiments, it was shown that CLL cells from patients with UM-CLL are more likely to undergo rapid spontaneous apoptosis than CLL cells from patients with M-CLL (Coscia et al. 2011). This suggests that CLL cells with unmutated IGHV are more dependant on survival stimuli from the microenvironment than cells with mutated IGHV.

ZAP70 expression has also been associated with poor prognosis of CLL (Crespo et al. 2003). It has been shown that $ZAP70^+$ CLL B cells have stronger migratory ability and are characterized by a special gene signature associated with migration, homing or CXCR5/CXCL12 pathways (Dubois et al. 2020).

Another prognostic marker for poor clinical outcome in CLL is the increased level of expression of CD38 (Damle et al. 1999). It was shown that CLL cells with high expression of CD38, together with ZAP30,

had a greater migratory potential, which was associated with aggressive disease (Deaglio et al. 2007). It was suggested that the changes in expression of CD38 during the course of disease reflect the dynamic status of the stromal cell-CLL cell interactions *in vivo* (Dubois et al. 2020).

Study by Herishanu et al. (2011) showed that levels of CCL3 and CCL4 were increased in CLL cells from bone marrow and lymph nodes (Herishanu et al. 2011). This increase is indicative of an *in vivo* interaction between CLL cells and NLCs as well as stromal cells (Dubois et al. 2020).

Collectively, the prognostic markers mentioned above are associated with the *in vivo* interactions between CLL and the microenvironment, which highlight the importance of further research in understaning the the molecular mechanisms mediating the interactions between CLL cells and components of the microenvironment.

1.6 Drug resistance: an area of unmet need

Despite the advancement of our understanding of the biology of the disease and progress in development of new drugs, patients with CLL still develop relapsed disease even though they initially respond to treatment (Bakker et al. 2016). Drug resistance is thus still a serious clinical challenge in management of the patients with CLL.

Advances in understanding the role of tumour microenvironment (TME) in leukaemia including CLL uncovered new therapeutic opportunities to target disease development and progression (Bakker et al. 2016; Woyach & Johnson 2015).

The BTK inhibiter ibrutinib has been successfully developed to treat the patients with CLL as a result of better understanding of the interaction of CLL cells with the microenvironment. As described earlier, BCR signalling plays an important role in CLL cell survival and proliferaltion in response to antigen stimulation within the CLL microenvironment and BTK is a critical component of the BCR signalling complex (Figure 1.2). Ibrutinib has been shown to reduce secretion of BCR-dependent chemokines (CCL3, CCL4) by the CLL cells, thus inhibiting chemoattraction of macrophages and T cells (Ponader et al. 2012). In the meantime, ibrutinib inhibited migration of CLL cells in response to tissue homing chemokines (CXCL12, CXCL13) secreted by T cells and macrophages (Niemann et al. 2016; Ponader et al. 2012). In patients on ibrutinib treatment, it has been shown that ibrutinib decreased overall T-cell numbers and disrupted the interaction between macrophages and CLL cells in the bone marrow (Niemann et al. 2016). Ibrutinib has also been shown to induce egress of CLL cells from the lymph nodes into the blood (Boissard et al. 2015b). Previous work from our Department has also shown that ibrutinib prevented CLL cells from entering into and retension within the lymph nodes by

inhibiting chemokine-induced integrin activation (Till, Pettitt & Slupsky 2015). Despite its impressive clinical activity, patients who fail to respond or relapse even after long periods of remission have been reported (Molica et al. 2020; Woyach & Johnson 2015).

Meanwhile, due to the fact that CLL cells over-express anti-apoptotic protein BCL-2 for reasons described previously in section 1.2.4 and that overexpression of BCL-2 is associated with chemotherapy resistance and shortened overall survival in CLL patients (Kang & Reynolds 2009), intensive efforts have been put into developing a therapeutic agent to target BCL-2 in CLL. Successful development of venetoclax, a small molecule inhibitor of BCL-2 (Souers et al. 2013), and its introduction into the CLL clinics have significantly improved the treatment of patients with CLL, particularly in those with refractory/relapsed disease or with defective p53 (Roberts et al. 2016). However, resistance to venetoclax has recently been reported (Blombery et al. 2019; Herling et al. 2018).

There are two main causes of drug resistance: intrinsic (i.e. mutations and defective activation of signalling pathways within cancer cells) and extrinsic (i.e. enhanced pro-survival signalling activated by certain components from the microenvironment) (Bakker et al. 2016). An example of intrinsic causes of resistance is seen in chronic myeloid leukaemia (CML) where mutations within the catalytic domain of ABL kinase render tyrosine kinase inhibitor imatinib ineffective as these mutations prevent binding of the imatinib to target effectively, resulting in drug resistance (Quintas-Cardama, Kantarjian & Cortes 2009).

Drug resistance caused by extrinsic factors, also known as 'environment-mediated drug resistance', occur as a result of protective effect provided by the microenvironment (Bakker et al. 2016). An example of this was seen in CLL cells localised in lymph node microenvironment where CLL cells were exposed to varieties of pro-survival stimuli such as CD40 and/or BCR stimulation and expressed high levels of anti-apoptotic proteins such as MCL-1 and BCL-XL, resulting in resistance to venetoclax (Bojarczuk et al. 2016; Elías et al. 2018; Thijssen et al. 2015; Vogler et al. 2009; Woyach & Johnson 2015)

Drug resistance can also be acquired from continuous presence of the chemotherapeutic drug, which leads to genetic and epigenetic changes in the cells that cause resistance (Bakker et al. 2016). An example of this is where in CLL patients receiving ibrutinib treatment acquired mutations occurs on BTK at C481 which is the binding site of ibrutinib. This leads to reduced binding affinity of ibrutinib for BTK, rendering ibrutinib ineffective (Woyach & Johnson 2015).

Regardless of what causes drug resistance, the outcome is the relapse of the disease following treatment (Woyach & Johnson 2015). Therefore, CLL is still an incurable disease. To improve the treatment of CLL, further research is required to better understand how drug resistance develop in the first place with the objective of developing a rational strategy for a therapeutic intervention to overcome drug resistance.

1.7 Hypothesis and Aim

CLL is still an incurable disease and the microenvironment play an important role in disease progression and development of drug resistance. As described in the previous section 1.2.5, the CLL microenvironment comprises of CLL cells and a mixture of accessory cells including BMSCs, T cells, endothelial cells and NLCs. Within the microenvironment, CLL cells interact with the various accessory cells. These interactions are believed to be bidirectional and CLL cells are actively involved in turning the surrounding into a supportive milieu, in favour of their survival and proliferation. NLCs is a major component of CLL microenvironment. However, molecular mechanisms mediating the interaction between NLCs and CLL cells are not yet fully characterised. I thus hypothesise that interactions between NLCs and CLL cells will activate certain pro-survival genes and pathways that are responsible for drug resistance.

To test the hypothesis, I set out to address the following research questions:

1. What are the optimum conditions to develop NLCs *in vitro*?
2. What are the main biological effects of NLCs on CLL cells in co-culture?
3. Whether the observed effects of NLCs on CLL cells can be reproduced using a cell line model?
4. By applying the next-generation-sequencing technology (e.g. RNA-Seq), can I identify any previously unknown, differentially expressed genes in CLL cells following co-culture with NLCs that are associated with CLL-cell survival and drug resistance?

The overall aim is to understand the molecular mechanisms mediating the interactions between NLCs and CLL cells at the transcriptional level with a particular emphasis on detecting changes in gene expression or pathways of CLL cells that are associated with drug resistance.

2 Methodology

2.1 Methods

2.1.1 Collection of primary CLL cells

2.1.1.1 CLL sample selection

Blood samples from patients diagnosed with CLL were obtained with informed consent and with the approval of the Liverpool Research Ethics Committee (REC reference no. 06/Q1505/82). The diagnosis of CLL was based on the revised Rai and Binet staging systems, standard morphological and immunophenotypic criteria (Cheson et al. 1988; Kotiah 2019; Mir et al. 2019; Rai et al. 1975). All the CLL samples were collected and stored by the Liverpool Blood Disease Biobank (LBDB). As there was a lack of readily available bone marrow or lymph node material, only peripheral blood mononuclear cells (PBMCs) from patients with CLL were used in the study.

2.1.1.2 Isolation of fresh CLL PBMCs

PBMCs were isolated by centrifugation of blood from CLL patients over Lymphoprep® solution (Axis-Shield PoC AS, Oslo, Norway), as indicated in Figure 2.1, as per LBDB protocol (see Appendix 7.14.1).

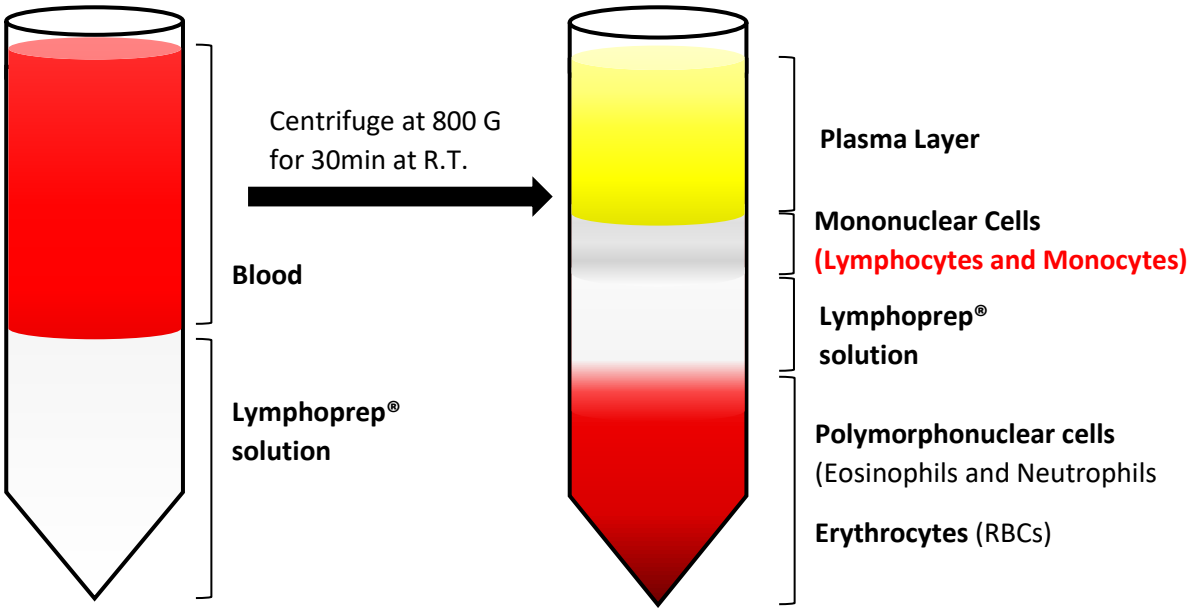

Figure 2.1 Peripheral blood mononuclear cells (PBMCs) preparation

Lymphoprep is added to the falcon tube in a volume ratio of 2:1 (blood to lymphoprep). Blood is gently poured on top (left). The tube is centrifuged at 800G for 30mins. The multiple layers are formed (right) at the end of centrifugation. The PBMC layer (highlighted in red) is collected using a sterile Pasteur pipette. This layer is then washed, resuspended in fresh complete medium and cell numbers counted on Cellometer. Some of the fresh CLL PBMCs are used for NLCs development experiments.

The rest of CLL samples was resuspended in ice-cold fetal bovine serum containing 10% DMSO and stored in the -150°C freezer in LBDB Biobank.

After separation by Lymphoprep, CLL PBMCs were washed in fresh medium and resuspended in 100% Fetal bovine serum (FBS) with cell numbers countered using Cellometer. A portion of this fresh CLL PBMCs was used for the purpose of development of NLCs. These CLL samples were spun and resuspended in standard RPMI conditions, as described below. The remaining CLL PBMCs were resuspended in ice-cold FBS containing 10 % DMSO and stored in -150°C freezer in the LBDB Biobank.

2.1.1.3 Thawing cryopreserved CLL PBMCs samples

Selected vials of cryopreserved CLL samples were thawed as per protocol from the LBDB Biobank (see Appendix 7.14.1) by adding complete RPMI 1640 medium supplemented with 100 U/mL penicillin, and 100 µg/mL streptomycin, 2 mmol/L L-Glutamine and 10 % heat inactivated FBS (Life Technologies/Thermo Fisher Scientific, Paisley, UK). After recovery for 1 h in the incubator containing 5% CO_2 at 37°C, cell numbers and viability (Trypan blue exclusion) were then measured on Cellometer and the cell concentration was then adjusted according to the desired experiment. Clinical and laboratory characteristics of the CLL samples that I used in my study are summarized in Appendix Table 7.1.

2.1.2 Cell culture of primary CLL cells

2.1.2.1 CLL cells cultured under standard conditions

Primary CLL cells were maintained in RPMI-1640 medium supplemented with 10 % heat-inactivated fetal bovine serum (FBS), 2 mM L-glutamine, 100 U/mL penicillin, and 100 µg/mL streptomycin (Life Technologies/Thermo Fisher Scientific, Paisley, UK), in a 37°C, 5% CO_2 humidified incubator.

For development of NLCs, initial viability and cell count were measured by trypan blue exclusion using the automated cell counter (Nexcelom USA Cellometer™ Auto T4 cell counter). Cells were cultured at a high density of 10 x 10^6/ml in RPMI medium in a 37°C incubator containing 5% CO_2 for up to 14 days, with partial replacement of fresh medium on alternate days. In co-culture experiments (with NLCs or THP-1 derived macrophages), CLL cells were plated at a cell concentration of 3 x 10^6/ml in complete RPMI medium.

2.1.2.2 Development of nurse-like cells (NLCs) from primary CLL PBMCs

To mimic the *in-vivo* interaction of NLCs with CLL cells in the lymph node microenvironment, NLCs were first developed from fresh CLL PBMCs for up to 14 days, as described earlier. The CLL cells from the original fresh PBMC cultures were washed away by gently pipetting (to avoid disrupting the monolayer of NLCs). The monolayer was observed under microscope to ensure minimum number of CLL cells remaining on the surface of the plate. NLCs in such conditions were ready for co-culture experiments Autologous CLL cells were thawed and resuspended in fresh RPMI medium at a concentration of 3 x 10^6/ml which were then plated on the monolayer of NLCs and maintained at 37^{o}C for an appropriate period of time.

2.1.2.3 CLL cells co-cultured with NLCs

Autologous CLL cells were thawed and resuspended in fresh RPMI medium at a concentration of 3 x 10^6/ml which were then plated on top of the monolayer of NLCs and maintained at 37^{o}C for an appropriate period of time. Care was taken in handling the plates during observations and partial replacement of medium to avoid dislodging monolayer of NLCs.

At the end of co-culture, CLL cells were harvested by gentle pipetting. The plate was checked under the phase contrast microscope to ensure most of the CLL cells have been collected. The collected CLL cells were then counted and used for analysis such as apoptosis assay by flow cytometry.

2.1.3 Cell culture of THP-1 cell line

2.1.3.1 THP-1 cells cultured under standard conditions

Human THP-1 cell line was obtained from European Collection of Authenticated Cell Cultures (ECACC 88081201). THP-1 cells were maintained in complete RPMI as mentioned above and incubated in a 37^{o}C, 5% CO_2 humidified Incubator. Similar to NLCs development as mentioned above, PMA-differentiated THP-1 cell line was prepared in advance by allocating 5 x 10^5 cells/ml of THP-1 cells in complete RPMI medium, followed by polarizing to M1 or M2 macrophages as required (see details below). Once the monolayers were prepared and confirmed by microscopy, the supernatant was removed and the monolayer of THP-1-derived macrophages was washed gently with PBS before introducing thawed CLL cells at a concentration of 3 x 10^6/ml.

2.1.3.2 Induction of differentiation of THP-1 cells into macrophages

2.1.3.2.1 THP-1 M0

Adjusted to a cell concentration of 5×10^5 cells/ml in complete RPMI 1640 medium (as described earlier), THP-1 cells were treated with 5ng/ml phorbol 12-myristate 13-acetate (PMA, Sigma-Aldrich, Gillingham, UK) for approximately 2 days to induce differentiation into macrophages, as described (Daigneault et al. 2010; Park et al. 2007).

The cells were checked under the light microscope and observed for formation of adherent macrophages, which was usually achieved after 24-48 h of incubation. These cells were generally considered as M0 macrophages (Daigneault et al. 2010; Park et al. 2007).

2.1.3.2.2 THP-1 derived M1 macrophages

Following differentiation of THP-1 cells to M0 macrophages, the supernatant was removed and replaced with complete RPMI medium with the addition of interferon-γ (IFNγ) (20ng/ml) (PeproTech EC Ltd, London, UK) and lipopolysaccharides (LPS) (Sigma-Aldrich) (10pg/ml) and incubated for 24 h, as described (Chanput, Mes & Wichers 2014; Jablonski et al. 2015; McWhorter et al. 2013; Park et al. 2007). The polarisation into M1 macrophages was confirmed upon visualising a 'large oval' appearance under phase contrast microscope, which was also confirmed later by immunophenotyping, as described (Chanput et al. 2013; Chanput, Mes & Wichers 2014; Genin et al. 2015; Jablonski et al. 2015; McWhorter et al. 2013).

2.1.3.2.3 THP-1 derived M2 macrophages

Following differentiation of THP-1 cells to M0 macrophages, the supernatant was removed and replaced with complete RPMI medium with the addition of interleukin-4 (IL-4) (30 ng/ml) (R&D Systems, Oxford, UK) for 72 h with additional 30ng/ml IL-4 added at 48 h (without replacement of supernatant). This method was considered optimal after more elongated cells were observed with this method as compared to other variations (Chanput et al. 2013; Chanput, Mes & Wichers 2014; Genin et al. 2015; Jablonski et al. 2015; McWhorter et al. 2013). The total duration of incubation with IL-4 is 72 h.

2.1.3.3 CLL cells co-cultured differentiated THP-1 cells

After THP-1 cells were differentiated into adherent macrophages with PMA, usually taking 24-48 h cryopreserved CLL cells from the Biobank were thawed and resuspended in complete RPMI medium

as per LBDB protocol (see Appendix 7.14.1 for detail). Cell count and viability were measured following staining cells with 0.1% Trypan blue dye on automated Cellometer (Nexcelom USA Cellometer^{TM} Auto T4 cell counter). CLL cells were then adjusted to 3 x 10^6/ml with complete RPMI medium and cultured alone or co-cultured with differentiated THP-1 cells. Before adding CLL cells to the monolayer of differentiated THP-1 cells, the culture medium of the THP-1 cells was fully removed and washed with fresh RPMI medium to remove any remaining PMA. CLL cells in suspension were then gently added onto the monolayer.

Preparation of M1 (24hr incubation with IFNγ and LPS) or M2 macrophages (72 h incubation with IL-4) from differentiated THP-1 cells also involved complete removal of culture medium of the THP-1 cells in order to remove residual PMA before addition of the respective stimuli. Again, before adding CLL cells to the monolayer of M1 or M2 macrophages, the culture medium of these cells was fully removed and washed with fresh RPMI medium to remove any remaining respective stimuli. Table 2.1 below provided a time plan when M0, M1 and M2 macrophages were prepared so that the co-culture experiments can start at the same time.

Afterwards, the CLL cells on co-cultures or cultured alone were harvested for viability assays using Annexin/PI on FACS.

Table 2.1 Timetable to prepare M0, M1 and M2 macrophage cultures

Day 0	Day 1	Day 2	Day 3	Day 4	Day 5	Population Desired
THP-1+ PMA		IL-4		IL-4	Experiment	M2
		THP-1+ PMA		IFNγ + LPS		M1
			THP-1+PMA			M0

As seen in Table 2.1, M2 macrophages were prepared first since they took the longest time to differentiate (5 days). M1 macrophages were then prepared afterwards (3 days) and M0 took the least time to be prepared (1-2 days).

2.1.3.4 Harvesting CLL cells from co-cultures with THP-1 cells derived macrophages

Similar to harvesting CLL cells from NLCs co-cultures, CLL cells co-cultured with THP-1 cells derived macrophages were collected by gentle pipetting. To ensure that most of the CLL cells were harvested, the culture plates were checked under the light microscope. After which, the harvested cells were counted and cell viability was examined on FACS with Annexin V/PI staining. Since the THP-1 cells derived macrophages were larger than the CLL cells, a gating strategy was followed to ensure that only the CLL cell population was analysed.

2.1.4 Light Microscopy

2.1.4.1 Basic principle

A typical microscope that uses transmitted light to observe targets at high magnification. Generally, a slide is placed on a flat stage, held by stage clips where a light source is directed and intensity is adjusted using diaphragm and brightness knobs. The image is magnified and visualised using the objective lens as well as eye piece. A camera may be attached as well. The image is focussed using coarse or fine adjustment.

The light microscope is often used to observe morphology of cells attached to slides which are stained with various dyes.

2.1.4.2 Staining the peripheral blood mononuclear cells with Romanowsky stain

May Grünwald Giemsa stain, a high quality Romanowsky stain (Hoffbrand, Moss & Pettit 2006; Lichtman et al. 2011b), was used with a phosphate buffer of pH6.8 for staining the cells cultured on slides after fixing them with absolute methanol.

Romanowsky stains contain both acidic and basic dyes in an optimal proportion dissolved in acetone free absolute methanol. The acidic and basic dyes stain the different cellular components with different intensity, thus producing shades of colours to give a good differentiation. The slides can then be inspected under the light microscope for the study of morphology of the NLCs and CLL cells.

2.1.5 Fluorescence microscopy

2.1.5.1 Basic principle

Fluorescence microscopy is a tool mainly used to visually examine the cell physiology, in particular the dynamic details of cellular events (Sanderson et al. 2014). Like all techniques to visualise cells, fluorescence microscopy is subject to practical physical limitations, the most important of which is resolution (Sanderson et al. 2014). Understanding the methods of microscope alignment, properties of light, wavelength selection, image recording techniques and image analysis all aid in achieving the best resolution of an image.

The principle of fluorescence microscope is essentially the same as described in flow cytometry, in that it involves the absorption of light energy (photon) by an indicator followed by the emission of some of this light energy a few nanoseconds later. Some energy is lost in this process, the emitted photon has less energy than the absorbed photon (Sanderson et al. 2014). Generally, the excitation and emission wavelengths should be distinct. However, due to the broad spectrum of emission and excitation wavelengths, sometimes it can be difficult to monitor the different fluorophores because of spill-over of wavelengths from one fluorophore to the other (Sanderson et al. 2014). The preferred approach is to take separate sequential images with filters designed for each fluorophore, but some spill-over is still possible (Sanderson et al. 2014).

A parallel beam of light simultaneously illuminates the whole specimen to excite the fluorophore(s) on the specimen (Sanderson et al. 2014). Care should be taken to minimize observation times and photo bleaching, where the area is illuminated but not captured, thus degrading the fluorophore due to prolonged exposure. This is why fluorescence microscopy is done in the dark. Auto-fluorescence occurs within cells as well as in whole tissues. It can interfere with imaging because it can mislead the observer into believing the fluorescent structure is related to the fluorophore conjugated anti-bodies used (Sanderson et al. 2014).

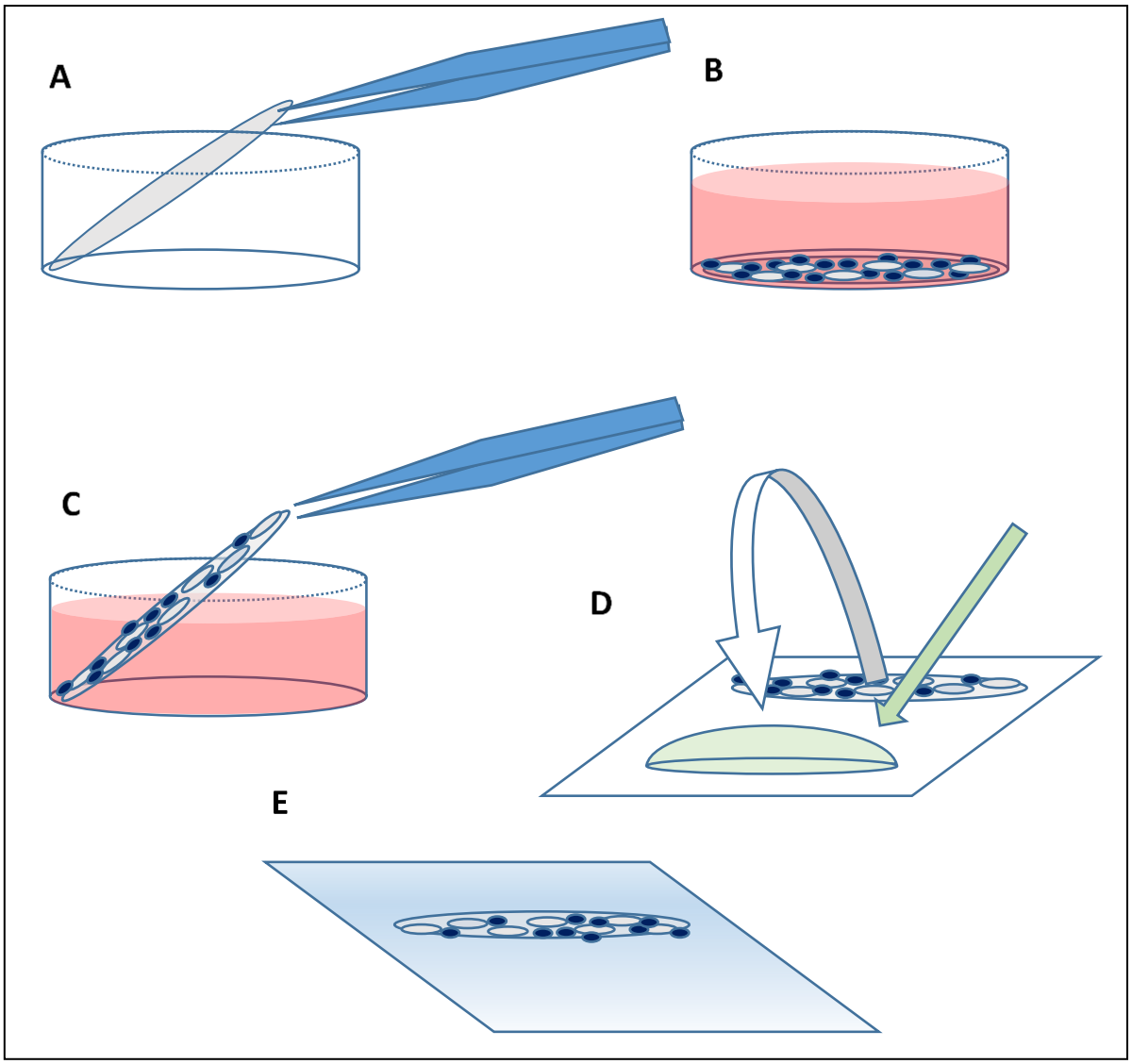

Figure 2.2 Schematic of Preparation of Cultures on coverslips for immunofluorescence microscopy

Cover slips are placed on the bottom of the culture plate wells (A), the cells are cultured as normally done (B). At the end of culture, the cover slips are removed carefully (C). The cover slips are placed on parafilm (D), fixed with absolute ethanol, blocked, incubated with antibodies by flipping the cover slip onto the droplet of the solutions (green arrow). Finally, the coverslip is placed on a droplet of mounting medium on a glass slide (E), to be stored in the dark at 4°C.

2.1.5.2 Applications

Fluorescence microscopes are used to visualise cells following staining with specific fluorochrome-conjugated antibodies. This technique can be used on tissue sections, cultured cell lines or individual cells. On viewing the slides, the distribution of cells, proteins, surface and intracellular markers can be analysed. The localization of the antigens of the cells can also be appreciated. Mixtures of cells can be distinguished and their physical characteristics can be appreciated in relation to each other. Multiple markers can be identified and overlapped to form an image that shows a complex representation of

all the stained regions. Additionally, when compared with an isotype control, the intensity of the fluorescence can be measured (Waters 2009) using ImageJ software and this can give a semi-quantitative assessment in the level of expression of the markers ('Quantification of Fluorescence Intensity of Labeled Human Mesenchymal Stem Cells and Cell Counting of Unlabeled Cells in Phase-Contrast Imaging: An Open-Source-Based Algorithm' 2010). A protocol was developed for measuring fluorescence using ImageJ software and was used (Burgess et al. 2010; McCloy et al. 2014).

2.1.5.3 Procedure

The steps in immunofluorescence microscopy includes preparing the cell culture on circular cover slips (13mm diameter, Appleton Woods, Cat. No. MS002) that fit into 24-well culture plates represented in Figure 2.2, so that the cells remain adherent on it. The supernatant is gently pipetted and the cover slip is collected. The cells are then immediately fixed and permeabilised onto the surface. 0.1% sodium borohydride ($NaBH_4$) is added to remove auto-fluorescence, the cells are blocked with donkey serum and Fc blocker to prevent non-specific binding. The cells are then incubated with the selected antibodies and counterstained with nuclear staining. The cover slip is gently mounted using a mounting medium on a pre-cleaned glass slide and left to dry in cold temperature (4^oC), stored in the dark, as it is prepared for microscopy.

When ready for microscopy, in the dark room the machine is switched on and warmed up. The lens is adjusted and with the viewing eye-piece, the cells are located and focused using the DAPI filter at low exposure. When satisfied with the field of view, the selection of filters is made and sequential photos are taken by the machine and overlapped using the machine software. The files are saved in a TIF format to be further analyzed using ImageJ software.

Using ImageJ software, the control images are used to determine the appropriate viewing parameters to use on the test images. The intensity of the images is thus normalized with their control images.

Further analysis to measure cell fluorescence using ImageJ is calculated using an established method (Fitzpatrick 2014).

2.1.6 Flow cytometry

2.1.6.1 Basic principle

Flow cytometry is a technique that has long been considered as the useful tool in clinical diagnosis as well as in research in the area of Haematology (Rane et al. 2017). Flow cytometry measures numerous characteristics of cells in liquid suspensions simultaneously in a quick and detailed form as they pass through a beam of light. Such examples of usage include immunophenotyping cells based on their surface markers to identify particular subsets of blood cells.

Cells or particles between 0.2-150µm are suitable for analysis by most flow cytometers. One of the limitations of flow cytometry is the need for cells of interest to be in suspension and therefore any solid tissue cells would require disaggregating into suspension form in order to be analysed (Depince-Berger et al. 2016). This would obviously affect the cell shape and there will also be loss of cells during the procedure, thus potentially introducing bias to the final results (Depince-Berger et al. 2016).

Flow cytometers measures and analyses multiple physical characteristics of a single cell/particles They measure the relative size, relative granularity/internal complexity and relative fluorescence intensity of the cells or particles of interest (Depince-Berger et al. 2016; Rane et al. 2017).

There are 3 main components of a flow cytometry: fluidics, optics and electronics.

Fluidics are the transportation of the cells in a stream to the laser beam for interrogation. Optics consists of lasers to illuminate cells in the sample stream and optical filters to direct the resulting light signals to detectors. Electronics converts the detected light signals into electronic signals that can be processed by a computer. Additionally, if the machine can sort, it is capable of initiating sorting decisions based on the parameters given (Depince-Berger et al. 2016).

In fluidics, there is hydrodynamic focusing which causes the individual cells to flow in a single file through a narrow tunnel, as seen in Figure 2.3. A higher sample pressure is used for more qualitative measurements, where there is increased flow rate and so more cells can pass through in a given time (Depince-Berger et al. 2016).

Light scatter depends generally on the size (forward scatter) and internal complexity (side scatter).

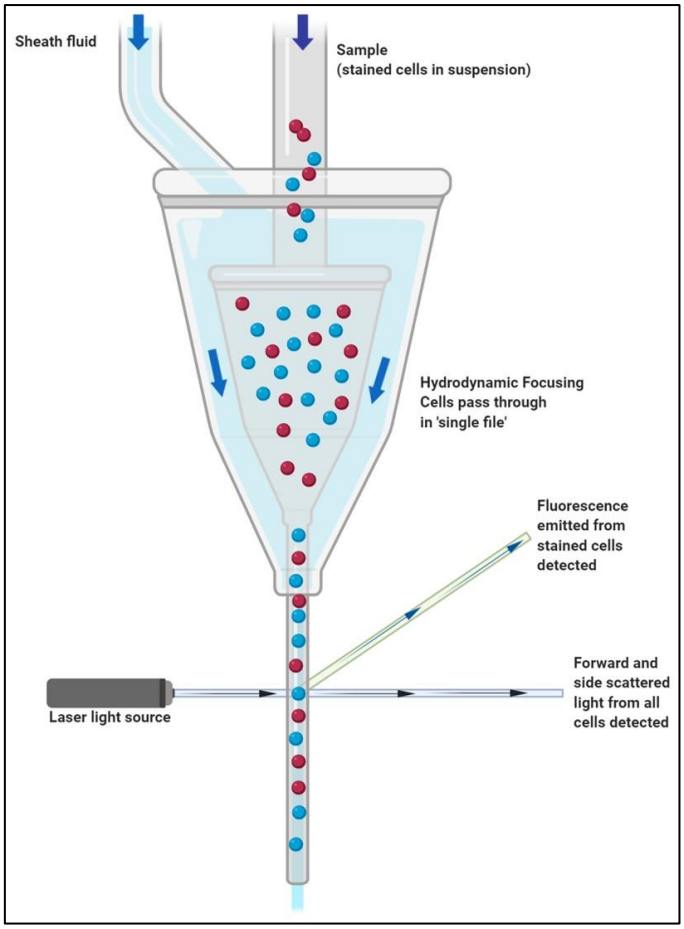

Figure 2.3 Fluidics schematic of flow cytometry.

Cell samples that are present in suspension are introduced in the collection column and hydrodynamically focused to a single file. The cells are then exposed to the laser light source on passing the channel and the resulting scatter of the light and fluorescence are detected by light detectors and converted in to electronic signals. Figure modified from abcam.com, using BioRender online tools.

Fluorescent compounds absorb light energy and the electrons are raised to a higher energy level (excitation level) where when the electron returns to original state, photons of light are emitted (emission level) (Figure 2.4). An ideal experiment should ensure that the excitation and emission wavelengths of the chosen fluorochromes do not overlap one another (Figure 2.4). Alternatively, a compensation tool is used to remove the overlapped section, however, care should be given on the extent of compensation as this would remove the data points that fall in those overlapped section.

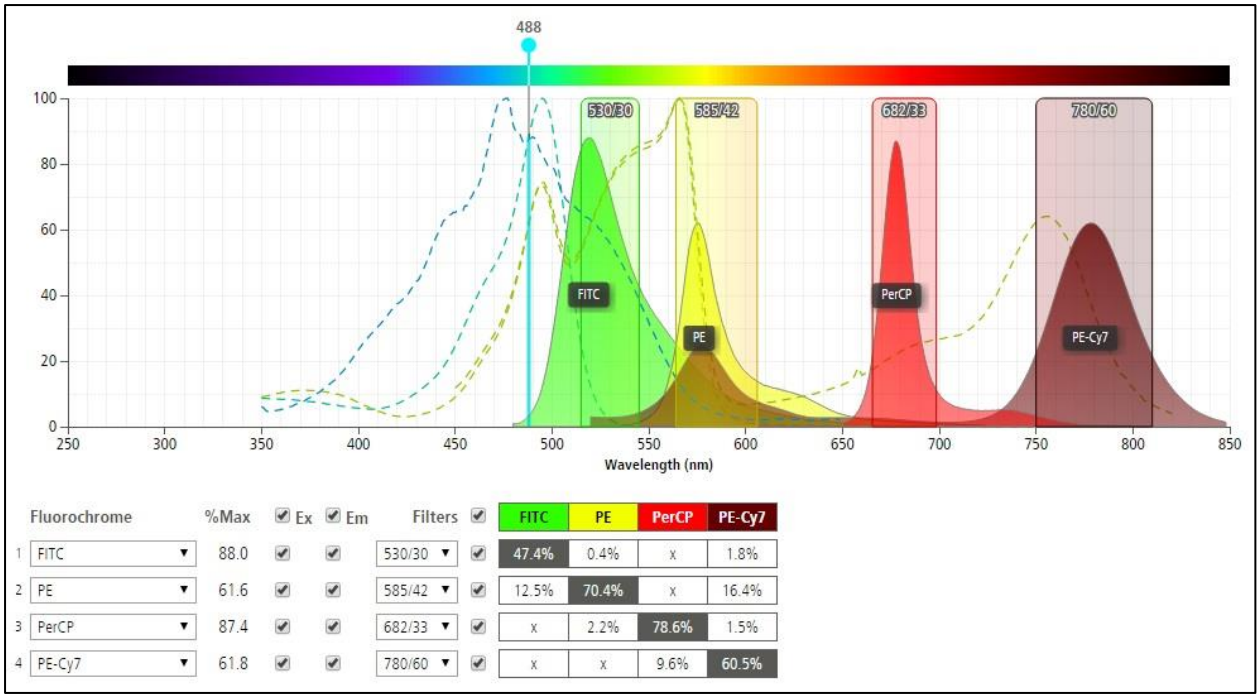

	Fluorochrome	%Max	Ex	Em	Filters	FITC	PE	PerCP	PE-Cy7
1	FITC	88.0	☑	☑	530/30	47.4%	0.4%	x	1.8%
2	PE	61.6	☑	☑	585/42	12.5%	70.4%	x	16.4%
3	PerCP	87.4	☑	☑	682/33	x	2.2%	78.6%	1.5%
4	PE-Cy7	61.8	☑	☑	780/60	x	x	9.6%	60.5%

Figure 2.4 Excitation and Emission waves of the fluorochromes used in Flow Cytometry.

The excitation of the fluorochromes are shown in dotted lines and the emission waves are the sold color lines. Each fluorochrome wavelength has a peak range which can be detected through certain filters, seen as rectangular bands. Figure image and legend taken from BD Biosciences Spectrum Viewer (https://www.bdbiosciences.com/en-us/applications/research-applications/multicolor-flow-cytometry/product-selection-tools/spectrum-viewer)

Optics involve laser and lens to shape and focus the laser beam, these are known as excitation optics. Collection optics are those that collect the light emitted and optical mirrors and filters to route specific wavelengths of collected light to the designated optical detectors as seen in Figure 2.5 (Depince-Berger et al. 2016). The protocol detailing the use of flow cytometer was provided in Appendix 7.14.5.

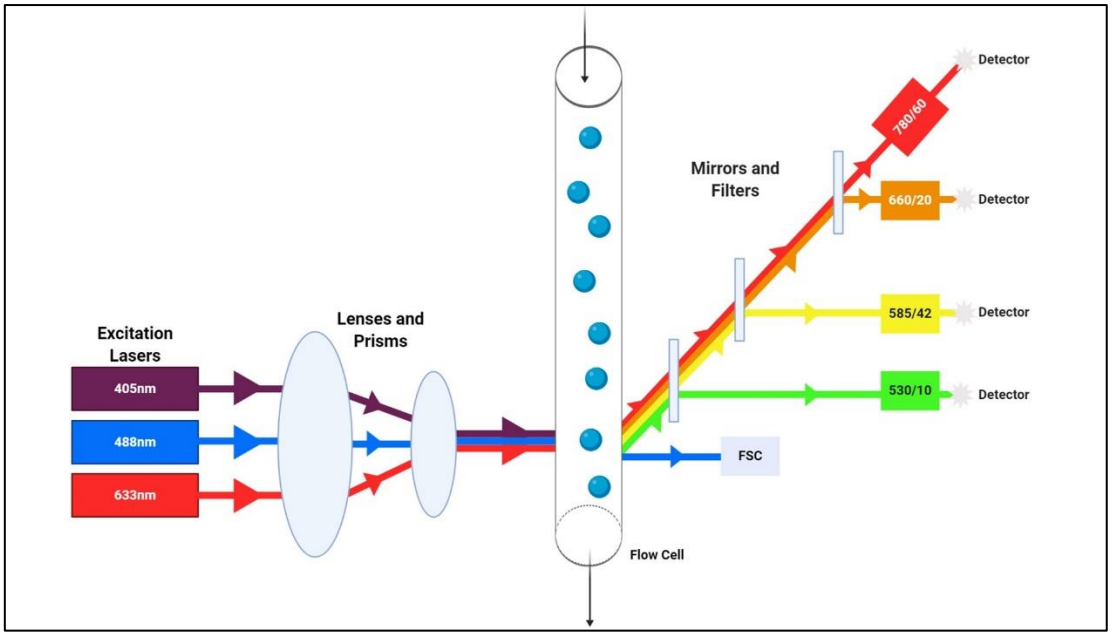

Figure 2.5 Optics and Electronics schematic diagram of flow cytometry.

As the cells pass through the column, they are hit by a single beam of laser light with a particular wavelength s. The light emitted from the cells is passed through multiple mirrors and filters to the respective detector. The amount of the fluorescence acquired by the detector is then converted into digital numbers which can be displayed in a graph. Figure adapted from bitesizebio.com, using BioRender online tools.

2.1.6.2 Applications

2.1.6.2.1 Analysis of Purity of CLL cells

In most cases, CLL cells were analysed for purity using flow cytometry. Fresh and thawed CLL cells ($1x10^6$) were incubated with fluorochrome-conjugated antibodies against CD19 and CD5 (PE and FITC, respectively) or with their respective isotype controls in order to identify the CLL B Cells. The gating strategies were applied to exclude debris and select the homogenous populations for subsequent analysis. The population that co-expressed both CD19 and CD5 was considered to be B-CLL cells as seen in Figure 2.6. The CLL samples containing greater than 90% B-CLL cells were used in subsequent experiments.

In practice, equal number of cells are collected and spun and washed with PBS and resuspended with staining buffer. The cells are then mixed with fluorochrome-conjugated anti-CD19 and anti-CD5 antibodies or respective isotype controls and incubated in the dark for 30-60mins. The cells were then spun to remove the excess antibodies and resuspended in appropriate volume of staining buffer and analysed using a flow cytometer (Attune, Life Technologies).

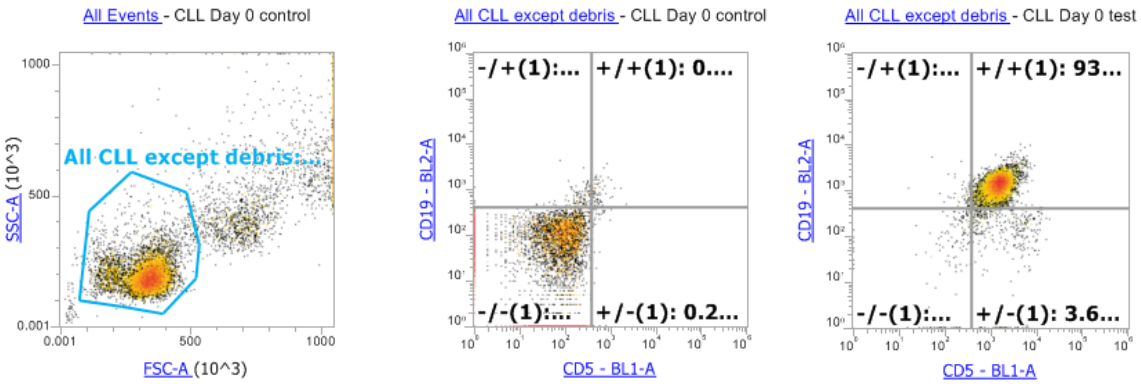

Figure 2.6 Gating strategies for measuring purity of CLL cells.

At the selected voltages, the CLL population (seen as the dense population) is gated excluding debris. This gated population is then analysed using BL1 and BL2 channels for their respective antibodies. A control is used (where isotype controls were used for the respective antibodies) as comparison. The B-CLL purity was assessed by CD19, CD5 positivity, using CD19-PE and CD5-FITC antibodies and control- PE, FITC antibodies on the Attune. Quadrant plots showing CD5+ CD19+ are displayed alongside the respective isotype control. Images produced from Attune software provided by the manufacturer.

2.1.6.2.2 Detection of cell death

Annexins are a family of calcium-dependent phospholipid-binding proteins that preferentially bind phosphatidylserine (PS) (Demchenko 2013). Under normal physiologic conditions, PS is predominantly located in the inner leaflet of the plasma membrane. Upon initiation of apoptosis, PS loses its asymmetric distribution across the phospholipid bilayer and is translocated to the outer leaflet of the membrane, marking cells as targets of phagocytosis. Once on the outer surface of the membrane, PS can be detected by fluorescently labelled Annexin V in a calcium-dependent manner.

In early-stage apoptosis, the plasma membrane of cells retains its integrity and excludes viability dyes such as propidium iodide (PI). These cells will stain positive for Annexin V but not a viability dye, thus distinguishing cells in early apoptosis. However, in late-stage apoptosis, the cell membrane loses integrity thereby allowing access of PS to the interior of the cell (Demchenko 2013; Rieger et al. 2011). The viability dye (PI) can be used to distinguish these late-stage apoptotic and necrotic cells (both Annexin V and viability dye-positive) from the early-stage apoptotic cells (Annexin V positive, viability dye negative) (Demchenko 2013; Rieger et al. 2011).

In practice, equal number of cells are collected, spun and resuspended in Annexin binding buffer. They are then incubated with Annexin V for approximately 10 minutes in the dark. PI is the added to the cells before flow cytometry analysis.

Analysis was carried out using the Attune Flow Cytometer (Life Technologies). Live cells appear as Annexin V-PI -/-, dying as Annexin V-PI +/- and dead cells as Annexin V-PI +/+, respectively seen in Figure 2.7.

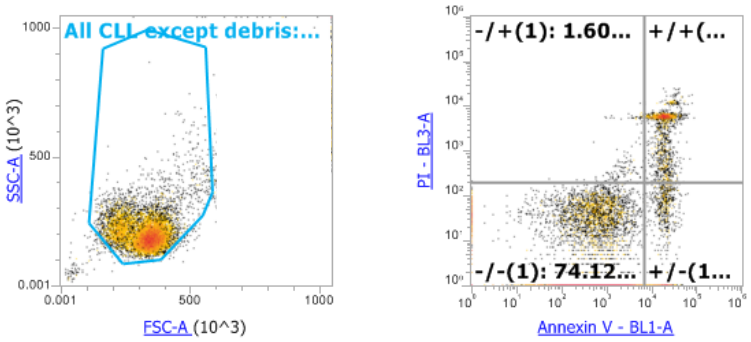

Figure 2.7 Viability assay of CLL cell population using Annexin V and PI

As an example, CLL sample (3631) at Day 0, where 10,000 events were analysed within the gated area in blue (87.75% of all events) and from there the included events were analysed for level of fluorescence with Annexin V (BL1 channel) and PI (BL3 channel) in a quadrant plot. Those that were double negative for Annexin and PI (-/-) were considered as the viable population (74.1%). Those that were single positive for Annexin (+/-) were the dying population and those that were double positive for Annexin and PI (+/+) were considered as the dead population (combined to be 24.28%).

2.1.7 Enzyme-linked immunosorbent assay

2.1.7.1 Basic principle

Enzyme-linked immunosorbent assay (ELISA) is a method of detecting and quantifying specific antigens in a solution with the use of enzyme-bound antibodies that emit a detectable light.

The method used was a sandwich ELISA Figure 2.8, whereupon a capture antibody is fixed on a solid surface. The antigen that we want to measure are added and incubated to allow binding at the designated sites. A detection antibody is then added which is bound to Biotin. Following this, a complex is formed with an enzyme-conjugated reagent. The enzyme in this complex can breakdown a specific substrate which produces a detectable colour. A stopping media is added to stop the function of the enzyme reaction and the colour is then detected by a spectrophotometer. The intensity of the colour detected is proportional to the amount of the antigen present and bound to the antibody coated on the surface of the plate. The antigen is therefore quantified using ELISA method.

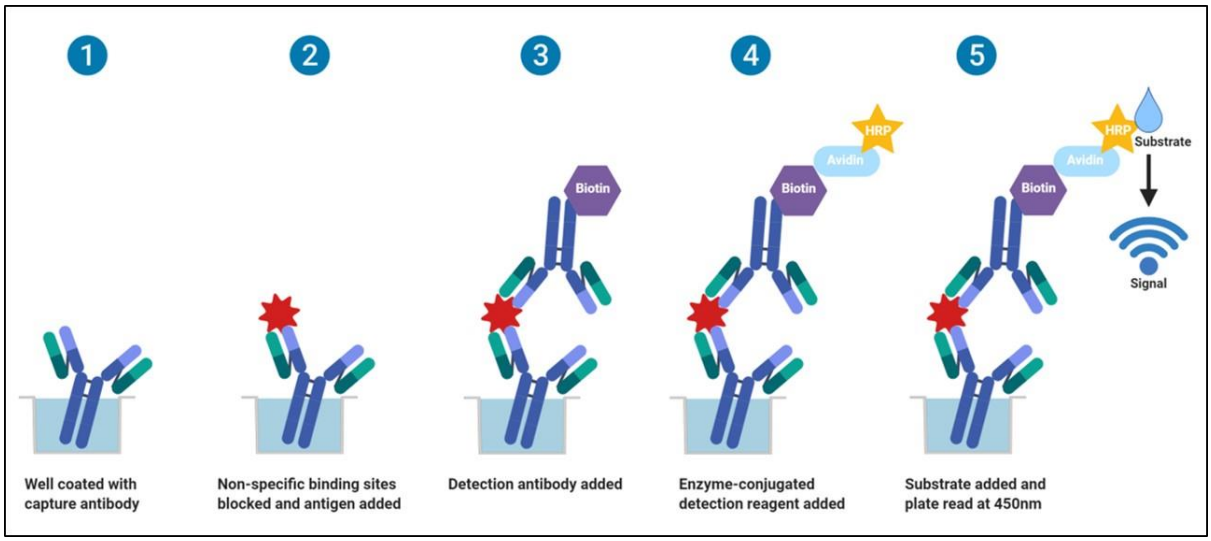

Figure 2.8 Diagram of Sandwich ELISA.

Schematic of Sandwich ELISA method. 1. A multiwall ELISA assay plate is coated with a known quantity of capture antibody. 2. Non-specific binding sites are blocked using blocking buffer and the antigen containing sample is added to the plate. 3. After washing to remove unbound antigen, a specific detection antibody (Biotin bound) is added which binds to the antigen. 4. Enzyme-conjugated detection reagent complex (Avidin-HRP bound to Biotin) is added and binds to the detection antibody. 5. A substrate is added which is converted by enzymes (Avidin-HRP) to produce a color and the reaction is stopped by an acidic solution. The resulting color is measured by spectrophotometer at 450nm which then determines the quantity of the antigen. Image was created using BioRender online tools.

2.1.7.2 Applications: Measurement of CCL3 and CCL4

The ELISA 96-well plates (Nunc-Immuno™ MicroWell™, Sigma-Aldrich) are coated with antibodies that bind specifically to human target antigens. We used ELISA to detect CCL3 and CCL4 (Thermo Fisher) proteins in the supernatant of cell cultures.

Human CCL3 (MIP-1 alpha) and Human CCL 4 (MIP-1 beta) detection kits were obtained from Affymetrix eBioscience which is now part of Thermo Fisher Scientific (Catalog Number 88703588 and 88703488 respectively).

Primary PBMC samples from CLL patients were placed in long-term cultures to generate NLCs as detailed earlier as well as co-cultured with differentiated THP-1 cells, described previously. Supernatants were obtained at 4, 5, 6, 8, 10 and 13 days of primary culturing and day 1, 2 and 3 after co-culture with the THP-1 cells. The supernatant samples were then assayed for CCL3 and CCL4 protein concentrations by ELISA (see Appendix 7.14.8 for detailed operation and sample selection for testing by ELISA).

2.1.8 Polymerase chain reaction (PCR)

2.1.8.1 Basic principle

PCR is an *in-vitro* procedure to amplify selected DNA fragments to reach a very high concentration. This allows researchers to exponentially copy and amplify regions of DNA of their choosing so that they can investigate them further by cloning, sequencing, quantification and size measurement, etc.

The double strand DNA template is separated in denaturation and nucleotide primers are annealed complementarily to each of the template strands. With the aid of a polymerase enzyme, the four free deoxynucleotide triphosphate nucleotides (A, C, G and T) bind to their complementary counterparts on the template, allowing an extension to produce a complimentary copy strand of the template. This cycle is repeated numerous times and the total strands increases in an exponential pattern each cycle. After a set number of cycles, the amplified product can then be measured.

In conventional PCR, the amplified product is detected by end-point analysis, by running the DNA on an agarose gel after the reaction is completed. In contrast, real-time PCR permits detection of amplified products as the reaction progresses. This is made possible by including a fluorescent molecule that reveals the increase in DNA products with proportional increase in fluorescence.

2.1.8.2 Applications

2.1.8.2.1 Major steps

2.1.8.2.1.1 mRNA extraction and cDNA generation

The RNA that was extracted (See 5.3.2) is converted to complementary DNA (cDNA) through reverse transcription. cDNA is much more stable and doesn't degrade very quickly even in room temperature compared to RNA. Usually, oligo (dT) primers were used to complementally binds to poly (dA) tail at the 3' end of the single strand RNA. The SuperScript III reverse transcriptase, which has a high thermal stability, is used to synthesize cDNA replacing U with T nucleotides. The transcriptase functions optimally at temperature range of 42-55^{o}C, giving a high specificity and great yield of full-length cDNAs. The cDNA then remains in its double stranded helix state. To perform reverse transcription, the condition requires RNAse free water, oligo (dT) primers, free nucleotides (dNTPs) and RNAse inhibitor and the Reverse Transcriptase (Superscript III). Given a known concentration of RNA measured at the start, an expected concentration of cDNA can thus be predicted to be later diluted for PCR experiments.

2.1.8.2.1.2 PCR procedure

As seen in Figure 2.9, the double stranded cDNA is denatured to be made single stranded again by raising the temperature to 95^{o}C, where the hydrogen bonds that link the double helix are broken. At lower temperatures (55-65^{o}C), this will trigger primer annealing with the DNA template at their complementary sequences.

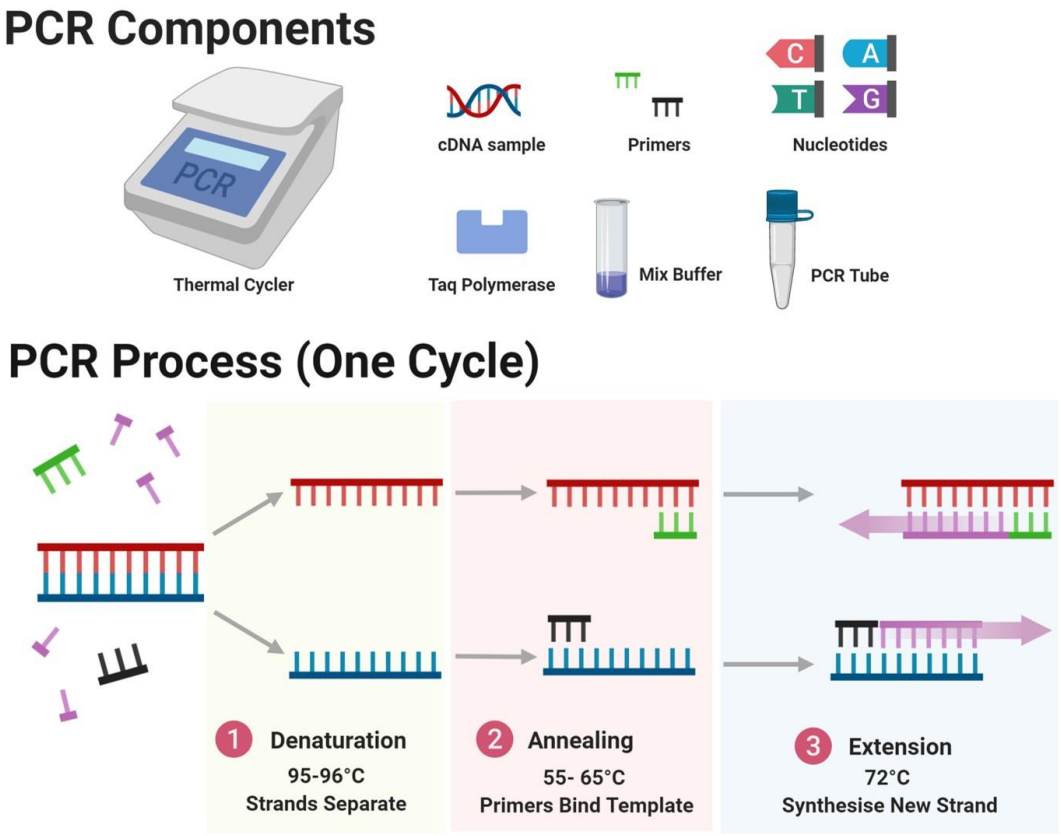

Figure 2.9 Diagram of PCR components and the steps of PCR.

PCR components (top) consisting of Thermal cycler, cDNA sample, primers, nucleotides, Taq Polymerase, mix buffer and PCR tubes. A single cycle of PCR (bottom) consists of Denaturation, Annealing and Extension. This process is repeated depending on the number of cycles programmed. Image adapted from bosterbio.com using BioRender online tools.

A pair of oligonucleotide primers (forward and reverse) initiates the process of annealing and extension. These primers are aligned alongside their respective starting points of the DNA fragments which will be amplified. Synthetic deoxynucleotides (dNTPs) are used as building blocks to extend the PCR products along the cDNA template from the primer using the DNA polymerase till they reach their respective ends (Figure 2.9). Taq-polymerase from *Thermophilus aquaticus* is used as this species of bacteria is extremophilic microorganism accustomed to living in such extremely high temperature conditions. This allows the enzyme to retain its function when denaturing temperatures are applied. The temperature is then cooled to allow the double strand to form and one cycle is ended.

After a period of time, the PCR solution is heated again at denaturing temperatures to initiate another cycle for several cycles to amplify the product exponentially (Figure 2.10). Usually 20-30 standard PCR cycles are enough to produce 10^6 to 10^9 of DNA fragments.

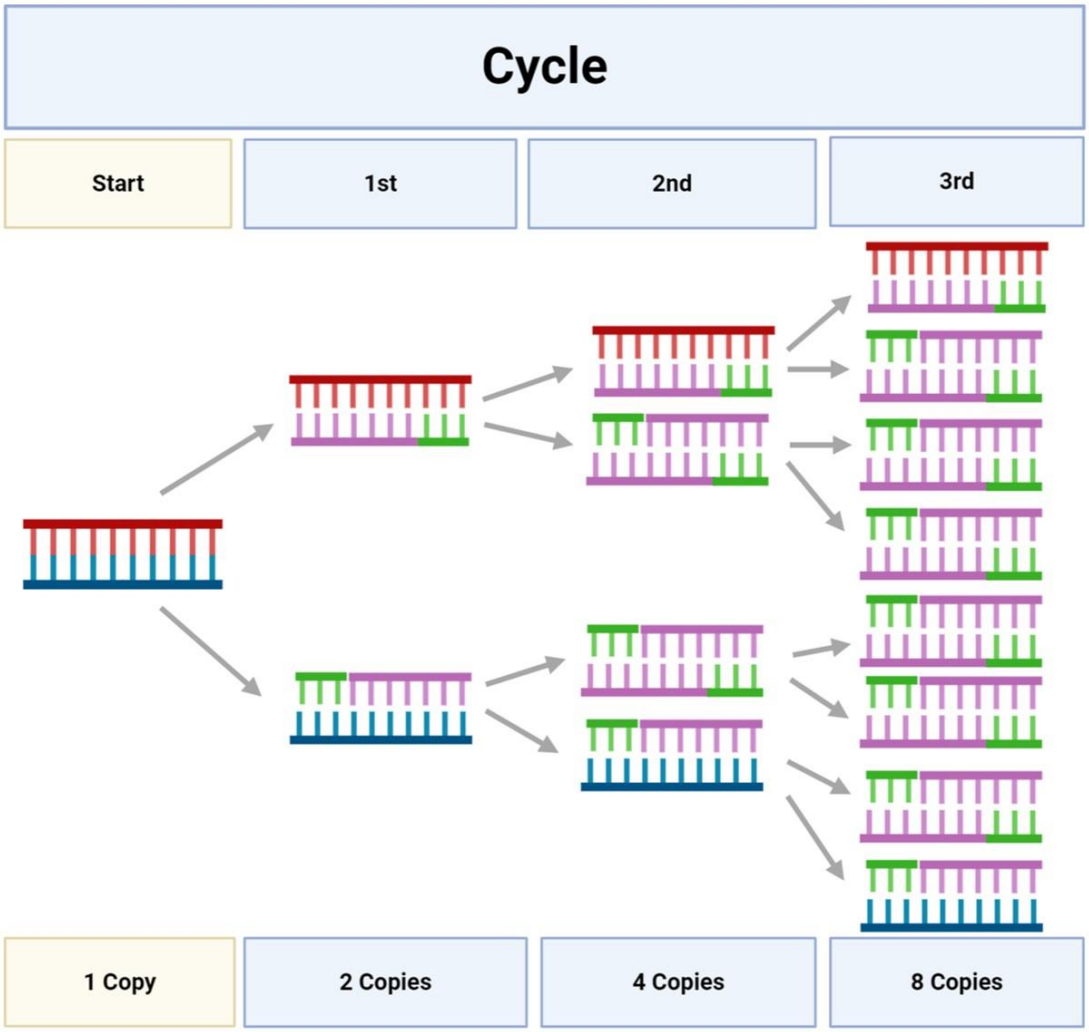

Figure 2.10 Diagram of Amplification of original template strand of cDNA to produce multiple copies per cycle

For every pair of strands to copied, another pair is made per cycle. There is an exponential increase in number of copies as the number of cycles increase. Eg. By the end of the 3rd Cycle there will be 8 copies, the 4th cycle would have 16 and so on. Eventually at the end of 30 cycles there will be 2^{30} copies. Diagram made using BioRender online tools

2.1.8.2.1.3 Reverse transcription quantitative PCR (RT-qPCR)

Since I am using reverse transcription PCR products from RNA and quantifying them in real time, it would be Reverse Transcription Quantitative PCR (RT-qPCR) following the MIQE guidelines on nomenclature (Bustin et al. 2009).

Following the MIQE guidelines (Bustin et al. 2009), Quantitative PCR methods allow estimation of an amount of sequence of a sample. This is an established tool to measure accumulation of DNA products after every round of amplification during PCR, which can then determine the level of gene expression (Bustin et al. 2009; Haimes & Kelley ; Livak & Schmittgen 2001).

The amplified sequences are measured in real-time using the fluorescence signal that is released from the SYBR green dye, as it binds to the minor groove of the newly synthesized DNA double strands during the elongation phase of the PCR reaction. Relative quantification is performed using a reference Housekeeping gene, in this case GAPDH, hereby described as Reference Gene (Bustin et al. 2009). The LightCycler 480 PCR machine is used to perform the RT-qPCR.

The samples prepared for PCR were optimized by using a control sample for comparison, a PCR grade water with only the primer as a negative control (to observe for contamination and primer dimers). See Appendix 7.14.17.3 for the arrangements.

When performing the experiment on optimized melting temperatures, the samples were all used, along with a control sample and negative control for each primer plate. See Appendix 7.14.17.4 for arrangements.

A specific threshold is set for when a fluorescence detection level is reached. The threshold is based on the overall parallel pattern of lines is seen from all the samples. This ensures that there is minimal bias on each sample/condition. The cycle in which the sample achieves the fluorescence, is quantified and used to compare with other samples. Whereby, an earlier cycle suggests a greater quantity of the targeted DNA fragment in this sample compared to a later cycle in another sample.

2.1.8.3 Designing Primers

Designing Primers was made possible using available resources in literature (Dieffenbach, Lowe & Dveksler 1993) and online guides by Premier Biosoft (http://www.premierbiosoft.com/tech_notes/PCR_Primer_Design.html) and online designing tools by NCBI (https://www.ncbi.nlm.nih.gov/tools/primer-blast/).

The primers were designed to satisfy certain conditions that was found to be most beneficial, such as the primer length was long enough to be specific to a targeted site on the DNA, but not too long to use up the nucleotides in the mixture during PCR steps (Dieffenbach, Lowe & Dveksler 1993).

The primer melting temperature (Tm) is the temperature where half of the DNA duplex will denature to become a single strand, indicating the stability of the duplex. Melting temperatures in the range of 53-58^{o}C is suggested to produce best results, where temperatures above 65^{o}C are prone to develop secondary annealing. The GC content of the sequence provides a decent estimate of the primer Tm, where it is the number of G's and C's in the primer as a percentage of total bases (Dieffenbach, Lowe & Dveksler 1993). The melting temperatures are calculated automatically through websites and programs when designing the primers.

The primer annealing temperature (Ta) is the melting temperature where it is an estimate of the DNA-DNA stability. Too high a Ta, would produce insufficient primer-template interaction, resulting in poor PCR product yield (Dieffenbach, Lowe & Dveksler 1993). Too low Ta, would results in multiple non-specific products decreasing the overall PCR specificity (Dieffenbach, Lowe & Dveksler 1993).

It is important to avoid chances of hairpins and self-dimer formations, where the primer folds on itself (hairpin) or anneals with another primer in the mix (self-dimer) at temperatures close to those in PCR steps. The presence of these artefacts results in less PCR yield from the DNA template and an inaccurate representation of the true expression from the DNA.

Using the NCBI BLAST tool, the primers design is check to ensure that the primer is specific to only the gene of interest. If it is not specific, then other genes may be amplified in the mixture and give a false positive reading of the desired gene expression level of interest.

When the primers are designed, they are ordered and received as lyophilized powder which is then resuspended with Molecular grade H2O into a Master stock and frozen down for storage. The Master stock (100x) of each primer is then diluted to produce a working stock (10x) for experiments.

2.1.8.4 Agarose Gel Electrophoresis

Agarose gel electrophoresis is a technique used in molecular biology for separation, quantification and purification of DNA fragments based on their length as measured by base pairs. The procedure uses an electrical field to separate DNA fragments within agarose gels where high percentage gels are used for small DNA fragments, and low percentage gels for large DNA fragments. The DNA fragment size is determined by comparison to a DNA ladder which is composed of DNA fragments of known base pair length.

Agarose gels were prepared by weighing the desired amount of granular agarose (ULTRAPURE) and adding 50ml of Tris-borate-ethylenediaminetetraacetic acid (EDTA)(TBE) buffer (diluted from a 10X stock consisting of 0.445M Tris borate, 0.01M EDTA pH=8.2-8.4). The agarose is then melted by heating in a microwave for about 1.5minutes. The agarose is mixed and left to cool down but not solidify. At this point 1ul of Midori Green Advance DNA Stain was added to the agarose solution before slowly pouring it into a gel tray in order to avoid air bubble formation. The dye is added so that DNA can be visualized under ultraviolet (UV) light. In the event there are bubble formations, the bubbles are quickly fished to the side using pipette tips. With the well comb in place, the agarose solution is then allowed to solidify for at least 20-30minutes.

The solid agarose gel is placed in an electrophoresis tank with the comb gently removed. This tank is then filled with TBE until the gel is covered. The DNA samples prepared by mixing DNA preparations with DNA buffer, and then carefully pipetted into the wells. Appropriate DNA ladders (Quick-Load Purple 100bp and 1kb) were also used.

An electrical field was then applied (110V constant voltage) for 1h. At this point separated DNA fragments were able to be seen under UV light using a manual adjust system for exposure time when obtaining images.

2.1.9 Statistical analysis

Where appropriate, a paired two-tailed Student's *t* test was performed to determine the statistical significance of the difference between the two groups of data. An alpha error of 0.05 was accepted as a cut-off of statistical significance. SPSS version 21 and Microsoft Office Excel 2017 was used.

2.2 Materials

2.2.1 Antibodies used for flow cytometry

The details of primary and secondary antibodies used for Phenotyping are provided in Table 2.2 and Table 2.3 for FACS analysis and Immunofluorescence Microscopy. Details of reagents used for Viability Assay is shown in Table 2.4. FACS analysis was performed on Attune NxT acoustic focusing Cytometer (Life Technologies).

Table 2.2 Antibodies used for flow cytometry and immunofluorescence microscopy

	Company	Description	Cat #
CD19	Merck Millipore	Mouse anti-Human	MAB1794
IgG2a kappa	BD Pharmingen	Mouse anti-Human	550339
PE-CD19 (4G7)	BD Pharmingen	Mouse anti-Human	345777
PE-IgG2a kappa	BD Pharmingen	Mouse anti-Human	555574
FITC-CD5 (L17F12)	BD Pharmingen	Mouse anti-Human	345781
FITC IgG2a kappa	BD Pharmingen	Mouse anti-Human	555573
CD20cy	Dako	Mouse anti-Human	IR604
CD14	BD Pharmingen	Mouse anti-Human	550376
FITC-CD14	BD Pharmingen	Mouse anti-Human	555397
PE-Cy7-CD14	BD Pharmingen	Mouse anti-Human	560919
PE-Cy7 IgG2a kappa	BD Pharmingen	Mouse anti-Human	557907
CD68	Dako	Mouse anti-Human	M087629-2
PE-CD68	BD Pharmingen	Mouse anti-Human	556078
PE-IgG2b kappa	BD Pharmingen	Mouse anti-Human	556078
CD163	Abcam	Rabbit anti-Human	ab100909
IgG	Abcam	Rabbit anti-Human	ab172730
PerCP-Cy5.5-CD163	BD Pharmingen	Mouse anti-Human	563887
PerCP-Cy5.5 IgG1 kappa	BD Pharmingen	Mouse anti-Human	550795
CD38	Abcam	Rabbit anti-Human	ab183326
PE-Cy5 CD38	BD Pharmingen	Mouse anti-Human	555461
PE-Cy5 IgG1 kappa	BD Pharmingen	Mouse anti-Human	555750
CD206	BD Pharmingen	Mouse anti-Human	555953
IgG1 kappa	BD Pharmingen	Mouse anti-Human	555746
FITC-CD206	BD Pharmingen	Mouse anti-Human	551135
FITC IgG1 kappa	BD Pharmingen	Mouse anti-Human	555748
EGR2	LifeSpan Biosciences Inc.	Mouse anti-Human	LS-C174298
APC-IgM	BD Pharmingen	Mouse anti-Human	551062
APC-IgG1 kappa	BD Pharmingen	Mouse anti-Human	555751
RPE-IgM	Dako	Rabbit anti-Human	R5111
RPE-F(ab')2	Dako	Rabbit anti-Human	X0930
PE-IgD	BD Pharmingen	Mouse anti-Human	555779

Table 2.3 Secondary antibodies

	Company	Description	Cat #
Alexa Fluor 488	Life Technologies	Donkey	A21202
Alexa Fluor 647	Life Technologies	Donkey	A31573

Table 2.4 Reagents for Viability Assay by Flow Cytometry

	Company	Cat #
FITC-Annexin V	BD Pharmingen	556420
Propidium Iodide (PI)	SIGMA-ALDRICH	25535164

2.2.2 Reagents used for MGG staining

Using standard glass slides and 8 well glass slides (Chamber slide, Lab-Tek™ glass, 8-well, Thermo Scientific Nunc, Cat. No. 10051021), May Grünwald Giemsa (MGG) staining was performed and viewed under standard light microscope. Table 2.5 provides details of reagents used for MGG staining.

Table 2.5 Reagents for MGG staining

	Company	Cat #
May Grünwald	SIGMA-ALDRICH	32856
Giemsa	SIGMA-ALDRICH	32884

2.2.3 Reagents used for immunofluorescent staining

Using coverslips (13mm diameter, Appleton Woods, Cat. No. MS002) and mounted on standard glass slides, the cells were viewed under Immunofluorescence Microscope in a dark room. Table 2.6 provides details of reagents and Table 6 provides details of antibodies used for Immunofluorescence staining.

Table 2.6 Reagents for Immunofluorescence staining

	Company	Description	Cat #
Aqua-Poly/Mount	Polysciences Europe GmbH	Mounting Media	18606-20
Donkey Serum	Merck Millipore	Donkey serum for blocking	S30-100ML
TruStain FcX	BioLegend	Fc Blocker	422302
Hoechst 33342	Thermo Fisher Scientific	Nuclear Stain	62249
4',6-Diamidino-2-Phenylindole, Dihydrochloride (DAPI)	Thermo Fisher Scientific	Nuclear Stain	D1306

2.2.4 Reagents used to induce differentiation of THP-1 cells into macrophages

Human THP-1 cell line was obtained from European Collection of Authenticated Cell Cultures (ECACC Cat. No. 88081201). The cell line was authenticated with 100% Match with ATCC® Number of TIB-202, Designated as THP-1 Acute Monocytic Leukemia Human and using 9 loci (D5S818, D13S317, D7S820, D16S539, VWA, TH01, AM, TPOX and CSF1PO). This was performed using Cell Line Authentication Services by Ms. Patricia Gerard and Dr Lakis Liloglou at the Department of Molecular and Clinical Cancer Medicine of University of Liverpool. Table 2.7 provides details of the reagents used to differentiate the THP-1 cell line.

Table 2.7 Reagents for Cell line differentiation

		Company	Cat #
M0	Phorbol 12-ymristate 13-acetate (PMA)	Sigma-Aldrich	16561-29-8
M1	Interferon Gamma (IFNγ)	Perprotech	300-02
M1	Lipopolysaccharide (LPS)	Sigma-Aldrich	8630
M2	Interleukin-4 (IL-4)	R&D Systems	6507-IL-010

2.2.5 Cytotoxic agents used to induce apoptosis

2.2.5.1 Fludarabine

Fludarabine (Cat. No. 21679141, Sigma-Aldrich) seen in Figure 2.11 was made up to 20 mM stock in DMSO and aliquoted in 10 µl/tube, stored in -20°C freezer.

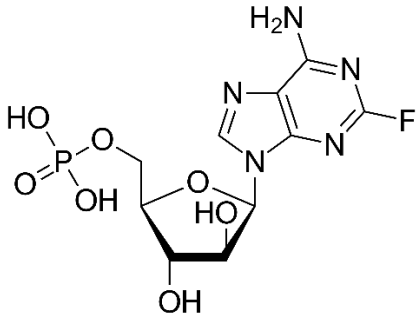

Figure 2.11 Fludarabine

2.2.5.2 ABT-199

ABT-199 (Cat. No. GDC-0199, Selleckchem.com) seen in Figure 2.12 was made up to 10 mM stock in DMSO and aliquoted in 5 µl/tube, stored in -20°C freezer.

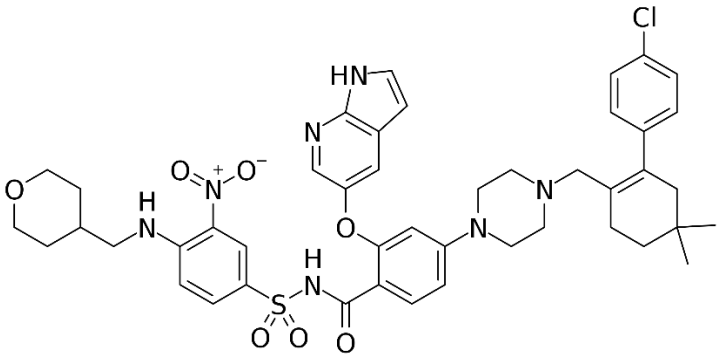

Figure 2.12 Venetoclax (ABT-199)

2.2.6 ELISA Kits

ELISA kits were ordered and ELISA was performed on 96-well plates (Nunc-Immuno™MicroWell™, Sigma-Aldrich, Cat. No. M9410-1CS), using manufacturer's instructions. The plates were measured using Densitometer µQuant (BioTek). Table 2.8 provides details of the kits used.

Table 2.8 ELISA Kits

	Company	Cat #
CCL3 (MIP-1 alpha)	Affymetrix eBioscience	887035
CCL4 (MIP-1 beta)	Invitrogen Thermo Fisher Scientific	887034

3 Characterising nurse-like cells derived from peripheral blood mononuclear cells of patients with CLL

3.1 Introduction

The study of nurse-like cells (NLCs) in CLL took off in the early 2000's with the initial reports of these cells appearing as 'large adherent cells' displaying morphologic and phenotypic features of macrophages and demonstrating pro-survival effect on CLL cells when co-cultured together (Burger et al. 2000; Tsukada et al. 2002).

The studies of NLCs continued and later established the critical role of NLCs within the CLL microenvironment. This led to the identification of, in addition to SDF1 (CXCL12), BAFF and APRIL that were expressed by NLCs to activate the pro-survival signalling pathways in CLL cells (Nishio et al. 2005). Meanwhile, chemokines such as CCL3 and CCL4 released from activated CLL cells in the lymph nodes have been shown to attract T cells and other immune cells to the tissue microenvironment (Burger et al. 2009b), supporting the notion that CLL cells are also actively involved in developing the favourable microenvironment (Burger 2011a; Caligaris-Cappio, Bertilaccio & Scielzo 2014). It is now known that NLCs most likely originate from blood monocytes and accumulate in the lymphoid tissues such as lymph nodes, bone marrow and spleen (Boissard et al. 2016a; Burger et al. 2000; Jia et al. 2014; Tsukada et al. 2002).

However, when my research was started back in 2015, the molecular mechanisms mediating the pro-survival and drug resistance following interaction of CLL cells with nurse-like cells were not well understood. In particular, cross-communication between nurse-like cells and CLL cells at the level of gene expression is not fully characterised. A good understanding of these molecular mechanisms is important as it may help identify key molecules that mediate survival and drug resistance *in vivo*. In turn, this may lead to discovery of novel therapeutic agents that could target these molecules and restore drug sensitivity.

Therefore, whilst the overall aim of my PhD study is to understand the molecular mechanisms mediating effects of NLCs on CLL and vice versa, the focus of this chapter is to independently validate the development of NLCs using primary peripheral blood mononuclear cells obtained from patients with CLL and confirm the biological effects of co-culture with NLCs on CLL cells that have been reported in the literature. The specific objectives of this part of my PhD study are therefore:

1. Validating the optimum culture conditions for developing NLCs in vitro;
2. Further characterisation of the morphology and immunophenotype of NLCs;
3. Expanding investigation of the cytoprotective effects of NLCs on CLL cells on co-culture;
4. Investigating effects of the co-culture on NLCs.

3.2 Methods:

3.2.1 Development of NLCs

To generate the nurse like cells, fresh mononuclear cells prepared from the peripheral blood of CLL patients were re-suspended in complete RPMI 1640 medium supplemented with 10 % heat-inactivated fetal bovine serum, 2 mM L-glutamine, 100 U/mL penicillin, and 100 µg/mL streptomycin (Life Technologies/Thermo Fisher Scientific, Paisley, UK). The cells were incubated in a 37°C, 5% CO_2 humidified incubator and followed up by observing for morphological changes under phase contrast microscope. They were initially cultured at different densities in 24 well plates.

Every day, the plates were viewed under microscopy for a minimum of 3 random fields. The visual changes relating to the cell shape, size, and general arrangement were noted and followed for each sample and compared with other densities and the previous day findings.

3.2.2 Replacement of media

In order to provide nutrition for the cells during the experiment involving long-term culture, I used partial replacement of media as a maintenance strategy as the cytokines/chemokines released from the cultured cells into the supernatant could be important for the longevity of the CLL cells as well as NLC differentiation. Partial replacement of either ½ or 1/3 of culture media with fresh complete RPMI medium was performed depending on the observations seen under microscope, as needed usually every 3-4 days. By gently tipping the plate to one side, without shaking the plate, the supernatant was collected from the top so as not to disturb the already settled cells. Fresh RPMI was added by gently pipetting along the walls of the wells. In the cases where there was too much localisation of cells to the centre, gentle drops were added to disperse the CLL cells, but not to dislodge the NLCs.

3.2.3 Co-culture of CLL cells with NLCs

To prepare a co-culture experiment, NLCs are first developed as described previously (Burger et al. 2000) up to 14 days where their condition is checked under microscope. The CLL cells that were present during the 14 days in fresh PBMC are gently washed away by combination of gentle agitation, tipping of the plate at an angle and collecting the supernatant by pipetting. Gentle washing using warm complete media is used on surfaces of the plate and the area is checked under microscope. The plates that are not to be co-cultured with autologous CLL cells are provided with equal volume of complete media and kept aside in the incubator. Plates to be used for co-culture experiments are temporarily resuspended with warmed complete media and kept in incubator while autologous CLL cells are

thawed and resuspended in fixed cell density of $3x10^6$/ml in warm complete media (as described in Methodology). The plates to be used are taken out and the supernatant is drained. The media mixture containing thawed CLL cells is then added onto the plates containing NLCs and is labelled as co-culture wells. A portion of thawed CLL cells is generally sent for viability testing by Trypan blue and or flow cytometry using Annexin/PI for record keeping as Day 0.

3.2.4 Statistical Analysis

Where appropriate, a paired two-tailed Students *t* test was performed to determine the statistical significance of the difference between the two groups of data. Chi squared test was performed to determine the statistical significance of the difference between two nominal and or ordinal groups of data and Fisher-Freeman-Halton exact test was used where Chi squared was not appropriate. SPSS version 21 and Microsoft Office Excel 2017 was used.

3.3 Results

3.3.1 Optimising cell density of CLL PBMCs in culture for developing NLCs

When I started my project, I noticed that the cell density of CLL PBMCs used to develop NLCs that was reported in the literature was different from study to study, ranging from 3 x 10^6 cells/ml (Filip et al. 2013b) to 10 x 10^6 cells/ml (Nishio et al. 2005) to 15 x 10^6 cells/ml (Burger et al. 2000). Therefore, I first set out to establish the optimal cell density to develop NLCs in standard culture conditions. When I first cultured fresh CLL PBMCs at low density (7.5 x 10^6/ml) (Figure 3.1 left), the development of NLCs were poor. This is most likely due to the lower number of cells used where cell-cell interaction was insufficient, resulting in earlier apoptosis of CLL cells.

At higher cell density (15 x 10^6/ml), the field of view looked very crowded with multilayers of cells heaped on top of each other (Figure 3.1, middle). This was therefore deemed an inefficient condition to develop NLCs from PBMC.

In contrast, at the cell density of 10 x 10^6/ml, I could observe clear morphology of cells under the microscope and appearance of NLCs with an enlarged oval or elongated shape (Figure 3.1, right). These NLCs continue to differentiate into macrophage-like cells over time.

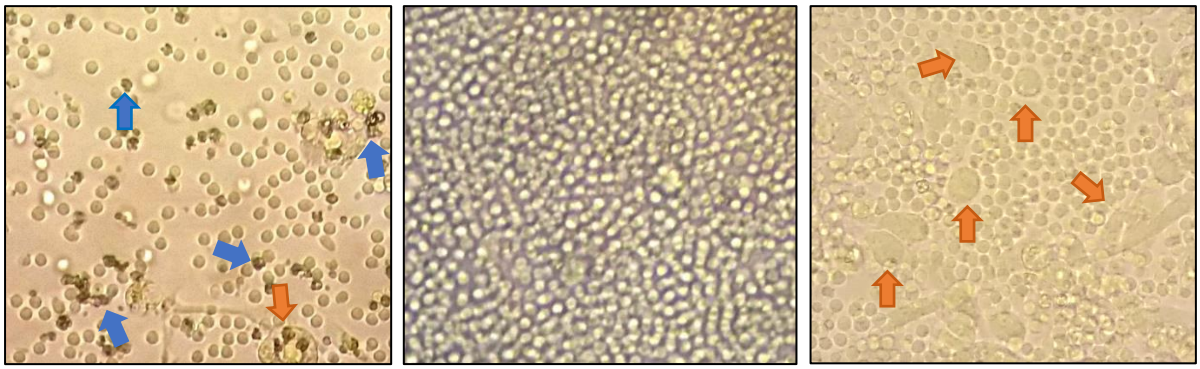

Figure 3.1 PBMCs cultured at different cell densities affects the development of NLCs.

Phase contrast image of fresh PBMC (3465 Day 8) cultured at cell density of 7.5 x 10^6/ml (left) giving a sparse arrangement of poor viability CLL cells (appearing as dark and shrivelled cells, blue arrows) and few NLCs (orange arrows). Phase contrast image of fresh PBMC (3460 Day 4) cultured at density of 15 x 10^6/ml (middle) giving multiple layers, obscuring the view in majority of viewing fields. Phase contrast image of fresh PBMC (3484 Day 6) cultured at cell density of 10 x 10^6/ml (right) giving a clear view of cells and their changes.

3.3.2 Morphological features of NLCs

3.3.2.1 Phases of monocyte/ macrophage differentiation observed via phase contrast microscopy and MGG staining.

Upon initial culturing the fresh CLL PBMCs in RPMI at Day 0, the appearance of monocytes was almost indistinguishable from lymphocytes seen in Figure 3.2, even though monocytes are generally larger than lymphocytes (Bain et al. 2012; Lichtman et al. 2011b).

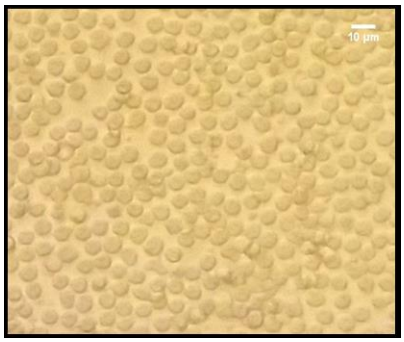

Figure 3.2 Monocytes indistinguishable from lymphocytes in fresh PBMCs cultured under standard conditions at Day 0.

Phase contrast microscopy of the fresh PBMCs (3470) plated on Day 0 in RPMI. Based on initial appearance upon plating, it was almost impossible to differentiate the monocytes from lymphocytes.

I next performed May Grünwald Giemsa (MGG) staining on the same cells that I observed under the phase contrast microscope.

With minimal agitation, the monocytes can be distinguished by having a slightly larger circular appearance and displayed mild adherent properties. This can be seen as early as 24 hours to 48 hours later. With MGG staining as seen in Figure 3.3 (left), the monocytes have a lower nuclear (N): cytoplasm (C) ratio, characteristic vacuoles in the cytoplasm which is not very granular and dense. The nearby lymphocyte is seen having a greater N:C ratio with a smaller size in contrast to the monocyte.

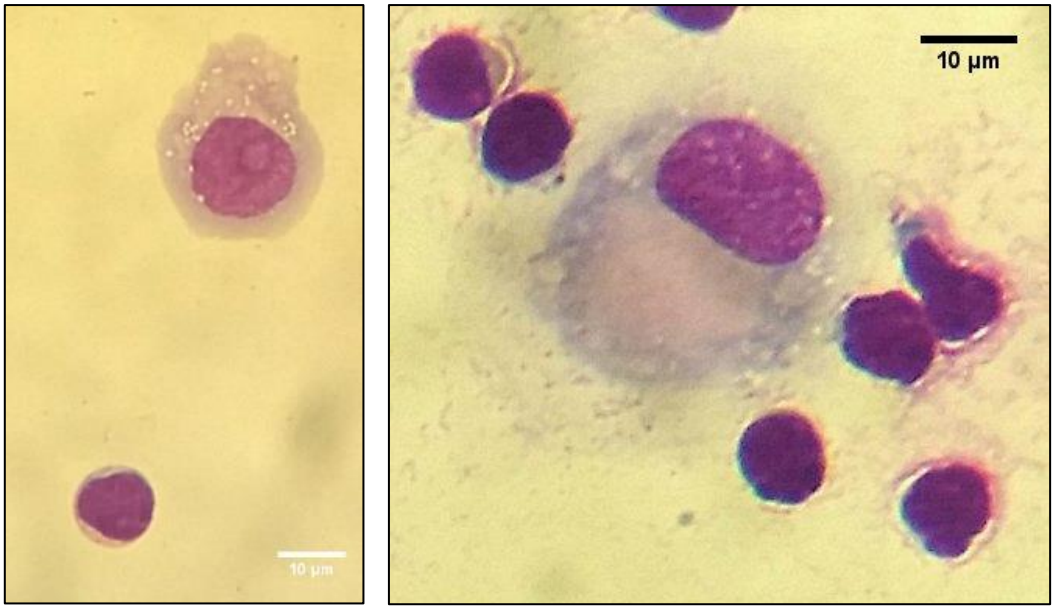

Figure 3.3 Monocytes and macrophages are distinguishable from lymphocytes by their morphology. (Sample 3464 Day 12) MGG-stained cells showing a single lymphocyte and a monocyte (left). The leukocyte is showing a high N:C ratio with diameter just under 10um. The monocyte is having a lower N:C ratio, showing characteristic vacuoles in the cytoplasm which is not very granular and dense. (Sample 3470 Day 4) MGG stained slide showing a group of lymphocytes in close proximity to a single big macrophage (right). The macrophage is having a very large oval appearance with cytoplasmic vacuoles and the cytoplasm appears to have ill-defined borders being heterogeneously stained as well.

Overtime, the monocytes were differentiated into large oval adherent cells, which is consistent with NLCs as previously described (McWhorter et al. 2013). As seen in Figure 3.3 (right), multiple lymphocytes are seen in close proximity to a single macrophage. The macrophage is having a large oval appearance with more cytoplasmic vacuoles, with the cytoplasm having an ill-defined border being heterogeneously stained as well.

Also, adherent cells with varying shapes were observed where the cytoplasm was stretched and the membrane appeared elongated. Illustrated in Figure 3.4 (A) is an example of an adherent cell with a stretched vacuolated cytoplasm of a macrophage-like cells giving an appearance of a tail-like projection.

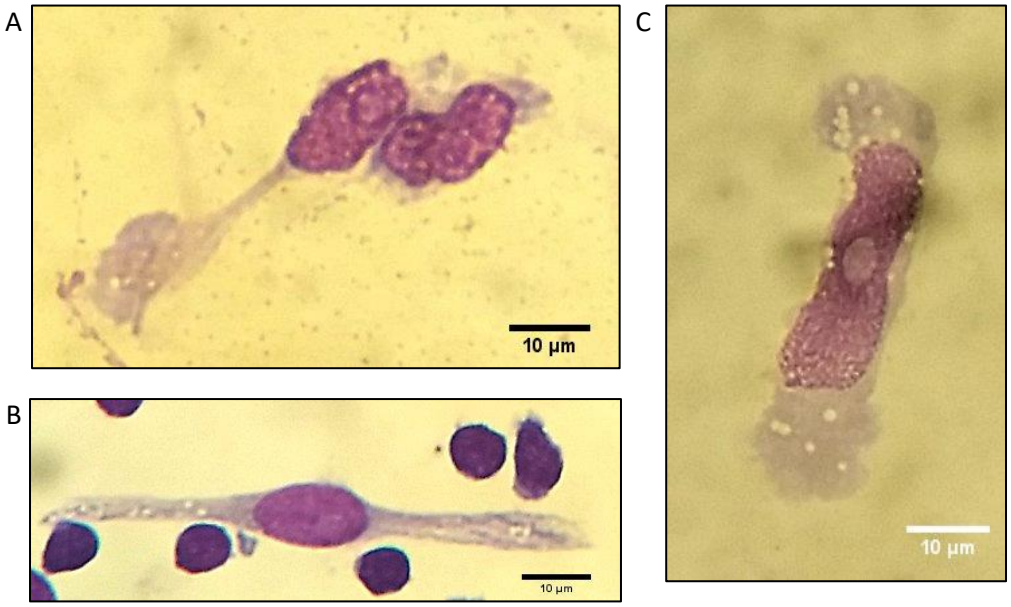

Figure 3.4 Tail-like projection, spindled-shaped and elongated appearance from an adherent cell.

(3464 Day 12) MGG stained slide showing a group of adherent cells with characteristic cytoplasmic vacuoles and lightly stained cytoplasm (A). One of the adherent cells has an extended cell membrane giving a tail-like appearance. (3464 Day 12) MGG stained slide showing a single macrophage in close proximity to lymphocytes (B). The lymphocyte is showing a high N:C ratio with diameter just under 10um as mentioned in literature. The Macrophage is having extension of the cell membrane of both poles from nucleus giving an elongated spindle shaped appearance. (3464 Day 12) MGG stained slide showing a single macrophage with characteristic cytoplasmic vacuoles, lightly stained cytoplasm and fine granules (C). The macrophage demonstrates an elongated appearance where the nucleus as well as the cell membrane are elongated. All macrophages are having a lower N:C ratio, showing characteristic vacuoles in the cytoplasm which is not very granular and dense.

Sometime, these tail-like projections increase in number to give a spindle shaped appearance, where the nucleus appears to be in the middle and the tails extending towards the two opposite directions as seen in Figure 3.4 (B).

Eventually some macrophages display an overall elongated appearance and seen in Figure 3.4 (C), the overall shape is as stated, with cytoplasmic vacuoles as well as fine granules within the cytoplasm. In fact, the nucleus is also appeared to be elongated in contrast to having a general oval appearance.

Usually these adherent cells were seen in close proximity with lymphocytes forming small clusters. An example is shown in Figure 3.5 (left) under phase contrast and Figure 3.5 (right) following MGG staining.

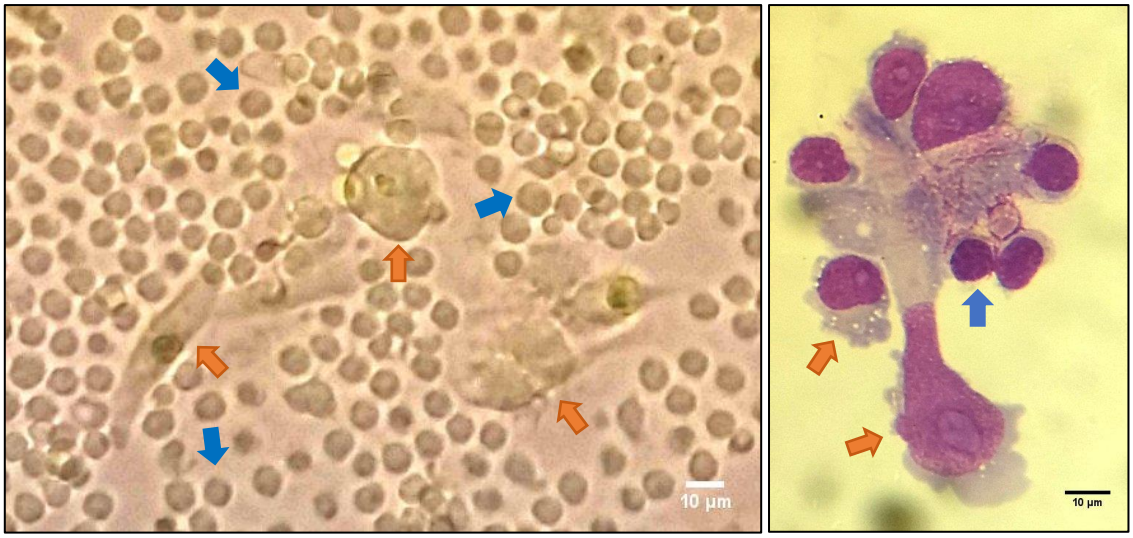

Figure 3.5 Pleomorphism and cluster formation of adherent cells developed after culturing CLL PBMCs under standard conditions.

CLL PBMCs (3460 Day 6) cultured in RPMI medium developed adherent cells with distinct appearance from lymphocytes (i.e. circular/oval cells with a diameter of just under 10um, blue arrow). These adherent cells appeared to have differentiated into macrophage-like cells displaying a larger more pleomorphic morphology with large oval or elongated shapes under phase contrast microscopy (left orange arrow). (3464 Day 12) MGG stained slide showing multiple lymphocytes and macrophage-like adherent cells forming a cluster (right). The lymphocyte (blue arrow) is showing a high N:C ratio with diameter of just under 10µm. The adherent cells (orange arrow) are having a lower N:C ratio, showing characteristic vacuoles in the cytoplasm which is not very granular and dense.

Figure 3.6 and Figure 3.7 shows more examples of adherent cells that have formed from the CLL PBMCs cultures. The lymphocytes are again seen as those with densely stained nuclei, having a large N:C ratio and appearing in close proximity to the adherent cells. The macrophage-like adherent cells are pleomorphic with the appearances described above, but all having characteristic cytoplasmic vacuoles, a smaller N:C ratio in contrast to the lymphocytes.

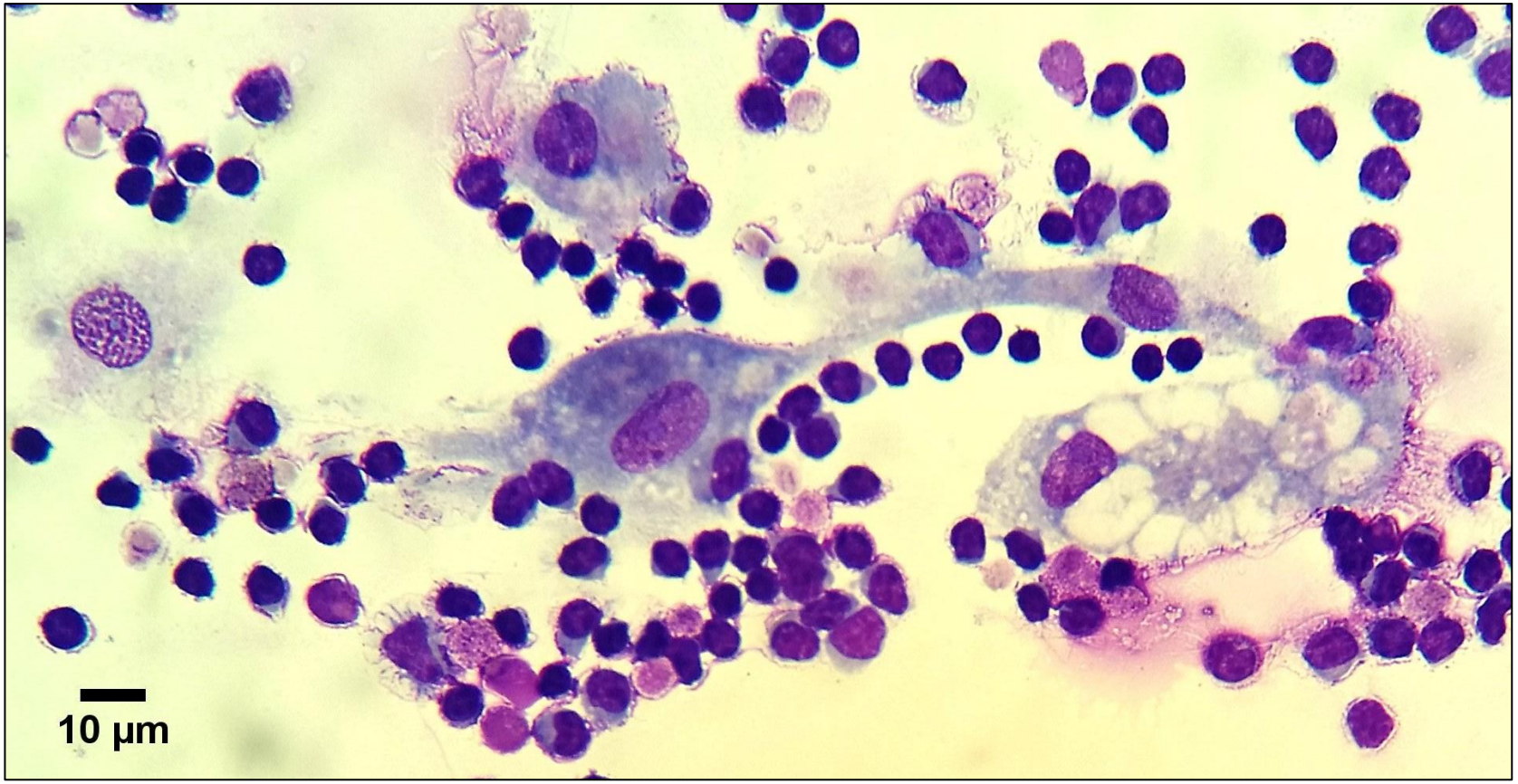

Figure 3.6 A diverse cluster of macrophage-like adherent cells with CLL cells emerges from CLL PBMCs culture.

(3469 Day 14) MGG stained slide showing a cluster of adherent cells with lymphocytes in close proximity. The adherent cells are distinguishable from their characteristic vacuoles in their cytoplasm of which is mildly granular with a lower N:C ratio than the leukocytes. The adherent cells are showing more pleomorphism where one is very large with heterogeneously densely stained cytoplasm and granularity.

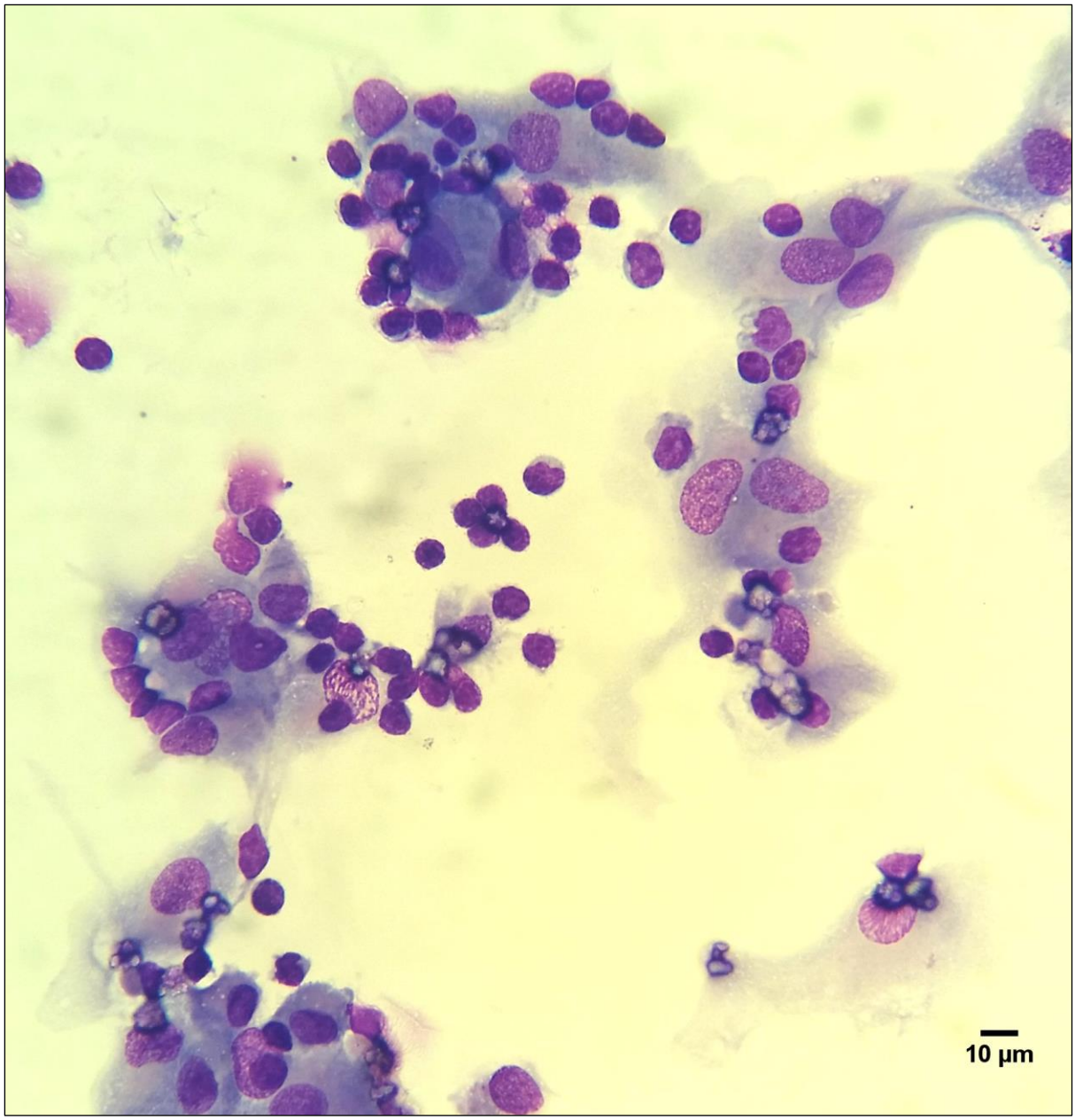

Figure 3.7 Clusters of adherent cells with CLL cells is apparent.

(3469 Day 14) MGG stained slide seen under oil immersion showing multiple clusters of pleomorphic adherent cells closely surrounded by leukocytes. The leukocytes have a high N:C ratio with a deeply stained nucleus. The NLCs have a broad range of morphology from large oval appearance to elongated and spindle shaped and having characteristic vacuoles with granular cytoplasm.

These groups of cells may then form clusters near a greater mix of spherical/oval and elongated, tailed monocytes. A cluster is considered as a collection of the cells in such close proximity and overlapping so that their margins are not distinguishable.

These clusters may then grow further consisting of more pleomorphic monocytes and lymphocytes to the point that it is seen with the naked eye in the culture plate thereby defined as colonies. As seen in

Figure 3.8, the visual field shows clusters formed consisting of multiple layers of cells that have aggregated there. Focusing on cells became difficult as a result.

Figure 3.8 Abundance of cells consisting of NLCs and CLL cells populated as dense islands.

Phase contrast a PBMC sample (3460 Day 13) where a close up is visualised of a colony formed by a very large collection of lymphocytes and macrophages.

There was a period of plateau where there were no obvious changes in size, shape, density appearance of monocytes or clusters.

After this point, the conditions of the clusters deteriorate. Eventually, dead/dying cells appear as floated or shrivelled cells with a darker granulated background which I considered as an apoptotic phase. As seen in Figure 3.9, the visual field shows multiple shrivelled cells where some have aggregated (left) and the macrophage-like adherent cells also start to lose their glow (right).

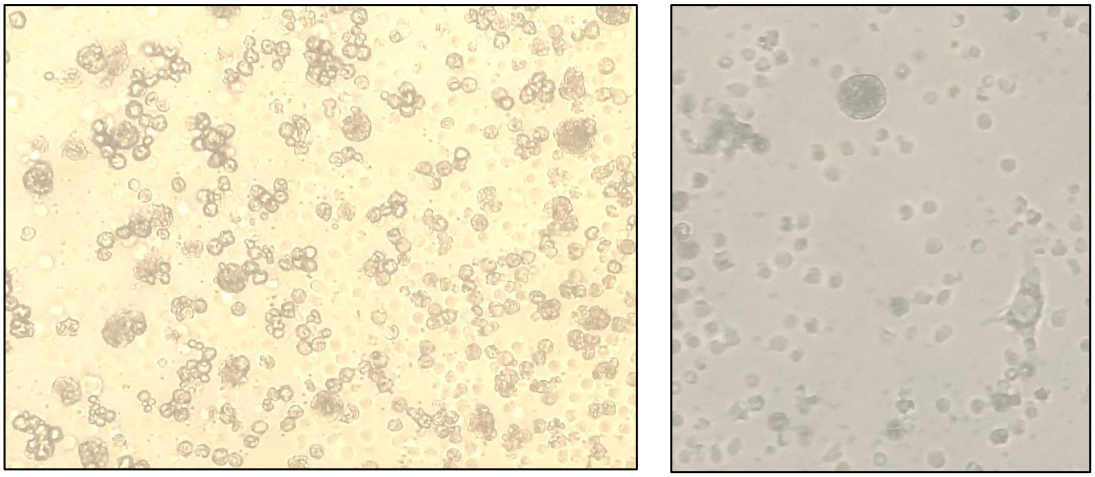

Figure 3.9 Apoptotic features start to occur in prolonged cultures.

Phase contrast images of CLL PBMCs (3460) cultured to Day 21 showing widespread apoptosis. The CLL cells appear as shrivelled cells either individually or clumped together with other shrunken cells (left). The adherent cells appear apoptotic as well based on their dense cytoplasm and blebbing (right).

Eventually there were few cells remaining adhered to the surface and the majority were dead cells.

Collectively, the above was the overall representation describing the development of macrophage-like adherent cells from the CLL PBMCs cultures from their initial appearance to their inevitable demise. The total duration of this was variable from sample to sample, however the phases described appeared to be consistent in all the samples examined. For the purposes of recording morphological features of these macrophage-like adherent cells in chronological pattern, a summary of detailed description of these features during different phases of their development was provided in the Appendix 7.4.

Therefore, using phase contrast microscopy and light microscopy following MGG staining I have characterised the morphological features of the macrophage-like adherent cells that developed from the CLL PBMCs cultures. All these features are consistent with that of NLCs described previously (Burger et al. 2000; Tsukada et al. 2002). I next examined the immunophenotype of these adherent cells because NLCs have been shown to display a phenotype similar to that of M2 macrophages (Filip et al. 2013a; Ysebaert & Fournie 2011).

3.3.3 Immunophenotyping of macrophage-like adherent cells

Following the morphological characterization of the macrophage-like adherent cells, I proceeded to investigate the expression of protein markers typical of the NLCs, including the M2 macrophage markers CD68 and CD163, as previously reported (Tsukada et al, 2002; Jia et al, 2014; Hume & Freeman, 2014; Mills, 2015; Boissard et al, 2015). First, I attempted a method of immunofluorescent staining for flow cytometry analysis. However, I faced many challenges.

These macrophage-like cells were firmly attached to the culture plates. Previous attempts at harvesting the cells (described in Methodology) included the use of enzyme Trypsin, or cold disodium ethylenediaminetetraacetic acid (EDTA) buffer or a combination of both (Tsukada et al. 2002) or a plate cell scraper (Filip, Cisel & Wasik-Szczepanek 2015).

I tried all the above methods to harvest the adherent cells and incubated these cells with antibodies against CD68 and CD163. As shown in Figure 3.10, the forward scatter and side scatter plots showed there wasn't a homogenous population of intact cells within the gated region for subsequent analysis. Most of the cells appeared to be broken, which formed a dense cluster of debris at the bottom of the plots. Another difficulty I faced was that immunophenotyping by flow cytometry method required a large number of adherent cells to begin with. This in turn required the use of even larger number of CLL PBMCs, which was not always possible to obtain. This is in contrast to other studies (Coscia et al. 2011; Giannoni et al. 2014; Jia et al. 2014; Polk et al. 2016; Tsukada et al. 2002). I therefore used immunofluorescence microscopy method instead.

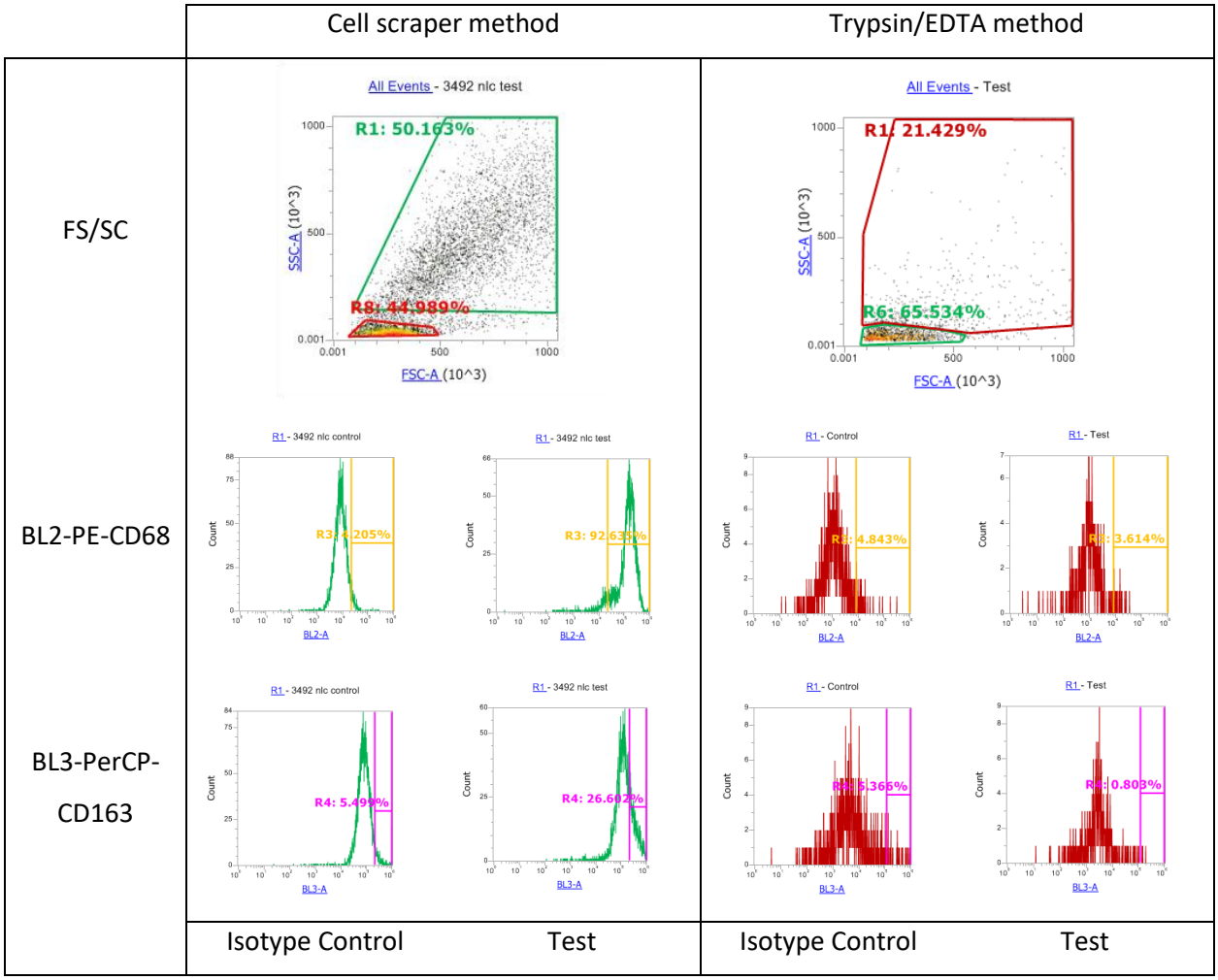

Figure 3.10 Immunophenotyping of adherent cells using flow cytometry.

Adherent cells were harvested using a plate cell scraper (left) or by Trypsin/EDTA (right) and stained with CD68 and CD163 antibodies as described in the Methods. 10,000 events were acquired on a flow cytometer and analysed using the channels BL2 and BL3 for CD68 and CD163, respectively. Histogram of fluorescence of gated events are shown. Isotype control antibodies were used in parallel.

Immunofluorescence (IF) microscopy was thus performed using 8-well chamber slides which can be viewed under fluorescence microscope (described in Methodology).

In order to optimize the conditions for IF staining, I used human monocytic THP1 cell line (see Appendix 7.14.6 for detail). I then applied the optimised IF conditions to immunophenotyping adherent cells. As shown in Figures 11-14, the lymphocytes were distinguishable from the adherent cells initially by their DAPI staining. The CLL lymphocytes were identified by dense DAPI staining (blue) and the size of the nucleus is generally smaller than that of NLCs.

Specific staining with respective antibodies also confirmed the differential expression of protein markers unique for each cell type. As seen in Figure 3.11, CD19 was detected only on the CLL cells,

following incubation with anti-CD19 antibody. This is in contrast to the adherent cells which were stained positive only for CD163 which covered the whole cells, consistent with the cytoplasmic localisation of this plasma membrane marker (Pontén, Jirström & Uhlen 2008).

A further example was seen in Figure 3.12 where the cells sample was immuno-stained on Day 9. Again, CD14 (a marker of monocyte) was detected in macrophage-like adherent cells but not in CLL cells. CD14 was localised in part of the cytoplasm and near the nucleus of the adherent cells. The staining by CD163 revealed an elongated structure of an adherent cell with the CLL cells closely positioned next to it.

Also shown in Figure 3.13 were images from dual staining of the cells cultured for 4 days with antibodies against CD68 and CD163, classical markers for NLCs (Boissard et al. 2015a; Hume & Freeman 2014; Jia et al. 2014; Mills 2015; Tsukada et al. 2002). Reassuringly, CD68 was detected only in macrophage-like adherent cells that were also positive for CD163, whereas CLL cells were clearly stained negative for either marker. CD68 expression was localised within the adherent cells near the nucleus as part of the cytoplasm.

The same CLL sample was dual-stained again at Day 11 of being in culture in order to detect changes in expression of these markers and morphology of the adherent cells. Again, the adherent cells were stained positive for both CD14 and CD163, whereas CLL cells were negative for either marker (Figure 3.14). The positioning of CLL cells was again in close contact with adherent cells.

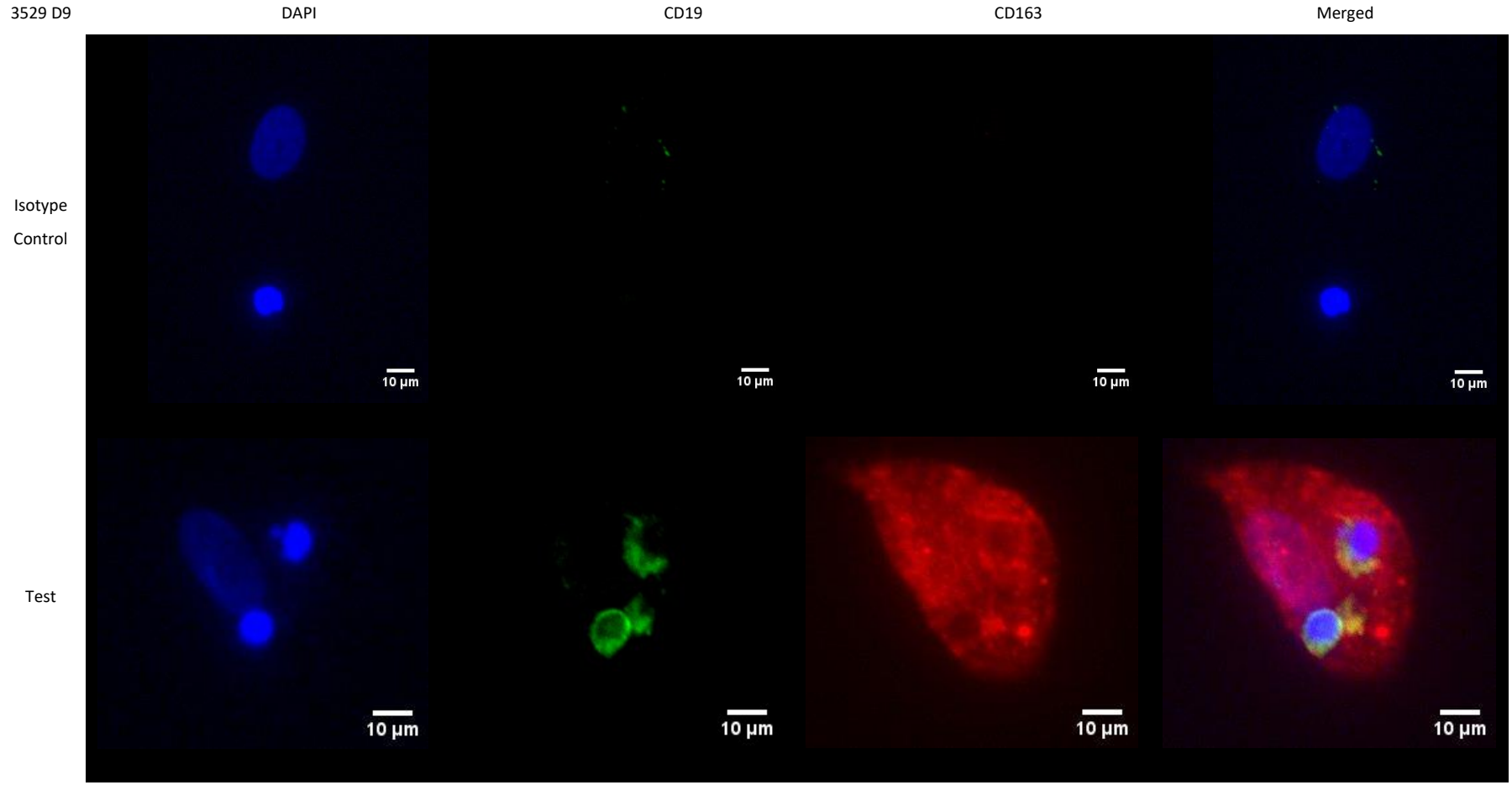

Figure 3.11 Immunofluorescence microscopy of adherent cells developed from CLL PBMCs culture.

Immunofluorescence staining of CLL PBMCs (sample 3529) culture at Day 9 using DAPI (blue), CD19 antibody (green) and CD163 antibody (red) and their respective isotype controls. Fresh PBMCs were cultured as described till Day 9, fixed, stained with primary antibodies against CD19 and CD163, followed by incubating with respective secondary antibodies, counterstained with nuclear staining dye DAPI and viewed under fluorescence microscope in the dark. Images were prepared using ImageJ software.

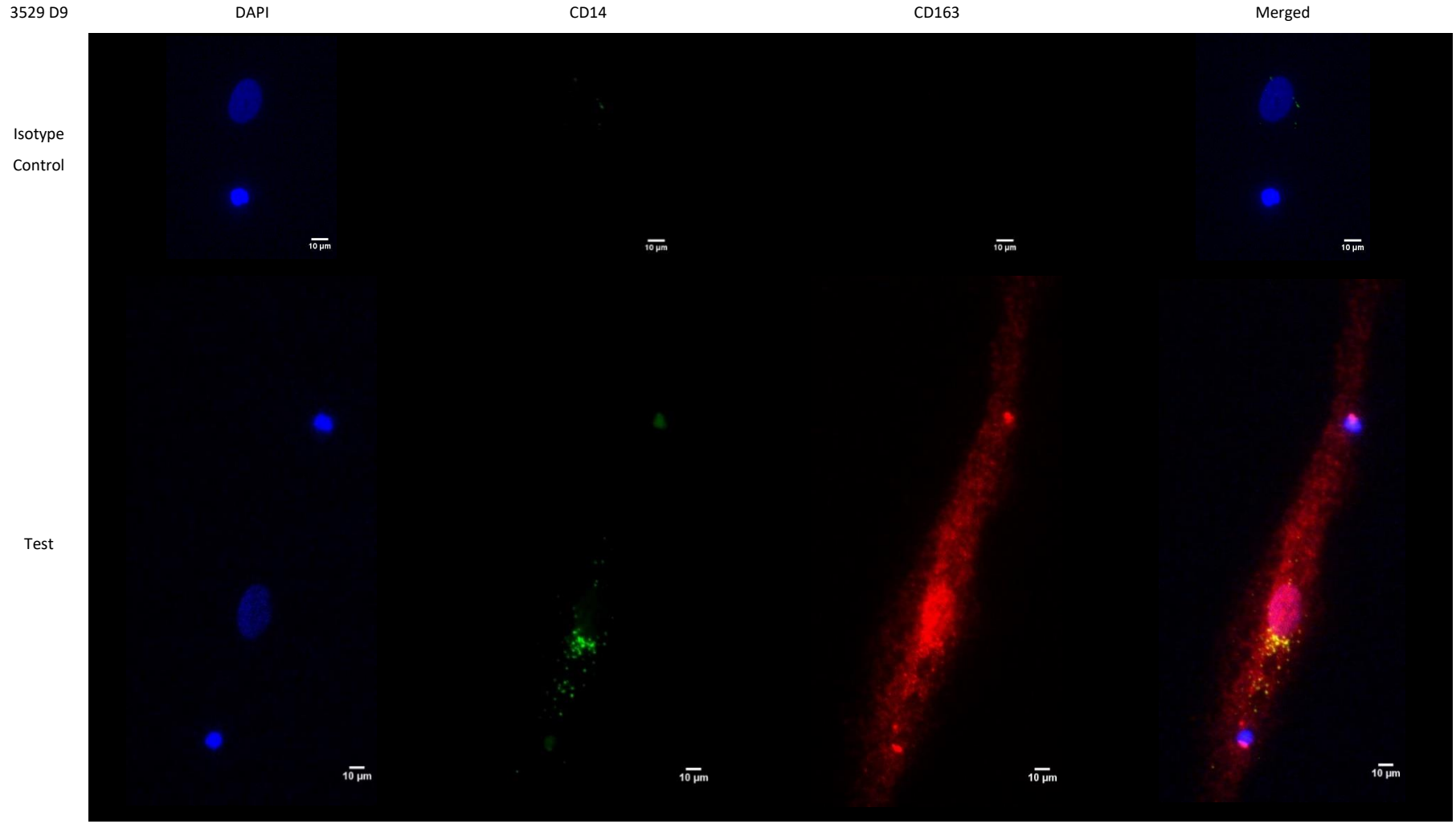

Figure 3.12 Immunofluorescence microscopy of adherent cells developed from CLL PBMCs culture at day 9.

Immunofluorescence staining of CLL PBMCs (sample 3529) culture at Day 9 using DAPI (blue), CD14 antibody (green) and CD163 antibody (red) and their respective isotype controls. Fresh PBMCs were cultured as described till Day 9, fixed, stained with primary antibodies against CD14 and CD163, followed by incubating with respective secondary antibodies, counterstained with nuclear staining dye DAPI and viewed under fluorescence microscope in the dark. Images were prepared using ImageJ software.

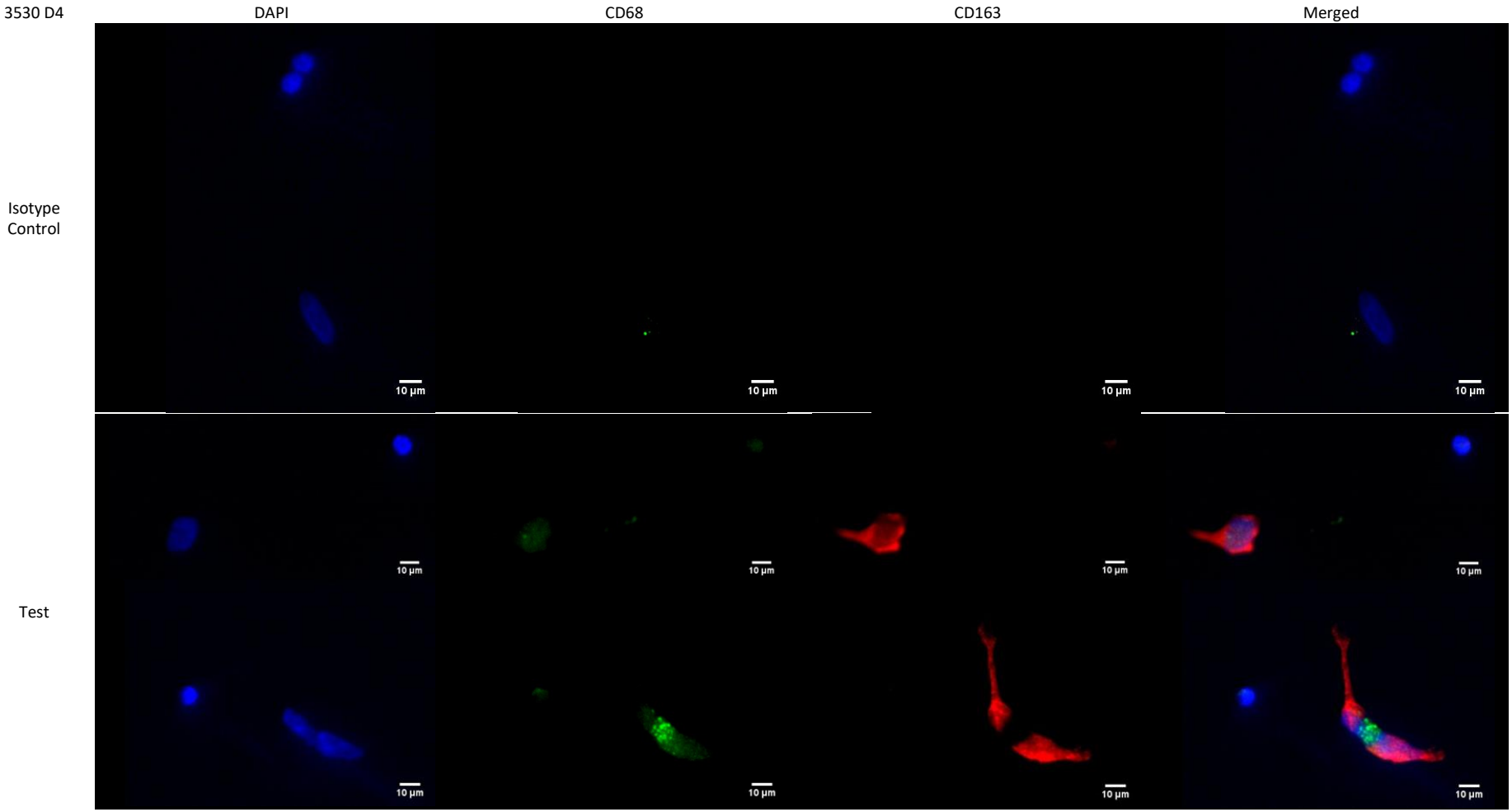

Figure 3.13 Immunofluorescence microscopy of adherent cells developed from CLL PBMCs culture at day 4.

Immunofluorescence staining of CLL PBMCs (sample 3530) culture at Day 4, using DAPI (blue), CD68 antibody (green) and CD163 antibody (red) and their respective isotype controls. Fresh PBMCs were cultured as described till Day 4, fixed, stained with primary antibodies against CD68 and CD163, followed by incubating with respective secondary antibodies, counterstained with nuclear staining dye DAPI and viewed under fluorescence microscope in the dark. Images were prepared using ImageJ software.

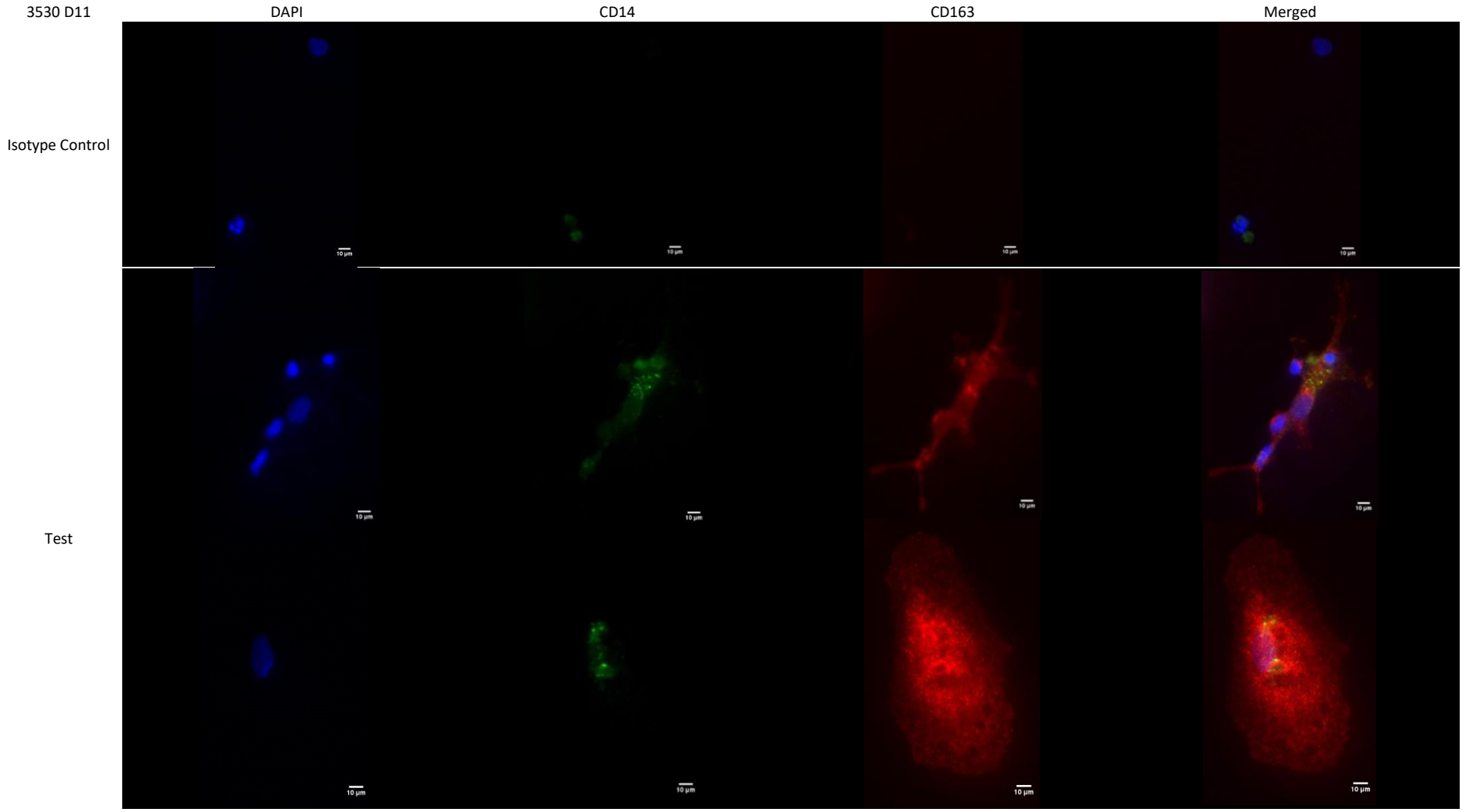

Figure 3.14 Immunofluorescence microscopy of adherent cells developed from CLL PBMCs culture at day 11.

Immunofluorescence staining of CLL PBMCs (sample 3530) culture on Day 11, using DAPI (blue), CD14 antibody (green) and CD163 antibody (red) and their respective isotype controls. Fresh PBMCs were cultured as described till Day 4, fixed, stained with primary antibodies against CD14 and CD163, followed by incubating with respective secondary antibodies, counterstained with nuclear staining dye DAPI and viewed under fluorescence microscope in the dark. Images were prepared using ImageJ software.

Taken together, the results from immunofluorescence microscopy showed that CD14, CD68 and CD163 were detected in adherent cells only, whereas CD19 was detected by CLL cells, as expected.

Therefore, combined observations from morphological study and immunofluorescence microscopy confirmed the macrophage-like adherent cells developed from the CLL PBMCs cultures under the conditions used in my study are indeed the nurse-like cells (NLCs). I will thus use the term NLCs in the thesis thereafter.

Whilst I successfully developed NLCs from the CLL PBMCs cultures, I also noticed considerable variation in the extent to which NLCs could be generated from fresh CLL blood samples under the experimental conditions I used. More specifically, the pace and number of the NLCs developed varied significantly from sample to sample.

3.3.4 Variation in the development of NLCs from the CLL PBMCs samples

Based on the morphological changes that were associated with the different phases during the development of NLCs that I have described (see Appendix 7.4), I noted down for each sample used and color-coded them in a time-course chart with the initial appearance of large oval adherent cells (coded purple) and appearance of maximum number of fully differentiated NLCs (coded orange) (Table 3.1). It was thus obvious that the majority of samples had initial adherent appearance of NLCs at Day 2-4, and the majority of samples reached maximum number of fully differentiated NLCs at Day 8-14.

Table 3.1 Phases of development of NLCs among CLL samples collected, from the appearance of large oval adherent cells (purple) to fully differentiated NLCs (orange).

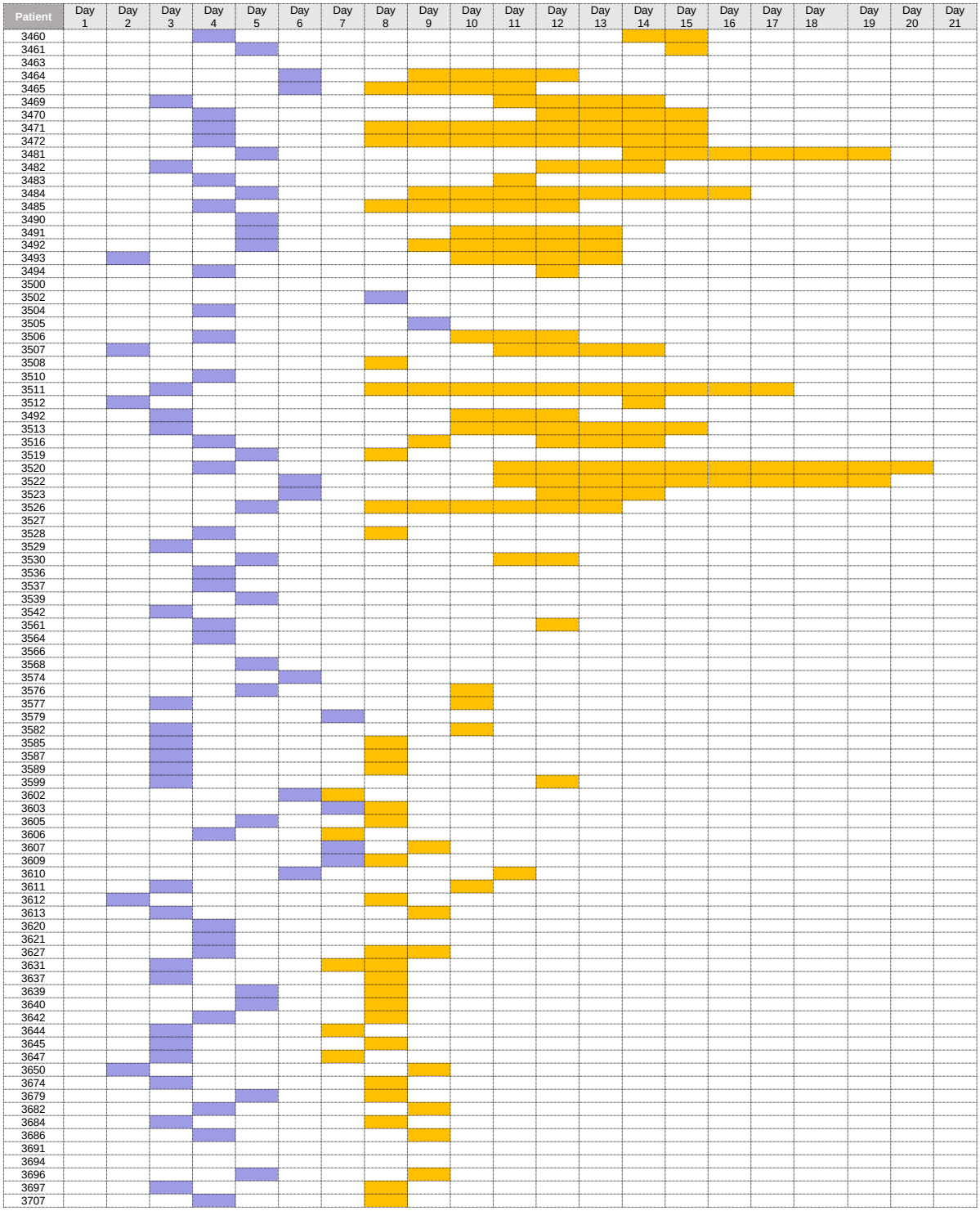

It was worth noting that some samples did not have any NLC development at all even the early phase presentation (e.g. #3536, #3537, #3539, #3542, #3564, #3568). Additionally, it was noted that not all samples gone through all the phases observed by the time they reached their plateau (e.g. #3519, #3528, #3602, #3603, #3609). The plateau period varied from sample to sample, where some samples

reached plateau on Day 8 (eg. #3465, #3471, #3472, #3485, #3511, #3519,) and others can last up to Day 14 (e.g. #3511, #3520, #3522).

3.3.4.1 Scoring of NLCs developed from individual CLL samples

Because of the considerable variation in development of NLCs among the CLL PBMCs samples used, I decided to assign a score of NLCs development to each individual CLL samples based on the following considerations:

- Day of first sight of large oval cells (usually Day 4-6)
- Number of NLCs of any morphology average per field at 200x magnification (≥30, 10-30, <10)
- Progression through different phases (all or some, up to plateau)
- Presence or absence of clusters of NLCs
- Day of plateau phase where maximum number of fully differentiated NLCs developed (usually day 8-12). Plateau phase also refers to a period of little or no significant changes. This period is generally followed by features of apoptosis.

Table 3.2 below provides a rough guide on how I assigned a score to individual samples. Figure 3.15, Figure 3.16, Figure 3.17 and Figure 3.18 were the microscopic images representative of morphology/ appearance of the NLCs assigned with different scores.

Table 3.2 NLC Scoring system

Description of Score	NLC Score
• Large oval cells seen at Day 4 (+/- 2 days) • Number per field >=30 cells • Progressed through all phases up to plateau • Cluster +ve And/ or • Plateau Reached (Day 8-12)	3 (+++)
• Large oval cells seen at Day 4 (+/- 2 days) • Number per field >=30 cells or 10-30 • Progressed through most phases up to plateau • Cluster +ve or -ve And/ or • Plateau Reached (Day 8-12)	2 (++)
• Large oval cells seen at Day 4 (+/- 2 days) or after • Number per field 10-30 cells or <10 • Progressed through phases (1-3) up to plateau • Cluster +ve or -ve And/ or • Plateau Reached (Day 8-12)	1 (+)
• Large oval cells seen well after Day 4 (+/- 2 days) or • Number per field <10 cells • Progressed through only one phase • Cluster -ve And/ or • Plateau Reached (Day 8-12) or apoptosis by day 12	0

3.3.4.1.1 NLC Score 0

Starting at the lowest score, as seen in Figure 3.15, a broad view (large circle) shows a generally homogenous appearance. Here there are no obvious presence of large oval cells. The number of NLCs are minimal to absent, therefore there was no development of NLCs. The samples that have had this score generally underwent widespread apoptosis in the early days of the culture.

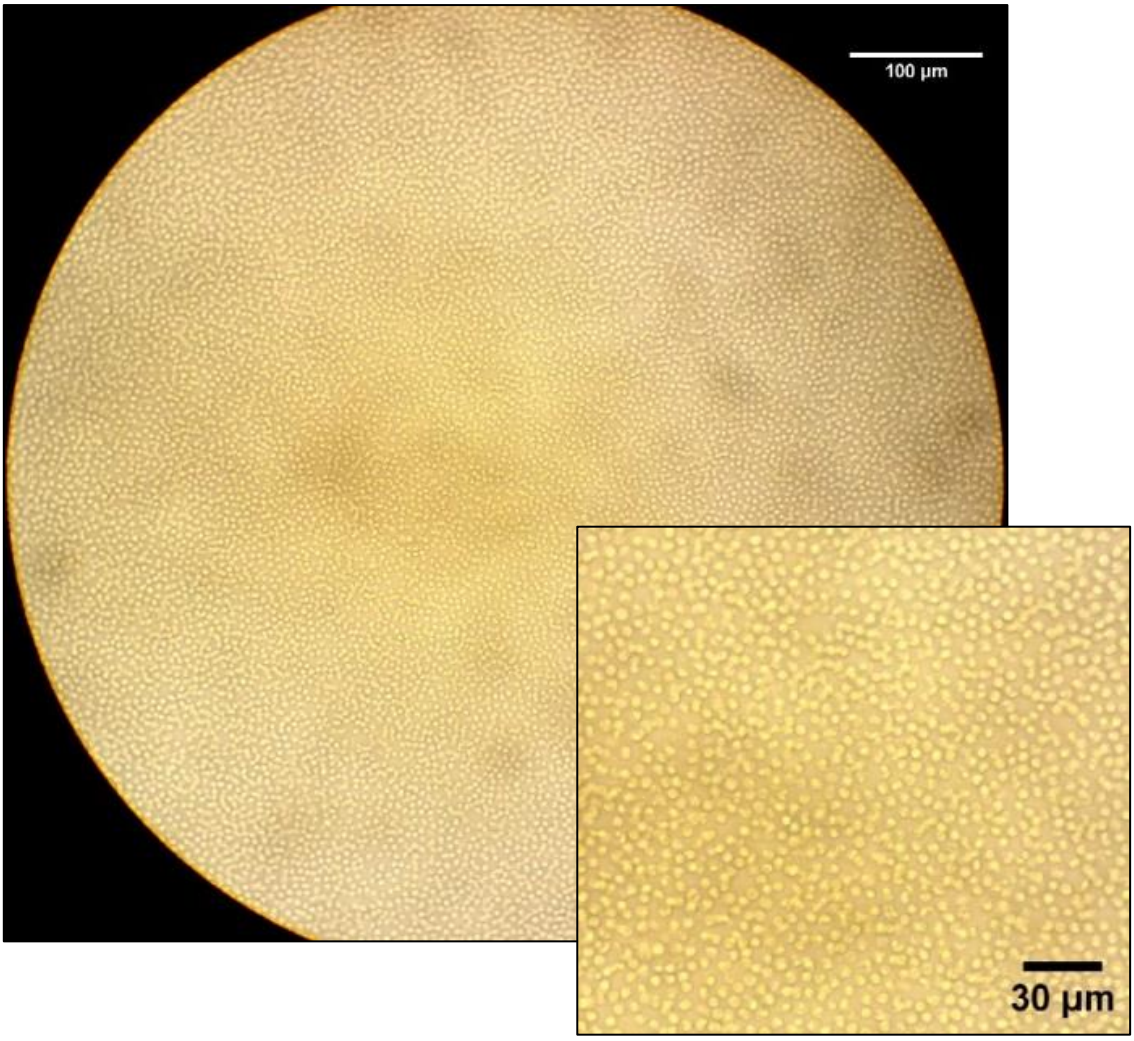

Figure 3.15 Example of NLCs with score 0.

Phase contrast image of CLL PBMCs (#3500) cultured over approximately 8 days to allow development of NLCs. Here the appearance of CLL cells was quite homogenous with minimum to no NLCs seen per visual field.

3.3.4.1.2 NLC Score 1+

As seen in Figure 3.16, few NLCs are present by broad visual inspection under the phase contrast microscope (large circle). At a closer look, the NLCs can be seen in contrast to the lymphocytes as large oval cells. Although the NLCs were present, their number is actually quite low. Upon follow-up checks, it was found that they had a very slow progression and reached their plateau after passing through only a few phases. Also, there were hardly any group/ cluster of NLCs to be seen. Apoptotic signs of the cells appear quickly in general.

Therefore, samples with NLC score 1+ generally presented with low number of NLCs at a later date, with hardly any clusters to be seen. This is followed by the sign of apoptosis.

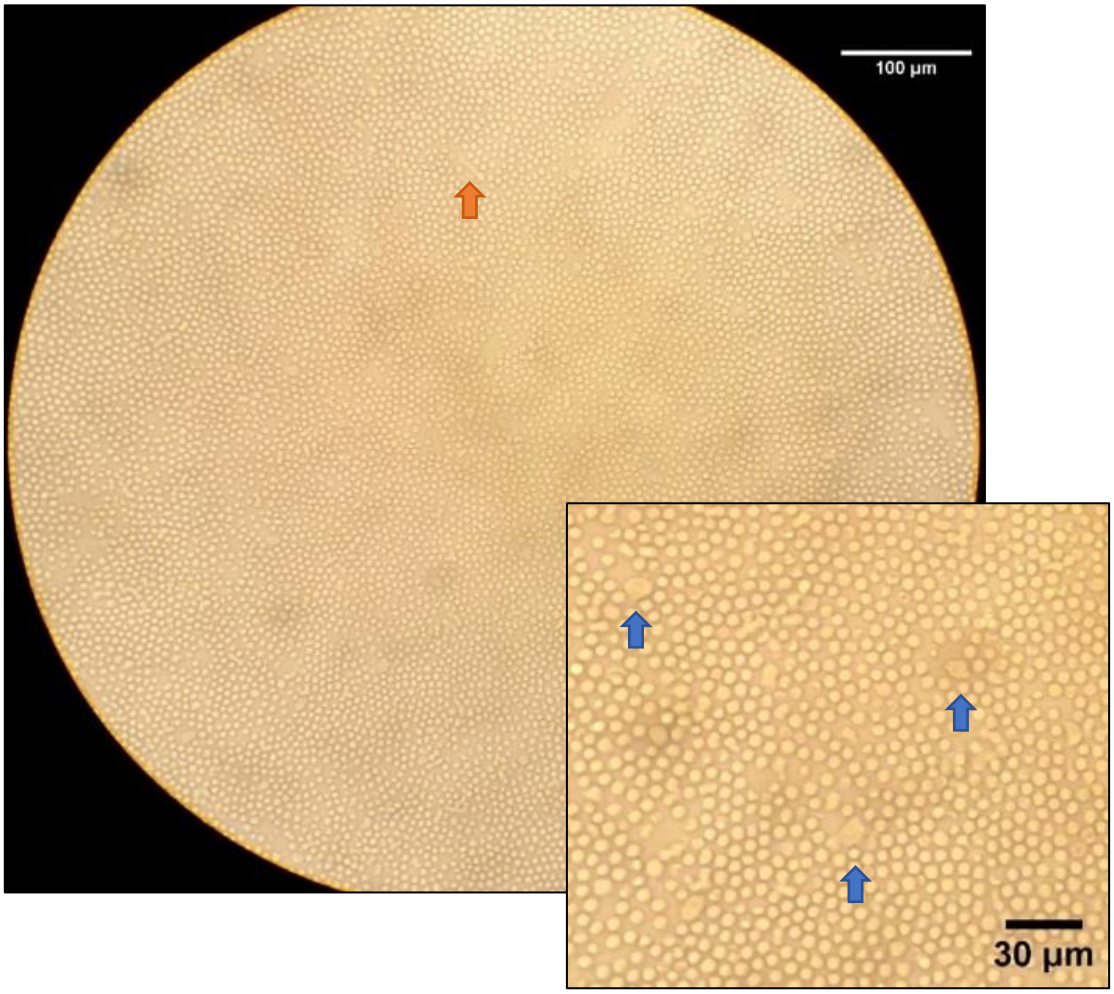

Figure 3.16 Example of NLCs with score 1.

Phase contrast image of CLL PBMCs (#3502) cultured over approximately 11 days, displaying a range of morphologies, from large oval (blue arrow) to elongated or spindle-shaped appearance (orange arrow).

3.3.4.1.3 NLC Score 2+

As shown in Figure 3.17, a greater number of NLCs is seen throughout the fields. On closer inspection a diverse collection of phases where the presence or absence of clusters were observed. These samples were considered as having moderate development of NLCs. Generally, samples with NLCs 2+ are suitable for most subsequent co-culture experiments.

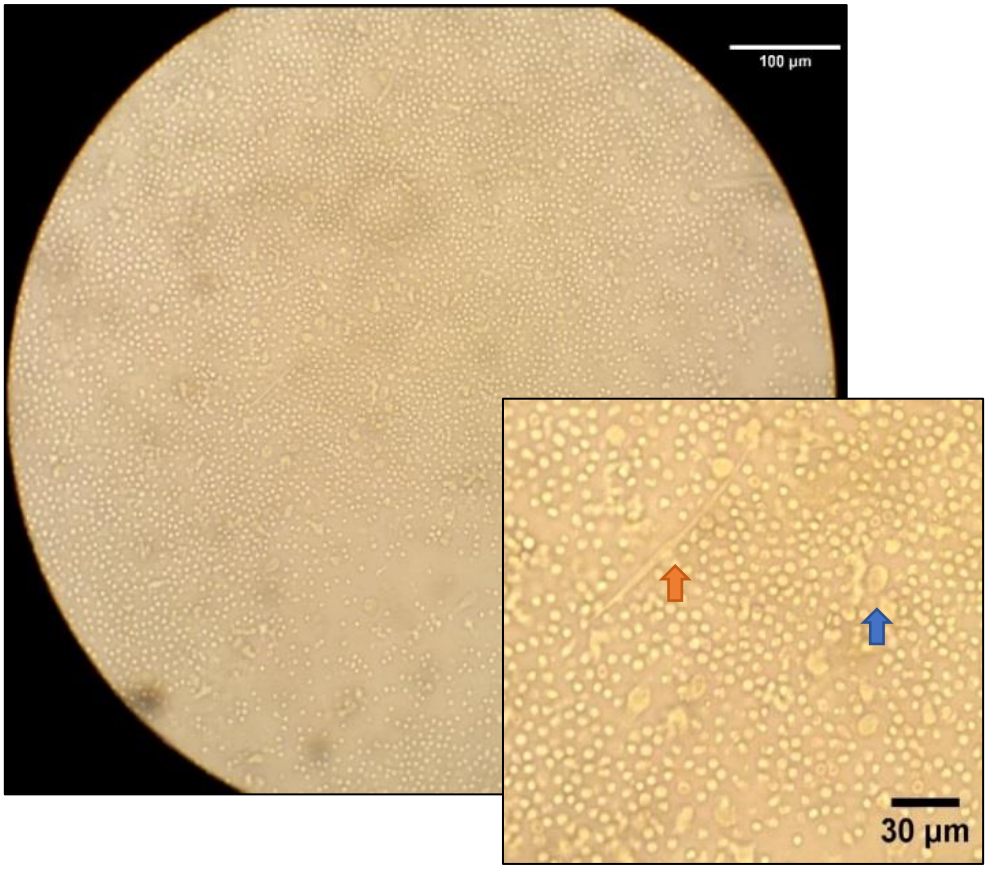

Figure 3.17 Example of NLCs with score 2.

Phase contrast image of CLL PBMCs (#3529) cultured over approximately 5 days, displaying a range of morphologies, from large oval shape (blue arrow) to elongated or spindle-shaped appearance (orange arrow). Here numerous NLCs are seen in each viewing field, scattered and in groups but with the absence of multi-layered clusters.

3.3.4.1.4 NLC Score 3+

This type of sample is considered as sample with fully developed NLCs. As shown in Figure 3.18, a very large number of NLCs can be seen broadly (large circle). On close inspection there were numerous cluster formations seen as multiple layers of cells, which make it difficult to distinguish the cells. The clusters consist of a very diverse group of monocytes/macrophages as well as lymphocytes. The clusters can be so big that it can be seen by the naked eye as small specs or spots on the plate (colonies). The samples with score 3+ are used for subsequent co-culture experiments.

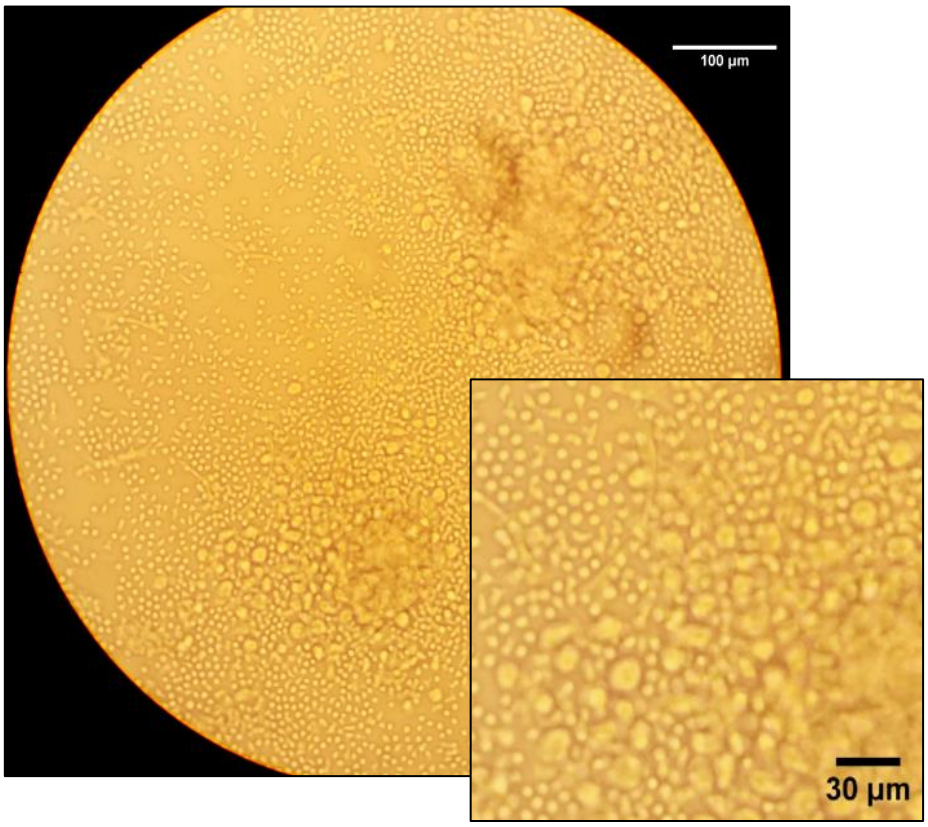

Figure 3.18 Example of NLCs with score 3.

Phase contrast image of CLL PBMCs (#3484) cultured over approximately 15 days, displaying a range of morphologies, from large oval shape to elongated or spindle-shaped appearance.

Using the NLC scoring system I carried out scoring all the CLL samples summarized in Table 3.3. It showed approximately half of all CLL samples had poor or no development of NLCs.

Table 3.3 Variation in generation of NLCs from all CLL samples studied

Category	No. of CLL samples examined	Proportion (out of 88 samples)
Well developed (3+)	24	27.3%
Moderately developed (2+)	18	20.5%
Poorly developed (1+)	43	48.9%
No NLC development (0)	3	3.4%
Total	88	100%

Samples with NLC score of 2 or 3 were therefore considered for the subsequent co-culture experiments, whereas those with 1 were left with morphology observations and phenotyping. Those with NLC score of 0 were unsuitable for any further experiments. To explain why this phenomenon was seen, I went back to the clinical data and performed some descriptive analysis.

3.3.4.2 Correlation of NLCs development with clinical features of the CLL samples

For this part of the study, a total of 88 CLL samples were used for NLC development, consisting of patients who gave re-bleeds (ie. Same patient gave more than one sample over time). The total number of samples that were not re-bleeds from the same patient was 65 and the summary of clinical information of these samples is displayed in Table 3.4. A more detailed view of the clinical data can be seen in Appendix Table 7.1.

Table 3.4 Summary of clinical features of non-repeat CLL case samples used in the study

Gender	Male	46
	Female	19
Age at diagnosis	Mean: 65.63	(95% CI: 62.33-68.93)
Prior therapy*	Yes	28
	No	36
WBC[#] (10^9/L)	Mean: 129.09	(95% CI: 105.60-152.59)
FISH[¶]	17p-	12/60
	11q-	11/60
	Tri 12	6/60
	13q-	18/60
	Normal	13/60
IGHV[Δ]	Mutated	14/26
	Un-mutated	12/26
Staging at the time of sample collection	A	22/60
	B	13/60
	C	25/60

*Prior therapy included steroid, chlorambucil, or fludarabine plus cyclophosphamide and rituximab.

[#]WBC (white blood cell count) was performed at the time of sampling.

[¶]FISH (fluorescence *in situ* hybridisation) was performed at or prior to sampling.

[Δ]IGHV status refers to somatic mutation in IGHV gene of CLL cells as compared with the gene sequence of the nearest germ-line using 2% as a cut-off.

Initial descriptive analysis of clinical information showed that there was a predominance of samples from males (>70%) over females (<30%) in this study, as well as more cases of mutated IGHV (M-IGHV) and un-mutated TP53 (Figure 3.19). The majority of cases (almost 50%) were of Stage C, followed by Stage A (31%) and Stage B (21%).

When categorising those treated and untreated, I grouped them into 'Untreated', 'Previously treated but not currently' and 'On current treatment'. As seen in Figure 3.19, almost 56% of cases in the study were untreated, almost 17% were previously on treatment but not on a current treatment and 27% were on treatment at the time of sample collection.

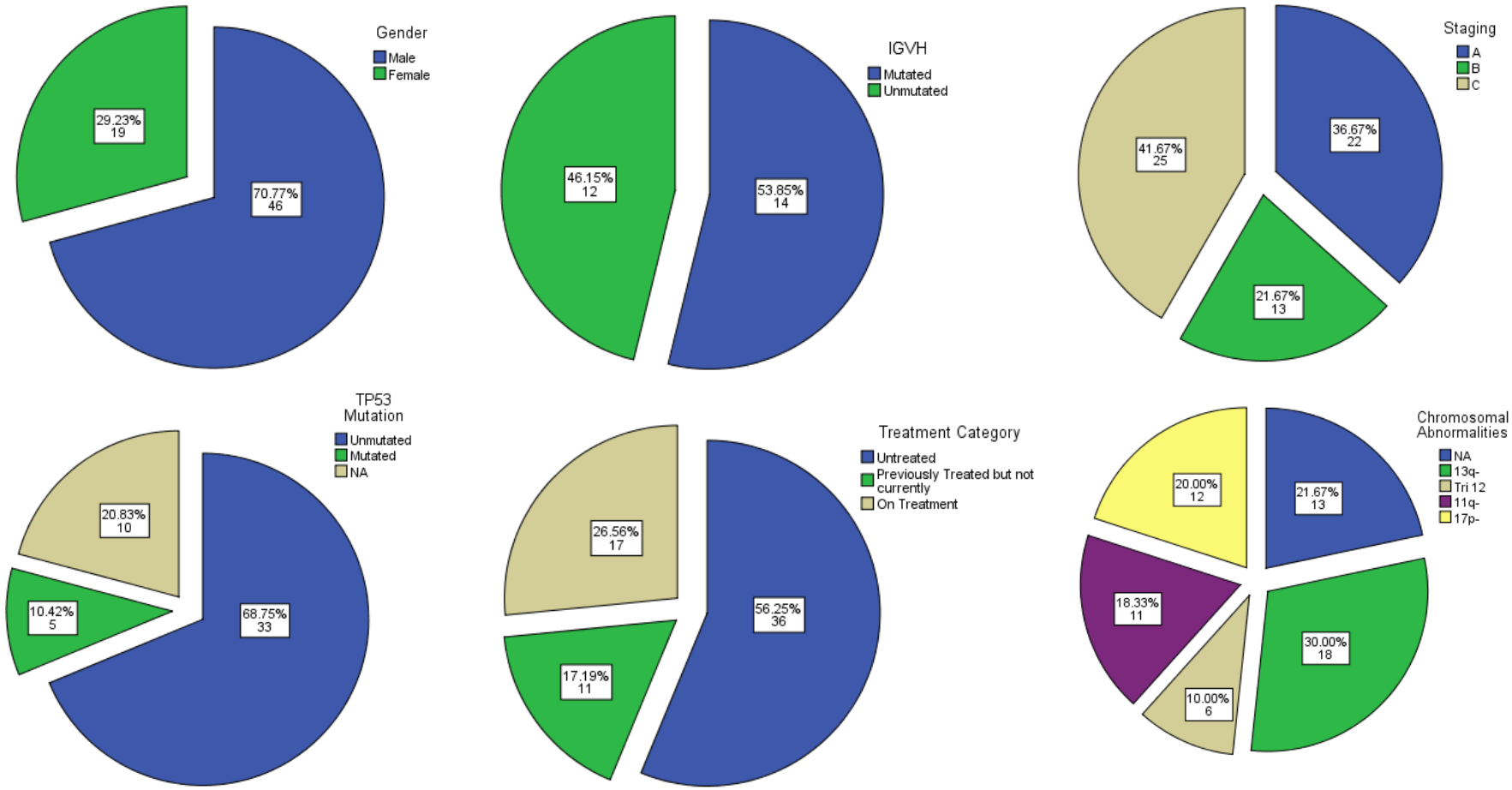

Figure 3.19 Summary of Clinical Data Analysis.

Percentage Distribution of cases based on Gender (top left), IGVH mutational status (top middle), Staging (top right), TP53 mutational status (bottom left), Treatment category (bottom middle) and Risk stratification based on chromosomal abnormalities (bottom right). Statistical Analysis and figures generated by SPSS 2.4

As seen in Figure 3.20, only 3 cases did not develop any NLCs (NLC Score 0) and combined with poor NLC Score (+), this gave just under 50% of all samples. Those that gave a Moderate NLC Score (++) accounted for about 20% of all cases and those that gave a High NLC Score (+++) accounted for about 30% of all cases (Figure 3.20 top left).

I then performed statistical analysis to see if there is a significant correlation between NLCs score and any of clinical features using Chi squared and Fisher-Freeman-Halton exact test. There was no significant trend seen when comparing the proportions of NLC Score distribution within IGHV mutational status (p=0.729), nor TP53 (p=0.259) and Chromosomal abnormalities (p= 0.175).

There was no trend seen with regard to NLC score distribution and treatment category with p=0.931 (Figure 3.20 top right).

When subdividing CLL samples according to the clinical stage, it appeared that samples with poor NLC Score (1+) covered just under half of Stage A and C but only 23% in Stage B (Figure 3.20, middle). Moderate NLC score (2+) samples accounted the most in Stage B cases (38%) followed by Stage C (28%) and finally Stage A (9%). High NLC score (3+) accounted the most in Stage A (45%), followed by Stage B (38%) and finally Stage C (16%). Interestingly, samples with the lowest NLC Score (0) were all in the category of Stage C (Figure 3.20, middle). This trend, however, was not significant using Fisher-Freeman-Halton exact test (p=0.54).

I wanted to find out if this pattern can be explained due to treatment, so I separated the samples into treated and untreated subgroups (See Appendix Table 7.2). The trend that was seen earlier was indeed replicated within untreated samples (Figure 3.20, bottom left) but not really seen with treated samples (Figure 3.20, bottom right). The NLCs score was inversely correlated with the clinical stage, which was statistically significant when analysed using Chi Squared test (p value <0.05).

Next, I wanted to see if there was a correlation between the amount of monocytes in circulation (i.e. in the PBMC) and the development of NLCs (i.e. NLC score). In order to answer this, I calculated and used the percentage of monocytes from the sum of absolute monocytes and lymphocytes for each PBMC samples used. As seen in Figure 3.21, there was no significant trend seen when comparing the percentage of monocytes in PBMC with NLC Score, nor with the mean percentage of monocytes in PBMC with NLC score.

Additionally, I analysed repeated samples (re-bleeds from same patients) to observe for any trends on NLC score with subsequent samples (See Appendix Figure 7.1). It is worth noting that generally with re-bleeds, it is usually taken before the start of treatment if not newly started. There were no significant trends seen with the NLC scores with repeat samples.

Figure 3.20 Summary of Clinical Data in the context of NLC Scores.

Distribution of cases based on NLC score (top left), NLC Score distribution based on treatment category (top right), Distribution of NLC scoring based on Staging (middle), NLC score distribution amongst samples that were Untreated (bottom left) vs Treated (bottom right) and their staging at the time of sample collection. The trend seen in staging with NLC Score 3 amongst untreated group was analysed using Chi Square test after subdividing the data into Low (0, 1, 2) and High (3) and was found to be statistically significant with p value < 0.05. Statistical Analysis and figures generated by SPSS 2.4.

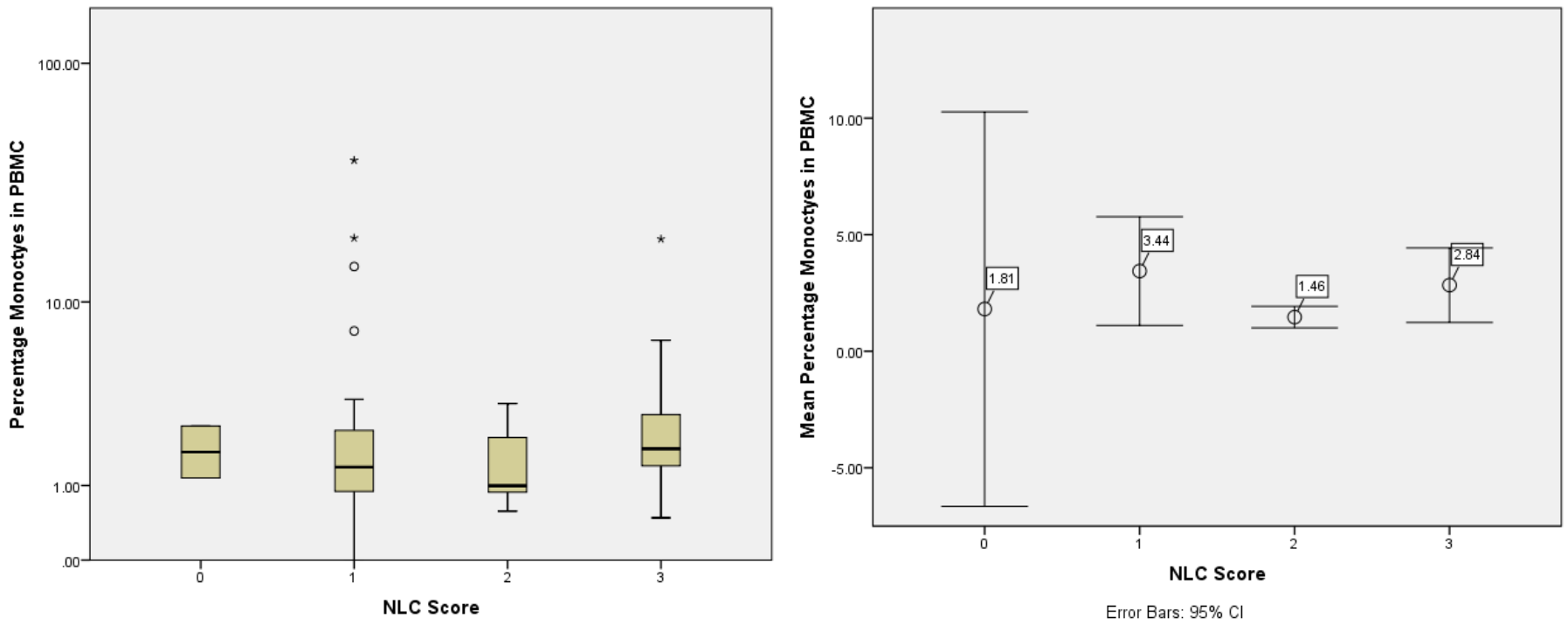

Figure 3.21 Summary of NLC Scores with levels of circulating monocytes.

Comparison of NLC scores with percentage monocytes in PBMC (left) and mean percentage monocytes in PBMC (right). With the percentage monocytes in PBMC (left) the y-axis is in log scale and the dark lines are Median average values. Using One Way ANOVA, there was no significant difference between the mean values (right) from the different groups. Statistical Analysis and figures generated by SPSS 2.4

3.3.5 Effects of co-culture on CLL cells

3.3.5.1 Preparing co-culture experiments

To confirm that NLCs exert cytoprotective effect on CLL cells when in co-culture, as previously reported (Burger et al. 2000), co-culture experiments were to be performed by culturing thawed autologous CLL cells with the NLCs developed from the same CLL samples. Viability of CLL cells with and without co-culture on the established NLC layer was quantified by FACS analysis (described in Methodology).

To prepare the NLC monolayer, the NLCs were developed as previously mentioned until they reached their plateau phase. Figure 3.22 provides an example what NLCs look like before co-culturing with autologous CLL cells (A) and during co-culture with CLL cells (B). The CLL cells were removed by gentle pipetting so as to leave behind the NLC monolayer (A). On close view it can be seen that minimal or no CLL cells remained. Given that the monolayer was prepared, autologous CLL cells were thawed and cultured at a density of $3x10^6$/ml.

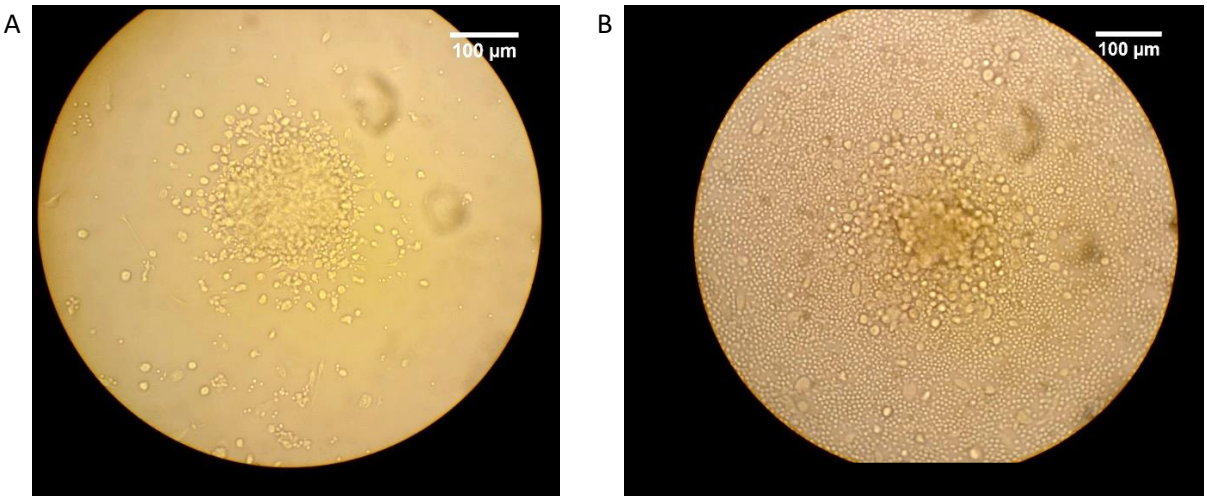

Figure 3.22 Phase contrast images of co-culture of CLL cells with NLCs.

Phase contrast images (#3484) of a typical visual field of a culture plate where NLCs were developed for about 15 days at low magnification. CLL cells were washed off, leaving behind the adherent NLCs at low magnification (**A**), autologous CLL cells were added (Day 4 after co-culture, **B**).

3.3.5.2 Analysis of spontaneous cell death

When preparing the co-culture experiments to evaluate effects of co-culture of CLL cells with NLCs, I also prepared both types of cells cultured alone so that I can not only directly compare the viability of the co-cultured CLL cells to that of CLL cells cultured alone, but also monitor how the NLCs behave in the absence of CLL cells. Therefore, I prepared wells on multi-well plates with CLL+NLC, NLC alone and CLL alone and observed for morphology and viability measured over 4 days. By morphological observation under the phase contrast microscope it was apparent that the CLL cells maintained their healthy, glowing appearance upon co-culture when compared with CLL cells cultured alone (Figure 3.23).

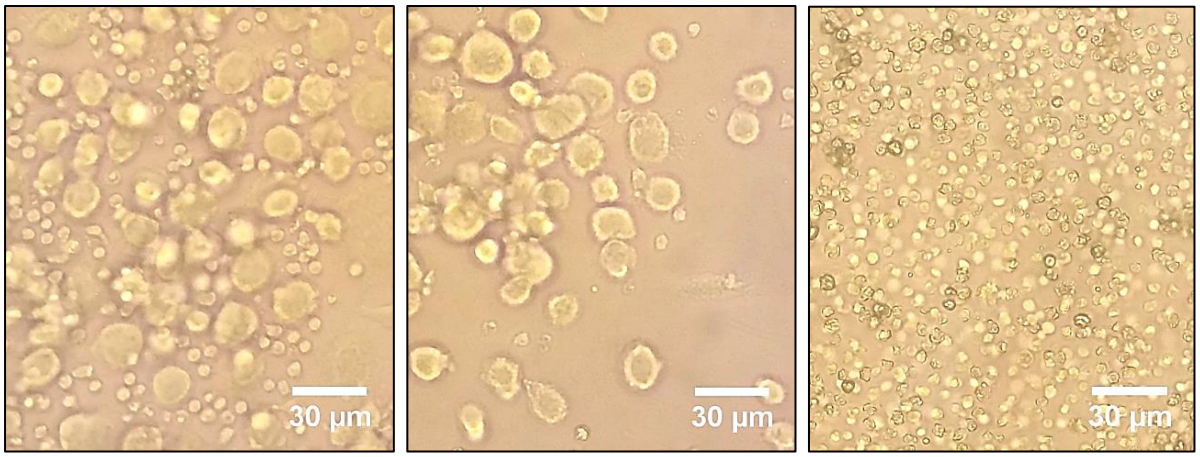

Figure 3.23 Co-culture conditions maintained healthy, glowing appearance of both NLCs and CLL cells when compared to their respective cells cultured alone.

Phase contrast images of co-cultured NLCs and CLL cells (3484) on Day 6 (left panel), NLCs cultured alone (middle panel) and autologous thawed CLL cells cultured alone (right panel). Fresh PBMCs was cultured as described till the fully developed NLCs appeared at approximately Day 14. Cryopreserved autologous CLL cells were then thawed and cultured with the NLCs.

Interestingly, the NLCs also displayed a healthy, glowing appearance when in co-culture with CLL cells as compared with NLCs cultured alone (Figure 3.23, compare right panel to middle panel). The NLCs cultured alone appeared to be dislodged from the groups/clusters and some NLCs seemed to lose glowing appearance. Eventually the NLCs also started to disintegrate. It was not possible to quantify the viability of the NLCs by flow cytometry due to the difficult and inefficient method of harvesting them form the culture plate. I therefore focused on analysis of cell death of CLL cells harvested from both culture conditions by flow cytometry.

As shown in Figure 3.24, in contrast to CLL cells cultured alone, the CLL cells in co-culture retained better viability throughout the 4-day period of observation. This coincided with what was seen under phase contrast microscope. In total, 8 CLL samples were used and the difference in viability between CLL cells in co-culture and cultured alone was statistically significant from Day 2 with a p value of less

than 0.05. Therefore, co-culturing CLL cells with NLCs protected them from spontaneous death, a result in agreement with previous reports (Burger et al. 2000; Tsukada et al. 2002).

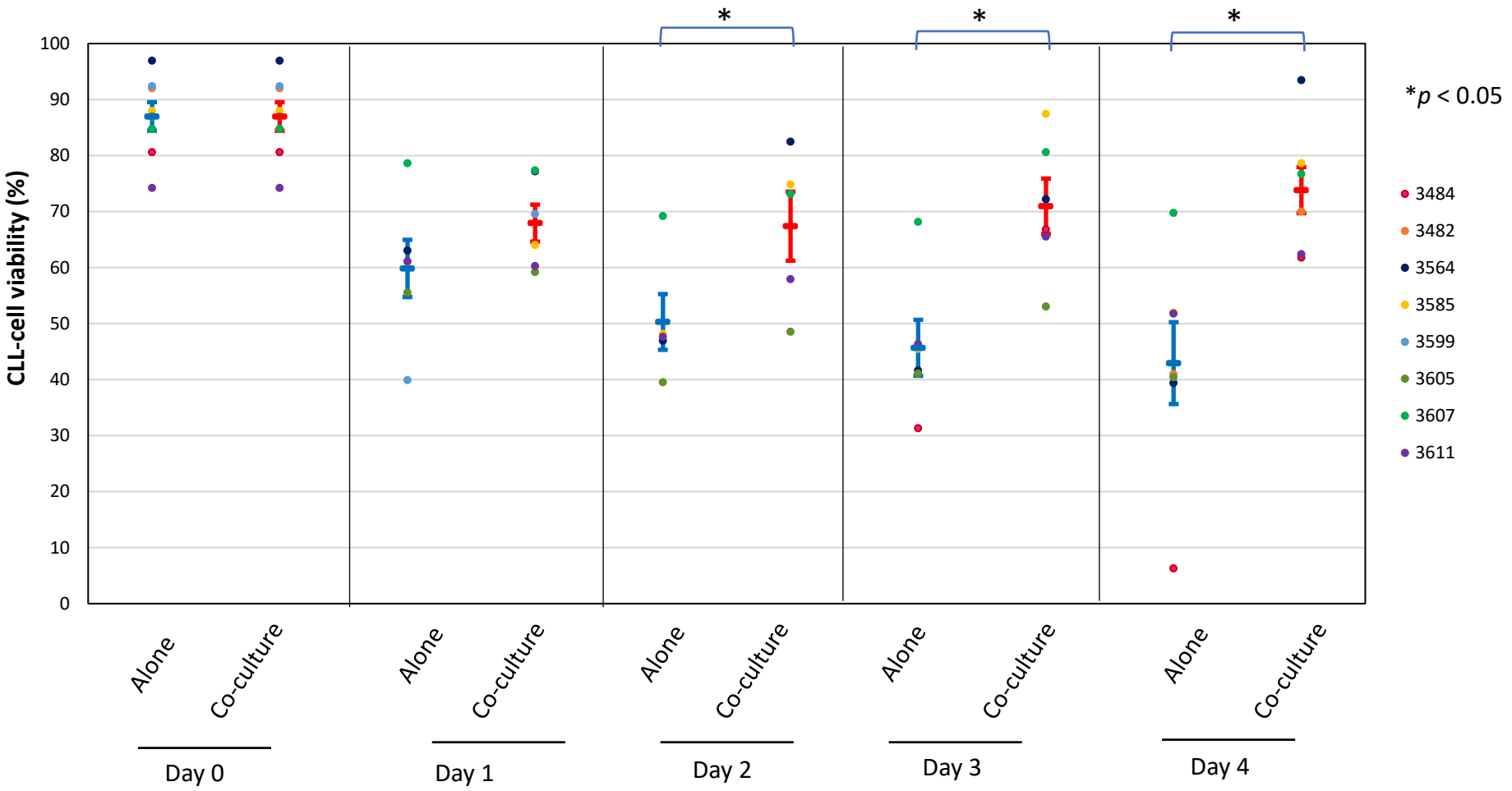

Figure 3.24 Co-culture with NLCs protected CLL cells against spontaneous cell death.

Cryopreserved CLL cells were thawed and co-cultured with NLCs as described in Methods. CLL cells cultured alone were used a control. Viability of CLL cells was monitored over 4 days by flow cytometry following Annexin V/ PI staining. Each data point represents mean ± SEM of 8 independent experiments using 8 different CLL samples. * refers to p value of <0.05 which is considered statistically significant.

3.3.5.3 Levels of CCL3 and CCL4 in the culture medium

It has previously been reported that NLCs induce CLL cells to secrete the T-cell chemokines CCL3 and CCL4 into the culture medium where they can be measured by ELISA (Burger et al, 2009). I therefore also measured levels of CCL3 and CCL4 in the supernatant collected from co-cultures of CLL cells with NLCs.

As seen in Figure 3.25, the levels of CCL3 (blue) and CCL4 (red) were increased from day 5 and reached a plateau by day 10, which continued to day 13. This result was similar to what has been reported (Burger et al. 2009b).

3.3.5.4 Expression of sIgM and sIgD

It has also been shown that CLL cells co-cultured with NLCs displayed significant reduction in surface expression of IgM and IgD, which may indicate that NLCs can engage B cell receptors (BCR) of CLL cells (Ten Hacken et al, 2016). I therefore monitored expression of surface IgM (sIgM) and IgD (sIgD) in CLL cells co-cultured with NLCs on days 0, 8/9 and 13/14 by flow cytometry.

As seen in Figure 3.26 (top), the average sIgM expression appeared to have been quite low at the start, then rose by two-fold on Day 8/9 of co-culture and then fell back to base-line on Day 13/14. Overall the changes in sIgM was not significant and there was no consistent trend of either direction (i.e. increase or decrease). The average sIgD expression was quite high at initial stage on Day 0, in contrast to sIgM (Figure 3.26 bottom). At the subsequent time points the levels of sIgD seemed to have decreased over the 14 days. Although a clear trend was seen, the changes were not statistically significant.

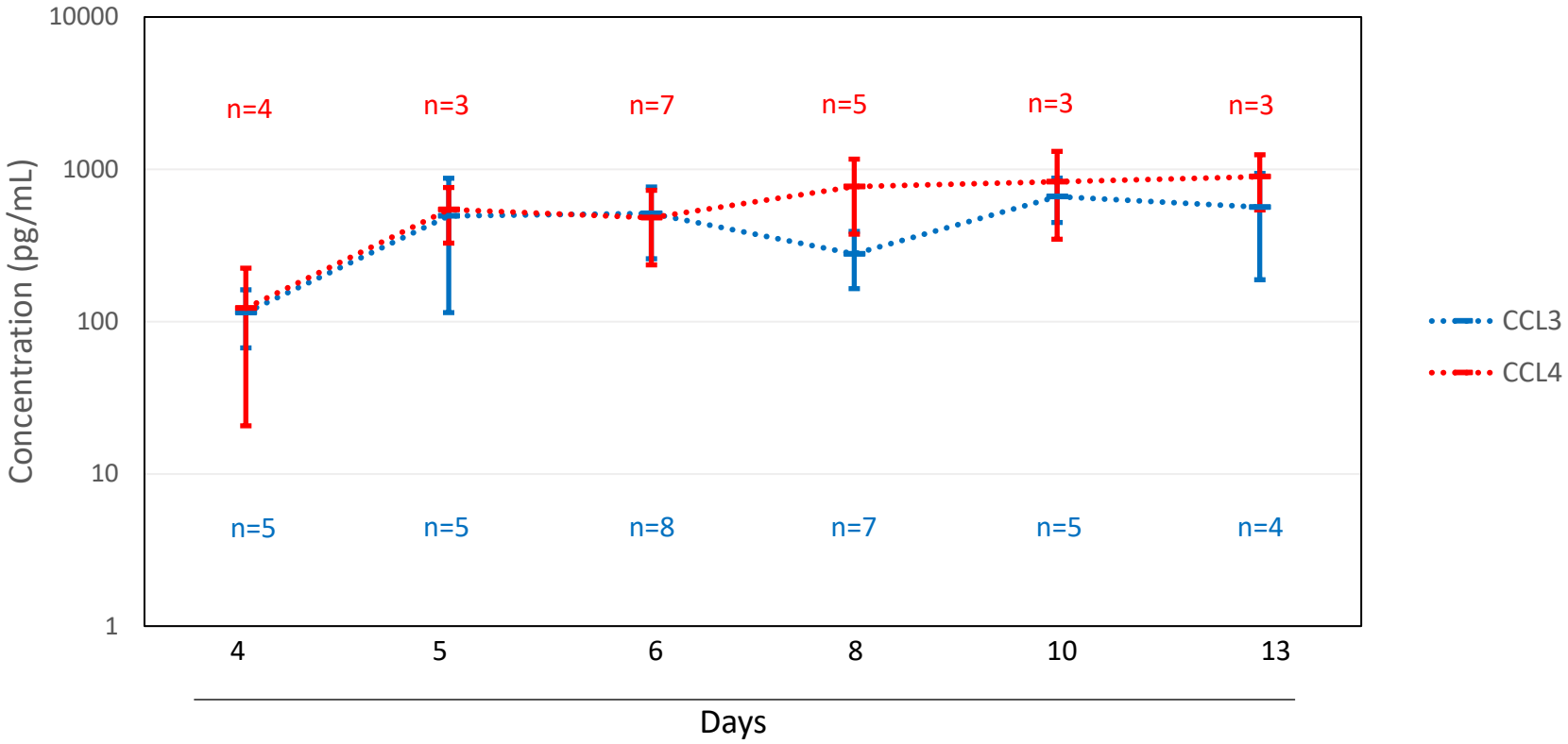

Figure 3.25 CCL3 and CCL4 protein expression in CLL-NLC cultures.

CLL PBMCs were cultured for up to 13 days with concurrent development of NLCs and supernatant samples at the indicated time points were collected for analysis of CCL3 (blue line) and CCL4 (red line) by ELISA, as described in Methods.

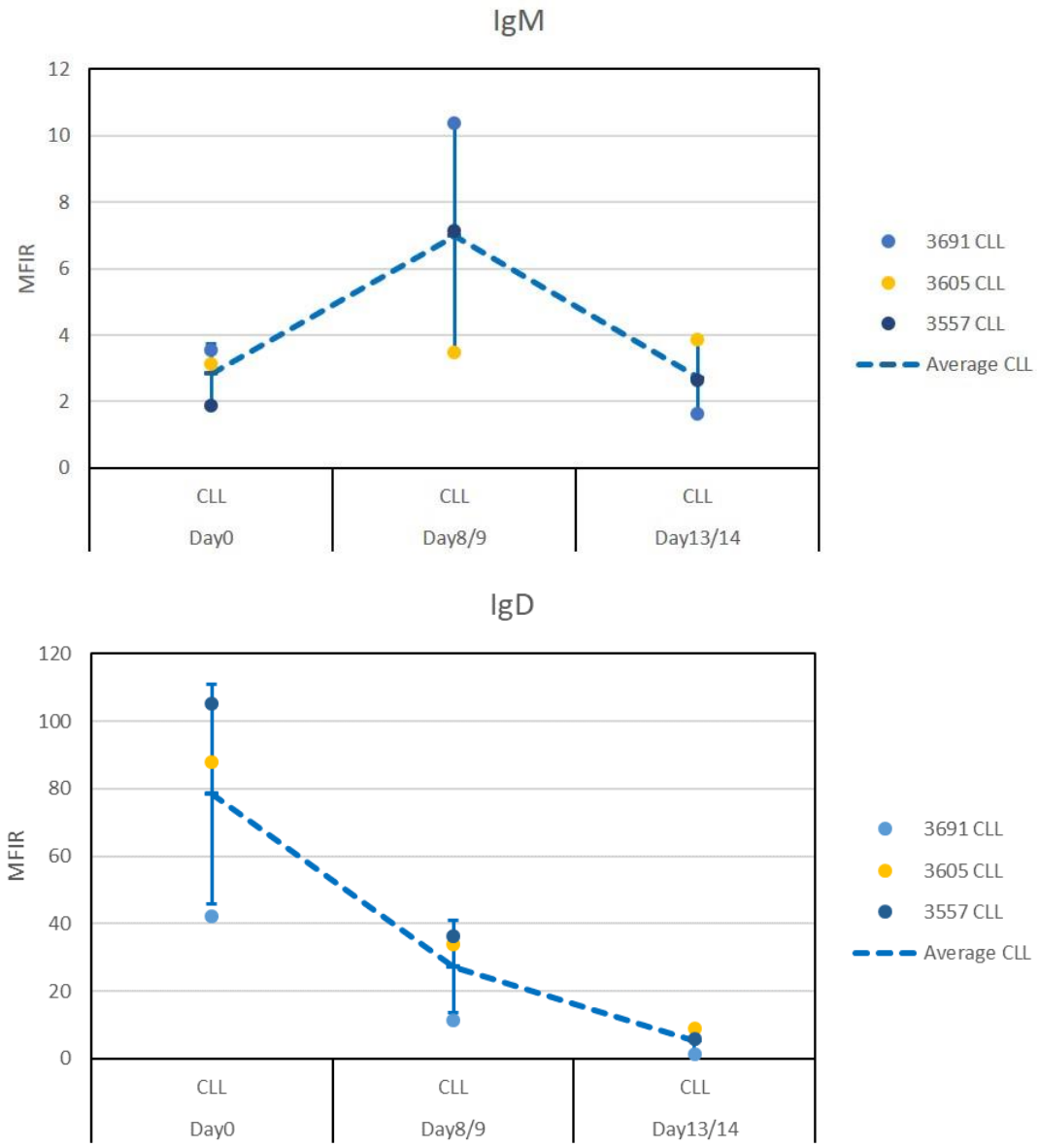

Figure 3.26 Surface expression of IgM and IgD of CLL cells cultured with NLCs over 14 days.

Surface expression of IgM (top) and IgD (bottom) of CLL cells cultured with NLCs over 14 days. Fresh PBMCs was cultured as described for up to 14 days. Surface IgM and IgD of CLL cells was monitored three times during the 14 days by flow cytometry as described. Data represent mean ± SD of independent experiments using 3 different CLL samples. Mean fluorescence intensity ratio (MFIR) of CLL cells stained with respective isotype control antibodies (Control) was also shown as mean ± SD.

Taken altogether, a pro-survival effect by NLCs on CLL cells was seen compared to CLL cultured alone. There was a trend of rising CCL3 and CCL4 in the supernatant of PBMC cultures till Day 5 where they remained high till the end of the experiment. sIgM of CLL cells did not give a clear trend with the presence of NLCs, however, sIgD had a trend of decreasing expression in the presence of NLCs.

3.4 Discussion

In this chapter, I confirmed and expanded the previous finding that NLCs can be developed using fresh PBMCs from CLL patients under standard culture conditions. The optimal cell density for development of NLCs I found was 10 x 10^6 cells/ml. This is consistent with conditions described previously by some researchers (Nishio et al. 2005). However, others have reported to develop NLCs using much lower cell densities of CLL PMBCs (Filip et al. 2009; Jia et al. 2014; Nishio et al. 2005; Polk et al. 2016). Use of higher cell densities to develop NLCs was also being reported (Burger et al. 2000). It thus indicates that, although the cell density of 10 x 10^6/ml was an optimal concentration of cells used to develop NLCs under the culture conditions in my study, it is not a critical factor in determining whether NLCs can be developed *in vitro*.

My description of NLCs detailing their pleomorphism (ranging from large oval, tail-like projections, spindle appearance, elongated, group/cluster formation, etc.) independently confirmed the dynamic process of NLCs development. The early description of NLCs in literature, e.g. being 'oval/adherent' by (Burger et al. 2000) or 'large/round/adherent' (Tsukada et al. 2002) provided a basic description of morphological features of NLCs. In my study, I used the MGG staining technique and produced images with more detailed cellular structure and shape of NLCs, revealing the vibrant process of differentiation from monocytes to macrophages. For example, the descriptions of large oval adherent and tail-like projections suggests that NLCs exhibited features of cell motility, similar to motile cells such as fibroblasts (Herant & Dembo 2010).

The time course observation that I recorded revealed that most CLL PBMCs samples present with distinguishable NLCs as early as 2 days after culturing and NLCs reach their plateau by Day 8-12. I performed my co-culture experiments as soon as NLCs reached plateau. This is in contrast with other researchers who performed their experiments at Day 14 (Burger et al. 2000; Gautam et al. 2016; Jia et al. 2014), which may explain the different results observed between the studies. Reassuringly, one of the earlier studies also mentioned the appearance of the NLCs after 3 days in culture, which increased in number in the following days and finally formed a layer of large, round adherent or fibroblast-like cells after 14 days in culture (Burger et al. 2000). This description was entirely consistent with what I have observed in my study.

The most striking observation I made was the wide variation in developing NLCs from primary CLL PBMC samples and this variation applied to both the kinetics and magnitude of NLCs generated. Although it has been previously reported that not all CLL PMBC samples developed NLCs (Jia et al, 2014), the extent of the variation prompted me to devise an NLC score system to assign an NLC score

for each and every samples used. To investigate if the NLC scores correlate with any clinical features of CLL samples, I collected available clinical information for all the samples used. Over the course of over 4 years, 88 samples were used for this chapter, 65 of which were samples not re-bled from the same patient. The clinical data analysis showed that the samples were primarily from male patients, almost half of samples from treatment naive patients, and majority of the patients with a Stage C progressive disease. Most of the samples had 13q- or no chromosomal abnormalities, accounting to over 50% of the cohort. The clinical information is thus very similar to the general population of CLL patients (Baliakas et al. 2019). The samples used in my study is thus a representative cohort of CLL patients.

When subgrouping CLL samples based on the NLC scores, I did not find any correlation between NLC score and IGHV mutation, TP53 mutation, treatment history nor chromosomal abnormalities. However, when analysing clinical staging I observed that samples with increasing NLC Scores inversely correlated with clinical staging of the disease. This inverse correlation was statistically significant in CLL samples from untreated patients. The exact cause is yet unknown and would thus require further work to explain.

Previous studies have reported the correlation between number of NLCs and clinical outcome of disease. In a study where authors examined the development of NLCs from CLL PBMC samples from 65 treatment naïve patients, they found that various number of NLCs was developed in 58 samples (Filip et al., 2009 and 2013). Among the samples that have developed NLCs, 49 CLL samples developed more than 20 NLCs/mm^2 and 9 samples developed fewer than 20 NLCs/mm^2. They found that the number of NLCs was positively correlated with serum level of β2-microglobulin and absolute monocyte count (AMC). However, no correlation was found between number of NLCs and clinical stage of the disease, whole blood count, lymphocyte count, or CD38 and ZAP70 expression. Interestingly, during a 6-year follow-up a shorter overall survival was observed in patients whose CLL samples produced a higher NLC count (i.e. >20 NLCs/mm^2), albeit not statistically significant (Filip et al., 2009 and 2013). Higher number of NLCs was also reported to correlate with shorter treatment-free survival and shorter overall survival (Boissard et al. 2016).

Meanwhile, higher AMC has been reported in CLL patients compared to normal healthy controls (Maffei et al. 2013). Higher AMC has been linked to progressive disease and early treatment in CLL (Herishanu et al. 2013, Friedman et al. 2016).

In my study, however, there was no significant correlation between the blood monocyte count and the NLC scores, which is in disagreement with the findings from the previous studies (Filip et al., 2009 and 2013). This may be due to the fact that the studies by Filip et al. (2013a) recorded the amount of

NLCs as absolute upon counting rather than categorising into NLC scores. Perhaps if I were to use meticulous methods to record absolute counts of NLCs, I may be able to perform accurate statistical analysis to correlate with absolute monocyte count. The NLC scoring could possibly be refined to include absolute NLC count.

Regarding the phenotypic marks of NLCs, I was able to confirm the expression of CD14, CD68 and CD163 in NLCs and CD19 CLL cells, respectively, by immunofluorescence microscopy. CD14 and CD68 were exclusively present in NLCs, localised within the cytoplasm near the nucleus. They also had variable levels of expression during the different phases of NLC development. CD163 was also present exclusively in NLCs and localised throughout the cytoplasm depicting the actual shape of the cells. It was also present throughout all phases of development of NLC. This suggests that CD163 may be a potential marker for NLCs *in vivo*. This notion is in agreement with the finding from a study investigating the relationship of NLCs with disease progression of CLL (Boissard et al. 2016a), where CD163 was considered to be the most reliable marker for NLCs as compared to CD68. The above result was also consistent with reports from others that NLCs express CD68, CD163 and CD14 (Boissard et al. 2015a; Fiorcari et al. 2015; Marchesi et al. 2015). Other studies had also shown that the expression of CD163 and CD68 was detected in monocytes/macrophages in the spleen (Nagelkerke et al. 2018; Ysebaert et al. 2010) and lymph nodes (Giannoni et al. 2014; Ysebaert et al. 2010). This suggests that what is seen *in vitro* of NLCs derived from CLL PBMCs culture is also relevant *in vivo* within the tumour microenvironment such as lymph nodes and spleen. I have observed the variation in levels of CD68 and CD14 during the different phases of development of NLCs. The levels of CD68 and CD14 expression may influence differentiation of the NLCs, particularly for the subsequent polarisation towards M2-type macrophages, as suggested by Gu et al. (2019). Therefore, the biological significance of the variation in expression of CD68 and CD14 by NLCs is still unclear and merits further investigation.

The co-culture experiments I have performed clearly demonstrated the protective effects of NLCs on CLL cells, which is entirely in agreement with the findings reported by numerous studies (Burger et al. 2000; Filip et al. 2013b; Nishio et al. 2005; Tsukada et al. 2002). My co-culture experiments predominantly used CLL samples with an NLC Score of 2 or 3. Co-cultured NLCs and CLL cells, as well as their respective counterparts cultured alone, were closely monitored under light microscope for morphologic changes. Indeed, compared with their counterparts cultured alone, CLL cells co-cultured with NLCs looked more viable, as indicated by their healthy-looking appearance. One study, however, reported that samples with lower viability developed NLCs faster and those with higher viability failed to develop NLCs in an experiment using 5 samples (Jia et al. 2014), which was not observed in my study.

Unexpectedly, compared to NLCs cultured alone, NLCs co-cultured with CLLs also displayed healthy-looking appearance. This suggests that CLL cells could also actively influence the wellbeing of NLCs. As of yet, there have been no report in the literature describing the effect that CLL cells have had on NLCs *in vitro*. This effect clearly merits further study as it could potentially unravel how CLL cells participate in shaping the microenvironment into a safe haven for the leukemic cells.

I also examined the levels of CCL3 and CCL4 in the medium of the co-cultures as it was shown that NLCs can induce CLL cells to express CCL3 and CCL4 and that increased levels of CCL3 and CCL4 were detected in the supernatant collected from medium of CLL PBMCs cultures over time (Burger et al., 2009; Zucchetto et al. 2009). The increased levels of CCL3 and CCL4 was also linked to unfavourable clinical outcome of CLL patients (Hartmann et al. 2016; Sivina et al. 2011). Solid cancers such as colon cancer, as well as local reaction to pathogenic challenge and wounding have been shown to secrete CCL3 and CCL4 which lead to recruitment of macrophages (Pollard 2004).

I also investigated the effect of NLCs on CLL cells regarding changes in surface expression of IgM and IgD of co-cultured CLL cells. Decrease in levels of sIgM and sIgD could be a result of activation of BCR signalling pathway, which plays a critical role in CLL biology (Ten Hacken et al. 2016). My results showed a continuous decrease in the level of sIgD in co-cultured CLL cells over the 14 days of co-culture, although the decrease is not statistically significant. In contrast to sIgD, changes in sIgM did not occur in a clear trend. Instead, overall expression of sIgM of CLL cells remained low throughout 14 days of co-culture. My results thus were in contradiction to a previous report where a significant decrease in both IgM and IgD of CLL cells was seen during a 14-day co-culture with NLCs using 4 CLL samples from patients with un-mutated IGHV (Ten Hacken et al. 2016). This discrepancy could be because of a low number of samples examined in my study. It is thus important that a greater number of randomly selected CLL samples should be used to get a clearer picture as to whether NLCs affect the expression of sIgM and sIgD in CLL cells.

In summary, after I optimised conditions to develop NLCs from fresh CLL PBMCs, I have confirmed many features of NLCs in terms of their morphology, expression of phenotypic markers and biological effects of on CLL cells. In addition, I made an important observation on the wide variation in both temporal and spatial terms in development of NLCs between individual CLL samples. This variation may well reflect the heterogeneous nature of the disease. This observation is thus relevant to the *in vivo* interaction between NLCs and CLL cells in the tumour microenvironment such as lymph nodes, bone marrow and spleen. To better understand the molecular mechanisms mediating the *in vivo* interactions of NLCs with CLL cells, further study is required to understand how NLCs and CLL cells cross-communicate each other at the level of the gene expression.

One further point to make is that study of NLCs requires continuous supply of fresh CLL PBMCs samples. Given the difficulty experienced in obtaining fresh CLL samples on a regular basis and the laborious, time-consuming techniques used to prepare the NLCs for subsequent experiments, together with the considerable variation in generating NLCs from CLL PBMC samples, there is clearly a need to explore the use of a cell line model of NLCs. In the next chapter, I will therefore describe the development of a cell line model of NLCs.

4 Development of a cell line model using THP-1 cells to mimic the pro-survival effects of NLCs on CLL cells

4.1 Introduction

I have shown in the previous chapter that the interaction between NLCs and CLL cells is a complex process which clearly impacted on the survival of CLL cells. Better understanding of this process is important as it may shed light to how CLL cells evade apoptosis within the tissue microenvironment via the interaction with NLCs and eventually develop resistance to therapies. However, I have also shown that there was a huge variation in the amount of NLCs generated from individual CLL samples. Among the 88 CLL samples I used in the previous part of the study, only about half of the samples developed adequate amount of NLCs that can be used for the subsequent co-culture experiments. Although this variation was not overly surprising given the heterogeneous nature of the disease, it caused a significant problem to me in obtaining consistent and reproducible results. This problem, together with some practical constraints such as entirely relying on supply of fresh CLL blood samples and continuous maintenance of primary cell cultures (for up to 2 weeks for each sample), prompted me to look for a cell line model of NLCs so that I can use it to perform experiments consistently and efficiently.

Cell lines have been used by cancer research scientists as model systems of cancer cells ever since the first human cancer cell line (i.e. Hela cells) was established in the 1950s (Masters 2002). Discoveries made from cell line-based research have complemented that from studies using tumor cells/tissues and animal models for different types of cancers. Together, they advanced our understanding of the biology of cancer and contributed to development of new treatment of cancer. Therefore, cell lines are valuable tool for discovery. However, cell lines have major limitations, namely the genetic instability acquired during long term culture, selective growth of subclones of cancer cells caused by culture condition and lack of interaction of components within the tumour microenvironment (Gazdar, Gao & Minna 2010; Kaur & Dufour 2012). Additional differences in other characteristics are summarized in Table 4.1. Therefore, with the advantages and limitations of cell lines in mind I set out to search a suitable cell line that can be developed as an *in-vitro* model for NLCs in my study.

Table 4.1 Brief summary of characteristics of primary cells vs cell Lines

Characteristics:	Primary Cells	Immortalized Cell Lines
Lifespan	Limited	Infinite
Resemblance of tissue characteristics	Good	Partial
Genetic mutations/Modifications	Low	High

Since NLCs are monocyte derived macrophages, I focused my search on cell lines of monocytic origin.

4.1.1 Choice of human monocytic cell lines

Monocytes are circulatory cells from myeloid origin that when migrating from circulation to tissues, can develop into macrophages or dendritic cells (Chanput, Peters & Wichers 2015). They serve three main functions in the immune system, namely phagocytosis, antigen presentation and cytokine production. The cell lines THP-1 and U937 are of monocytic origin that can be differentiated into various types of macrophages (Chanput, Peters & Wichers 2015).

4.1.1.1 THP-1 cell line

The THP-1 cell line is derived from leukemic cells from a patient with acute monocytic leukemia, with the cell line established in 1980 (Chanput, Peters & Wichers 2015; Tsuchiya et al. 1980). THP-1 cells retain morphological and differentiation properties of primary monocytes and macrophages. They appear in a large, round single-cell morphology and express distinct monocytic markers (Chanput, Peters & Wichers 2015; Tsuchiya et al. 1980). They can be differentiated into macrophages with the addition of phorbol 12-myristate 13-acetate (PMA). They grow in suspension and do not adhere to surface of the plastic culture plates/flasks (Chanput, Peters & Wichers 2015; Takashiba et al. 1999; Tsuchiya et al. 1980).

THP-1 cells have relatively homogenous genetic background, resulting in fewer changes in cell phenotype (Chanput, Mes & Wichers 2014; Chanput, Peters & Wichers 2015). Their average doubling time is around 35-50 h (Chanput, Mes & Wichers 2014). The growing rate in complete RPMI medium is much higher as compared to that of primary PBMC-derived monocytes (Chanput, Mes & Wichers

2014). There is no report for presence of infectious viruses in the THP-1 cells, making them relatively easy and safe to use (Chanput, Mes & Wichers 2014). It was reported that this cell line can be cultured *in vitro* for up to 25 passages (approximately 3 months) with no detectable changes in cell phenotype and function (Chanput, Mes & Wichers 2014). The availability of primary PBMC-derived monocytes is often limited and these monocytes are not suited for long-term storage in liquid nitrogen (Tedesco et al. 2018). THP-1 cells, however, can be stored for a number of years following appropriate storage protocol, without any obvious effects on monocyte-macrophage features and cell viability (Chanput, Mes & Wichers 2014). Co-cultivation of THP-1 cells with other cell types has been reported for use as cell line models to mimic *in-vivo* situation (Chanput, Mes & Wichers 2014).

4.1.1.2 U937 cell line

The U937 cell line is derived from human myeloid leukaemia cells that was isolated from the histiocytic lymphoma of a 37-year-old male patient (Chanput, Peters & Wichers 2015). Similar to THP-1 cells, U937 cells also exhibit many features of monocytes, differentiate into macrophages with typical morphology and characteristics (Chanput, Peters & Wichers 2015; Mendoza-Coronel & Castanon-Arreola 2016). It is used to study the behaviour and differentiation of monocytes, as U937 cells can be induced to differentiate in response to a number of stimuli (Chanput, Peters & Wichers 2015; Rots et al. 1999; Strefford et al. 2001).

Similar to THP-1 cells, U937 cells can also be cultured *in vitro* for up to passage 25 or higher (Chanput, Peters & Wichers 2015). Unlike THP-1 cells originated from blood monocytes with less differentiation characteristics, U937 cells are of tissue origin, thus maintain more differentiation features (Chanput, Peters & Wichers 2015). For example, U937 cells can be induced to differentiate into macrophages with the use of 1,25-dihydroxyvitamin D_3 (VD_3 at 100nM) or 12-O-tetradecanoylphorbol-13-acetate (TPA at 20ng/ml) (Chanput, Peters & Wichers 2015).

Other cell lines with similar properties to THP-1 and U937 cells include ML-2, HL-60 and Mono Mac 6 cells, but there are far fewer reported studies using them (Chanput, Peters & Wichers 2015).

Given the information described above, together with the fact that far more studies were published using THP-1 cells than U937 cells and that THP-1 cells closely resemble primary monocytes, I decided to use THP-1 as the cell line of choice in an attempt to mimic NLC behaviour.

4.1.2 PMA vs VD_3 for chemically differentiating the cell line monocytes to macrophages

PMA inhibits the growth and allow differentiation of THP-1 and U937 cell line in dose dependent pattern. PMA does this by activation of Protein Kinase C (PKC) because it mimics the physiological Diacylglycerol (DAG) which is a PKC activator (Chang et al. 2012; Schwende et al. 1996). PKC comprises of a series of kinases that are involved in the regulation of cell proliferation, differentiation, and other cellular functions (Schwende et al. 1996).

High concentrations of phorbol ester results in downregulation of certain isoforms of PKC and decreased activity of PKC so this will lead to downregulation of certain transcriptional factors (Schwende et al. 1996).

According to one study, THP-1 responded better with PMA with an almost complete arrest in proliferation but VD3 was less effective with unchanged division up to 48h (Schwende et al. 1996). THP-1 cells incubated with PMA became adherent and developed a macrophage-like appearance but not with exposure to VD3 (Schwende et al. 1996). THP-1 was able to phagocyte target foreign bodies and the phagocytic activity was enhanced with PMA and VD3-differentiated cells. PMA-differentiated cells showed almost 2-fold higher phagocytic activity than those with VD3 (Schwende et al. 1996).

Based on literature, $0.5x10^6$/ml of THP-1 monocytes fully differentiated into macrophages after 48h incubation at minimal concentration of 100ng/ml of PMA, resulting in macrophages with a phagocytic capacity for latex beads and expressing cytokine profiles that resembled PBMC monocyte-derived macrophages (Chanput, Mes & Wichers 2014; Chanput, Peters & Wichers 2015).

Given the information, I decided to use PMA as the agent of choice to chemically differentiate the THP-1 cell lines to macrophages for the study.

4.1.3 Polarization of THP-1 macrophages

THP-1 cell lines have been shown to differentiate into macrophages using phorbol 12-myristate 13-acetate (PMA) (Aldo et al. 2013; Chang et al. 2012; Chanput et al. 2013; Daigneault et al. 2010; Genin et al. 2015; Kohro et al. 2004; Park et al. 2007; Ramprasad et al. 1996; Schwende et al. 1996). Once differentiated with PMA (M0), they do not proliferate further and adhere to the surfaces of culture plates (Aldo et al. 2013; Chanput et al. 2013; Chanput, Mes & Wichers 2014; Chanput, Peters & Wichers 2015; Daigneault et al. 2010; Forrester et al. 2018; Genin et al. 2015; Kohro et al. 2004; Park et al. 2007; Qin 2012; Ramprasad et al. 1996; Schwende et al. 1996; Takashiba et al. 1999; Tsuchiya et al. 1980).

When exposed to interferon gamma (IFN-γ) and lipopolysaccharide (LPS), the M0 cells differentiate to M1 phenotype (Chanput et al. 2013; Genin et al. 2015; Park et al. 2007; Takashiba et al. 1999), and with exposure to interleukin-4 (IL-4) the M0 cells differentiate into M2 phenotype (Chanput et al. 2013; Genin et al. 2015; GmbH 2015; Gordon 2003; Gordon & Martinez 2010; Italiani & Boraschi 2014; Jablonski et al. 2015; Mantovani et al. 2002; McWhorter et al. 2013; Mills 2015; Roszer 2015; Sica et al. 2008).

It is important that the monocyte be PMA-differentiated first (M0) and then polarized to either M1 or M2, as the THP-1 cell (unexposed to PMA) would not change their morphology into macrophage-like, and only mild expression of some M1/M2 marker genes were observed (Chanput, Mes & Wichers 2014).

This THP-1 cell line was also used in co-culture experiment studies, with platelets, T-lymphocytes, vascular smooth muscle cells (Aslam et al. 2007; Azenabor et al. 2011; Chanput, Mes & Wichers 2014; Qin 2012; Zhang et al. 2008), and interestingly with adipocytes where it was shown that co-cultured primary human adipocytes with THP-1 macrophages resulted in a induced shift of THP-1 macrophages to M2 phenotype (Chanput, Mes & Wichers 2014; Spencer et al. 2010).

4.2 Objectives

- To determine if THP-1 cells can be developed as an *in-vitro* model of NLCs,
- To compare the similarities and differences of the cell line model to NLCs in aspects of morphology, phenotype and biological functions.

4.3 Methods

4.3.1 Summary of CLL samples used for this part of the study

For this chapter, a total of 14 CLL samples were used and the summary of clinical information of these samples is displayed in Table 4.2. A more detailed view of the clinical data can be seen in Appendix Table 7.1. The samples were selected based, in part, on their sensitivity to fludarabine.

Table 4.2 Summary of clinical features of the CLL samples used in this chapter

Gender	Male	11
	Female	3
Prior therapy*	Yes	4
	No	8
FISH¶	17p-	1/10
	11q-	2/10
	13q-	7/10
IGHV#	Un-mutated	2
Staging at the time of sample collection	A	2/10
	B	5/10
	C	3/10

*Prior therapy included steroid, chlorambucil, or fludarabine plus cyclophosphamide and rituximab.

¶FISH (fluorescence *in situ* hybridisation) was performed at or prior to sampling.

#IGHV status refers to somatic mutation in IGHV gene of CLL cells as compared with the gene sequence of the nearest germ-line using 2% as a cut-off.

Of the 14 samples were used, the majority were from male patients, untreated and were of stage B.

4.3.2 Culturing and differentiation of THP-1 cells.

The THP-1 cell line (derived from human monocytic leukaemia cells) was obtained from the European Collection of Authenticated Cell Cultures (Salisbury, UK), and maintained in culture flasks containing the complete RPMI-1640 medium as described above. To induce differentiation into macrophages, THP-1 cells (5 x 10^5 cells/mL) were treated with 5 ng/mL phorbol 12-myristate 13-acetate (PMA) (Sigma-Aldrich, Gillingham, UK) for 2 days, as previously described (Daigneault et al. 2010; Park et al. 2007). For polarization to M1 macrophages, the medium of PMA-differentiated THP-1 cells was removed and replaced with fresh complete medium containing 20 ng/mL interferon- γ (IFN-γ) (PeproTech EC Ltd, London, UK) and 10 pg/mL lipopolysaccharides (LPS) (Sigma-Aldrich) for 24 h, as previously described (Chanput, Mes & Wichers 2014; Genin et al. 2015; Jablonski et al. 2015). To induce M2 macrophages, the medium of PMA-differentiated THP-1 cells was removed and replaced with the fresh complete medium containing 30 ng/mL interleukin-4 (IL-4) (R&D Systems, Oxford, UK) and incubated for 72 h, with additional IL-4 (30 ng/mL) being added at 48 h (Chanput, Mes & Wichers 2014; Jablonski et al. 2015; McWhorter et al. 2013; Park et al. 2007). As described in Methodology, to perform a combined set of experiments using M0, M1 and M2 a timetable (Table 2.1) is followed to allow all conditions to be ready by the time the experiments are started.

4.3.3 Co-culture experiments

As described in Methodology, cryopreserved CLL samples were thawed and co-cultured at 3 x 10^6 cells/mL with differently differentiated THP-1 cells for the indicated times.

4.3.4 Analysis of cell death by flow cytometry

As described in Methodology, CLL cells co-cultured with differentiated THP-1 cells in the presence or absence of cytotoxic agents were harvested at the end of indicated time points and analysed for cell death by flow cytometry following staining with FITC-labelled Annexin V (BD Biosciences, Oxford, UK) and propidium iodide (Sigma-Aldrich).

4.3.5 Immunofluorescence microscopy

As described in Methodology, cells were fixed with 4% paraformaldehyde and permeabilized in PBS + 0.2% Triton X-100 in accordance with the manufacturer's protocol (BD Biosciences) before staining with primary antibodies and their corresponding isotypic controls. Fluorescence-labelled secondary

antibodies were then applied to amplify the signal and the nuclei counterstained with diamidino-2-phenylindole (DAPI).

4.3.6 Measuring CCL3 and CCL4.

As described in Methodology, levels of human CCL3 and CCL 4 in the culture medium were measured using commercial ELISA kits, in accordance with the manufacturer's instructions (Thermo Fisher Scientific). The colour-metric changes were read using a spectrophotometer at 450nm.

4.3.7 Surface IgM and IgD

The THP-1-derived M0 and M2 macrophages are prepared as previously described. A level of surface IgM and IgD on CLL after thawing is measured as described (Ten Hacken et al. 2016) and used as a basal level of expression (Day 0). The levels of expression in IgM and IgD on CLL cells co-cultured with M0 or M2 macrophages were measured for 3 consecutive days using 3 different CLL samples and then compared to Day 0. Following 3 days in co-culture, CLL cells were collected from the co-cultures and incubated at $3x10^6$/ml under standard culture conditions and the levels of IgM and IgD on CLL cells were monitored for another 3 days. The expression levels are measured at 24, 48 and 72hrs, as described in Methodology.

4.3.8 Measuring drug-induced cell death

To determine drug-specific effect on cell death, cells that were not treated with the drug was used as a control. The amount of cell death in the control is considered as spontaneous cell death. Using Equation 4.1 below, the percentage of drug induced cell death can be calculated, as previously described (Zhuang et al, 2014).

Equation 4.1 Drug Induced Cell Death

$$\% \text{ drug-induced cell death} = 100 \times \left[\frac{(\% \text{ cell death of drug-treated cells} - \% \text{ cell death of untreated cells})}{(100 - \% \text{ cell death of untreated cells})} \right]$$

4.3.9 Statistical analysis

Where appropriate, the paired, two-tailed Student's *t* test was performed to determine the statistical significance of the difference between the two groups of data using SPSS (version 21) and Microsoft Office Excel 2017.

4.4 Results

4.4.1 Morphological features of PMA-treated THP-1 cells resembled that of macrophages

As shown previously, NLCs were developed from circulating monocytes and exhibited a macrophage phenotype. To differentiate THP-1 cells into macrophages, I added phorbol 12-myristate 13-acetate (PMA) as described in Methods. This caused the cells to become adherent and their proliferation ceased as expected from other studies (Chanput, Peters & Wichers 2015; Spano, Barni & Sciola 2013).

As seen in Figure 4.1 (left), the PMA-treated THP-1 cells became adherent with a flattened oval and elongated shape, which resembled NLC cells. Next, I wanted to see if there were any further changes of the PMA-treated THP-1 cells in the presence CLL cells.

It is known from other studies that PMA induces differentiation of CLL B cells (Ghamlouch et al. 2014), so it was imperative to remove PMA from the differentiated THP-1 culture medium. Therefore, I removed the supernatant and washed the culture plate with pre-warmed PBS to remove residual PMA and any undifferentiated THP-1 suspension cells. I then plated thawed CLL cells on top of adherent THP-1 cells (Figure 4.1, middle). CLL cells were plated alone as a control (Figure 4.1, right).

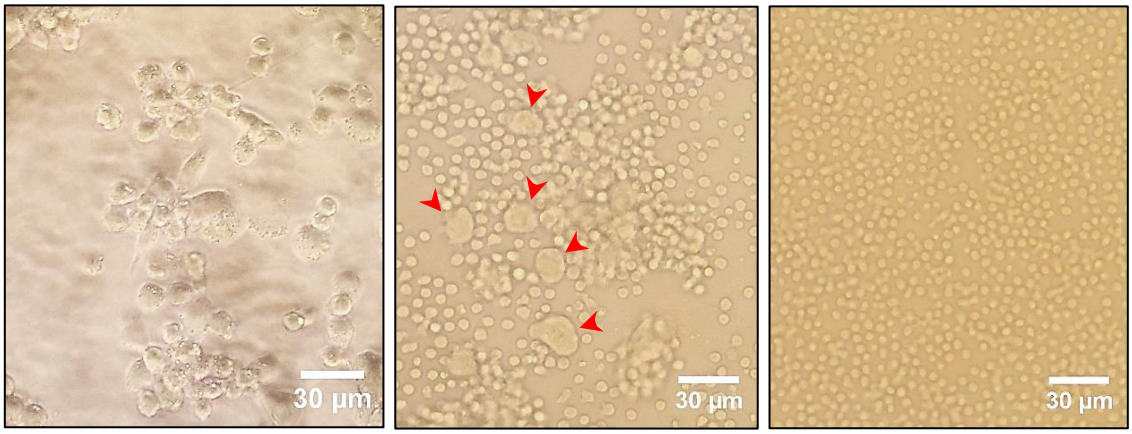

Figure 4.1. PMA-treated THP-1 cells co-cultured with CLL cells when compared to their counterparts cultured alone.

Phase contrast images of THP-1 cells treated with PMA for 48 h when cultured alone (left), co-cultured with CLL cells (middle, red arrow head) and CLL cells cultured alone (right). THP-1 cells were plated at 5 x 10^5/ml and treated with PMA as described. Supernatant was removed and the monolayer was gently washed with PBS before adding CLL cells. CLL cells were thawed as described and plated with PMA-treated THP1 cells as well as cultured alone as described.

A previous study has examined morphology of PMA-treated THP-1 cells using MGG staining and shown that they looked similar to NLCs displaying a flattened adherent morphology (Tsai et al. 2016). Thus, PMA-treated THP-1 cells displayed morphology similar to NLCs. Next, I looked at the immunophenotype of these cells using immunofluorescence microscopy.

4.4.2 Immunophenotype of PMA-treated THP-1 cells resembled that of NLCs

There had been numerous studies characterising the phenotype of differentiated THP-1 cells where expressions of CD14 and CD68 were reported (Aldo et al. 2013; Forrester et al. 2018; Genin et al. 2015) as well as CD163 (Chimal-Ramirez et al. 2016; Genin et al. 2015; Riddy et al. 2018). In my study, immunofluorescence microscopy showed that the PMA-differentiated THP-1 cells expressed both CD14 and CD163 (Figure 4.2). As seen in Figure 4.2, the DAPI staining revealed the location of the cell nuclei. CD163 was scantly detected in the cytoplasm of the cells, whereas CD14 expression was more confined within the cytoplasm.

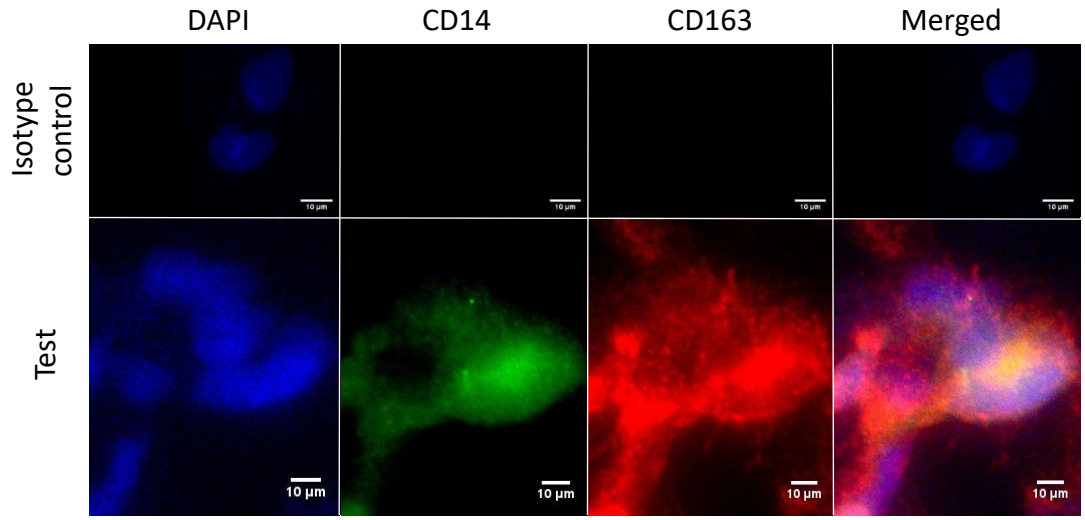

Figure 4.2. PMA-treated THP-1 cells expressed CD14 and CD163.

Immunofluorescence microscopy of PMA-differentiated THP-1 cells stained with DAPI (blue), antibodies against CD14 (green) and CD163 (red), and their respective isotype controls. Images were prepared using ImageJ software.

The above result was in agreement with phenotype of NLCs described in the previous chapter where the expression of both CD14 and CD163 was detected. Expression of CD68 in PMA-treated THP-1 cells was also confirmed in previous studies (Genin et al. 2015; Maeß et al. 2014).

Taken together, the morphology and phenotype of PMA-differentiated THP-1 cells resembled that of NLCs. I then proceeded to assess the functional features of PMA-treated THP-1 cells.

4.4.3 Effects of co-culture of PMA-treated THP-1 cells on CLL cells

To investigate if PMA-differentiated THP-1 cells exert any cytoprotective effect on CLL cells when in co-culture like NLCs, I performed the co-culture experiments the same way as previously described with NLCs. Cryopreserved CLL cells were first thawed and recovered and then cultured at a density of 3 x 10^6/ml over the washed monolayer. CLL cells cultured alone were used as controls. Viability of CLL cells with and without co-culture with the PMA-differentiated THP-1 monolayer was measured using FACS analysis (described in Methodology).

4.4.3.1 Analysis of spontaneous cell death

As seen in Figure 4.3, the co-cultured conditions preserved the viability of CLL cells significantly better than CLL cells cultured alone from as early as day 1 after co-culture. The average viability of CLL cells alone (blue) decreased following initial culturing, however, the average viability of CLL cells in co-culture (red) did not decrease as drastically. From Day 1 the co-cultured CLL cells had a significantly higher viability can those cultured alone.

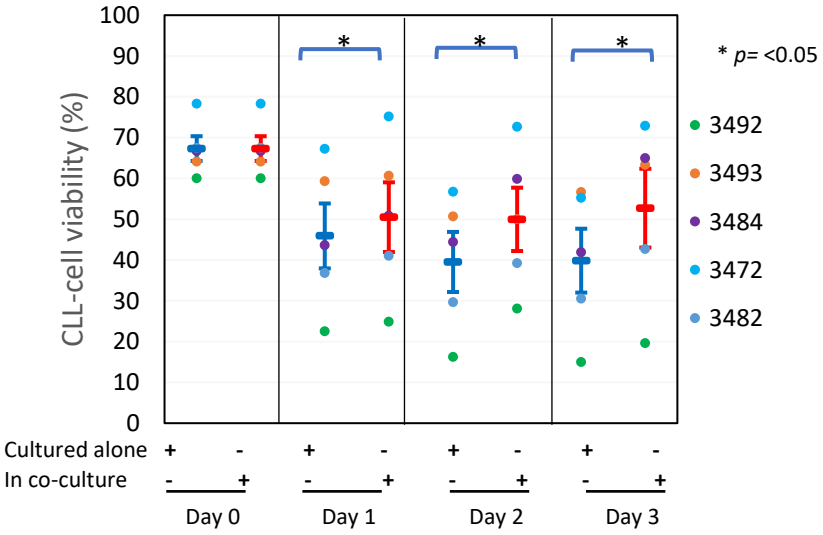

Figure 4.3 Co-culture with PMA-treated THP-1 cells preserved the viability of CLL cells over 3 days when compared to CLL cells cultured alone.

CLL cells were cultured alone and with PMA-differentiated THP-1 cells and the viability was monitored over 3 days. Viability of CLL cells was measured using Annexin V/ PI staining by flow cytometry. Data points represent mean ± SEM of 5 independent experiments using 5 different CLL samples. * refers to p value of <0.05 which is considered statistically significant.

Thus, like NLCs, PMA-treated THP-1 cells protected CLL cells from spontaneous cell death when in co-culture. Next, I wanted to examine if PMA-treated THP-1 cells also protect CLL cells against drug-induced cell death.

4.4.3.2 Analysis of drug-induced cell death

Fludarabine, a major component of first line therapy in treatment of CLL was used as a cytotoxic agent to assess if the co-culture conditions could protect CLL cells from fludarabine-induced cell death. It was previously shown that 10μM fludarabine is capable in killing CLL cells following 48h incubation under standard culture conditions (Zhuang et al. 2014). Also, since CLL cells with 17p deletion do not respond to fludarabine-induced apoptosis (Turgut et al. 2007), I selected CLL samples that do not contain 17p deletion for the experiment. I incubated CLL cells with 10μM fludarabine for 48h and cell death was measured by flow cytometry.

Percentage of fludarabine-induced cell death was calculated as described (Zhuang et al, 2014). Figure 4.4 showed that there was a significant difference in cell death between co-cultured CLL cells and CLL cells cultured alone. On average, fludarabine killed ~50% of CLL cells when they were cultured alone, whereas only ~20% of CLL cells co-cultured with PMA-differentiated THP-1 cells were killed. This suggests that the PMA-differentiated THP-1 cells protected CLL cells from fludarabine-induced cell death.

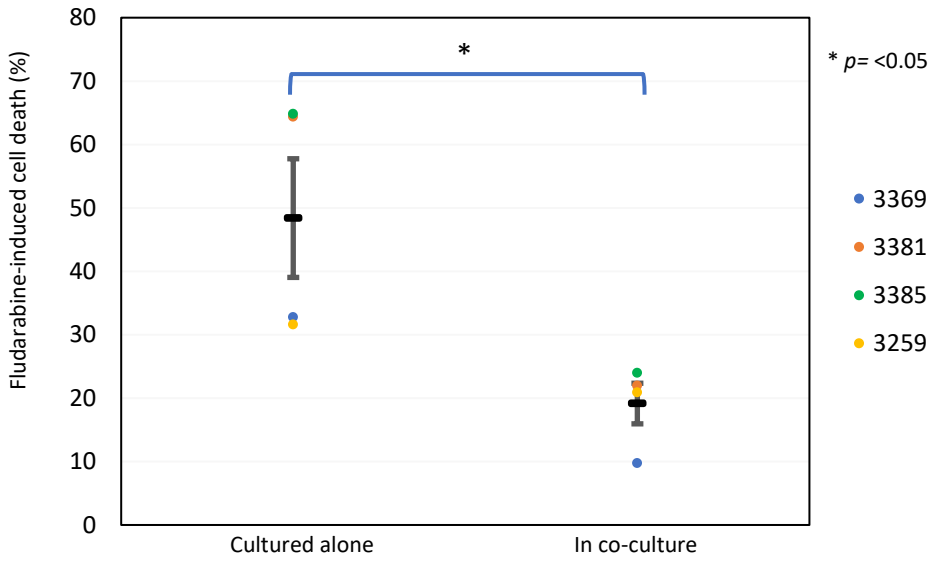

Figure 4.4 Fludarabine drug-induced cell death was significantly reduced in CLL cells co-cultured with PMA-treated THP-1 cells when compared to CLL cells culture alone.

Cryopreserved primary CLL cells were thawed and plated in co-culture with PMA-treated THP-1 cells or cultured alone in standard conditions. CLL cells cultured in respective conditions were incubated with 10μM fludarabine for 48 hrs. The viability of CLL cells was measured by flow cytometry following annexin V/ PI staining. The percentage of drug-induced killing was calculated as described in Methods. Data points represent mean ± SEM of 2 independent experiments, each experiment performed using 4 different CLL samples. * refers to p value of <0.05 which is considered statistically significant.

Taken altogether, the above results have shown that similar to NLCs, PMA-treated THP-1 cells conferred protection to CLL cells against spontaneous and drug-induced apoptosis. Importantly, co-culture with PMA-treated THP-1 cells significantly protected CLL cells from fludarabine-induced cell death, resulting in drug resistance in CLL cells.

As NLCs have been shown to more closely resemble M2 than M1 macrophages (Ysebaert et al, 2011; Filip et al, 2013), I further polarized PMA-differentiated THP-1 cells (here designated as M0 macrophages) into M1 macrophages by IFN-γ and LPS, and into M2 macrophages by IL-4, as previously described (McWhorter et al, 2013; Chanput et al, 2014; Genin et al, 2015; Jablonski et al, 2015). In doing so, I hope to establish the relative contribution of M1 and M2 macrophages to the cytoprotective effect seen.

4.4.3.3 M1 and M2 macrophages can be distinguished using CD38 and EGR2

Using the protocols reported from other studies to differentiate THP1 cells to M1 and M2 macrophages (Chanput, Mes & Wichers 2014; Genin et al. 2015; Jablonski et al. 2015), I optimised conditions of polarisation of M1 and M2 macrophages from PMA-differentiated THP-1 cells for my study (See Appendix 7.14.7). To confirm phenotype of M1 and M2 macrophages, I examined the expression of the respective markers CD38 and EGR2 (Jablonski et al. 2015) by immunofluorescence microscopy. As seen in Figure 4.5, M0 macrophage did not express EGR2 nor CD38 (top row), M1 macrophage expressed only CD38 (middle row) and M2 macrophage expressed only EGR2 (bottom row).

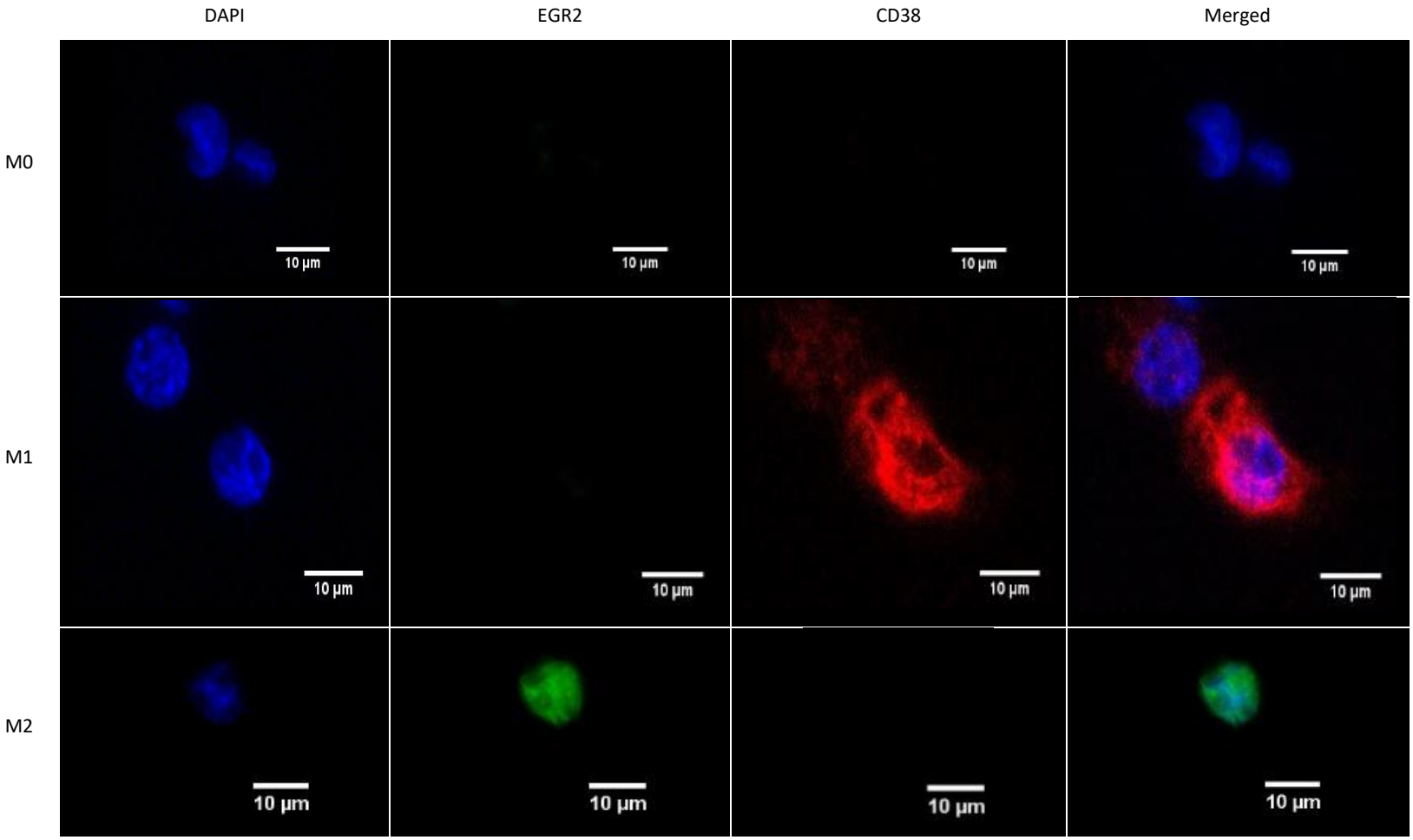

Figure 4.5. M0, M1 and M2 macrophages were distinguishable by the unique expression of EGR2 or CD38.

Immunofluorescence microscopy of PMA-differentiated THP-1 cells (M0 macrophages) and M1 and M2 macrophages, stained with anti-EGR2 (green), anti-CD38 (red) antibodies and counterstained with DAPI (blue). THP-1 cells were PMA differentiated for 24-48 hr (top row), M1 macrophages were prepared using IFN-γ and LPS (middle row) and M2 macrophages were prepared using IL-4 (bottom row) as described in the Methods. Images were prepared using ImageJ software.

4.4.3.4 M1 and M2 macrophages have distinguishable morphological features

I also examined morphological features of M1 and M2 macrophages using corresponding polarising protocols. As seen in Figure 4.6 it was noted that M1 macrophages appear as large, oval-shaped cells (top left panel) whereas M2 macrophages are large and elongated (top right panel). These observations were consistent with the respective morphology of M1 and M2 macrophages (McWhorter et al. 2013).Co-culture with CLL cells did not alter the distinct morphology of M1 or M2 macrophages (Figure 6, bottom panels).

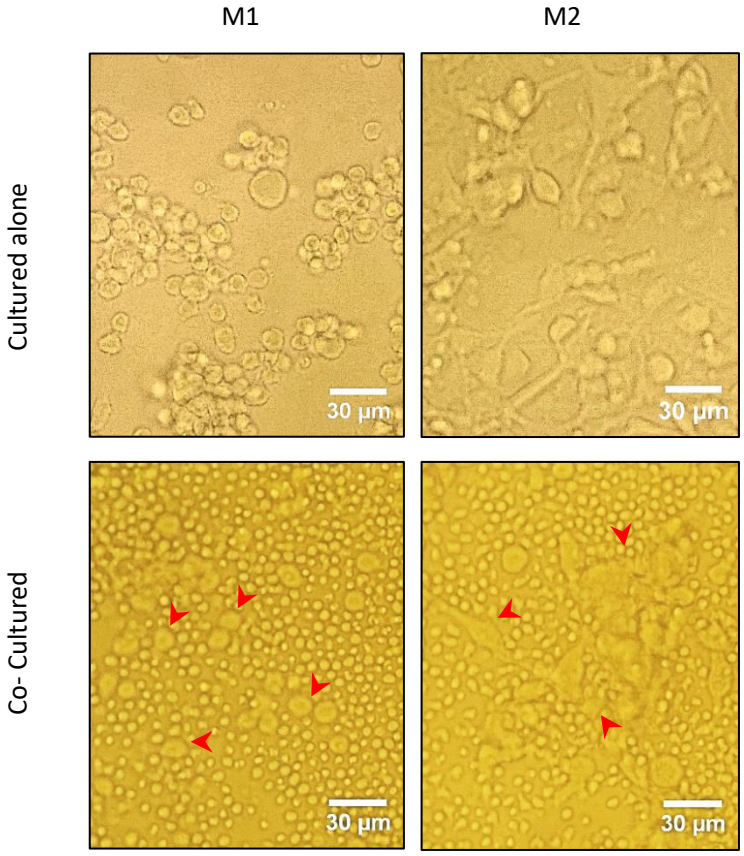

Figure 4.6. M1 and M2 macrophages have distinct morphological features with or without CLL cells.

Phase contrast microscopy of PMA-differentiated THP-1 cells which were further polarized to M1 (Top left), and to M2 macrophages (Top right). M1 and M2 macrophages were prepared using IFN-γ + LPS and IL-4, respectively as described in Methods. Bottom panels showed the respective images of M1 and M2 macrophages (red arrow heads) in co-culture with CLL cells.

4.4.4 Effects of co-culture with Polarised macrophages on CLL cells

4.4.4.1 Analysis of spontaneous cell death

I next repeated the same co-culture experiments I performed with M0 macrophages described previously, but this time using M1 and M2 macrophages for up to 3 days (Figure 4.7). CLL cells cultured alone were used for comparison. As shown in Figure 4.7, CLL cells co-cultured with M1 macrophages retained a higher viability than CLL cells cultured alone, however, the difference was not significant. In contrast, CLL cells co-cultured with M2 macrophages retained greatest viability than that of CLL cells cultured alone, which was statistically significant as early as 24h after co-culture. Furthermore, the viability of CLL cells co-cultured with M2 macrophages was significantly higher than those with M1 macrophages from day 2 onwards.

Therefore, both M1 and M2 macrophages provided protection against spontaneous apoptosis of CLL cells. However, M2 macrophages provided significantly greater protection than M1 macrophages.

I next investigated the cytoprotective effect of M1 or M2 macrophages on drug-induced cell death of CLL cells.

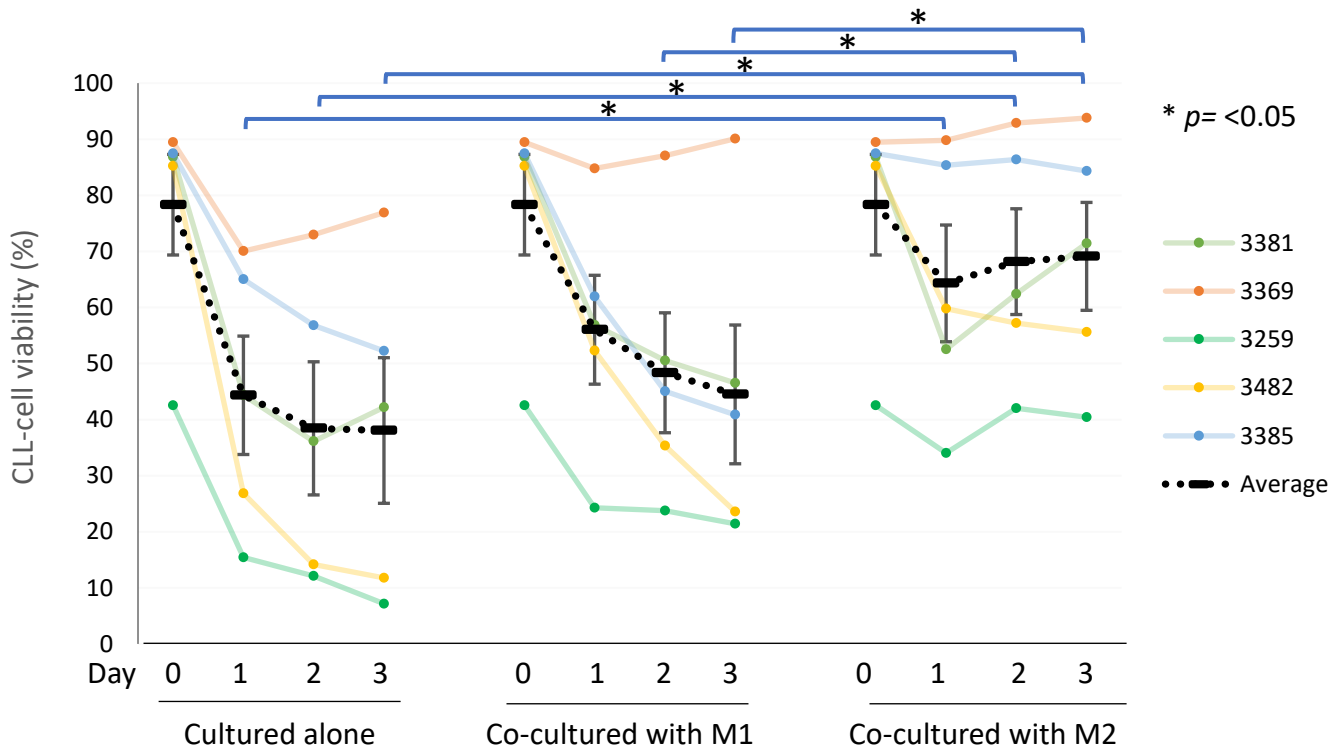

Figure 4.7 Co-culture with M2 macrophages provided greater protection than M1 macrophages against spontaneous apoptosis of CLL cells over 3 days.

Primary CLL cells were cultured alone or co-cultured with M1 or M2 macrophages derived from differentiated THP1 cells and their viability was monitored over 3 days by flow cytometry following annexin V/ PI staining. M1 and M2 macrophages were prepared using IFN-γ + LPS and IL-4 respectively as described in Methods. Data points represent mean ± SEM of independent experiments using 5 different CLL samples. * refers to p value of <0.05 which is considered statistically significant.

4.4.4.2 Analysis of drug-induced cell death

I repeated the same co-culture experiments I performed with M0 macrophages described earlier but this time with M1 and M2 macrophages in the presence of 10μM fludarabine CLL cells cultured alone were used for comparison. As shown in Figure 4.8, co-culture with M0 macrophages significantly protected CLL cells from fludarabine-induced cell death, compared to CLL cells cultured alone. CLL cells co-cultured with M2, and to a lesser extent M1, macrophages were also protected from fludarabine-induced cell death, although not statistically significant. Interestingly, protection against fludarabine-induced cell death provided by M2 macrophages was not as great as M0 macrophages.

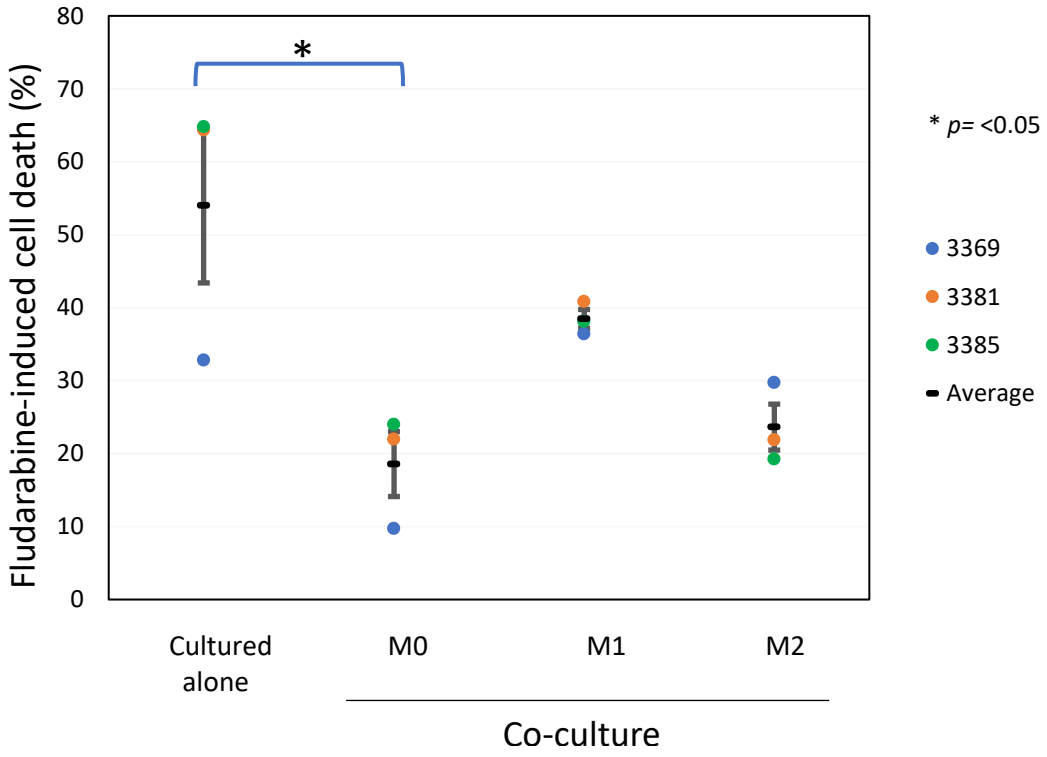

Figure 4.8. Co-culture with M0 macrophages provided the greater protection than M1 or M2 macrophages against fludarabine-induced cell death of CLL cells.

M0, M1 and M2 macrophages derived from PMA-differentiated THP-1 cells were prepared as described in Methods. Primary CLL cells were incubated alone or in co-culture with M0, M1 or M2 macrophages, as described in Methods, in the presence of 10μM fludarabine for 48 h and their viability were monitored by flow cytometry following annexin V/ PI staining. The percentage of drug-induced killing was calculated as described in Methods. Data points represent mean ± SEM of 2 independent experiments, each experiment performed using 3 different CLL samples. * refers to p value of <0.05 which is considered statistically significant.

Next, I was interested to see what effect the co-culture condition would have with ABT-199, a BCL-2 specific inhibiter, which showed impressive clinical activity in CLL (Roberts et al. 2016). As expected, ABT-199 caused concentration-dependent cell death in CLL cells cultured alone (Figure 4.9, red line).

However, ABT-199-induced cell death of CLL cells were not affected by co-culture with M0 (yellow line), M1 (blue line) or M2 macrophages (green line). The above result showed that the cytoprotective effect against fludarabine shown earlier was lost in the presence of ABT-199, suggesting that this protective effect is BCL-2-dependent. It also showed that ABT-199 is effective killing n CLL cells that are in co-culture with macrophages.

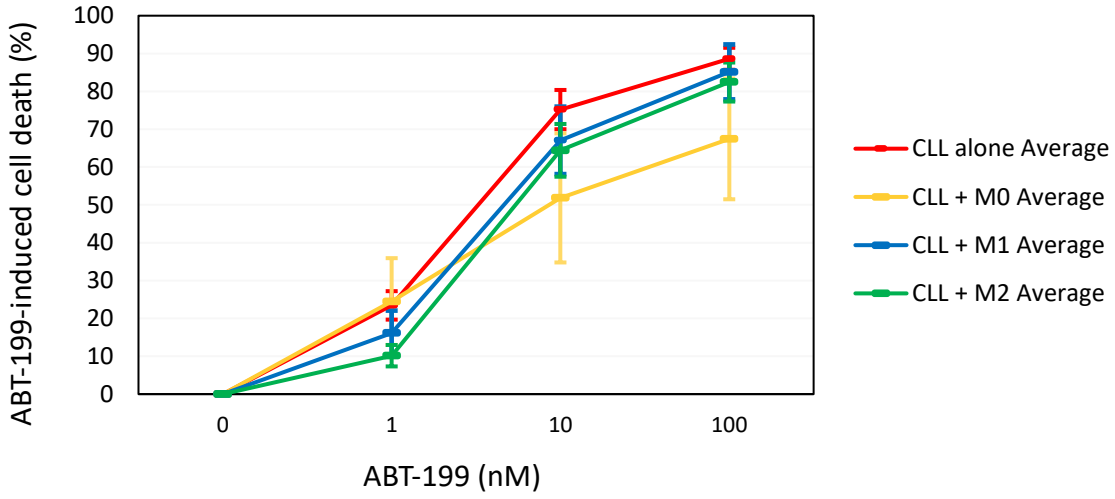

Figure 4.9 Co-culture with M0, M1 or M2 macrophages failed to protect CLL cells against ABT-199-induced cell death.

M0, M1 and M2 macrophages derived from PMA-differentiated THP-1 cells were prepared as described in Methods. Primary CLL cells were incubated alone or in co-culture with M0, M1 or M2 macrophages, as described in Methods, in the presence of ABT-199 at the indicated concentrations for 24 h and their viability were monitored by flow cytometry following annexin V/ PI staining. The percentage of drug-induced killing was calculated as described in Methods. Data points represent mean ± SEM of 2 independent experiments, each experiment performed using 3 different CLL samples.

Taken together, the cytotoxic effect of fludarabine on CLL cells was impeded by co-cultures with M0, M1 and M2 macrophages derived from PMA-differentiated THP-1 cells, but the greatest protection was provided by co-cultures with M0 macrophages. Co-cultures with M2 macrophages provided the greater protection than M1 macrophages against fludarabine-induced cell death of CLL cells, even though not as great as M0 macrophages.

In contrast, the cytotoxic effects of ABT-199 on CLL cells was not impeded by co-cultures with M0, M1 or M2 macrophages, suggesting that the drug is still effective in killing co-cultured CLL cells and that the protection against fludarabine-induced cell death shown earlier is most likely mediated by BCL-2.

4.4.4.3 Levels of CCL3 and CCL4 in the culture medium

It has previously been reported that NLCs induce CLL cells to secrete the T-cell chemokines CCL3 and CCL4 into the culture medium where they can be measured by ELISA (Burger et al. 2009b). I therefore sought to establish if the differentiated THP-1 cells have the same effect. As described in the previous chapter, the levels of CCL3 and CCL4 proteins in the culture medium were increased from day 5 and reached a plateau by day 10 from fresh CLL PBMC cultures. I thus measured levels of CCL3 and CCL4 in the supernatant of differentiated THP-1 cells. As shown in Figure 4.10, PMA-differentiated THP-1 cells (M0 macrophages) alone secreted high levels of CCL3 and CCL4. In keeping with previous reports (Mantovani et al. 2004; Mantovani et al. 2002), THP-1 cell-derived M1 macrophages cultured alone secreted even more CCL3 and CCL4 (Figure 4.10). In contrast, levels of CCL3 and CCL4 in the medium of M2 macrophages cultured alone were similar to those produced by CLL cells alone (Figure 4.10). Culturing CLL cells with various differentiated THP-1 cells (M0, M1 or M2) did not increase the total amount of CCL3 and CCL4 that were secreted into the supernatant for up to 3 days (Figure 4.10). My results thus indicated that, THP-1 cell-derived M0 and M1 macrophages secreted CCL3 and CCL4, but did not induce CLL cells to secrete these chemokines.

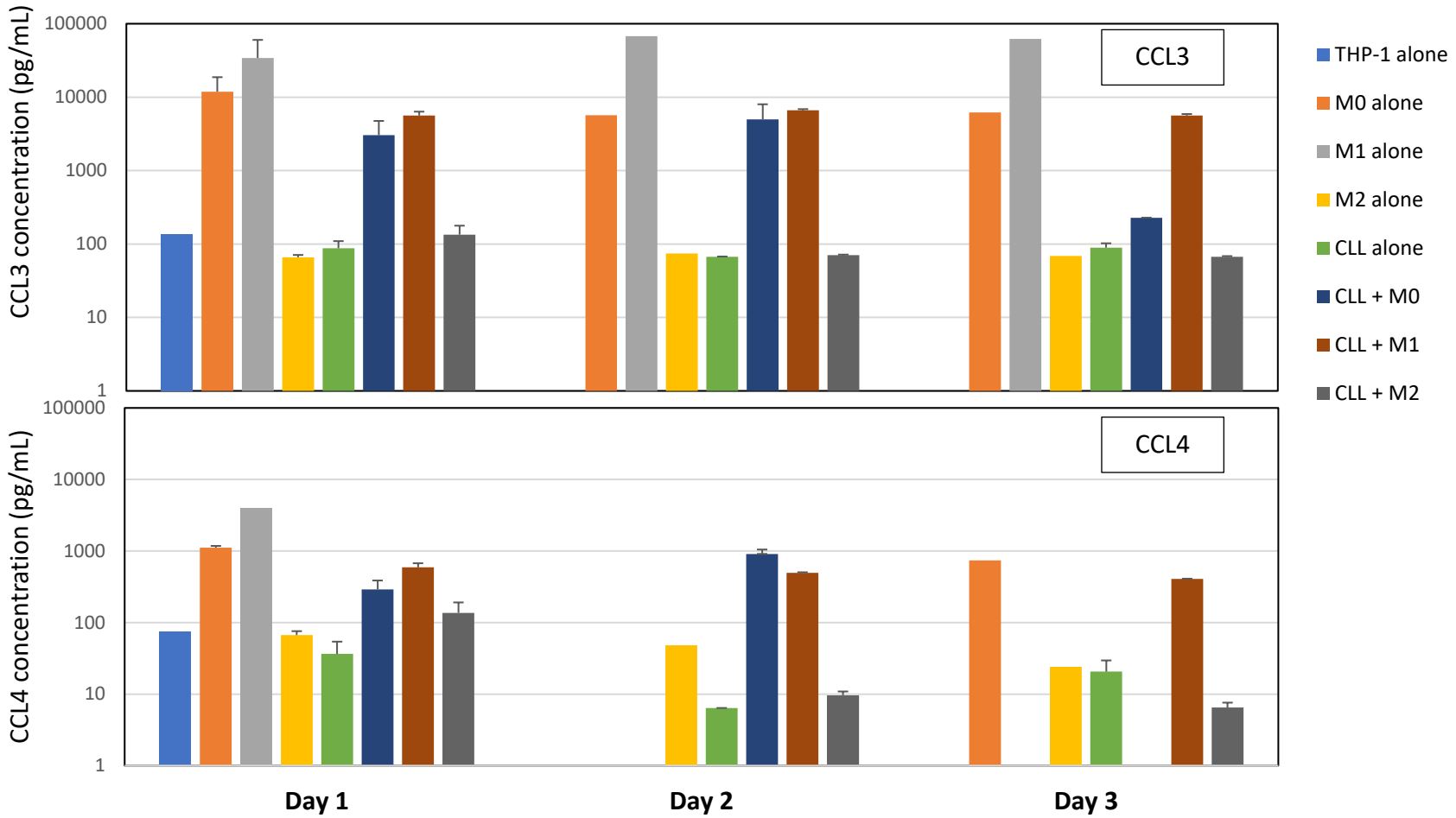

Figure 4.10 Co-culture conditions did not affect the levels of CCL3 and CCL4 in the medium of CLL cells co-cultured with M0, M1 or M2 macrophages.

CLL cells were cultured alone or with various differentiated THP-1 cells for 3 days and supernatant samples at the indicated time points were collected for analysis of CCL3 (top panel) and CCL4 (low panel) by ELISA. The medium of M0, M1 and M2 macrophages cultured alone was also collected for analysis of CCL3 and CCL4 in a similar manner. Levels of CCL3 and CCL4 were measured using ELISA kit as described in the Methods. The concentrations of CCL3 and CCL4 are displayed in log scale. Data points represent mean ± SEM of independent experiments from available samples.

4.4.4.4 Expression of sIgM and sIgD

It has also been reported that CLL cells co-cultured with NLCs displayed significant reduction in sIgM and sIgD expression and that these CLL cells re-expressed both IgM and IgD following *in-vitro* culture in the absence of NLC, indicating that NLCs can engage B cell receptors (BCR) of CLL cells (Ten Hacken et al. 2016). I thus tried to determine if the cell line model replicated this activity. First, I screened CLL samples to select those that recover the expression of IgM when cultured alone under standard conditions This is because it has been shown that not all CLL samples are able to recover the expression of IgM under such culture conditions and that ability to re-express IgM is strongly correlated to BCR signalling capacity (Mockridge et al. 2007). As shown in Figure 4.11, on average the expression of IgM in all 9 CLL samples increased over three days of incubation under standard culture condition. However, CLL samples 3557, 3609 and 3691 clearly recovered expression of IgM well, whereas sample 3684 hardly recovered expression of IgM (Figure 4.11).

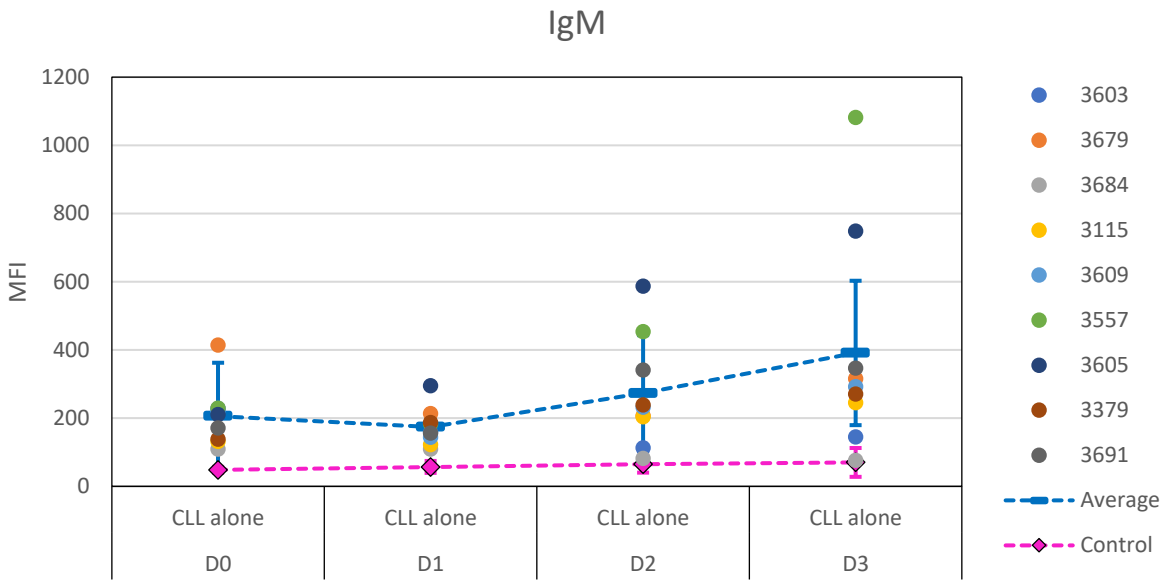

Figure 4.11 Surface expression of sIgM on CLL cells when cultured for three days under standard conditions.

Surface expression of IgM on CLL cells cultured under standard conditions over 3 days were measured by FACS as described in Methods. Data points represent mean ± SD of independent experiments using 9 different CLL samples.

I next measured expression of IgD of these samples in a similar manner. To my surprise, these CLL cells did not recover their IgD expression over the three days in culture (Figure 4.12).

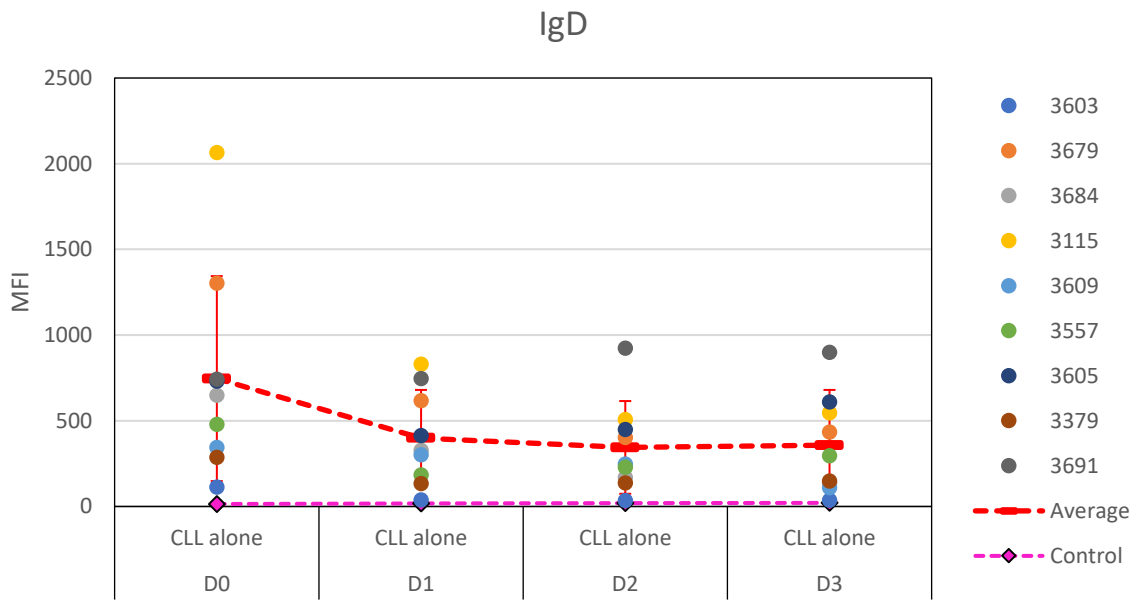

Figure 4.12 Surface expression of sIgD was not increased on CLL cells when cultured for three days under standard conditions.

Surface expression of IgD on CLL cells cultured under standard conditions over 3 days were measured by FACS as described in Methods. Data points represent mean ± SD of independent experiments using 9 different CLL samples.

Next, I decided to use M2 macrophages for co-culture experiments as NLCs were described as displaying predominantly 'M2 subset' by literature (Ysebaert & Fournie 2011). I used M0 for comparison as the unpolarised macrophage subset. I also used CLL cultured alone as a control.

As shown in Figure 4.11, all nine CLL samples initially exhibited reduced expression of IgM 24 h after incubation *in vitro*. However, some but not all samples recovered their expression of IgM at 48 h. We next used these samples for co-culture with M0 or M2 macrophages for up to 72 h and compared the surface expression of IgM and IgD on co-cultured CLL cells to that on CLL cells cultured alone (Figure 4.13). As shown in Figure 4.13, the expression of IgM on CLL cells cultured alone was reduced at 24 h, but recovered at 48 h and further increased at 72 h. Similar to CLL cells cultured alone, CLL cells co-cultured with M0 or M2 macrophages expressed reduced IgM at 24 h, but restored expression of IgM at 48 h and increased the expression further at 72 h (Figure 4.13). At all these time points the levels of expression of IgM on CLL cells co-cultured with either M0 or M2 macrophages were not lower than that on CLL cells cultured alone.

I monitored the expression of IgD on CLL cells cultured in the three culture conditions described above and observed a similar trend of the increase in expression of IgD as with IgM on CLL cells over 72 h (Figure 4.14). Overall, the surface expression of IgM and IgD was not reduced in CLL cells co-cultured with M0 nor M2 macrophages over a 72h incubation period.

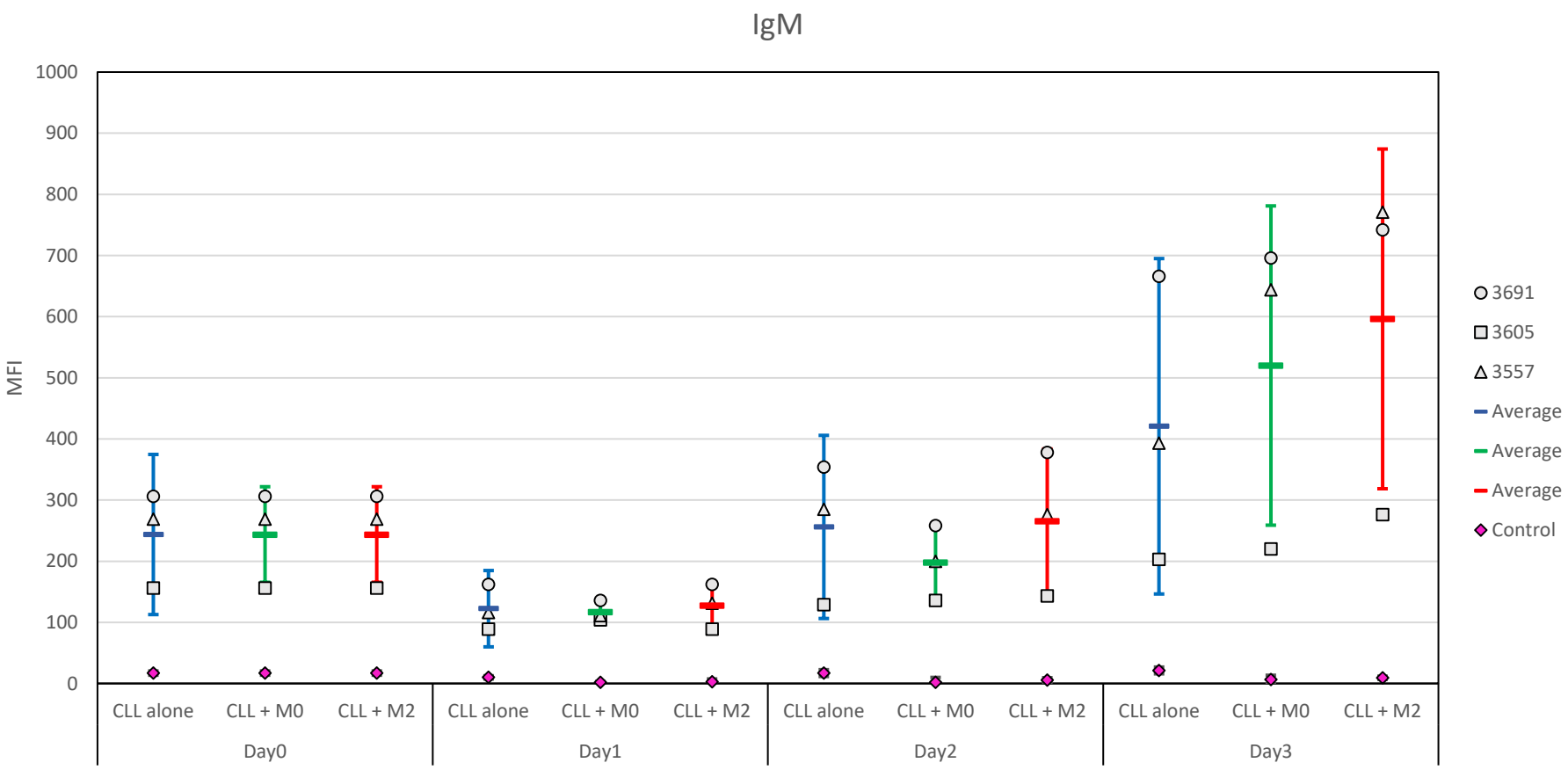

Figure 4.13 Surface expression of IgM was not decreased in CLL cells co-cultured with M0 or M2 macrophages for 3 days.

THP-1 cells were differentiated into M0 or M2 macrophages as described in the Methods. Primary CLL cells were cultured alone or co-cultured with M0 or M2 macrophages over 3 days and surface expression of IgM on CLL cells was analyzed by flow cytometry as described in Methods. Data points represent mean ± SD of independent experiments using 3 different CLL samples.

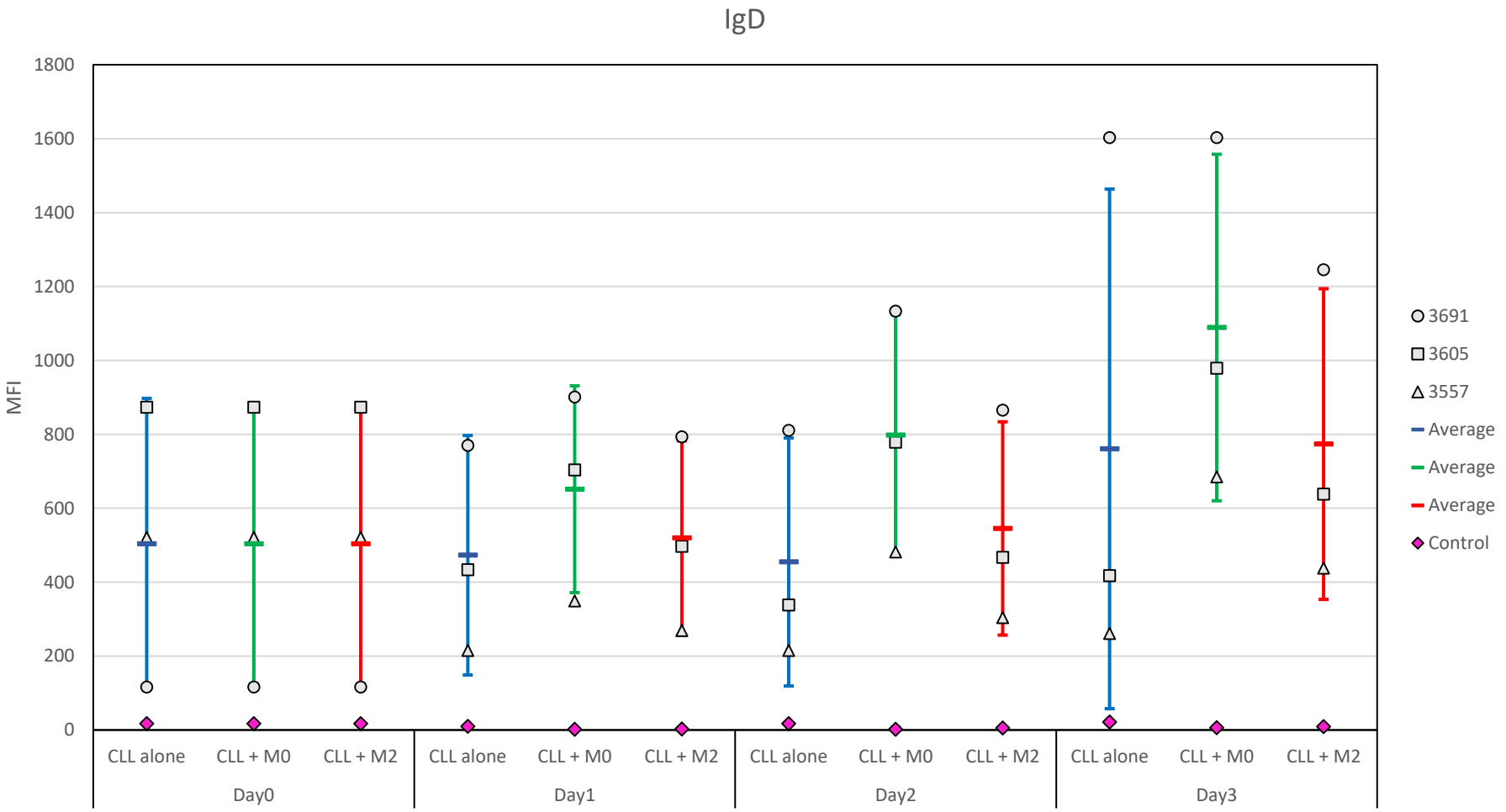

Figure 4.14 Surface expression of IgD was not decreased in CLL cells co-cultured with M0 or M2 macrophages for 3 days.

THP-1 cells were differentiated into M0 or M2 macrophages as described in Methods. Primary CLL cells were cultured alone or co-cultured with M0 or M2 macrophages over 3 days and surface expression of IgD on CLL cells was analyzed by flow cytometry as described in the Methods. Data points represent mean ± SD of independent experiments using 3 different CLL samples.

Taken altogether, a pro-survival effect was seen by co-cultures with differentiated THP1 on CLL cells when compared to alone. Co-culture with M2 macrophages provided the best survival environment for CLL cells against spontaneous apoptosis.

M0 and M2 co-cultures offered the best protection against fludarabine-induced cell death upon CLL cells, where M0 was the best condition. There was no protection seen at all against ABT-199 induced cell death.

There was no clear trend seen on the levels of CCL3 and CCL4 in the supernatants of co-culture conditions. Rather, it appears that there is a very high level of CCL3 and CCL4 secreted by the cell lines, which may conceal any minor changes expected.

Finally, although I demonstrated that the CLL samples selected regained their sIgM expression when cultured alone, the expression levels were not decreased when in co-culture with M0 and M2 macrophage conditions.

4.5 Summary of Results

I showed that THP-1 cell line can be used to differentiate into macrophages by incubating with PMA. In order to mimic the distribution of NLCs seen in the previous chapter, a density of $5x10^5$/ml was preferred. Upon PMA differentiation, the THP-1 cells demonstrated the morphological features of adherent macrophages with oval and elongated shapes. The differentiated THP-1 cells (M0 macrophages) were distinguishable from CLL cells by their shape and size when in co-cultures.

Through IF staining, the M0 macrophages demonstrated some expression of CD14 and CD163. Although the expressions were weak, this was consistent with the observations from other studies who performed more in-depth investigations on PMA differentiated THP-1 cells (Chimal-Ramirez et al. 2016; Neu et al. 2013; Tedesco et al. 2018).

Co-culture with M0 macrophages showed significantly improved viability of CLL cells over 3 days of co-culture compared to CLL cells cultured alone. This co-culture condition also showed significant protection against fludarabine-induced cell death of CLL cells.

The phenotype of M1 and M2 macrophages were confirmed by IF techniques for CD38 and EGR2. When comparing morphology of M1 and M2 macrophages that were developed by using the respective polarising techniques, they exhibited distinct morphological features. Co-culture of CLL cells with M1 or M2 macrophages showed an improved viability of CLL cells for 3 consecutive days comparing to CLL cells cultured alone. The protection against fludarabine-induced cell death of CLL cells was found to be most pronounced with co-culture conditions with M0 macrophages, followed by with M2 macrophages with M1 macrophages offering the least protection.

However, no such protective effect against ABT-199-induced apoptosis was seen in CLL cells co-cultured with M0, M1 or M2 macrophages.

M0 and M1 macrophages produced high levels of CCL3 and CCL4 in the culture medium, whereas M2 produced low levels of the two chemokines when cultured alone. There was no increase in the amount of CCL3 and CCL4 in the culture medium for up to 3 days when CLL cells were co-cultured with M0 or M1 macrophages. These findings suggested that M0 and M1 macrophages derived from THP-1 cell line secreted CCL3 and CCL4 but did not induce CLL cells to secrete them.

CLL cells were found to recover the expression of sIgM upon thawing for up to 3 days, however in co-culture conditions it was not found to be decreased. CLL expression of sIgD was generally found to decrease upon thawing for up to 3 days but upon culture conditions was also found not to decrease further.

4.6 Discussion

In this chapter I showed that THP-1 cell line can be used to investigate the function of NLCs by differentiating them into macrophages using PMA. Generally, human primary monocytes from circulation are isolated and commonly used as precursors for study of macrophages *in vitro* (Tedesco et al. 2018). However, these primary monocyte-derived macrophages (MDMs) cannot be stored in liquid nitrogen, plus the evident heterogeneity between the monocyte samples (Tedesco et al. 2018). Cell lines are thus used to compensate these issues as they can be easily expanded and stocked in frozen temperatures in non-differentiated state (Tedesco et al. 2018). THP-1 cell lines have been used in numerous studies demonstrating that they can be differentiated to macrophages which can be further polarised to M1 and M2 macrophages (Aldo et al. 2013; Daigneault et al. 2010; Forrester et al. 2018; Park et al. 2007; Tedesco et al. 2018). Alternatives to THP-1 cell line are U937, ML-2, HL-60 and Mono Mac 6 cells (Chanput, Peters & Wichers 2015), however there are limited information available in the literature because of significantly fewer published studies reporting using these cell lines. Between THP-1 and U937 cells, the choice was based the fact that THP-1 cell line was derived from blood monocytic cells whereas U937 cells from tissue resident monocytic cells (Chanput, Peters & Wichers 2015). In addition, in studies comparing the difference and similarities of two cell lines, it has been found that, although they both can be differentiated into macrophages with the similar stimuli, U937 cells can also be differentiated into macrophages using retinoic acids, Vitamin D3 and TPA (Chanput, Peters & Wichers 2015; Chun et al. 2001). Differentiated THP-1 cells yielded a 'macrophage-only' phenotype where there was no expression of dendritic cell markers CD80 or CD86 (Riddy et al. 2018). U937 cells did not migrate in response to any chemoattractant whereas THP-1 cells and PBMCs migrated well in response to chemoattractant using trans-well migration assay (Riddy et al. 2018). PMA was the preferred choice for differentiating into macrophages as it was the most widely used chemical for differentiation of monocyte cell lines (Riddy et al. 2018).

I selected a density of $0.5x10^6$/ml of THP-1 cells to be differentiated into macrophages for subsequent experiments because this closely represent the distribution of well-developed NLCs as described in the previous chapter. This cell density used in my study was similar to that reported by some studies (Forrester et al. 2018; Park et al. 2007; Takashiba et al. 1999), but different to that from other studies (Aldo et al. 2013; Daigneault et al. 2010; Schwende et al. 1996; Genin et al. 2015). Since the studies using the density of $0.5x10^6$/ml had also prepared THP-1 cells for co-culture experiments, I therefore used this density for my co-culture experiments. Next, I was able to demonstrate the similarities in morphology and phenotype of PMA-differentiated THP1 (M0 macrophages) with those of NLCs described in the previous chapter.

The morphology and phenotype of CD14 in M0 macrophages observed were consistent with the results found with studies from Genin et al. (2015) and Chimal-Ramirez et al. (2016). They showed the macrophages displayed a flattened appearance with mild expression of CD14. Regarding the expression of CD163, some studies did not observe the expression of CD163 in PMA-differentiated THP-1 cells (Forrester et al. 2018; Tedesco et al. 2018) whereas others did observe its expression (Chimal-Ramirez et al. 2016; Genin et al. 2015; Riddy et al. 2018). Thus, my study agreed with the latter group where expression was observed in PMA-differentiated THP-1 cells by immunofluorescence microscopy.

I further polarised M0 macrophages into M1 or M2 subtype. This was carried out by using an established procedure of polarising the M0 into M1 and M2 using LPS+ IFNγ and IL-4, respectively. To distinguish the subsets, I observed the morphology under phase-contrast microscope and IF following staining the cells using CD38 and EGR2. The M1 macrophages expressed CD38, whereas M2 expressed EGR2 and M0 expressed neither. This is in agreement with a study using these markers to define the M1 and M2 populations (Jablonski et al. 2015).

Furthermore, by observation of morphology, I found that M1 macrophages as appeared to be round and flattened after the addition of LPS and IFNγ and M2 macrophages displayed the elongated appearance upon addition of IL-4. It has been reported that the degree of elongation correlates with the phenotypic polarization of M2 macrophages (McWhorter et al., 2013). The study showed that preventing cell elongation inhibits the complete polarization of M2 macrophages following incubation with IL-4. Therefore, elongation and polarisation possibly represent a unified process leading to fully differentiated M2 macrophages. Reassuringly, elongated and polarised NLCs similar to M2 macrophages were also seen in CLL PBMC cultures as described in the previous chapter, thus providing further evidence that NLCs resemble M2 macrophages (Hanna et al, 2015; Marchesi et al, 2015, Ysebaert and Fournie, 2011; Ysebaert et al, 2010).

Likewise, I was also able to demonstrate the pro-survival effects of THP-1-derived macrophages on CLL cells as compared to CLL cells cultured alone. Unexpectedly, co-culture with M0 macrophages displayed the greatest protection against spontaneous and fludarabine-induced apoptosis of CLL cells, with M2 macrophages offering modest protection and M1 macrophages with the least protection. My result was thus in disagreement with that reported by a study where HepG2 (human hepatoma) and A549 (lung adenoma) cancer cells were co-cultured with THP-1 cells-derived M1 or M2 macrophages and etoposide-induced apoptosis was significantly reduced in cancer cells that were incubated with M2 macrophages (Genin et al. 2015).

The reason why M0 macrophage condition was better than M2 macrophage condition, to protect against fludarabine induced cell death, is still unclear. A study by Caras et al. (2011) using tumour-secreted soluble factors on THP-1 cell line, found that THP-1 macrophages were able to switch their phenotype or induce functional polarization towards a mixture of M1/M2 phenotype. This occurred when the macrophages were incubated with supernatant of primary tumour cells which contained tumour-secreted soluble factors (Caras et al. 2011; Chanput, Mes & Wichers 2014). In my study, I did not inspect the phenotype of M2 macrophages after co-culture with CLL cells. Therefore, further studies are required to check if the phenomenon of phenotype switching occurs and thus be able to offer some explanation. The differentiated THP-1 cells offered no protection against Venetoclax (ABT-199)-induced cell death, the result is consistent with a report that NLCs failed to protect CLL cells from ABT-199 induced apoptosis (Boissard et al. 2015b).

In an attempt to reproduce the effect of NLCs in inducing CLL cells to express CCL3 and CCL4 chemokines when in co-culture, I co-cultured CLL cells with the THP-1 cells-derived macrophages and monitored the level of CCL3 and CCL4 in the culture medium. Although there was an increase in levels of CCL3 and CCL4 in the medium from CLL cells co-cultured with M0 or M1 macrophages compared to CLL cells cultured alone, similar increases were also observed in the medium from the corresponding macrophages cultured on their own. Thus, the increase in levels of CCL3 and CCL4 was likely due to the presence of differentiated THP-1 cells in the co-culture system. It has been shown that M1 macrophages intrinsically expressed higher levels of certain chemokines such as CCL3 and CCL4 than M2 macrophages (Mantovani et al. 2002). My results were thus consistent with the findings reported in this study. In this regard, the cell-line model therefore does not appear to fully recapitulate the chemokine-inducing properties of primary NLCs (Burger et al. 2009b).

Another functional difference between primary NLCs and cell-line model was highlighted by the finding that CLL cells co-cultured with M0 or M2 macrophages over 72 h did not express reduced levels of IgM or IgD, whereas CLL cells co-cultured with primary NLCs displayed significant reduction in surface expression of IgM and IgD (Ten Hacken et al. 2016). One possible explanation can be that IL-4 enhances the expression of sIgM in CLL cells (Aguilar-Hernandez et al. 2016) and that IL-4 has been shown to be secreted in small amounts by macrophages themselves (La Flamme et al. 2012), although it is unclear if NLCs specifically secrete IL-4. To confirm this, an experiment observing the levels of IL-4 in CLL cells co-cultured with M0/M1/M2 as well as cultured alone needs to be performed, in parallel to the experiment using primary NLCs as a comparison.

Taken together, I have shown that the THP-1 cells derived macrophages do share many functional similarities to NLCs. However, I have also found some differences between THP-1 cells derived macrophages and NLCs. Here, I gave my explanations to potential causes to these differences.

One possible explanation for the dissimilarities with NLC experiments is the use of PMA to differentiate THP-1 cells to M0 macrophages. PMA is a known potent mitogen which activate many immune cells including monocytes and induces TNF-α production in these cells (Mendoza-Coronel & Castanon-Arreola 2016). TNF-α signals through the receptors TNFR1 and TNFR2 and regulates cell functions such as proliferation, survival, differentiation and apoptosis. Macrophages secrete TNF-α and are also highly responsive to TNF-α, thus rendering TNFα as a "master-regulator" of inflammatory cytokine production where it mediates the cytokine cascade in inflammatory diseases (Parameswaran & Patial 2010).

Therefore, cell line model is subject to manipulation by PMA which could result in non-naturally occurring functions. This may explain why the cell line model could not recapitulate the effects of BCR stimulating and chemokine induction of CLL cells by NLCs. Another explanation is that, as M1 and M2 macrophages represent the two opposing ends of a continuum (Mantovani et al, 2002) whereas NLCs are heterogeneous in their development as described in previous chapter, it is possible that NLCs could be a mixture of M1 and M2 macrophages, despite that they have been shown to resemble predominantly the M2 macrophages. Therefore, the results from the cell line model that M0 macrophages conferred greater protection than the M1 or M2 macrophages against spontaneous and fludarabine-induced cell death may reflect what NLCs did to CLL cells.

Last but not the least, it is important to recognise the weakness of *in-vitro* cell cultures, both primary cells and cell lines, where they are being studied in the absence of their local environment *in-vivo*. It is also well established that cell lines cannot replace primary cells despite their ease to use and providing consistent results (Kaur & Dufour 2012; Riddy et al. 2018). Therefore, great caution was needed when interpreting the results from studies using cell lines. In addition, validation experiments should ideally be replicated in primary cells. For these reasons, in the next part of my study to investigate how CLL cells and NLCs influence each other at the level of gene expression, I chose to use primary NLC cells as the overall objective of my study is to understand the mechanisms mediating the interactions of CLL cells with NLCs.

5 Identification of differentially expressed genes and significantly enriched functional pathways in CLL cells co-cultured with NLC cells

5.1 Introduction

From the previous chapters I have shown that NLCs can be developed from CLL PBMC samples from patients with CLL and that they displayed many morphological features of macrophage and expressed CD68 and CD163, the phenotypic markers of M2 subset of macrophages. The NLCs were able to reduce spontaneous apoptosis of CLL cells when in co-culture, as compared to CLL cells cultured alone. I have also shown that human THP-1 cell line can be used to mimic many behaviours of NLCs, particularly on the pro-survival effect on CLL cells against spontaneous apoptosis. However, the THP-1 cell line model did not replicate all of biological effects of NLCs, especially in regulating the release of chemokines and expression of surface IgM and IgD on CLL cells. This disparity was further highlighted by the observation that cell lines such as THP-1 cells can only partially reproduce the genotypic and phenotypic properties of monocytes isolated from fresh PBMC samples (Riddy et al. 2018). Therefore, to investigate the mechanisms mediating the interaction between NLCs and CLL cells at the level of gene expression, I chose to use fresh CLL PBMCs samples to develop NLCs and use cryopreserved autologous CLL cells for co-culture experiments.

So far, the studies that have looked into the difference in gene expression between CLL cells co-cultured with or without NLCs have relied on microarray techniques using a limited number of established gene sets to acquire targeted gene expression profiles (Bhattacharya et al. 2011; Boissard et al. 2016b; Burger et al. 2009b; Burgess et al. 2016; Fiorcari et al. 2015; Maffei et al. 2013). These studies helped identify several molecules potentially important in mediating the pro-survival effect of NLCs on CLL cells. The molecules included ICAM-1 and CD31 (Boissard et al. (2016b) and CSF-1 (Polk et al. (2016). However, subsequent studies showed that inhibition of these molecules or blocking NLC development did not significantly increase the spontaneous apoptosis (Boissard et al. 2016b) or ibrutinib-induced cell death of CLL cells (Polk et al. 2016), indicating that other yet-to-be-identified mechanisms may operate concomitantly to compensate the inhibition of the known targets. Further studies are thus still required in order to gain better understanding on how NLCs and CLL cells influence each other, resulting in sustained survival and expansion of CLL cells in the tissue microenvironment.

RNA-sequencing (RNA-seq), also called whole-transcriptome shotgun sequencing, is a newly developed, high throughput sequencing technology for characterising RNA content and composition in a sample of cells (Hrdlickova, Toloue & Tian 2017; Wang, Gerstein & Snyder 2009; Wolf 2013).

Until the arrival of RNA-seq, microarrays were the standard method of gene expression quantification. However, RNA-seq can not only quantify the gene expression, but also give the precise location of transcript boundaries to a single base resolution (Wang, Gerstein & Snyder 2009). Short reads of 30-base pair (bp) can uncover how two exons are connected whereas longer reads or pair-end short reads can reveal the connectivity between multiple exons (Wang, Gerstein & Snyder 2009). This allows the sequencing-based technique to identify different transcripts of individual genes.

Compared with microarrays, RNA-seq can capture a wider range of expression values. The "Count data" is a digital measure and can be scaled linearly with no upper limit, whereas microarrays can display saturation of analogue-type fluorescent signals (Wolf 2013). It is structured as a table where it reports the number of sequence fragments detected to each gene for each sample (Nguyen et al. 2016). RNA-seq has a very low background signal because sequences can be mapped to unique regions of the gene (Hrdlickova, Toloue & Tian 2017; Wang, Gerstein & Snyder 2009; Wolf 2013). RNA-seq can give information on RNA splice events, which are not easily detected by microarray (Wolf 2013). Thus, short reads of 30-base pair (bp) can uncover how two exons are connected whereas longer reads or pair-end short reads can reveal the connectivity between multiple exons (Wang, Gerstein & Snyder 2009). This allows the sequencing-based technique to identify different transcripts of individual genes. RNA-seq produces results with high levels of reproducibility. As it does not involve cloning or amplification step, RNA-seq requires less RNA sample (Wang, Gerstein & Snyder 2009).

In this Chapter, I will therefore describe the findings obtained through comparison of globe gene expression profiled by RNA-seq in different populations of cells, namely between CLL cells co-cultured with NLCs versus CLL cells cultured alone and between NLCs co-cultured with CLL cells versus NLCs cultured alone.

5.2 Objectives

- Establish a comprehensive list of differentially expressed genes in primary CLL samples cultured with or without NLCs through RNA-seq analysis,
- Validate the RNA-seq results using RT-qPCR on selected genes from the list,
- Identify molecules and pathways critically involved in survival and resistance of CLL cells to therapy *in vivo* through bioinformatics analysis.

5.3 Methods

5.3.1 CLL cell samples and coculture

In order to carry out the experiments, the NLCs were developed as described in Methodology and for this chapter the cases chosen had NLC Score of 2 or 3. This was to ensure a good number of NLCs were developed so enough RNA can be extracted. 6 CLL cases were used for the RNA-seq analysis and validation (#3577, #3599, #3627, #3682, #3679 and #3684). A further 8 cases were used for validation of RNA-seq results (#3620, #3645, #3686, #3605, #3607, #3621, #3631 and #3637). Clinical information of CLL samples used in this part of the study was provided in Table 5.1. To meet the objectives of the study, I designed the following 4 populations:

- CLL alone (CLL cells cultured alone)
- CLL + NLC (CLL cells co-cultured with NLCs)
- NLC alone (NLCs cultured alone)
- NLC + CLL (NLC co-cultured with CLL cells)

The changes seen on CLL + NLC when compared to CLL alone is due to the effects that NLCs have on CLL cells. Conversely, the changes seen on NLC+CLL when compared to NLC alone is due to the effects CLL cells have on the NLCs. 24-hour period of culture/co-culture was chosen based on the results described in the previous chapters where protection of CLL cells against spontaneous apoptosis was detected at that time point (see previous chapters). This means that at the cellular level the protective effect of NLCs on CLL cells can be seen in 24 hours and that the changes in gene expression caused by the co-culture condition should have taken place within 24 h of co-culture.

As illustrated in Figure 5.1, fresh CLL PBMC sample was first cultured under standard conditions in a multi-well culture plate until the NLCs have developed and reached their plateau. The CLL cells in the PBMC co-cultures were then removed by gentle pipetting to leave NLCs behind. Wells containing NLCs were equally divided. For NLCs cultured alone, standard RPMI medium was added to the wells. For NLCs selected for co-culture, autologous CLL cells were thawed and resuspended in complete RPMI medium and added onto the wells. Aliquots of thawed CLL cells from the same sample were cultured alone in a separate well as CLL alone. The three groups of cells were incubated for 24 hours in humidified incubator at 37^{o}C at 4% CO_2. Following the 24-hour incubation, the cells from the 3 groups were harvested and prepared for RNA extraction.

Table 5.1 Clinical Data of Samples used for RNA-seq and RT-qPCR.

Details of each sample with clinical data information and RNA sample information. Samples with blue highlight are indicated on those that were not included in RT-qPCR analysis, red marked samples are those that were sent for RNA-seq and green Highlight are those that are from the same patient. RIN is from QC performed by the outsourced Novogene. Purity was measured using Nanodrop as described in Methods.

Sample number	WBC	Absolute Lymphocyte Count	Absolute Monocyte Count	Drug Treatment	IGHV status	Chromosomal status	Age at Diagnosis	Age at collection of samples	Gender	Staging	Date of sample collection	Percentage Monocytes of PBMC	PBMC total	RIN on sending to RNAseq		Purity	
														CLL alone	CLL+NLC	CLL alone	C+ N
3577	85.7	75.8	1.4	ibrutinib	NA	17p-		55	Male	A	28/07/2017	1.813	77.2	9.3	9.1	2.1	2.09
3599	63.9	59.2	0.9	untreated	NA	13q-	62	70	Female	A	13/09/2017	1.498	60.1	7.7	9.2	2.08	2.1
3627	136.7	129.4	2	ibrutinib	unmutated	13q del	58	68	Male	C	06/12/2017	1.522	131.4	8.7	9	2	2.08
3682	33.2	25.8	0.5	untreated	NA	normal	71	74	female	A	13/06/2018	1.901	26.3	8.8	9.2	1.97	2.01
3679	171.4	164.7	1.6	untreated	NA	13q-	53	54	male	C	06/06/2018	0.962	166.3	8.8	8.2	1.92	1.97
3684	230.1	220.8	NA	untreated	mutated	13q-	75	84	male	A	18/06/2018			8.4	9	1.97	1.98
3620	145.9	142.6	1.2	untreated	mutated	normal	69	76	Female	C	15/11/2017	0.834	143.8			1.91	1.95
3645	264.1	258.8	1.5	untreated	unmutated	normal	68	72	male	C	14/03/2018	0.576	260.3			2.09	2.07
3686	38.5	31.3	1	untreated	mutated	trisomy 12	70	71	female	A	25/06/2018	3.0960	32.3			1.97	1.94
3605	252.8	244	1.6	untreated	mutated	13q-	60	63	Male	B	27/09/2017	0.651	245.6			2.15	2.21
3607	254.2	247.7	2.2	untreated	mutated	normal	66	69	Male	B	02/10/2017	0.880	249.9			2.05	2.1
3621	70.2	60.6	2	ibrutinib	mutated	13q-	58	59	Female	B	15/11/2017	3.195	62.6			1.93	1.91
3631	256.1	>200	4.7	ibrutinib	mutated	13q-	60	64	Male	B	13/12/2017					1.9	1.89
3637	144.6	134.9	2.2	untreated	unmutated	11q-, 13q-	66	69	Male	A	24/01/2018	1.605	137.1			2.15	2.02

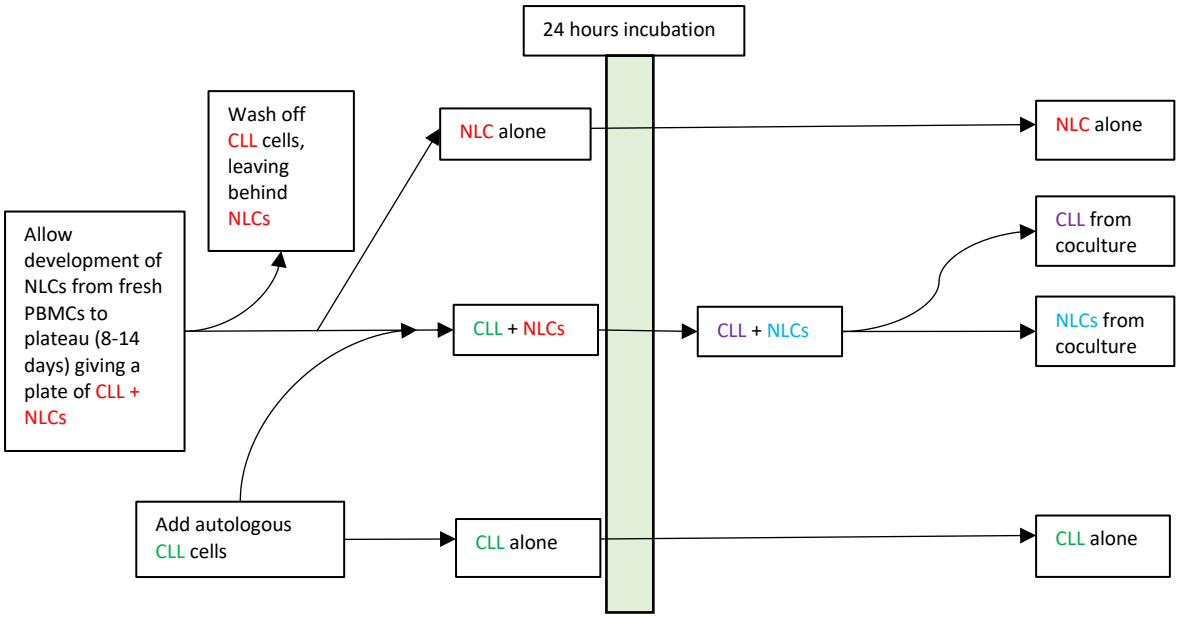

Figure 5.1 Schematic of preparing samples for RNA extraction

Diagram of experiment design to produce 4 populations to compare the effects of CLL cells on NLCs and NLCs on CLL cells. The starting CLL PBMC culture (red) produces developed NLCs (8-14 days later) and the CLL cells are washed off. Autologous CLL cells (green) are added. After the incubation period of 24 hours, the new co-culture condition CLL cells (purple) are collected leaving behind the new conditioned NLCs (blue). By the end of the 24 h incubation, all 4 populations of cells are harvested and RNAs from respective cell populations extracted.

5.3.2 RNA preparation

As seen in Figure 5.1, CLL cells from CLL alone and CLL in co-culture with NLCs are harvested by gentle washing and collected into 1.5 ml Eppendorf tubes total RNA was extracted using a commercial kit (RNeasy Mini Kit, Qiagen).In brief, the cell pellet was resuspended in 400ul RNA lysis buffer and mixed thoroughly before it was transferred to the 2ml Shredder spin column (QIAshredder, Qiagen).

To extract RNA from NLCs cultured alone and NLCs in co-culture with CLL cells, NLCs were lysed by adding the RNA lysis buffer directly on the surface of the culture plate. The cell lysate was then collected and transferred to the shredder spin column, as described above.

As shown in Figure 5.2, RNA was extracted following the Manufacturer's instruction. Isolated RNA was then kept in ice cold temperature to assess for purity and quantity. The remaining RNA was then stored and kept at -80°C.

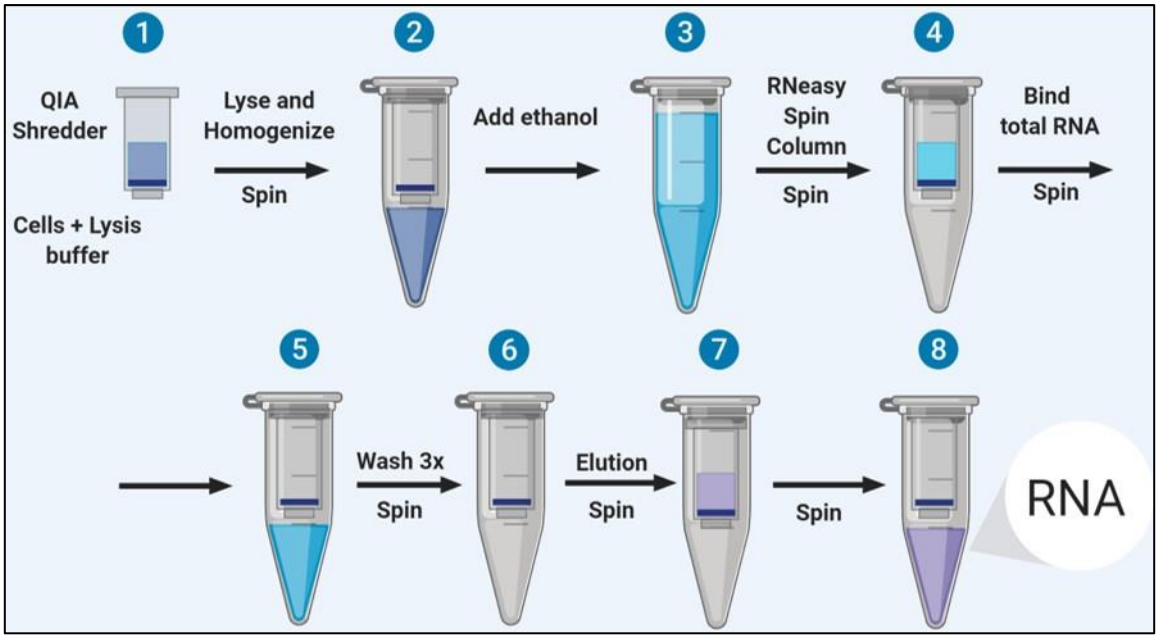

Figure 5.2 Procedure for extracting RNA from cells by Qiagen RNeasy Mini kit.

Using the Qiagen RNeasy Kit and the Qiagen Shredder, a lysis buffer is prepared as per instructions and added to the cell samples. The lysate is then transferred to the QIA Shredder Column for homogenization to reduce viscosity (1). Together with the shredder it is spun for 2 minutes at max speed in a microcentrifuge (2). After discarding Shredder column, ethanol is added to flow-through solution and mix (3). The mixture is transferred to RNeasy Spin Column (4) and spun for 15s at ≥8000g and the flow through is discarded while the RNA is bound to membrane on the RNeasy Spin Column (5). The column is washed three times with washing buffers provided within the kit and the follow through is discarded (6). Finally, RNAse free water is added to the column and the RNA is eluted (7) from the column as follow through (8). The RNA sample is then measured for purity and quantity and stored in freezer. Image adapted from Qiagen RNEasy Mini kit manual using BioRender online tools.

5.3.3 Measuring Purity and Quantity of RNA

The quality of extracted RNA was assessed using a Nanodrop 2000 spectrophotometer (Thermo Fisher Scientific, UK) and quantity was measured Qubit® 2.0 Fluorometer (Thermo Fisher Scientific, UK).

In brief, 1ul of each RNA sample was used to measure the purity of the RNA extracted using the Nanodrop machine where it measures the absorbance ratio at OD260/280 and OD260/230, with RNAse-free water as a control.

5.3.3.1 Quantification using Qubit

Qubit® 2.0 Fluorometer is an instrument used for quantification of protein, DNA and RNA in the same principle as Beer-Lambert Law (relates to the reduction of amount of light to the properties of the media through which the light is travelling through). The Qubit uses fluorescent dyes to measure the

concentration where each dye is specific for one molecule i.e. DNA, RNA or protein. The natural absorbance light at 260nm is used to measure DNA and RNA whereas 280nm is used to measure for proteins. The dyes have a low fluorescence until they bind to their targets, where upon their binding, they intensely fluoresce, which is then measured by the Qubit.

Qubit is preferred for the quantitative measurement over Nanodrop due its greater sensitivity and specificity. Quantification is done by Qubit giving a concentration of ng/ul. The kit used for quantifying was the Qubit® RNA HS Assay Kit with quantitation range of 5-100ng (Thermo Fisher Scientific Life Technologies). Using this kit, including a buffer, a fluorochrome and the standards Standard 1 (with no RNA) and Standard 2 (with high RNA quantity), a linear curve is made. Based on that the sample RNA quantity would be measured against the concentrations within the ranges of the standard curve.

Those RNA samples that had good quality and quantity as defined in 5.3.4 were reserved for commercial RNA-seq service, as described in Methods. The remaining RNA samples that had good quality but enough quantity for RNA-seq were stored in -80^{o}C freezer. These RNA samples were subsequently used to synthesise cDNA (as described in Methodology) to be used for optimising and validation by RT-qPCR. The summary information of the RNA samples is provided in Table 5.2.

The quality and quantity of the RNA was verified by Novogene as well as assessing the integrity of the RNA with RNA integrity number (RIN) values of 7 and higher. For more information on Integrity of RNA, please refer to Appendix 7.5.

Table 5.2 Summary information of RNA samples regarding RNA quality and quantity

Sample ID	Purity of CLL sample from Biobank (CD5 CD19)	Viability of CLL sample from Biobank	Population	Purity (Nanodrop) 260/280	Quantity (Qubit as ng/ul)	Volume (ul)	Total (ng)
3577	95.04%	95.10%	CLL alone	2.1	238	30	7140
			NLC alone	2.07	33.02	25	825.5
			CLL from NLC+CLL	2.09	458	30	13740
			NLC from NLC+CLL	2.08	57.3	25	1432.5
3599	99.20%	96.10%	CLL alone	2.08	258	29	7482
			NLC alone	2.1	187	29	5423
			CLL from NLC+CLL	2.1	323	29	9367
			NLC from NLC+CLL	2.12	101	29	2929
3621	91.94%	92.80%	CLL alone	1.93	550	30	16500
			NLC alone	2.05	37.2	30	1116
			CLL from NLC+CLL	1.91	578	30	17340
			NLC from NLC+CLL	1.99	68.8	30	2064
3627	90%	78%	CLL alone	2	212	30	6360
			NLC alone	2.07	344	30	10320
			CLL from NLC+CLL	2.08	220	30	6600
			NLC from NLC+CLL	2.07	364	30	10920
3605	98.64	87	CLL alone	2.15	488	35	17080
			NLC alone	NA	7.48	35	261.8
			CLL from NLC+CLL	2.21	391	35	13685
			NLC from NLC+CLL	NA	11.2	35	392
3607	93.64	84.77	CLL alone	2.05	358	30	10740
			NLC alone	2.53	21	30	630
			CLL from NLC+CLL	2.1	570	30	17100
			NLC from NLC+CLL	2.1	27	30	810
3631	93.911	74.11	CLL alone	1.9	165	30	4950
			NLC alone	1.98	14.88	30	446.4
			CLL from NLC+CLL	1.89	230	30	6900
			NLC from NLC+CLL	1.92	22.2	30	666
3637	84.15	80.11	CLL alone	2.15	51.8	30	1554
			NLC alone	2.18	12.4	30	372
			CLL from NLC+CLL	2.02	282	30	8460
			NLC from NLC+CLL	2.21	28.8	30	864
3645	84	85.6	CLL alone	2.09	103.5	30	3105
			NLC alone	2.26	11.4	30	342
			CLL from NLC+CLL	2.07	124.5	30	3735
			NLC from NLC+CLL	2.07	22.4	30	672
3620	NA	20.35	CLL alone	1.91	990	29	28710
			NLC alone	1.95	28.8	27	777.6
		36.55	CLL from NLC+CLL	1.9	420	29	12180
			NLC from NLC+CLL	1.95	63.6	28	1780.8
3679	97.12%	90.90%	CLL alone	1.92	520	30	15600
			NLC alone	2.01	58	30	1740
			CLL from NLC+CLL	1.97	830	30	24900
			NLC from NLC+CLL	1.96	63	30	1890
3682	95.00%	89.00%	CLL alone	1.97	251	30	7530
			NLC alone	2.07	189.6	30	5688
			CLL from NLC+CLL	2.01	112	30	3360
			NLC from NLC+CLL	2.05	118.4	30	3552
3684	97.38%	86.40%	CLL alone	1.97	730	30	21900
			NLC alone	2.09	49.2	30	1476
			CLL from NLC+CLL	1.98	5000	30	150000
			NLC from NLC+CLL	2.01	65.2	30	1956
3686	83.60%	83.00%	CLL alone	1.97	289	30	8670
			NLC alone	2.1	98.8	30	2964
			CLL from NLC+CLL	1.94	306	30	9180
			NLC from NLC+CLL	2.1	66.4	30	1992

5.3.4 RNA sequencing

The samples that met the quality control criteria for RNA-seq sequencing, i.e. having ≥1µg RNA measured by Qubit®, purity measured by Nanodrop of OD260/280 ≥2.0 and OD260/230 ≥2.0, with a volume ≥20µL and RIN values ≥7.0 were used for sequencing by RNA-seq technology at Novogene (Novogene (UK) Ltd, Cambridge, UK). The details of RNA sequencing were described in Methodology. The completed sequencing data was returned electronically and analysed by the Bioinformatics specialists at Computational Biology Facility (CBF) of the University of Liverpool.

Due to the technological requirement for sequencing, the population of RNA is converted to a library of cDNA fragments with adaptors attached to one or both ends of up to several base pairs which will undergo short reads. The transcripts first need to be reconstructed with these reads, referred to as *de novo* assembly. In the case where transcript or genome information readily available, the reads are aligned onto the reference. The number of reads that fall to a given transcript provides a digital measurement of the level of expression of each gene, which is a starting point for a biological conclusion (Hrdlickova, Toloue & Tian 2017; Wang, Gerstein & Snyder 2009; Wolf 2013).

5.3.5 Sequencing Data Analysis

The analysis portion was performed under the supervision of Professor Francesco Falciani of Computational Biology Facility (CBF) of the University of Liverpool.

5.3.5.1 Quality Control

The data generated by RNA-seq is in the format of bam and FastQ files. FastQ files contain sequences and quality scores for each nucleotide. 10% of the data was fed into FASTQC tool to check the quality of FastQ files. FASTQC generates an html file for each sample. All of this is fed into MultiQC which then gives an overview of quality control of all samples in a single html file as a one report. The graphs that are generated determine whether the samples pass or fail (see Appendix Figure 7.10).

The sequence counts give number of reads sequenced from either direction. The base quality in DNA sequencing is presented by Phred Score. The larger the value the better the quality of a sequenced base. The average GC content of reads was also analysed in the QC report. The Sequence Duplication levels counts the degree of duplication for every sequence in the library and the plot shows the relative number of sequences with different degrees of duplication. A low level indicates a high level of coverage without enrichment bias. The frequency of A/T/C/G on each base position is measured as a

percentage and should be approximately constant across the read. Due to the very sensitive measurement, this commonly results in a 'failed' parameter in the report.

5.3.5.2 Obtaining Counts

The sequence reads are aligned onto a reference genome using Bowtie 2 and SAM tools. The reference genome chosen was homo_sapiens _NCBI_GRCh38. The prerequisite for mapping is having index files for the genome, which were built using Bowtie 2. Bowtie 2 outputs the alignments in SAM format where it is then processed using SAMtools resulting in bam files. From bam files, counts were generated using htseq_count tool. The counts were then used for data processing.

5.3.6 Data Processing

From the starting number of genes and their corresponding counts, the CBF team filtered out genes which had a sum of counts over all samples <10. The filtered counts were fed into DESeq2 which then makes corrections for library size. DESeq2 generates log2fold change values (CN vs CL), p-values and p-adj values using Benjamini-Hochberg correction.

5.3.6.1 Principle Component Analysis

Principal Component Analysis (PCA) is a method of spreading the whole data observations of possibly correlated variables as far apart based on the overall spatial orientation. PCA calculates the most separation among the data points. Therefore, if the data includes outliers, the outlier and the data points will have the largest separation. Through transformations of data, multiple PC values were obtained, labelled as PC1-PC20. The first principal component accounts for as much of the variability in the data as possible, and each succeeding component accounts for as much of the remaining variability as possible. The amount of variance that can be described by a principle component is usually represented as a percentage, where it represents how much of the variance is explained in the direction of the vector.

5.3.6.2 Differential Gene Expression Analysis

Two packages for R software (Bioconductor website) were applied to the RNA sequencing data in performing gene expression analysis: DESeq2 (Love, Huber & Anders 2014) and SAM using SAMseq method (Li & Tibshirani 2013).

5.3.6.2.1 DESeq2/SAM

This file is input to DESeq2 / SAM function to give out statistical information. DESeq2 and SAM are both methods of statistical analysis. From this the genes of statistically significant difference are separated out using adjusted p value of 0.05 as a cut-off. Those that are positive log2fold values are upregulated, whereas negative values are considered downregulated.

While performing DESeq2 analysis, False Discovery Rate (FDR) 5% was used with Benjamini-Hochberg correction and genes with adjusted p value <0.05 were considered significantly upregulated/downregulated.

For SAM, which is a more stringent method, the FDR was lowered to 10%.

5.3.6.3 Functional annotation against Database for Annotation, Visualization and Integrated Discovery (DAVID)

DAVID was originally a web based functional annotation tool that identifies enriched biological Gene Ontology (GO) terms and clusters the redundant ones (Dennis et al. 2003). A newer version provides a greater integrated annotation knowledgebase, built on the newly developed 'DAVID Gene Concept'. It provides a more complex set of tools to methodically summarize relevant biological patterns from user-classified gene list (Dennis et al. 2003).

5.3.6.4 Gene Set Enrichment Analysis

All of the filtered genes were ranked based on "stat" values provided by DESeq2. Stat is a measure of log2fold change divided by its standard error. Gene sets selected (KEGG and Gene Ontology) were mapped onto the ranked genes. A gene set is considered to be either positively or negatively enriched if its genes are clustered high or low on the ranked list, respectively, and with the family-wise error rate (FWER) p-value <0.05 (Figure 5.3).

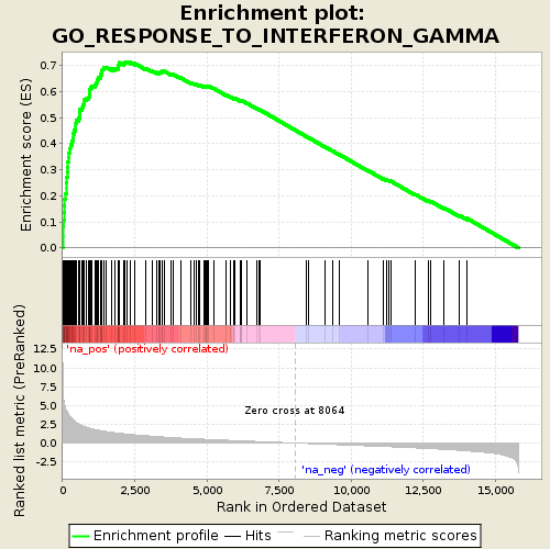

Figure 5.3 Example of Positive enrichment gene set

Enrichment plot of a gene set 'GO_RESPONSE_TO_INTERFERON_GAMMA'. The Enrichment score (ES) seen in the Y-axis (top). The score at the peak of the plot (the score furthest from 0.0) is the ES for the gene set (green). Gene sets with a distinct peak at the beginning (such as the one shown here) or end of the ranked list are generally the most interesting. The bottom portion of the plot shows the value of the ranking metric as you move down the list of ranked genes. The ranking metric measures a gene's correlation with a phenotype. A positive value indicates correlation with the phenotype profile and a negative value indicates no correlation or inverse correlation with the profile. Image taken from Gene Set Enrichment Analysis website (https://software.broadinstitute.org/gsea/doc/GSEAUserGuideFrame.html)

In order to visually represent Gene Set Enrichment Analysis (GSEA) results a bioinformatics analysis tool, REVIGO, was used that takes a long list of Gene Ontology terms and summarizes them by removing redundant GO terms (Supek et al. 2011). From GSEA results, they extracted GO terms only, fed them into the web server 'Reduce and Visualize Gene Ontology' (REVIGO) and the results are shown in a "TreeMap" as well as scattered plot representation (Supek et al. 2011). Each rectangle is representative of a single cluster. The representatives are joined into 'superclusters' of loosely related terms which are then visualized with different colors (Supek et al. 2011). The size of the rectangles may be modified to either the p-value, or the frequency of the GO term in the underlying GOA database (Supek et al. 2011).

In scatterplot representation, cluster representatives (i.e. terms remaining after the redundancy reduction) are shown in a two dimensional space based on semantic similarity (Supek et al. 2011).

5.3.6.5 Ingenuity Pathway Analysis (IPA)

5.3.6.5.1 Downstream Effector Analysis (DEA)

The IPA database of diseases and biological functions contains information on whether a gene is known to promote or inhibit a certain function. From gene matching, depending on the logFC, an input gene is matched to an increase or decrease of activity of a certain function. This is visualised by a "TreeMap" or a hierarchical heatmap, where the major boxes represent a family or category of related functions or diseases. Each individually coloured rectangle is referring to a particular biological function and if the function is found to be increasing, it will be shown in orange, otherwise it is shown in blue as decreasing (Kramer et al. 2014). A table of top categories of Disease and Function from IPA database is also generated.

5.3.6.5.2 Upstream Regulator Analysis

Differentially expressed genes in CLLcc (up and downregulated) along with their logFC were selected and input in the IPA database of prior knowledge of expected effects between transcriptional regulators and their target genes. Analysis examines how many known target genes of each transcription regulator are present in the input and compares target genes direction of change with the expected change if the transcriptional regulator increases/decreases its activity. If the direction is mostly consistent with activation/inhibition of the transcriptional regulator, a prediction is made about the activation state (Dennis et al. 2003). Upstream regulators were fed as official gene symbols into DAVID to classify them by function. Through DAVID, enriched biological themes (GO terms) can be identified, clustering of annotation terms can be made, genes can be visualized on KEGG pathway maps and more.

5.3.7 Real time Quantitative PCR (RT-qPCR)

A selected number of genes from a list of differentially expressed genes from RNA-seq dataset (see Appendix Table 7.7) was chosen for validation by RT-qPCR following literature search for their function and relevance to CLL. Due to the large number of differentially expressed genes identified, for practical reason those genes with the biggest log2 fold-changes and the known association with the CLL microenvironment and NLC function were given the priority to be included for validation. In total, 20 genes were initially selected for validation purposes.

5.3.7.1 Primer Designing

Designing primers is a very meticulous, but important step in ensuring correct amplification of a gene of interest (Ye et al. 2012). In brief, sensitivity and specificity of the primers to the complementary sequence of the genes of interest were carefully taken into accounts. A forward and reverse primer would ensure an accurate amplification during the polymerase chain reaction. The primer are designed in such a way that the primer itself is stable with melting temperatures (Tm) of 50-60^{o}C. The primer pairs should have a Tm within 5^{o}C of each other. The primer pairs are designed to avoid complementary regions or be possible hairpin structures. The primers are prepared using the online tools from Ensembl Genome Browser (https://www.ensembl.org/Homo_sapiens/Info/Index), NCBI Primer Designing (https://www.ncbi.nlm.nih.gov/tools/primer-blast/), Oligonucleotide Properties Calculator (http://biotools.nubic.northwestern.edu/OligoCalc.html) and NCBI Homo sapiens (human) Nucleotide BLAST (https://blast.ncbi.nlm.nih.gov/Blast.cgi?PAGE_TYPE=BlastSearch&BLAST_SPEC=OGP__9606__9558). Detailed sequences of the primers used for this chapter were provided in Appendix Table 7.7.

5.3.7.2 Selection of Reference Gene

GAPDH, RPL27 and ACTB were used for housekeeping/reference genes based on consensus in the literature (Eisenberg & Levanon 2013; Nakayama et al. 2018). Using the counts for each sample, the three mentioned genes were compared with each other using linear correlation. Those that had good correlation of at least 2/3 combinations was considered to be used as the Reference Gene of choice. Further details are seen in Appendix Figure 7.11.

5.3.7.3 The use of a Calibration Sample

A calibration sample had to be included in all batches of RT-qPCR with all the primers. Ideally, the calibration sample had to have a high expression of all the primers to ensure appropriate technical replicates. Addition to that there must be enough cDNA of the calibration sample to be used in optimising as well as in the actual RT-qPCR experiments. Within the raw data of the RNAseq, the sample with the highest counts, for each primer was considered a good candidate. The CN of 3679 and 3627 were therefore considered to be the calibration positive control samples.

5.3.7.4 Calculation of Relative Gene expression

The Livak Method for relative gene expression analysis (Livak & Schmittgen 2001) was used where the result was expressed as the fold change of the expression of target gene in the test sample over that in the calibrator sample with expression of target gene in both test and calibrator sample normalized to the expression of a reference gene. Normalizing the expression of the target gene to that of the reference gene compensates for any difference in the amount of sample tissue.

The C_T of the target gene is normalised to that of the reference gene for both test sample and the calibrator sample to give $\Delta C_{T(test)}$ (Equation 5.1). This is then normalised to that of the calibrator. Finally, the expression ratio is calculated, where the gene expression is considered increased if >1.0 and decreased if <1.0.

Equation 5.1 Calculation of Relative Gene expression.

Calculation of relative gene expression is by normalising the CT (1) and then normalising that of the test sample to that of the calibrator (2). Finally, the normalised expression ratio is calculated (3).

1. Normalise the C_T

$$\Delta C_{T(test)} = C_{T(target,\ test)} - C_{T(ref,\ test)}$$

$$\Delta C_{T(calibrator)} = C_{T(target,\ calibrator)} - C_{T(ref,\ calibrator)}$$

2. Normalise the ΔC_T of the test sample to the ΔC_T of the calibrator:

$$\Delta\Delta C_T = \Delta C_{T(test)} - \Delta C_{T(calibrator)}$$

3. Calculate the expression ratio:

$$2^{-\Delta\Delta C_T} = \text{Normalized expression ratio}$$

The RT-qPCR data, must meet the following criteria for analysis.

1. GAPDH must be expressed in all sample pairs.
    a. If it is not expressed in one, the pair is excluded from interpretation.
2. C_T of the sample pair should ideally be less than 45 cycles.
    a. If both the sample pair is more than 45 cycles then the pair should be excluded.
    b. If one sample in the pair has C_T more than 45 cycles then the sample pair can follow the equation provided that the weakest expression sample is set at default C_T of 45.

5.4 Results

5.4.1 Case Summary

In this chapter a total of 14 CLL samples were used and the summary was displayed in Table 5.3. A more detailed description of the clinical information of the CLL samples used in the study was provided in Appendix Table 7.1. 6 CLL cases were used for RNA-sequencing and validation by RT-qPCR (3577, 3599, 3627, 3682, 2679 and 3684) and 8 cases for validation of RNA-seq results (3620, 3645, 3686, 3605, 3607, 3621, 3631 and 3637).

Table 5.3 Summary of clinical features of the CLL samples used in this chapter

	RNAseq		**RT-qPCR**	
Gender	Male	4	Male	9
	Female	2	Female	5
Prior therapy*	Yes	2	Yes	4
	No	4	No	10
FISH¶	17p-	1/5	17p-	1/10
	13q-	4/5	11q-	1/10
			Trisomy 12	1/10
			13q-	7/10
IGHV#	Mutated	1/2	Mutated	7/10
	Un-mutated	1/2	Un-mutated	3/10
Staging at the	A	4/6	A	6/14
time of sample	B	0/6	B	4/14
collection	C	2/6	C	4/14

*Prior therapy included steroid, chlorambucil, or fludarabine plus cyclophosphamide and rituximab.

¶FISH (fluorescence *in situ* hybridisation) was performed at or prior to sampling.

#IGHV status refers to somatic mutation in IGHV gene of CLL cells as compared with the gene sequence of the nearest germ-line using 2% as a cut-off.

5.4.2 Bioinformatics analysis of sequencing data generated by RNA-seq

5.4.2.1 Quality Control

After receiving the RNA-seq data, the Bioinformatics specialists at the Computational Biology Facility (CBF) of the University did the initial data quality control check and concluded that the quality of the sequencing data for each sample had passed the minimum requirement for downstream bioinformatics analysis. The details of their report were provided in the Appendix Figure 7.10.

5.4.2.2 Data Processing

After performing the quality control test on the RNA sequencing data, the Bioinformatics team was able to include 33,121 genes for subsequent data analysis. They filtered out genes which had a sum of counts of <10 over all samples, resulting in a total of 19,595 genes. Next, a file was produced after feeding the read counts into DESeq2, where log2fold change values were generated. The fold change was comparing the CLL cells cocultured with NLC (CN) versus CLL cells cultured alone (CL). Addition to log2fold change, p values and adjusted p values (padj) values were generated using Benjamini-Hochberg correction method which can reduce the false discovery rate (FDR).

5.4.2.2.1 Principle Component Analysis (PCA)

PCA was then performed using the 19,595 genes from all 4 groups of samples. As seen in Figure 5.4, overall there was a clear separation between CLL and NLC populations among the 24 samples. Also, there was a separation among the 12 samples of CLL cells in the two groups, i.e. cultured alone versus co-culture. Regarding NLCs, however, there was no clear separation among samples in the two groups, i.e. cultured alone versus co-culture.

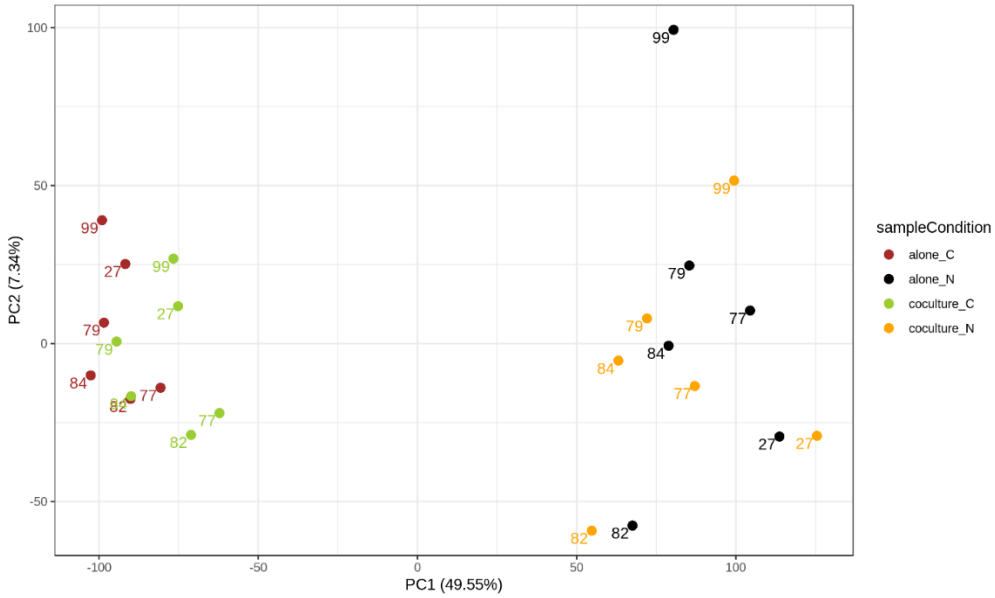

Figure 5.4 Principal Components of all groups from filtered genes separates the CLL samples from the NLC samples

The data observations on the left are those from CLL alone (red) and CLL co-cultured with NLCs (green) and on the right are those from NLCs alone (black) and NLCs co-cultured with CLL cells (orange). This PCA plot used 24 samples and all genes from the filtered set of 19,595.

PCA was repeated using only the CLL samples (alone and co-cultured). As shown in Figure 5.5, a mild form of separation was again seen.

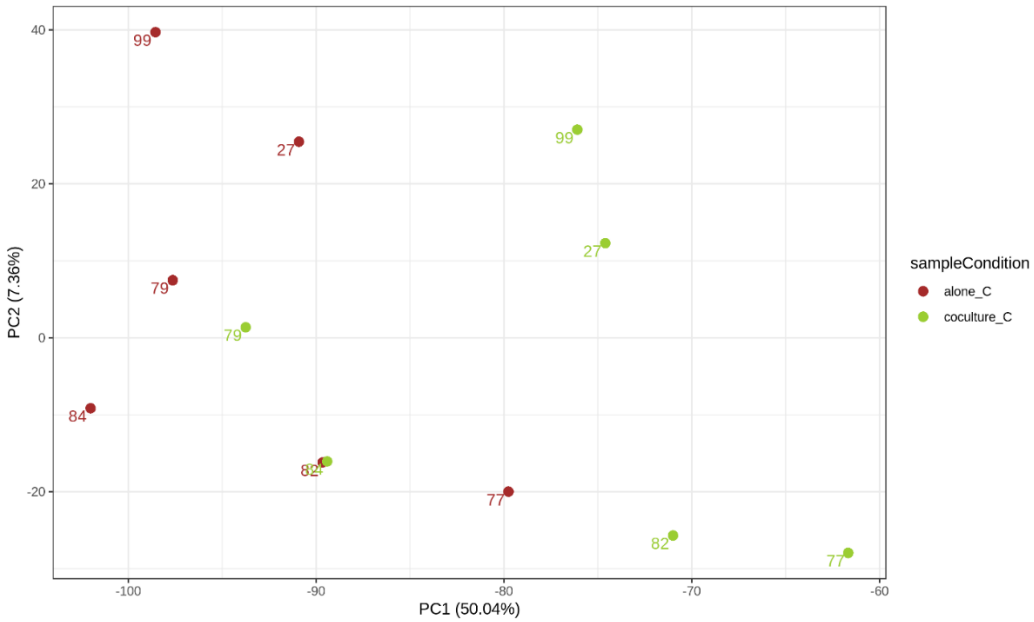

Figure 5.5 Principle Component analysis of CL vs CN samples among the filtered genes

The data observations are those from CLL alone (red) and CLL co-cultured with NLCs (green) This PCA plot used 12 samples and all genes from the initial filtered set of 19,595.

PCA was also repeated using only the NLC samples (alone and co-cultured). As shown in Figure 5.6, there was again no obvious separation among the samples.

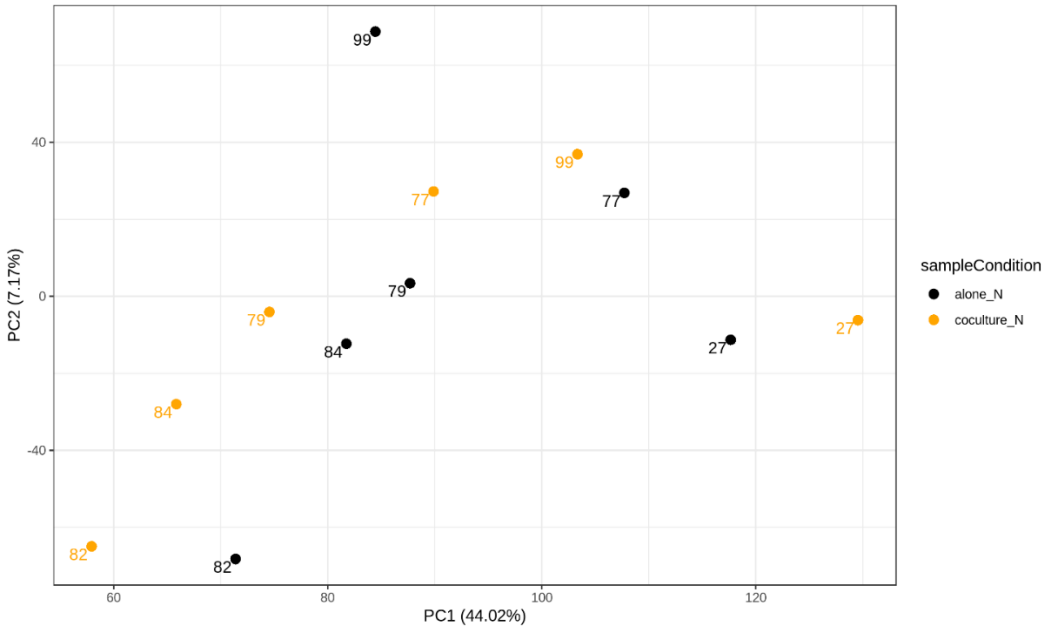

Figure 5.6 Principle Component analysis of NL vs NC samples among the filtered genes

The data observations are those from NLCs alone (black) and NLCs co-cultured with CLL cells (orange). This PCA plot used 12 samples and all genes from the initial filtered set of 19,595.

Upon performing differential expression analysis using DESeq2 (as described in Methods) on the 19,595 genes, 333 genes were identified as significantly differentially expressed among all samples, with 326 differentially expressed genes from CLL samples (alone versus co-culture) and 7 from NLCs (alone versus co-culture) (for details, see Appendix Tables 7.3, 7.4, 7.5 and 7.6). PCA was again performed using the 333 differentially expressed genes. As seen in Figure 5.7, the CLL group was clearly separated from the NLC group.

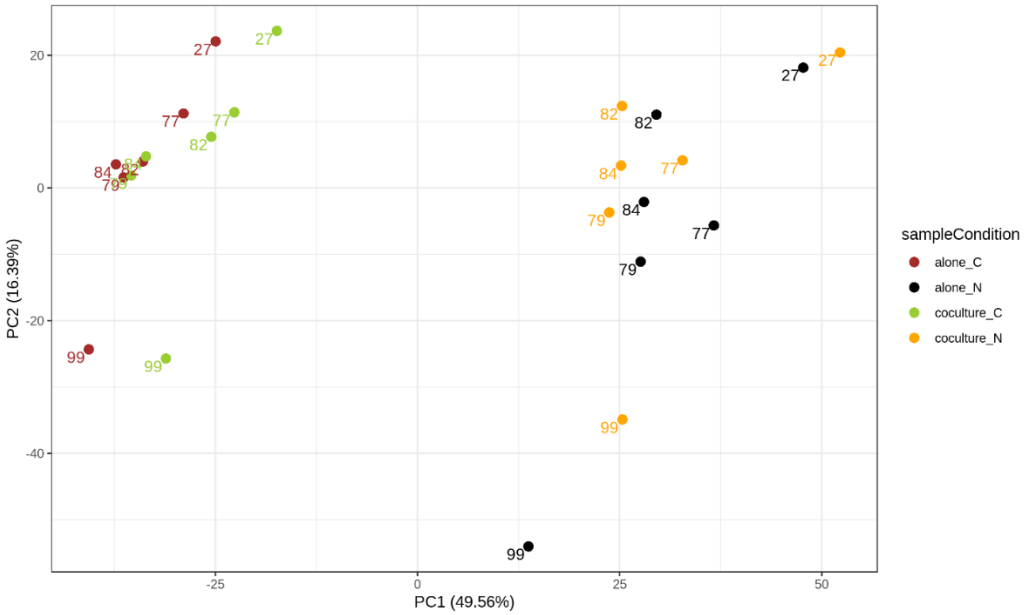

Figure 5.7 Principal Components of all groups from filtered 333 genes that were significantly dysregulated, showed separation between the CLL samples and NLC samples.

The data observations on the left are those from CLL alone (red) and CLL co-cultured with NLCs (green) and on the right are those from NLCs alone (black) and NLCs co-cultured with CLL cells (orange). This PCA plot used 24 samples and all genes from the filtered set of 333 significant genes from DESeq2 results with $p_{adjusted}$<0.05, FDR 5% and use of Benjamini-Hochberg correction.

PCA was repeated only for CLL groups using 326 significantly differentially expressed genes. As seen in Figure 5.8, a separation between the CLL cells cultured alone (within the blue) and the CLL cells co-cultured with NLCs (within the pink).

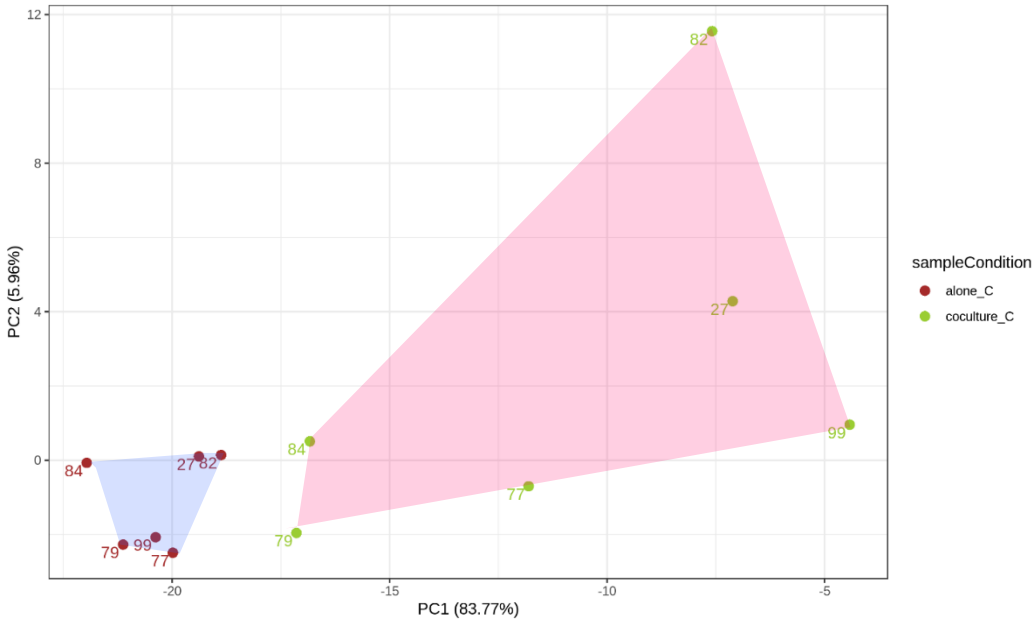

Figure 5.8 Principle Component analysis of CL vs CN samples among the filtered 326 significant genes.

The data observations are those from CLL alone (red) and CLL co-cultured with NLCs (green) This PCA plot used 12 samples and all significant genes from the initial filtered set of 326 from DESeq2 results with $p_{adjusted}$<0.05, FDR 5% and use of Benjamini-Hochberg correction.

PCA was repeated on the NLC group using 7 significantly differentially expressed genes. As shown in Figure 5.9, even with only 7 genes, there was a mild separation between the NLCs cultured alone versus in co-culture.

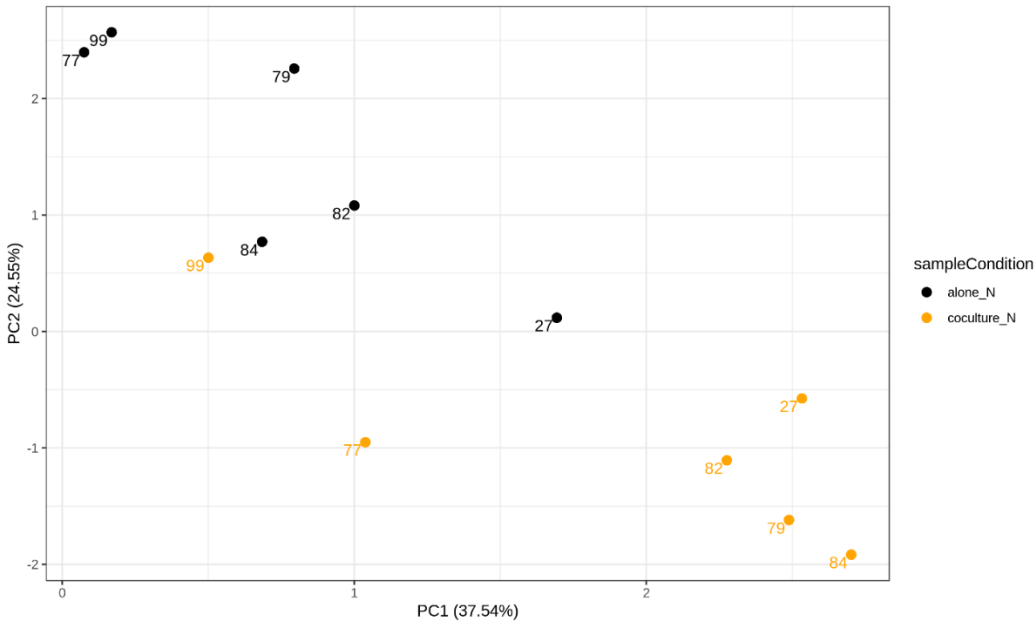

Figure 5.9 Principle Component analysis of NL vs NC samples among the filtered genes

The data observations are those from NLCs alone (black) and NLCs co-cultured with CLL cells (orange). This PCA plot used 12 samples and all significant genes from the initial filtered set of 7 from DESeq2 results with $p_{adjusted}$<0.05, FDR 5% and use of Benjamini-Hochberg correction.

Based on the plots from PCA, there was clear indications that the global gene expression from the 4 cell populations were indeed distinct from each other.

5.4.2.2.2 DESeq2 vs SAM

Differential Gene Expression Analysis (DGEA) was performed comparing the list of differentially expressed genes using DESeq2 and SAM R software packages. As described in Methods, the number of differentially expressed genes from DESeq2 was compared to SAM with their respective FDR on the CLL and NLC groups. Those with positive and negative log2fold values were upregulated and downregulated respectively. When comparing CLL alone (CLL) with CLL in co-culture (CLLcc) as seen in Figure 5.10, it was seen that more significant genes were detected using DESEq2.

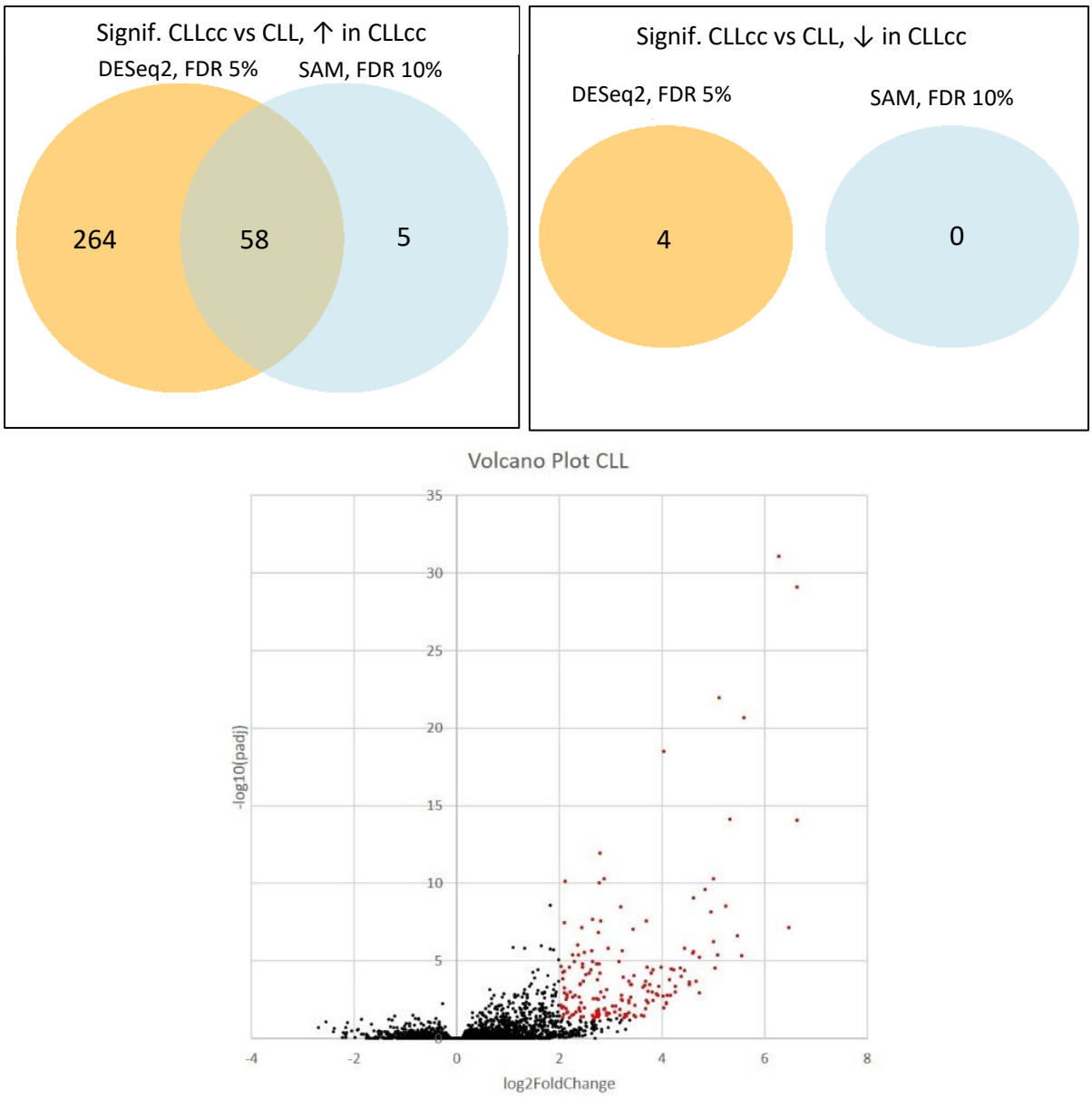

Figure 5.10 Differential Expression with two method comparing DESeq2 with SAM for CLL cells

Venn diagrams (top) showing the number of genes that were upregulated (left) and downregulated (right) among the CLL comparison group using DESeq2 and SAM method of differential gene expression analysis. DESeq2 (orange) results with $p_{adjusted}$<0.05, FDR 5%, Benjamini-Hochberg correction was used and SAM (blue) results with FDR 10%, Benjamini-Hochberg correction. Volcano plot (bottom) displaying the number and expression of genes, based on DESeq2 analysis, according to the log2foldchange and adjusted p value. The red indicates the genes that are having log2foldchange more than 2 with a significant p adjusted value.

When comparing NLC alone (NLC) with NLCs in co-culture (NLCcc) as seen in Figure 5.11, more significant genes were detected in DESeq2.

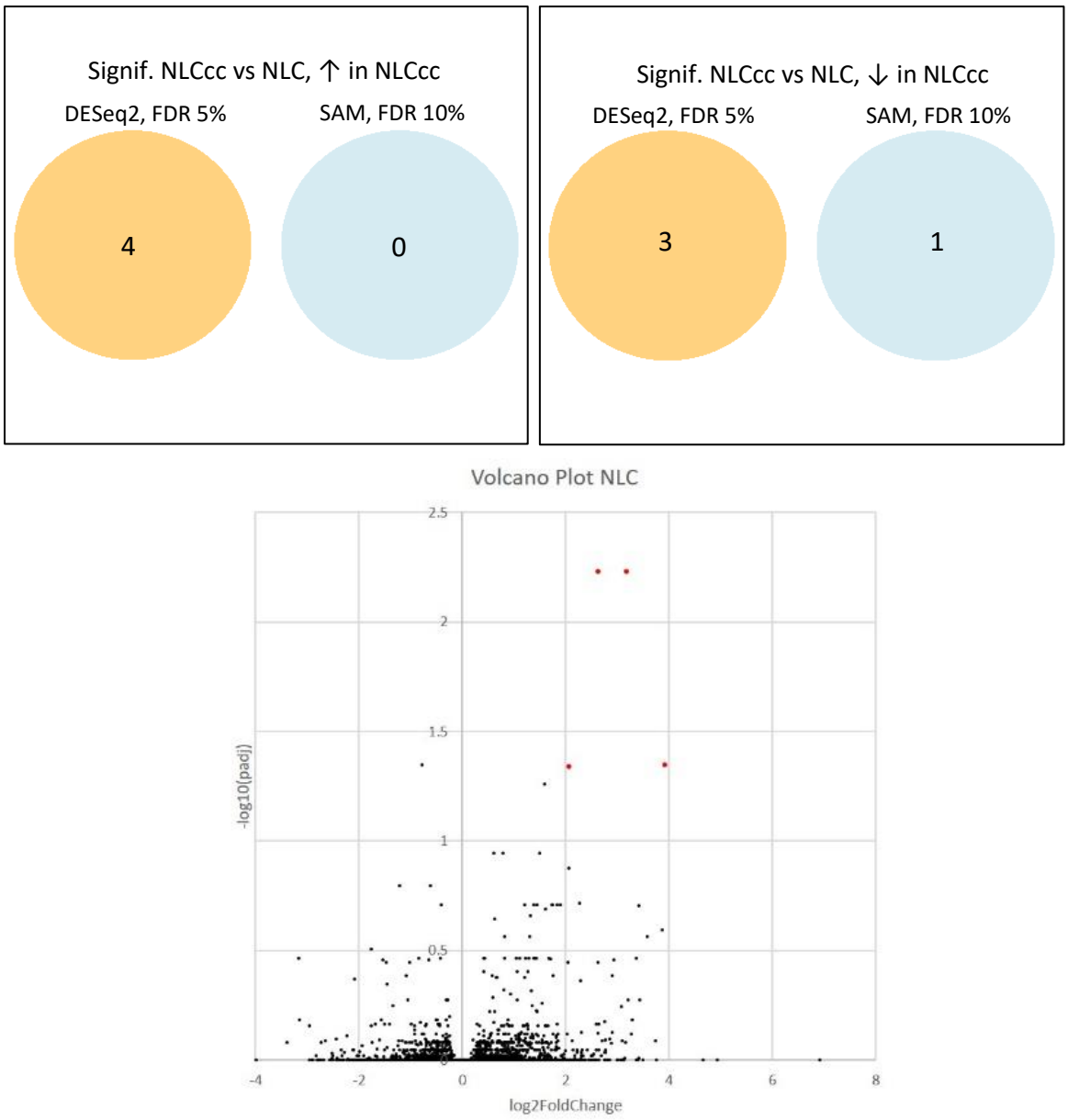

Figure 5.11 Differential Expression with two method comparing DESeq2 with SAM for NLCs

Venn diagram (top) showing the number of genes that were upregulated (left) and downregulated (right) among the NLC comparison group using DESeq2 and SAM method of differential gene expression analysis. DESeq2 (orange) results with $p_{adjusted}$<0.05, FDR 5%, Benjamini-Hochberg correction was used and SAM (blue) results with FDR 10%, Benjamini-Hochberg correction. Volcano plot (bottom) displaying the number and expression of genes, based on DESeq2 analysis, according to the log2foldchange and adjusted p value. The red indicates the genes that are having log2foldchange more than 2 with a significant p adjusted value.

Based on the findings, DESeq2 was preferred to be the method of choice for subsequent analysis as it was not as stringent as SAM. The list of differentially expressed genes were those from DESeq2 analysis.

5.4.2.3 Comparison of differential gene expressions with those of microarray data on tissues

A study that investigated effects of tumour-host interactions in vivo (Herishanu et al. 2011), were compared with our data. In that study, peripheral blood (PB), bone marrow (BM) and lymph node (LN) biopsy samples were collected from treatment naïve CLL patients and matched samples were taken from different anatomic compartments on the same day, processed and were analysed at the same time (Herishanu et al. 2011). The CLL patient cohort were a mix of male and female, Rai stage 1-4, mutated and unmutated IGHV and all common chromosomal aberrations investigated in CLL (Herishanu et al. 2011). SAM differential expressions on microarray data from the study, where gene expression profiling was performed on peripheral blood (PB), bone marrow (BM) and Lymph Nodes (LN), were compared with that of our data using FDR 0.5%, Benjamini correction.

Gene set enrichment analysis was performed three times, each time using different differential expression microarray tissue data as input ranked list, comparing Lymph/Marrow, Lymph/Blood and Marrow/Blood.

Four custom gene sets were generated using our differentially expressed genes (CLL_up, CLL_down, NLC_up, NLC_down, DE genes overlapping with tissue data only), when CLLcc was compared with CLL alone and NLCcc was compared with NLC alone as described earlier.

The Bioinformatics team generated 322 genes that were significantly upregulated when comparing CLLcc with CLL alone. 4 genes were significantly downregulated when comparing CLLcc with CLL alone. These were then made into custom gene sets, however only CLL upregulated passed the size threshold. Therefore, this could not be performed with NLC genes of total of only 7.

Using the microarray data from the study as described in Methods, the custom gene sets were compared with LN/BM and LN/PB ranked- retrieved positive enrichment only, and showed statistically significant comparisons (FWER p-value <0.05). Among the statistically significant gene sets were 61 genes which can be seen in Table 5.4. This significant finding was not detected when comparing with BM/PB ranked- retrieved positive enrichment only.

Table 5.4 Core enriched genes from Custom Gene sets vs LN/PB

	PROBE	RANK IN GENE LIST	RANK METRIC SCORE	RUNNING ES
1	RRM2	5	11.533	0.0376
2	ICAM1	106	6.935	0.0543
3	CTSB	111	6.899	0.0767
4	EGR2	158	6.321	0.0947
5	MKI67	170	6.269	0.1147
6	HJURP	296	5.412	0.1249
7	PKMYT1	530	4.467	0.1254
8	OAS3	565	4.384	0.1377
9	RCN1	581	4.339	0.1511
10	C1QA	582	4.338	0.1653
11	LILRB4	621	4.213	0.1769
12	PTGDS	637	4.175	0.1897
13	C1QC	652	4.142	0.2025
14	PKM	769	3.903	0.2082
15	MMP9	777	3.857	0.2205
16	MRC1	1018	3.457	0.2173
17	CXCL9	1064	3.383	0.2257
18	GALNT6	1075	3.366	0.2361
19	PLIN3	1122	3.298	0.2442
20	C1QB	1125	3.29	0.2549
21	EBI3	1131	3.284	0.2654
22	APOE	1158	3.234	0.2744
23	SIRPA	1361	2.961	0.2719
24	TAP1	1398	2.917	0.2793
25	STEAP3	1579	2.733	0.2773
26	TNFRSF9	1596	2.717	0.2853
27	ITGB2	1624	2.687	0.2925
28	C17orf96	1628	2.682	0.3011
29	PGD	1709	2.603	0.3048
30	LAP3	1802	2.524	0.3075
31	PLOD1	1882	2.443	0.3108
32	GBP1	1903	2.424	0.3175
33	BHLHE41	1943	2.395	0.323
34	COL8A2	1951	2.384	0.3304
35	STAT1	1974	2.36	0.3369
36	PARP9	2080	2.258	0.3379
37	TICRR	2109	2.231	0.3435
38	PHLDA3	2111	2.23	0.3508
39	FNDC3B	2168	2.177	0.3546
40	CR1	2197	2.145	0.3599
41	WDFY1	2292	2.067	0.361
42	GADD45G	2588	1.856	0.3492
43	MREG	2596	1.845	0.3548
44	FBXO6	2670	1.797	0.3563
45	UBE2L6	2698	1.776	0.3605
46	CSF1	2700	1.773	0.3663
47	PARP14	2716	1.762	0.3712
48	C1S	2851	1.669	0.3685
49	EGLN3	2958	1.598	0.3673
50	BPGM	3028	1.56	0.3683
51	CCL22	3042	1.55	0.3726
52	MT1E	3124	1.489	0.3725
53	NUPR1	3203	1.443	0.3726
54	FSCN1	3229	1.436	0.3758
55	PRR11	3314	1.388	0.3752
56	QPRT	3416	1.328	0.3735
57	CXCL12	3526	1.278	0.371
58	PLAU	3531	1.275	0.375
59	MMP14	3581	1.247	0.3761
60	GPRC5B	3634	1.219	0.377
61	PRRG4	3643	1.214	0.3805

List of genes generated when comparing custom gene sets vs Lymph/Marrow, ranked – retrieved positive enrichment only. This custom gene set were inlcuding genes upregulated in CLLcc vs CLL, and was ranked with those from the study microarray data (Herishanu et al. 2011).

To confirm the RNA-seq results, some of the differential expressed genes identified by RNA-seq were to be selected for validation in RT-qPCR.

5.4.3 Validation by RT-qPCR

5.4.3.1 Selection of Primers

I decided to select genes from my Differential Gene Expression Analysis (DGEA) list that were also found to be in the study of microarray genes as described in Methods. Among the 61 genes listed, I selected 13 candidate genes. Primer designing difficulties and lack of available resources forced us to exclude the other genes of interest. On deciding the most appropriate reference gene out of GAPDH, RPL27 and ACTB, the comparison using R^2 calculation in linear correlation and regression analyses revealed that GAPDH has a closer positive correlation with other two and is therefore used as house-keeping gene (see Appendix Figure 7.11). I proceeded to test all the cDNA samples for their expression of GAPDH using gel electrophoresis. As seen in Figure 5.12, it was clear that GAPDH are not amplified to an acceptable level in some samples, likely due to insufficient RNA, thus unsuitable for RT-qPCR. These samples (3599, 3577 and 3637) were therefore scrutinised with caution when interpreting the results.

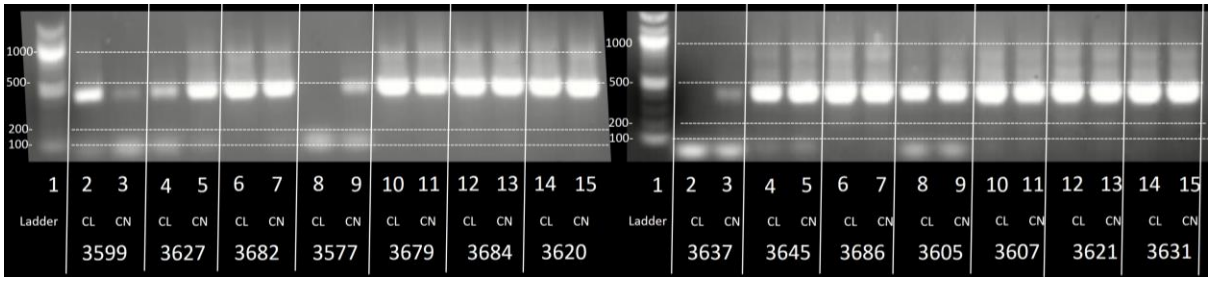

Figure 5.12 PCR gel of GAPDH Primer for all the samples used with a DNA ladder, to determine which samples are suitable to be used for comparison. Here 3599, 3577 and 3637 are seen as unsuitable samples.

Agarose gel electrophoresis was performed, as described in Methodology, on PCR products of the cDNA samples (as described). The Quick-Load Purple 100bp DNA ladder was used. Both CN and CL samples were used for each sample.

5.4.3.2 Optimising Conditions of the RT-qPCR

All the primers were prepared as described and RT-qPCR was performed for each of them using either of the mentioned calibration samples with a negative water control. I first observed the melting curves for each primer. As seen in Figure 5.13, there are two peaks formed. The start of the bigger peak is the temperature which should be set for detection of maximum fluorescence.

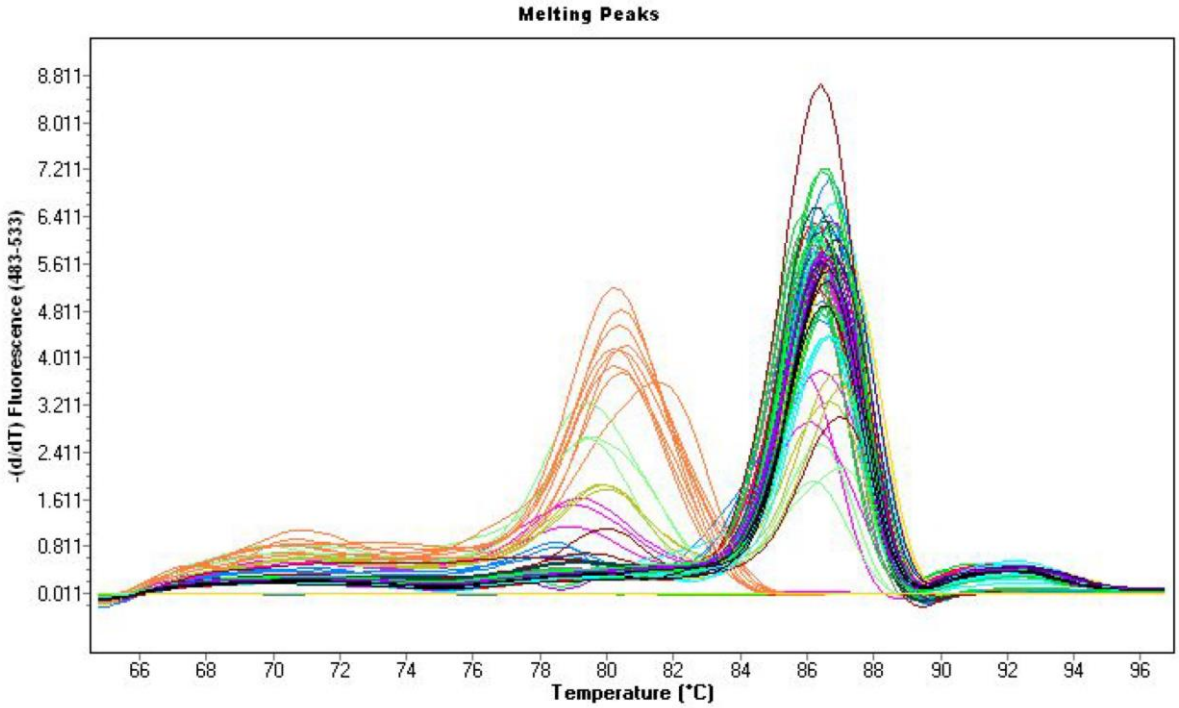

Figure 5.13 Example of Melting curve of all samples with GAPDH Primer run on RT-qPCR.

Melting curve from RT-qPCR of all cDNA samples showing the presence of primer dimer formation at 77-83°C (left peak). The detection temperatures should be adjusted to 84°C. cDNA is synthesised from RNA as described. cDNA for RT-qPCR is prepared as described using standard protocol available in Appendix. Image is generated by the Lightcycler 480 PCR machine.

It is seen that the smaller peak is the location of primer dimer formation which appeared to be present in most of the samples. Individually, this phenomenon can be seen per sample, as seen in Figure 5.14. The use of water control without cDNA shows at what temperature the primer forms primer dimers.

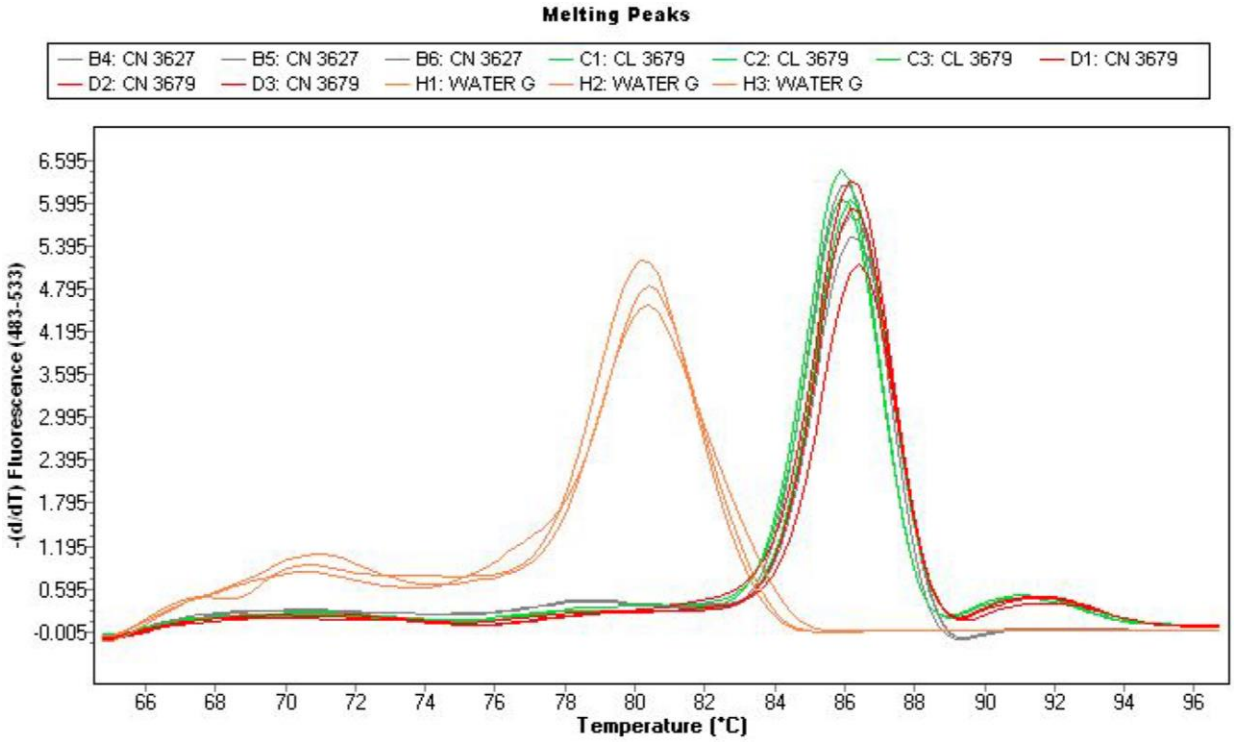

Figure 5.14 Melting curve of sample 3679, control positive sample and control negative water, all with GAPDH Primer showing the presence of primer dimer formation at 77-83°C

Melting curve from RT-qPCR of cDNA sample 3679, control positive sample and control negative water, all with GAPDH Primer showing the presence of primer dimer formation at 77-83°C (left peak). The detection temperatures should be adjusted to 84°C to detect the peak formed *(right)*. Control negative water is used with GAPDH primer to show the position of primer dimer formations. cDNA is synthesised from RNA as described. cDNA for RT-qPCR is prepared as described using standard protocol available in Appendix. Image is generated by the Lightcycler 480 PCR machine.

Addition to melting curves made by the LightCycler 480 PCR machine, I also ran an agarose gel (described in Methodology) to observe how specific the Primers were. As seen in Figure 5.15, most of the primers were working well. This was also agreed upon by their qPCR results from their melting curves.

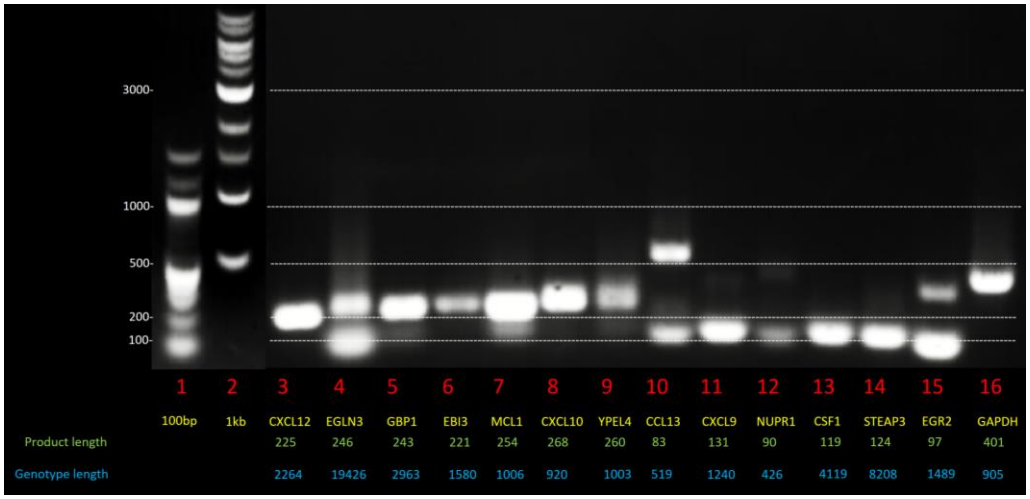

Figure 5.15 Agarose gel using a control sample with all the primers of interest.

Using a control sample with all the primers of interest (column #3-#16). The Quick-Load Purple DNA ladders 100bp (column #1) and 1kb (column #2) were used to compare the bp. The agarose gel electrophoresis was performed as described in Methodology. This was performed to determine which primers are suitable to be used. Here a primer dimer formation is seen for EGLN3 and nonspecific binding is seen with CCL13 and EGR2, thereby making these primers unsuitable to test on samples.

Based on the results (Figure 5.15), depicting the presence of primer dimers identified as detection at half the expected product length (eg. EGLN3) as well as non-specific binding as detection higher than the product length (eg. CCL13), these primer results were to be highly scrutinized with caution.

Based on all the data from position of melting curves of RT-qPCR as well as bands formed from PCR gel electrophoresis, an optimised set of conditions was prepared to read the level of fluorescence for each primer (Table **5.5**).

Table 5.5 Optimal conditions to read the level of fluorescence for each primer

Temp for signal capture ^{o}C	Genes	Comments
80	MCL1	
82	CXCL12	
	CSF1	
84	GAPDH	
	GBP1	
	EBI3	
	YPEL4	Expected to be downregulated
	STEAP3	
86	EGLN3	
NOT GOOD	CXCL10	Overlap with dimers
	CCL13	gDNA amplified
	CXCL9	Overlap with dimers
	NUPR1	Overlap with dimers, gDNA amplified
	EGR2	Partially overlap with dimers, non-specific amplification

The conditions were therefore optimised, supported by evidence of PCR products on agarose gel and I could go ahead and confirm the findings of DGEA of RNAseq.

5.4.4 Confirmation of differentially expressed genes by RT-qPCR

Using the conditions optimised for RT-qPCR for all the primers, I performed the experiment on all the CLL paired samples (14 CL and 14 CN) for all the primers (8 primers). The method is described in Methodology with the grid outlines in the Appendix Table 7.14.

As seen in Figure 5.16, the amplification curves were produced for all the samples (pooled) in their replicates for each primer.

Individually, the cases can be analysed to compare each case (CLL alone and CLL co-cultured with NLC) with positive control and negative water control. As seen in Figure 5.16, the negative (water) control did not amplify anything suggesting no contamination. The presence of the positive control shows the experiment ran correctly. Observed a parallel exponential curve at threshold level, suggested the appropriate threshold level and quality of the experiment. The presence and distance of parallel waves between CL and CN shows the change in level of expression. This was performed on all primers for all case pairs. A representative example of #3620 is shown for each primer in Figure 5.16, where the negative control (water with primer), positive control (control sample) and the pair of CLL alone and CLL in co-culture with NLCs can all be appreciated. When one of the curves reach threshold (C_T) later,

this means the expression of that gene is lower than a curve that reaches threshold (C_T) earlier. Each report generated the C_T at the selected fluorescence threshold. Now that all the RT-qPCR data was acquired, I was ready to calculate and compare the gene expression changes with that of RNAseq data.

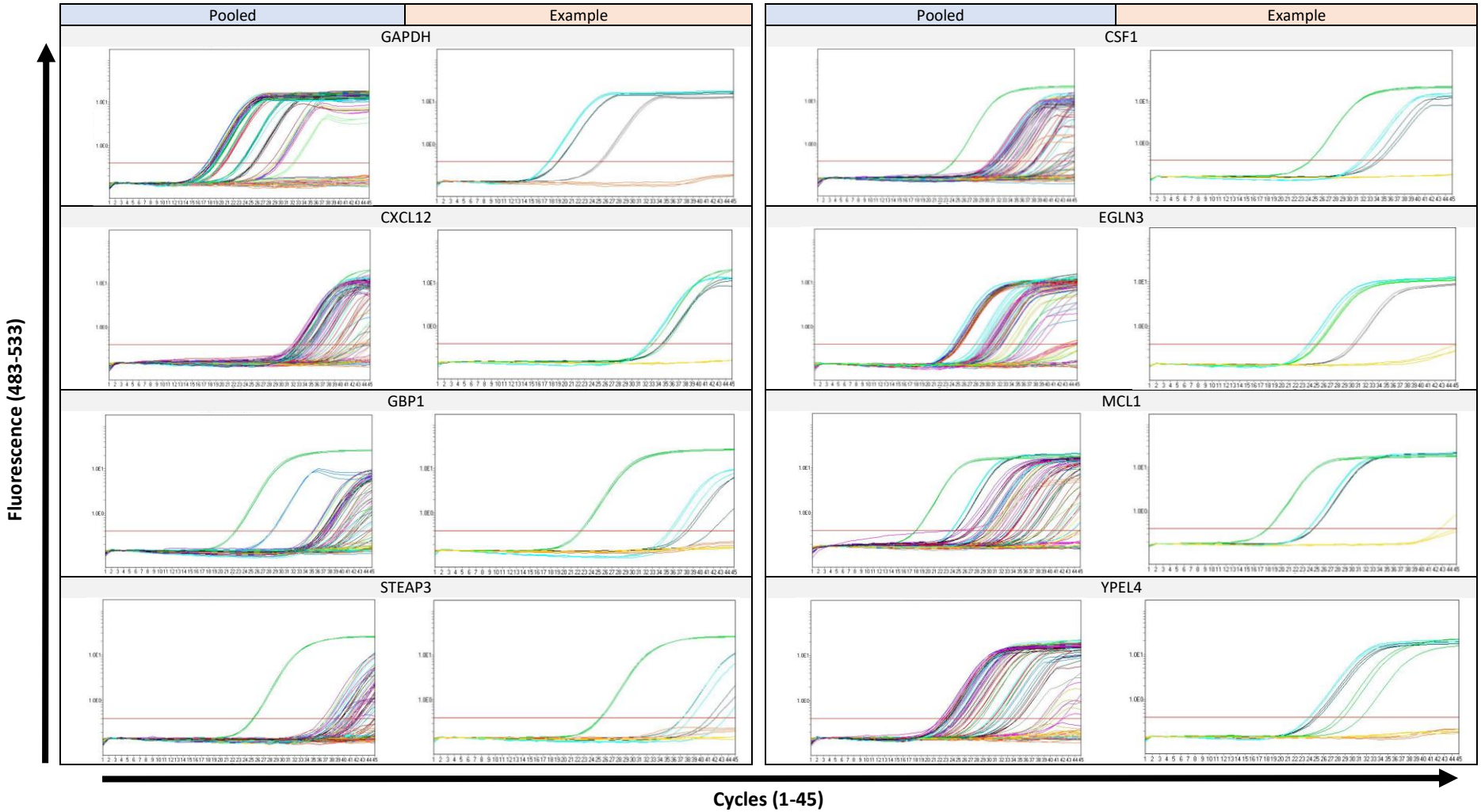

Figure 5.16 Amplification Curves of cDNA samples (Pooled in Blue column and #3620 as representative example in Orange column) for each primer at their optimised conditions.

A control positive (CN 3627 as grey for GAPDH, green for others) and a control negative (PCR grade water with respective primer) in beige colour. For GAPDH, #3620 pair of CLL alone as dark green and CLL in coculture with NLCs as pale blue. For remaining primers, #3620 pair of CLL alone as green and CLL in coculture with NLCs as pale blue. Fluorescence measured in log scale and threshold (red horizontal line) set at 0.4. The point in which the wave for each sample passes the red line is the C_T. RT-qPCR was performed as described and the images were generated using Lightcycler 480 machine software.

5.4.4.1 Relative Gene expression changes

Here the gene expression values were calculated by the method described (Equation 5.1). It became clear that with the additional evidence by the PCR products on agarose gel, the samples #3577 and #3637 were degraded. Additionally, EBI3 were not detected at all in any of the samples. In order to calculate gene expression ratio values, there was a strict requirement of GAPDH C_T values to be present to perform the calculation. If samples from either CLL cells cultured alone or in co-culture with NLCs or both did not have GAPDH values, then that case cannot be used in further analysis. The next strict requirement is that samples from either CLL cells cultured alone or in co-culture with NLCs should have C_T values for each primer. If both were absent then the calculation cannot be performed. As seen in Table 5.6, based on the values as either >1 or <1 corresponding to upregulated or downregulated respectively, it was colour coded for ease in visual representation.

Table 5.6 RT-qPCR results displaying gene expression changes across all the samples for each primer.

	3682	3679	3684	3620	3645	3686	3605	3607	3621	3631
MCL1										
CXCL12										
CSF1										
GBP1										
YPEL4										
STEAP3										
EGLN3										

Increased

Decreased

RT-qPCR results displaying gene expression changes as green (increased) or blue (decreased) compared between CLL alone and CLL in co-culture with NLCs. Samples in purple font are those that were also sent for RNAseq. Gaps are indicated where qPCR data was not obtainable. C_T values were obtained from Lightcycler 480 machine software. Gene expression ratio was calculated as described in Methods. Each sample was normalised to a calibration sample, and each of that was normalised to reference gene GAPDH.

The samples #3577, #3599, #3627 and #3637 had to be excluded because calculation of gene expression ratio was not possible for the majority of the primers. #3627 was excluded entirely because the GAPDH of CL was very weakly expressed which would not have given a justifiable analysis of the primers. The empty spaces are where both the samples in the pair could not be used to calculate the

relative gene expression. As seen in Table 5.6, of the 10 cases remained for 7 primers (excluding GAPDH) there was an increased expression of most of the genes for the majority of samples, except #3621 and #3631. I then proceeded to compare the expression changes of these remaining 10 cases, with that of the expected changes from RNAseq analysis.

5.4.4.2 Compared results from RT-qPCR with RNA-seq data

Using the gene expression changes from Table 5.6, I compared with the expected changes from RNAseq analysis, where if the RT-qPCR data coincided with the expected change in gene expression, the applied colour coding is green and similarly if they go against the expected change in gene expression, the applied colour coding is red (Table 5.7).

Table 5.7 Comparison of RT-qPCR gene expression changes with that of expected changes from RNAseq analysis.

	3682	3679	3684	3620	3645	3686	3605	3607	3621	3631
MCL1										
CXCL12										
CSF1										
GBP1										
YPEL4										
STEAP3										
EGLN3										

As expected

Not expected

Comparison of gene expression changes obtained from RT-qPCR with that from RNAseq DGEA as green (as expected with RNAseq results) or red (not expected with RNAseq results) compared between CLL alone (CL) and CLL in co-culture with NLCs (CN). Gaps are indicated where RT-qPCR data was not obtainable. The samples that were also used in RNAseq are in purple.

Here it can be seen in Table 5.7, 24 gene expression change observations (red) did not agree with that of RNAseq analysis, but 41 did (green). It can be seen that the sample #3679 displayed all the changes in RT-qPCR that was expected from DGEA of RNAseq data. The next best samples were #3620 and #3682. A further detailed descriptive analysis seen in Table 5.8, show that among the RNAseq samples, 3 primers were consistently differentially expressed as expected, namely MCL1, CSF1 and GBP1.

Table 5.8 Descriptive analysis of RT-qPCR vs RNA seq data

	RNAseq samples (3)		Other Samples (7)		All samples (10)	
MCL1	3 out of 3	100.00%	3 out of 7	42.86%	6 out of 10	60.00%
CXCL12	2 out of 3	66.67%	4 out of 7	57.14%	6 out of 10	60.00%
CSF1	3 out of 3	100.00%	4 out of 7	57.14%	7 out of 10	70.00%
GBP1	3 out of 3	100.00%	4 out of 5	80.00%	7 out of 8	87.50%
YPEL4	1 out of 3	33.33%	3 out of 7	42.86%	4 out of 10	40.00%
STEAP3	1 out of 2	50.00%	3 out of 6	50.00%	4 out of 8	50.00%
EGLN3	2 out of 3	66.67%	5 out of 6	83.33%	7 out of 9	77.78%

Descriptive analysis of gene expression changes of RT-qPCR compared with DGEA of RNAseq data. 7 primers were compared among 3 groups: RNAseq samples themselves, other samples and all samples combined. Highlighted in blue are the primers that were differentially expressed as expected by all the samples within their respective groups.

To further understand why these specific primers (MCL1, CSF1 and GBP1) were faithful in their expression changes detectable by RT-qPCR and RNA-seq DGEA, I looked at the raw read counts from the RNA-seq data.

5.4.4.3 Read counts from RNA-seq

As shown in Table 5.9, the read counts obtained from RNA-seq in order to calculate differential gene expression analysis, revealed a wide range of absolute values from 0-18079.

Table 5.9 Read counts of Primers investigated for each RNA sample sent for RNAseq.

CL

	CL27	CL77	CL79	CL82	CL84	CL99	Average read
YPEL4	61	32	51	53	33	90	53.33333
CXCL12	1	0	1	1	0	0	0.5
EGLN3	2	0	1	1	0	0	0.666667
GBP1	34	13	12	59	26	12	26
EBI3	2	2	0	3	3	0	1.666667
CSF1	55	76	31	48	30	44	47.33333
MCL1	6418	6256	4451	8709	6264	4898	6166
STEAP3	8	189	26	18	7	14	43.66667
GAPDH	3701	3804	2847	4037	2983	1929	3216.833

CN

	CN27	CN77	CN79	CN82	CN84	CN99	Average read
YPEL4	32	30	32	25	7	85	35.16667
CXCL12	2	22	2	7	6	14	8.833333
EGLN3	10	7	7	6	0	5	5.833333
GBP1	224	59	28	1586	47	231	362.5
EBI3	17	4	0	45	10	2	13
CSF1	498	314	75	815	80	231	335.5
MCL1	10638	10221	6281	18079	9243	9546	10668
STEAP3	141	497	55	45	37	263	173
GAPDH	3909	4220	2814	4534	3800	2312	3598.167

Raw read counts for each sample sent for RNAseq for each primer investigated. Green indicates the gene that was significantly differentially downregulated by DGEA. Yellow indicates genes that were significantly differentially upregulated by DGEA. Orange indicates the reference gene selected. Red indicates the Genes whose RT-qPCR data completely coincided with expected changes of RNAseq DGEA. CLL alone (CL) are those on top and CLL Co-cultured with NLCs (CN) are those bottom. The individual samples have numbers after their designated culture condition. Raw counts were obtained during DGEA by the Bioinformatics department of Computational Biology Facility.

Interestingly, the genes MCL1, CSF1 and GBP1 had a much higher read count (2-4 digits) than the remaining genes across all the samples. (1-2 digits). Those with 2 digit read counts but compared poorly in RT-qPCR had counts in the lower range (ie 10-50) such as YPEL4, CXCL12, EGLN3, EBI3 and STEAP3. The average read count for those with poor comparison with RT-qPCR were 0.5-53 (CL) and 5.8-173 (CN).

Given that the majority of Primers (6/7) were validated with more than 50% of samples we can have good confidence on the validity of the RNAseq data by the differential gene expression analysis.

So far, the analysis of samples for qPCR and RNAseq was more or less validated. The samples that were not sent for RNAseq but had qPCR performed gives a similar picture, though the findings can be explained by the heterogeneity of the CLL disease (Table 5.3).

5.4.5 Functional and Pathway analysis

5.4.5.1 Functional annotation (DAVID)

With the use of DAVID, as shown in Table 5.10, CLLcc vs CLL comparison showed 322 upregulated genes as input data, out of which 313 genes were mapped in by DAVID, resulting in 10 clusters. Out of these 10, 2 clusters had significant Benjamini corrected p-values. The first cluster is of inflammatory response (26/313 genes) and the second cluster is of platelet degranulation (10/313 genes).

The number of differentially expressed genes in NLC was not enough to perform DAVID analysis.

Table 5.10 Functional Annotation (DAVID) in CLLcc vs CLL comparison

Annotation Cluster 1	Enrichment Score: 4.76			Count	P_Value	Benjamini
GOTERM_MF_DIRECT	chemokine activity	RT		11	5.2E-9	2.6E-6
GOTERM_BP_DIRECT	inflammatory response	RT		26	1.0E-8	1.7E-5
GOTERM_BP_DIRECT	chemotaxis	RT		15	2.4E-8	2.0E-5
GOTERM_BP_DIRECT	cellular response to interleukin-1	RT		11	3.6E-7	2.0E-4
GOTERM_BP_DIRECT	chemokine-mediated signaling pathway	RT		11	3.6E-7	2.0E-4
GOTERM_BP_DIRECT	positive regulation of inflammatory response	RT		10	4.3E-6	1.8E-3
GOTERM_BP_DIRECT	cellular response to interferon-gamma	RT		9	5.6E-6	1.6E-3
GOTERM_BP_DIRECT	monocyte chemotaxis	RT		8	6.7E-6	1.6E-3
GOTERM_BP_DIRECT	immune response	RT		22	1.4E-5	2.5E-3
GOTERM_BP_DIRECT	cell chemotaxis	RT		9	1.5E-5	2.5E-3
GOTERM_BP_DIRECT	cellular response to tumor necrosis factor	RT		11	2.0E-5	3.1E-3
GOTERM_MF_DIRECT	CCR chemokine receptor binding	RT		6	2.9E-5	7.1E-3
GOTERM_BP_DIRECT	positive regulation of ERK1 and ERK2 cascade	RT		13	5.2E-5	7.3E-3
GOTERM_BP_DIRECT	lymphocyte chemotaxis	RT		6	1.0E-4	1.2E-2
GOTERM_BP_DIRECT	cell-cell signaling	RT		15	1.4E-4	1.4E-2
GOTERM_BP_DIRECT	neutrophil chemotaxis	RT		8	1.4E-4	1.3E-2
GOTERM_BP_DIRECT	cellular calcium ion homeostasis	RT		8	1.1E-3	7.0E-2
GOTERM_BP_DIRECT	eosinophil chemotaxis	RT		3	9.8E-3	3.3E-1
GOTERM_BP_DIRECT	G-protein coupled receptor signaling pathway	RT		26	1.3E-2	3.8E-1
GOTERM_BP_DIRECT	positive regulation of GTPase activity	RT		14	1.8E-1	9.3E-1
Annotation Cluster 2	**Enrichment Score: 3.24**			**Count**	**P_Value**	**Benjamini**
GOTERM_BP_DIRECT	platelet degranulation	RT		10	7.1E-5	9.2E-3
GOTERM_CC_DIRECT	platelet alpha granule lumen	RT		7	2.5E-4	6.6E-3
GOTERM_BP_DIRECT	negative regulation of endopeptidase activity	RT		9	1.2E-3	7.1E-2
GOTERM_MF_DIRECT	serine-type endopeptidase inhibitor activity	RT		7	5.1E-3	3.9E-1

CLLcc vs CLL comparison: 322 upregulated genes were fed into DAVID and found 10 clusters, of which only 2 had significant Benjamini corrected p-values.

5.4.5.2 Gene Set Enrichment Analysis (GSEA)

Gene sets were selected (KEGG and Gene Ontology) and were mapped onto the ranked genes. When comparing CLLcc with CLL, 15,796 were selected and 104 positively enriched gene sets were found to be significant when FWER p-value <0.05. As seen in Table 5.11, the top 10 enriched and upregulated gene sets included those involved in chemokine and cytokine signalling.

Table 5.11 Gene set enrichment analysis of CLL co-cultured with NLC (CLLcc) vs CLL alone (CLL)

	GS follow link to MSigDB	GS DETAILS	SIZE	ES	NES	NOM p-val	FDR q-val	FWER p-val	RANK AT MAX	LEADING EDGE
1	GO_RESPONSE_TO_INTERFERON_GAMMA	Details ...	115	0.7	2.6	0	0	0	2225	tags=53%, list=14%, signal=61%
2	GO_CHEMOKINE_RECEPTOR_BINDING	Details ...	40	0.8	2.6	0	0	0	1936	tags=65%, list=12%, signal=74%
3	GO_CELLULAR_RESPONSE_TO_INTERFERON_GAMMA	Details ...	96	0.7	2.5	0	0	0	1970	tags=49%, list=12%, signal=56%
4	GO_CHEMOKINE_ACTIVITY	Details ...	32	0.8	2.5	0	0	0	1075	tags=59%, list=7%, signal=64%
5	GO_CHEMOKINE_MEDIATED_SIGNALING_PATHWAY	Details ...	49	0.8	2.5	0	0	0	1936	tags=61%, list=12%, signal=70%
6	KEGG_COMPLEMENT_AND_COAGULATION_CASCADES	Details ...	41	0.8	2.5	0	0	0	440	tags=44%, list=3%, signal=45%
7	GO_CYTOKINE_MEDIATED_SIGNALING_PATHWAY	Details ...	350	0.6	2.4	0	0	0	2558	tags=43%, list=16%, signal=50%
8	GO_PROTEIN_ACTIVATION_CASCADE	Details ...	35	0.8	2.4	0	0	0	1186	tags=51%, list=8%, signal=55%
9	GO_INNATE_IMMUNE_RESPONSE	Details ...	419	0.6	2.4	0	0	0	2344	tags=39%, list=15%, signal=45%
10	GO_INTERFERON_GAMMA_MEDIATED_SIGNALING_PATHWAY	Details ...	63	0.7	2.4	0	0	0	2130	tags=52%, list=13%, signal=60%

Top 10 gene sets that were enriched based on their rank on the list and with FWER p-val <0.05. Data sets are predefined by KEGG or GO and is ranked based on "stat" values provided by DESeq2.

Furthermore, as seen in Figure 5.17, REVIGO was used to visualize the GSEA results and showed involvement of 'Regulation of response to wound' and 'Lymphocyte migration'.

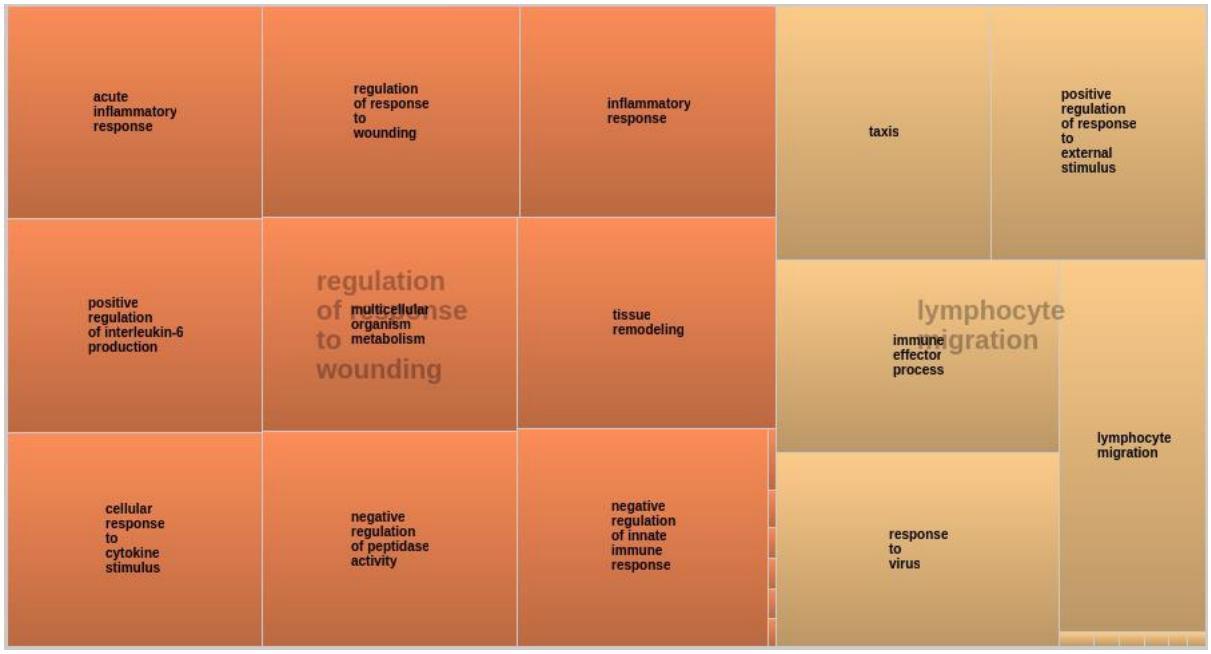

Figure 5.17 "TreeMap" view of REVIGO Gene Set Enrichment Analysis comparing CLL co-cultured with NLC vs CLL alone

Each rectangle is a single cluster representative. The representatives are joined into 'superclusters' of loosely related terms, visualized with different colors. Size of the rectangles may be adjusted to reflect either the p-value, or the frequency of the GO term in the underlying GOA database.

A ‘‘Scatterplot & Table’’ view of REVIGO was also generated when comparing CLLcc with CLL alone, as seen in Figure 5.18, and showed the involvement of lymphocyte migration, extracellular matrix disassembly, tissue remodelling, inflammatory response, regulation of response to wounding, positive regulation of ERK1 and ERK2 cascade and positive regulation of vasculature development.

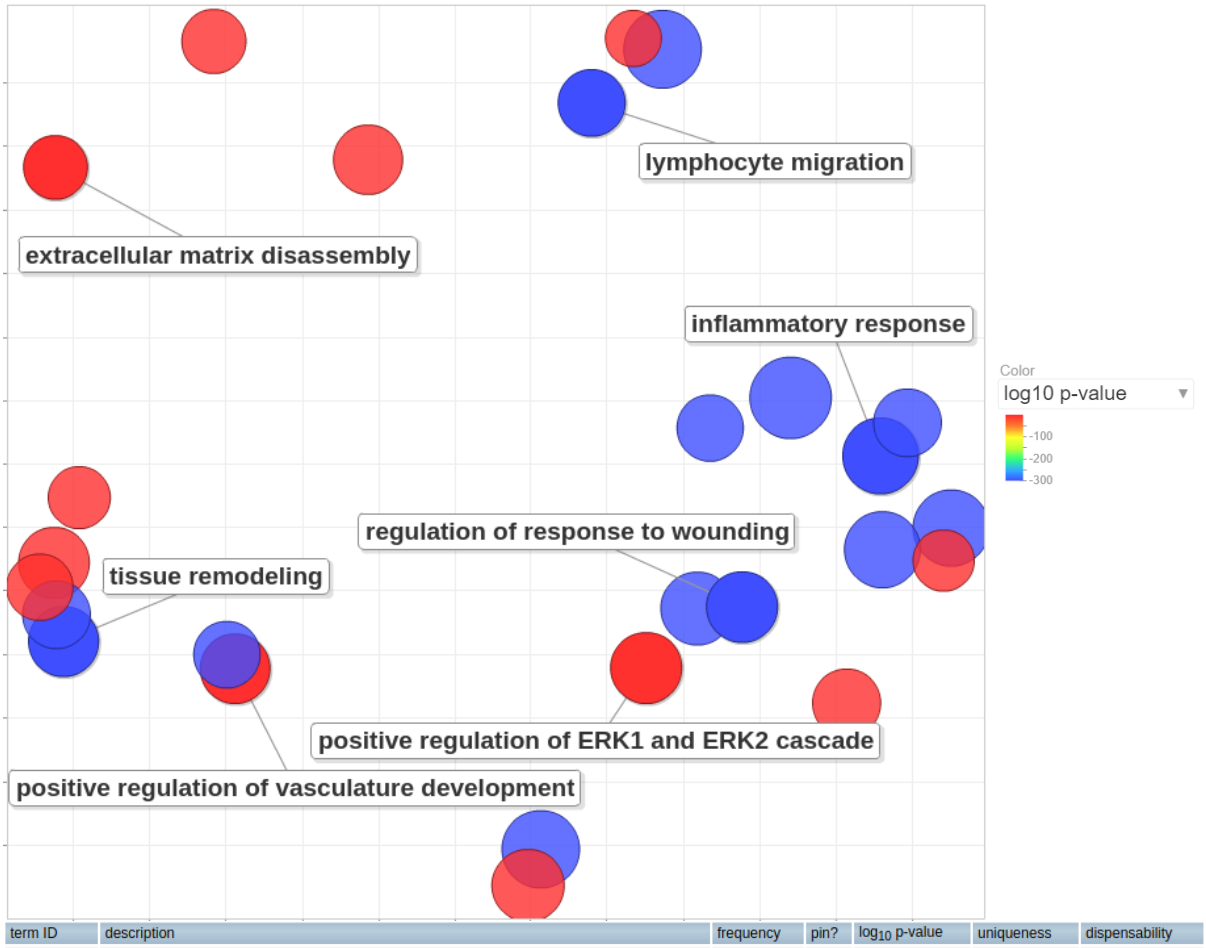

term ID	description	frequency	pin?	log_{10} p-value	uniqueness	dispensability
GO:0072676	lymphocyte migration	0.013 %		-300.0000	0.38	0.00
GO:1903034	regulation of response to wounding	0.033 %		-300.0000	0.47	0.00
GO:0022617	extracellular matrix disassembly	0.007 %		-1.8539	0.91	0.10
GO:0006692	prostanoid metabolic process	0.007 %		-1.9208	0.91	0.10
GO:0032755	positive regulation of interleukin-6 production	0.013 %		-300.0000	0.59	0.16
GO:0010466	negative regulation of peptidase activity	0.170 %		-300.0000	0.76	0.18
GO:0072376	protein activation cascade	0.018 %		-1.4949	0.71	0.22
GO:0071345	cellular response to cytokine stimulus	0.122 %		-300.0000	0.50	0.25
GO:0006954	inflammatory response	0.110 %		-300.0000	0.53	0.40
GO:0001893	maternal placenta development	0.005 %		-1.4815	0.82	0.41
GO:0044259	multicellular organismal macromolecule metabolic process	0.012 %		-3.0000	0.82	0.44
GO:0044236	multicellular organism metabolic process	0.016 %		-300.0000	0.82	0.44
GO:0048771	tissue remodeling	0.028 %		-300.0000	0.82	0.46
GO:0002475	antigen processing and presentation via MHC class Ib	0.001 %		-1.8539	0.54	0.51
GO:0022612	gland morphogenesis	0.033 %		-1.3565	0.81	0.54
GO:0033280	response to vitamin D	0.004 %		-1.4089	0.59	0.55
GO:0042330	taxis	0.480 %		-300.0000	0.45	0.64
GO:0032103	positive regulation of response to external stimulus	0.055 %		-300.0000	0.38	0.66
GO:0002526	acute inflammatory response	0.016 %		-300.0000	0.57	0.66
GO:0052192	movement in environment of other organism involved in symbiotic interaction	0.022 %		-1.3665	0.76	0.66
GO:0045824	negative regulation of innate immune response	0.012 %		-300.0000	0.24	0.67
GO:0002252	immune effector process	0.185 %		-300.0000	0.42	0.67
GO:1904018	positive regulation of vasculature development	0.025 %		-1.7447	0.59	0.67
GO:0070374	positive regulation of ERK1 and ERK2 cascade	0.034 %		-2.6990	0.42	0.69
GO:0050730	regulation of peptidyl-tyrosine phosphorylation	0.045 %		-1.4559	0.78	0.69
GO:0009615	response to virus	0.117 %		-300.0000	0.56	0.70

Figure 5.18 ‘‘Scatterplot & Table’’ view of REVIGO comparing CLL co-cultured with NLC vs CLL alone

The scatterplot shows the cluster representatives (i.e. terms remaining after the redundancy reduction) in a two-dimensional space derived by applying multidimensional scaling to a matrix of the GO terms’ semantic similarities.

This GSEA was performed the same way again in the comparison between NLCcc and NLC using 19,595 genes and found 18 significantly enriched gene sets with positive enrichment when p<0.0.5, which is displayed in Table 5.12.

Table 5.12 Gene set enrichment analysis of NLC co-cultured with CLL (NLCcc) vs NLC alone (NLC)

	GS follow link to MSigDB	GS DETAILS	SIZE	ES	NES	NOM p-val	FDR q-val	FWER p-val	RANK AT MAX	LEADING EDGE
1	KEGG_RIBOSOME	Details ...	85	0.6	2.4	0	0	0	4281	tags=60%, list=22%, signal=76%
2	GO_ESTABLISHMENT_OF_PROTEIN_LOCALIZATION_TO_ENDOPLASMIC_RETICULUM	Details ...	102	0.6	2.4	0	0	0	4281	tags=57%, list=22%, signal=72%
3	KEGG_SPLICEOSOME	Details ...	125	0.6	2.4	0	0	0	3422	tags=46%, list=17%, signal=55%
4	GO_CHEMOKINE_MEDIATED_SIGNALING_PATHWAY	Details ...	59	0.6	2.4	0	0	0	4238	tags=56%, list=22%, signal=71%
5	GO_CYTOSOLIC_RIBOSOME	Details ...	105	0.6	2.3	0	0	0	4281	tags=54%, list=22%, signal=69%
6	GO_RIBOSOMAL_SUBUNIT	Details ...	156	0.5	2.3	0	0	0	3861	tags=48%, list=20%, signal=59%
7	GO_CYTOSOLIC_SMALL_RIBOSOMAL_SUBUNIT	Details ...	42	0.7	2.3	0	0	0	3693	tags=60%, list=19%, signal=73%
8	GO_RRNA_METABOLIC_PROCESS	Details ...	249	0.5	2.3	0	0	0	5074	tags=49%, list=26%, signal=66%
9	GO_CHEMOKINE_ACTIVITY	Details ...	38	0.7	2.3	0	0	0	3458	tags=50%, list=18%, signal=61%
10	GO_RIBOSOME	Details ...	212	0.5	2.3	0	0	0	4281	tags=45%, list=22%, signal=57%
11	GO_RIBOSOME_BIOGENESIS	Details ...	298	0.5	2.3	0	0	0	5089	tags=49%, list=26%, signal=65%
12	GO_SMALL_RIBOSOMAL_SUBUNIT	Details ...	66	0.6	2.3	0	0	0.001	3693	tags=53%, list=19%, signal=65%
13	GO_PROTEIN_LOCALIZATION_TO_ENDOPLASMIC_RETICULUM	Details ...	121	0.5	2.2	0	0	0.003	4281	tags=53%, list=22%, signal=67%
14	GO_PROTEIN_TARGETING_TO_MEMBRANE	Details ...	149	0.5	2.2	0	0.001	0.02	4281	tags=46%, list=22%, signal=59%
15	GO_CCR_CHEMOKINE_RECEPTOR_BINDING	Details ...	26	0.7	2.1	0	0.002	0.033	4238	tags=54%, list=22%, signal=69%
16	GO_RIBONUCLEOPROTEIN_COMPLEX_BIOGENESIS	Details ...	419	0.4	2.1	0	0.002	0.034	5089	tags=44%, list=26%, signal=59%
17	GO_CHEMOKINE_RECEPTOR_BINDING	Details ...	47	0.6	2.1	0	0.002	0.034	3103	tags=40%, list=16%, signal=48%
18	GO_CYTOSOLIC_LARGE_RIBOSOMAL_SUBUNIT	Details ...	56	0.6	2.1	0	0.002	0.039	4281	tags=55%, list=22%, signal=71%

All 18 gene sets that were enriched based on their rank on the list and with FWER p-val <0.05. Data sets are predefined by KEGG or GO and is ranked based on “stat” values provided by DESeq2.

5.4.5.3 Ingenuity Pathway Analysis (IPA)

IPA was performed as described in Methods to identify any pathways that is suggested to be involved based on the genes that is known to promote and inhibit a function. As seen in Figure 5.19 (top), the TreeMap shows an involvement of several functions.

5.4.5.3.1 Diseases and Functions

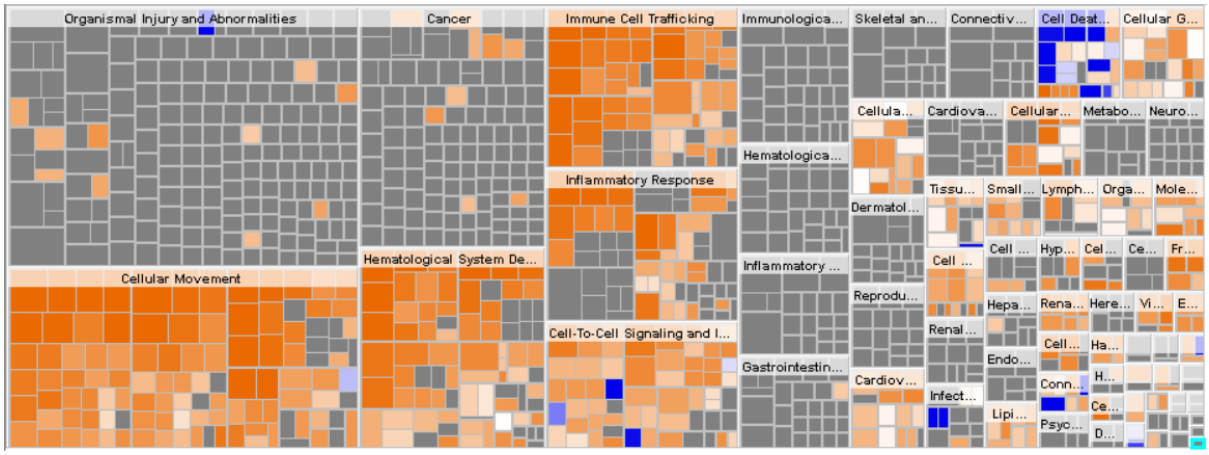

Categories	Function	Diseases or Functions Annotation	p-Value	Predicted Activation State	Activation z-score	Molecules	# Molecules
Cellular Movement	migration	Migration of cells	1.06E-19	Increased	4.5	A2M,ACTN1,AD	87
Cellular Movement	cell movement	Cell movement	1.29E-18	Increased	4.809	A2M,ACTN1,AD	91
Cell-To-Cell Signaling and Interaction	adhesion	Adhesion of blood cells	3.23E-15	Increased	3.07	A2M,APOE,CCI	27
Inflammatory Response	inflammatory response	Inflammatory response	8.25E-15	Increased	3.258	APOE,CCL1,CC	34
Cellular Movement	cell movement	Cell movement of myeloid cells	1.24E-14	Increased	4.372	CCL1,CCL13,C	27
Cell-To-Cell Signaling and Interaction	binding	Binding of blood cells	2.01E-14	Increased	2.948	A2M,APOE,CCI	28
Cellular Movement,Hematological System Develop	cell movement	Cell movement of leukocytes	3.86E-14	Increased	4.573	ADGRE2,CCL1	32
Cell-To-Cell Signaling and Interaction,Hematologic	adhesion	Adhesion of immune cells	5.14E-14	Increased	2.455	A2M,APOE,CCI	24
Cellular Movement	cell movement	Cell movement of tumor cell lines	8.63E-14	Increased	4.261	A2M,ACTN1,BC	61
Cellular Movement	migration	Migration of tumor cell lines	1.77E-13	Increased	3.645	A2M,ACTN1,BC	55
Cellular Movement,Hematological System Develop	migration	Migration of phagocytes	2.34E-13	Increased	3.21	CCL1,CCL22,C	19
Cellular Movement,Immune Cell Trafficking	migration	Leukocyte migration	3.05E-13	Increased	4.702	ADGRE2,CCL1	37
Cellular Movement	chemotaxis	Chemotaxis	4.65E-13	Increased	4.501	ACTN1,ADGRE	32
Cellular Movement,Hematological System Develop	cell movement	Cell movement of phagocytes	9.12E-13	Increased	4.07	CCL1,CCL22,C	25
Cellular Movement,Hematological System Develop	chemotaxis	Chemotaxis of leukocytes	1.3E-12	Increased	4.062	CCL1,CCL13,C	24
Free Radical Scavenging	metabolism	Metabolism of reactive oxygen species	2.3E-12	Increased	3.35	APOE,APOL6,C	27
Cellular Movement,Hematological System Develop	cell movement	Cell movement of mononuclear leukocy	2.42E-12	Increased	3.783	CCL1,CCL13,C	25

Figure 5.19 "TreeMap" (hierarchical heatmap) of downstream effector analysis (DEA) comparing CLLcc with CLL alone cells

DEA results for CLL cells in co-culture with NLCs. The visualization is a TreeMap (top) where the large boxes represents a category of related functions. Each smaller box are coloured at a particular biological function or disease. Orange is the predicted increase and blue is the predicted decrease. Darker colours indicate higher absolute Z-scores. The image has been cropped for better readability. The details of the functions that are top increases is listed (bottom).

Among the top categories are cellular movement, cell-cell signalling interaction (adhesion, binding), inflammatory response, free radical scavenging, cellular proliferation, shape change, cell death and cell viability. Details of those that are increased are shown in Figure 5.19 (bottom).

5.4.5.3.2 Upstream Regulator analysis

326 differentially expressed genes in CLLcc (up and downregulated) along with their logFC were selected and input in the IPA database. The database then analysed these genes with those of its own from other studies to identify the common upstream regulators for a dataset of genes. As seen in Table 5.13, a list of upstream regulators according to their p-value of overlap shows the involvement of TNF, NF-κB, ERK and TLR4.

Table 5.13 Upstream Regulator analysis of the 326 differentially expressed genes in CLL co-cultured with NLCs

Upstream Regulator	Expr Log Ratio	Molecule Type	Predicted Activation State	Activation z-score	p-value of overlap	Target molecules in dataset
TNF		cytokine	Activated	4.249	2.42E-22	ALOX15B,APOE,CCL18,CD59,CDKN1
IFNG		cytokine	Activated	4.786	2.31E-21	ACE,APOL6,C1QA,C1QB,C1QC,CCL1
IL1B		cytokine	Activated	3.921	1.23E-17	APOE,CCL13,CCL7,CHI3L1,CXCL10,C
STAT1	1.982	transcription regulator	Activated	3.756	6.96E-17	C1S,CDKN1A,CXCL10,CXCL9,GBP1,C
IL1A		cytokine	Activated	3.447	3.95E-15	ALDH1A1,CCL8,CDKN1A,CSF1,CXCL
NFkB (complex)		complex	Activated	4.426	1.37E-14	CCL1,CCL22,CCL8,CDKN1A,CXCL10,
Interferon alpha		group	Activated	2.034	3.81E-14	ADAR,CCL22,CDKN1A,CXCL10,CXCL
RELA		transcription regulator	Activated	3.488	5.23E-13	CD59,CDKN1A,CXCL10,CXCL5,CXCL
TREM1		transmembrane receptor	Activated	2.527	3.07E-12	ARRDC4,CCL18,CCL7,CRTAM,CSF1,
IFNA2		cytokine	Activated	3.113	4.43E-12	APOL6,CISH,CXCL10,GBP1,IFIH1,IFIT
RNASE2		enzyme	Activated	3.113	5.49E-12	CCL1,CCL22,CCL24,CCL7,CCL8,CSF
TGM2	3.191	enzyme	Activated	4.518	9.66E-12	ADGRE2,CCL22,CCL24,CXCL10,CXC
IL27		cytokine	Activated	3.032	1.21E-11	CCL7,CR1,CXCL10,CXCL8,CXCL9,ICA
JUN		transcription regulator	Activated	2.47	1.21E-11	CCL8,CDKN1A,CXCL10,CXCL5,CXCL
RNASE1		enzyme	Activated	2.97	1.34E-11	CCL1,CCL22,CCL24,CCL7,CCL8,CXC
TLR7		transmembrane receptor	Activated	3.642	6.13E-11	CD38,CXCL10,CXCL8,CXCL9,ICAM1,I
IL13		cytokine	Activated	2.117	8.92E-11	ADAMDEC1,ARNTL2,CCL18,CCL22,C
Immunoglobulin		complex	Activated	3.138	1.97E-10	CCL1,CCL7,CCL8,CISH,CXCL10,CXC
PRL		cytokine	Activated	3.039	7.78E-10	ADAR,CDKN1A,CISH,CTSB,CXCL10,C
IFNL1		cytokine	Activated	3.41	9.01E-10	APOL6,CXCL10,CXCL8,CXCL9,GBP1,
EGFR		kinase	Activated	3.011	1.63E-09	CDCP1,CHI3L1,CXCL8,E2F2,F3,GBP1
PRKCD		kinase	Activated	2.901	1.77E-09	CD4,CDKN1A,CTSB,CXCL10,CXCL12
TLR9		transmembrane receptor	Activated	3.229	2.61E-09	CD38,CXCL10,CXCL8,CXCL9,IFIT3,IL4
P38 MAPK		group	Activated	3.384	2.73E-09	CCL8,CDKN1A,CXCL10,CXCL12,CXC
NFKB1		transcription regulator	Activated	2.744	3.64E-09	CD59,CHI3L1,CXCL10,CXCL8,CXCL9,
TGFB1		growth factor	Activated	3.263	7.06E-09	CD59,CDKN1A,CHI3L1,COL6A3,CXCL
ERK		group	Activated	3.045	7.75E-09	CDKN1A,CXCL10,CXCL8,ICAM1,IL6,IT
JAG2		growth factor	Inhibited	-2.121	2.01E-08	CCL13,CCL24,CXCL5,CXCL9,IL13RA1
TLR4		transmembrane receptor	Activated	2.401	5.72E-08	CCL8,CD38,CXCL10,CXCL8,ICAM1,IL

Segment of upstream Regulator Analysis as part of Ingenuity Pathway Analysis of 326 differentially expressed genes. The regulators are listed according to p-value of overlap and activation z-score. A total of 102 upstream regulators were produced.

Just over 100 upstream regulators produced were fed as official gene symbols into DAVID to classify them by function. The genes were analyzed with DAVID online tool for KEGG (Kyoto Encylopedia of Genes and Genomes) pathways analysis. As seen in Table 5.14, KEGG pathway were listed according to count, genes and FDR in order to plot out pathways connected.

Table 5.14 DAVID Top 12 KEGG pathways analysis of genes directed from validated mRNA targeting

KEGG pathway	Count	Genes	FDR
Toll-like receptor signaling pathway	17/78	IL6, TNF, RELA, MAP2K3, NFKB1, TLR4, CD40, STAT1, TAB1, CCL5, TLR7, TLR9, IFNA2, JUN, IL1B, IRF3, SPP1	5.22E-13
Cytokine-cytokine receptor interaction	19/78	IL4, CSF2, IL6, TNF, IL18, IL13, CD40, CCL5, TGFB1, OSM, IFNA2, IFNL1, IL17A, CD40LG, IFNG, TNFRSF18, IL1B, PRL, IL1A	2.14E-09
NF-kappa B signaling pathway	12/78	TNF, PTGS2, CD40LG, RELA, IL1B, NFKB1, TLR4, UBE2I, CD40, MAP3K14, TAB1, ATM	2.47E-07
TNF signaling pathway	12/78	CSF2, IL6, TNF, PTGS2, RELA, JUN, MAP2K3, IL1B, NFKB1, CCL5, MAP3K14, TAB1	2.38E-06
HIF-1 signaling pathway	11/78	EGFR, IL6, HIF1A, RELA, ERBB2, VEGFA, IFNG, NFKB1, TLR4, EGF, GAPDH	1.22E-05
Pathways in cancer	18/78	CEBPA, EGFR, IL6, PTGS2, ERBB2, RELA, FOXO1, NFKB1, STAT1, MMP1, TGFB1, GLI1, HIF1A, JUN, VEGFA, RARB, EGF, FGF2	4.24E-05
T cell receptor signaling pathway	10/78	IL4, CSF2, TNF, CD40LG, RELA, JUN, IFNG, CTLA4, NFKB1, MAP3K14	2.56E-04
MAPK signaling pathway	14/78	EGFR, TNF, JUN, MAP2K3, RELA, IL1B, NFKB1, MAP3K14, TAB1, EGF, ECSIT, FGF2, TGFB1, IL1A	3.26E-04
Jak-STAT signaling pathway	11/78	OSM, IL4, CSF2, IFNA2, IFNL1, IL6, SOCS1, IFNG, IL13, STAT1, PRL	6.32E-04
NOD-like receptor signaling pathway	8/78	IL6, TNF, IL18, RELA, IL1B, NFKB1, CCL5, TAB1	6.63E-04
Cytosolic DNA-sensing pathway	8/78	IFNA2, IL6, IL18, RELA, IL1B, NFKB1, IRF3, CCL5	0.001678771
PI3K-Akt signaling pathway	14/78	EGFR, OSM, IL4, IFNA2, IL6, RELA, VEGFA, NFKB1, TLR4, FOXO3, EGF, FGF2, PRL, SPP1	0.010648413

Upstream regulators were fed into DAVID to classify them by function. The KEGG pathways are listed according to the count, genes involved and the FDR.

5.4.5.3.3 KEGG Pathways generated

KEGG pathway analysis revealed pathways being the most relevant to CLL-NLC interaction and produced figures for Toll-like receptor (TLR) signalling (Figure 5.20) and NF-Kappa B (NF-κB) signalling (Figure 5.21) as among the top ranked pathways.

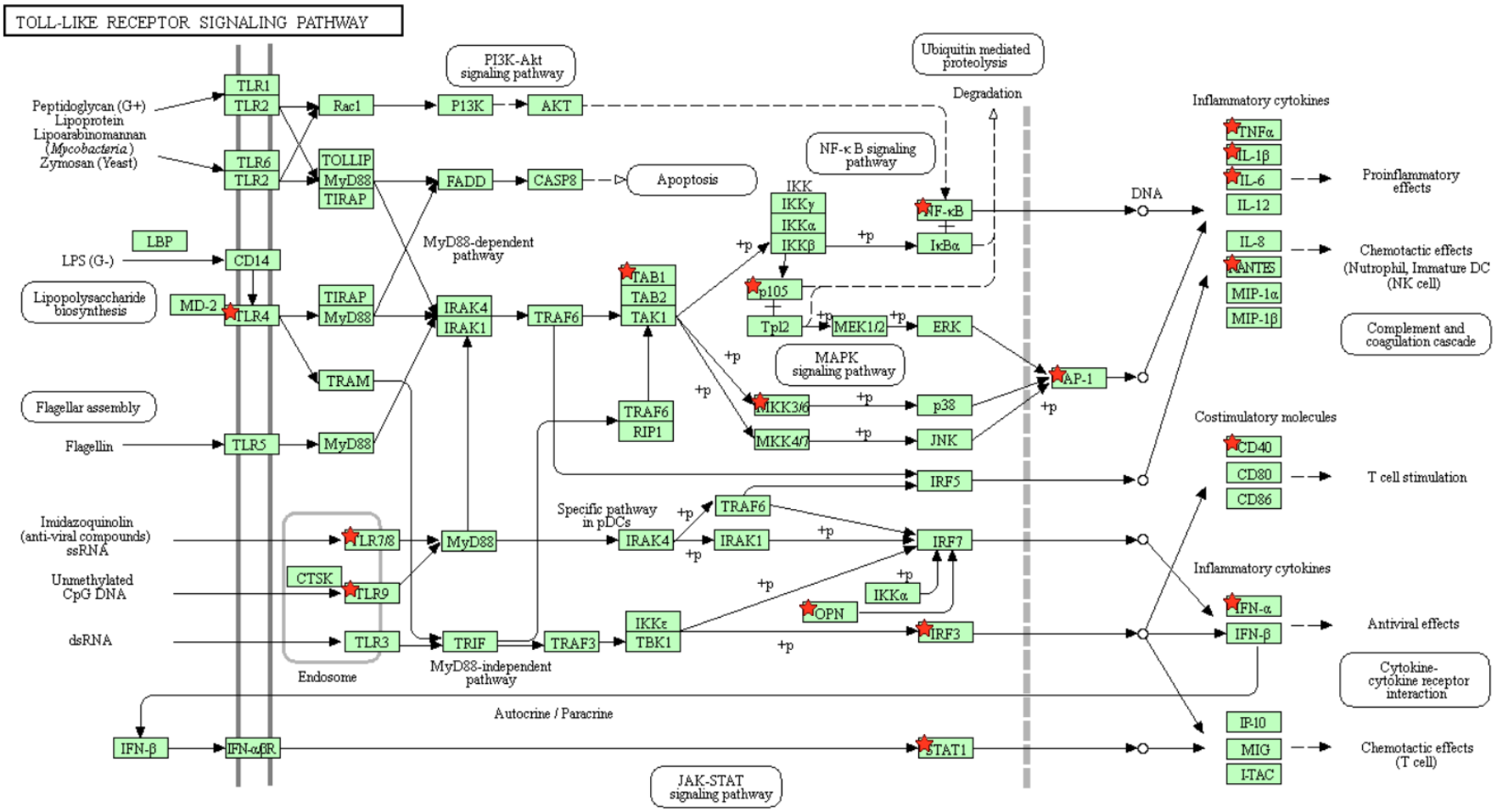

Figure 5.20 DAVID KEGG pathway analysis; mRNA targeted genes (red star) are involved in Toll-Like Receptor Signalling Pathway

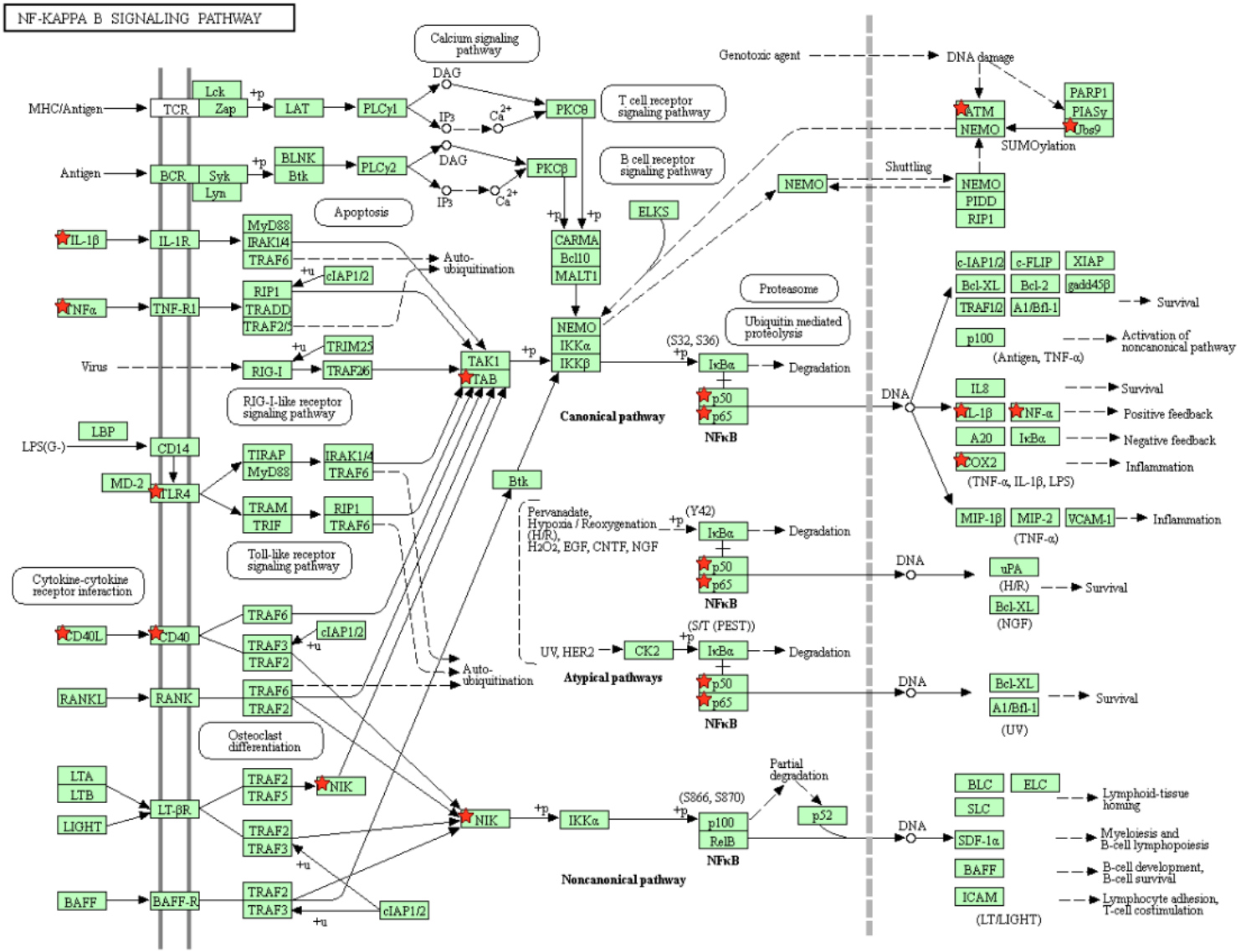

Figure 5.21 DAVID KEGG pathway analysis; mRNA targeted genes (red star) are involved in NF-Kappa B Signalling Pathway

In addition to TLR and NF-κB signalling pathways, other pathways were also produced as being relevant to CLL-NLC interaction, (see Appendix 7.13) including but not limited to Tumor necrosis factor (TNF) signalling (Appendix Figure 7.12), Hypoxia-inducible transcription factor (HIF) signalling (Appendix Figure 7.13), T cell receptor signalling (Appendix Figure 7.14), Mitogen-activated protein kinase (MAPK) signalling (Appendix Figure 7.15), Janus kinase (JAK) and signal transducer of activator of transcription (STAT) signalling (Appendix Figure 7.16), phosphoinositide-3-kinase (PI3K-AKT) signalling pathway (Appendix Figure 7.17) as well as general pathways involved in cancer (Appendix Figure 7.18). Other pathways (see Appendix 7.13) produced by KEGG pathway analysis include nucleotide-binding oligomerization domain (NOD)-like receptor signalling pathway (Appendix Figure 7.19), cytosolic DNA-sensing pathway (Appendix Figure 7.20) and cytokine-cytokine receptor pathway (Appendix Figure 7.21).

On closer inspection of the pathways, it was revealed that NF-κB pathway seemed to be the most mutually connected pathway in the network of all the mentioned pathways. To decide which genes to investigate for further work, a number of areas of Bioinformatics results should be considered.

The first area to investigate are the GSEA visualized by REVIGO, where Regulation of response to wounding was quite prominent. The next area is from IPA under diseases and functions where cellular movement and adhesion was among the highest rank of predicted involvement.

Next, are the upstream regulators derived from IPA (and used for KEGG analysis) indicating which genes are predicted to be activated or inhibited which lead to the differentially expressed genes initially found.

I decided to look into upstream regulators predicted as well as those differentially expressed in order to narrow down which genes could be investigated on next.

Of the listed genes from the KEGG pathways, three were found to be significantly upregulated in CLL cells co-cultured with NLCs, namely STAT1, SPP1 and IL6. Table 5.15 summarises the genes mentioned in their rank, log2fold change and read count from each sample.

Table 5.15 Summary of Genes of interest

Gene	Rank on DESeq2 List	log2fold increase	Mutual pathway involved	Read count from CLL cells		
				Range	Mean among CL	Mean among CN
IL6	47	3.82	TLR signalling	0-15	0.33 ± 0.816	8.33 ± 5.28
SPP1	102	2.79		15-1260	65 ± 49.52	463 ± 411.76
STAT1	179	1.98		443-6979	510.67 ± 118.09	2774.3 ± 2563.07

Based on the information from Table 5.15, it appears that TLR signalling was the mutual pathway among these three genes, which is of no surprise as it was ranked as highest from Bioinformatics analysis. TLR itself is linked with NFκB pathway quite closely. Based on the read count and experience during validation during RT-qPCR, the genes SPP1 and STAT1 would be most appropriate to investigate further in the practical setting. SPP1 and STAT1 are also among the highest ranked clusters in a number of functional annotation pathways such as inflammatory response and cell adhesion. I therefore suggest the genes STAT1 and SPP1 to be chosen for further work up in the setting of CLL-NLC interaction.

5.5 Summary of Results

Through outsourcing the RNA sequencing, using RNA that were of good quantity and quality, >100GB of data was generated from the 6 cases (24 samples). With the crucial help of the Bioinformatics team of Computational Biology Facility, a comprehensive analysis of data was performed. Using DESeq2 package for R software, a list of differentially expressed genes were generated when comparing CLLcc with CLL alone and NLCcc with NLC alone. The overall number of genes that were upregulated were significantly greater when CLL cells were exposed to NLCs for 24hrs.

Comparing with a study using ranked microarray data, generated 61 genes that were upregulated and coincided with my data. Using these 61 genes, I prioritized the selection process of genes to validate using RT-qPCR. I concluded with testing 13 designed primers for their respective genes on cDNA synthesised from the RNA extracted. With the aid of agarose gel electrophoresis, control samples and the reference gene GAPDH, I was able to optimise and run an intricate RT-qPCR on 14 case pairs with 9 primers.

I was able to generate relative gene expression ratio values after normalising the C_T with control and reference gene. Through exclusion of samples that were not fit to calculate relative gene expression and one primer that did not give confident results, I was able display an overall increase or decrease in gene expression.

On comparing with the expected changes from DGEA of RNA-seq, the primers for MCL1, CSF1 and GBP1 gave the most parallel findings with the samples sent for RNA-seq. When looking at all the samples, 41/65 gave parallel findings with the expected changes. This gave an overall confidence of validating the data from DGEA. The differences can be speculated as due to heterogeneity of CLL disease.

From the data generated from RNA-seq, it was shown by PCA that there was clear separation of all 4 populations of cells cultured under different conditions. The most significant differences were between CLL cells co-cultured with NLCs and CLL cells cultured alone. A subset of 326 genes were identified that discriminate between both cell conditions (CLLcc vs CLL) and was able to link these genes to relevant biological functions and pathways. Biological functions included inflammatory response and platelet degranulation. Cellular functions involved included, but not limited to, lymphocyte migration, cell death, cellular proliferation, tissue remodelling and regulation of response to wounding.

My study data have shown some discrepancy of results between RNA-se and RT-qPCR. This emphasizes an necessary of validating RNA-seq data, particularly those with low depth of read cover.

Through DAVID, KEGG analysis showed the involvement of upstream pathways including TLR signalling, NF-κB signalling and cytokine-cytokine receptor interactions. Pathways which are relevant to CLL-NLC interaction included, but not limited to, tumour necrosis factor (TNF) signalling pathway, Hypoxia-Inducible Factor-1 (HIF-1) signalling pathway, T cell receptor signalling pathway, MAPK signalling pathway, JAK-STAT signalling pathway and PI3K-AKT signalling pathway. By observing the pathways, it showed that NF-κB was the most commonly involved pathway. Addition to that, the genes STAT1, SPP1 and IL6 were found to be common among the TLR pathway as well as significantly upregulated in CLL cells co-cultured with NLCs. Comprehensive pathway analysis indicated that the genes SPP1 and STAT1merit further investigations.

5.6 Discussion

5.6.1 Quality of RNA samples used for sequencing

RNA samples from a total of 9 cases (4 samples each) were sent for RNA sequencing using RNA-seq technology by Novogene. In the end, RNA samples from 6 cases were used for RNA-seq due to the low quantity of RNA extracted from NLC populations in the other 3 cases. The main reason to exclude RNA samples with low quantity is the unreliable global profiling of miniscule RNA generated by RNA-seq (Ozsolak & Milos 2011). Additionally, to ensure that samples were free from contamination of non-CLL cells, I checked purity of CLL samples by CD5 & CD19 co-expression by flow cytometry purity testing (described in Methods) after observing by microscopy. The Qubit 2.0 is considered to be a more accurate instrument than Nanodrop in quantitating RNA, as it was found to be highly reproducible and consistent with qPCR measurements (Simbolo et al. 2013). It was also reported that Nanodrop was not as accurate in quantifying very low levels of RNA as Qubit (Nakayama et al. 2016). Therefore, I relied on Qubit for the measurement of RNA before sending the RNA samples to be sequenced.

When the RNA sequencing data was produced by Novogene and released to us, it was analysed by Bioinformatics team of Computational Biology Facility at the University.

5.6.2 Quality control of sequencing data used for subsequent analysis

MultiQC software was initially used, as described (Ewels et al. 2016), to produce a single report visualising the data from all 24 samples. The sequence reads were aligned onto the reference genome homo_sapiens_NCBI_GRch38 (*NCBI - Genome Reference Consortium Human Build 38*) and subsequently levels of gene expression were estimated by counting the number of reads that maps to an exon (Kukurba & Montgomery 2015). Initially 33,121 genes were identified. However, after removing genes that had a sum of counts of <10 over all 6 samples within each group, 19,595 genes were taken forward for subsequent analysis. This included all the 24 samples i.e. 12 CLL and 12 NLC samples. Out of 19,595 genes, 322 genes were significantly upregulated and 4 were significantly downregulated in co-cultured CLL cells when compared to CLL cells cultured alone. However, only 4 genes were significantly upregulated and 3 were downregulated in co-cultured NLCs when compared to NLCs cultured alone.

5.6.3 Comparison of gene expression profile from my study with that from other studies

A study performed cDNA gene expression analysis of CLL samples after 14 days of co-culture with NLCs (Burger et al. 2009b). The top genes induced by 14 days of NLC co-culture with at least 3-fold up-regulation were CC chemokine CCL4, BCMA (TNFRSF17), EGR3, CCL3, PSAT1, MYCN, EGR2, K1AA0101, KMO and FCRL5 (Burger et al. 2009b). Down regulated genes included HRK, RGS2, TUBB2A, KLF6, TSC22D3, TMEM66, CHPT1, MXI1, MAFF and RHOB (Burger et al. 2009b). They performed DNA microarray analysis and identified a homogenous gene expression response across 9 different CLL cells after 14 days of co-culture with NLCs (Burger et al. 2009b).

A study (Boissard et al. 2016b) compared NLCs from CLL patients with monocytes of healthy donors and found 2589 overexpressed genes, while CLL cells compared to healthy B-lymphocytes over expressed 225 genes. After filtering out genes by applying different functional ontology criteria, the genes involved with NLC/CLL cell interaction included VCAM1, CD28, PECAM1 (for CD31 antigen), SELPLG (for LFA-1 antigen), CD2, CD86, CTLA4, SELP (for CD62 antigen) and CD58 (for LFA-3 antigen) (Boissard et al. 2016b).

A study generated NLCs from CLL patients for 10 days and treated with lenalidomide, that were then harvested and microarray was performed to give whole-genome expression profiles (Fiorcari et al. 2015). 584 genes were differentially expressed with lenalidomide treatment, of which 352 were up regulated and 232 were downregulated (Fiorcari et al. 2015). Categorised by Gene Ontology, the genes enriched by lenalidomide were those involved in immune responses, activation/proliferation of T cells, complement activation, antigen processing and presentation and regulation of cellular movement, cytokine and chemokine activity (Fiorcari et al. 2015). Specifically, CXCL11, CXCL9, CCL19, XCL1 XCL2, CCL2 and CCL12 was apparent (Fiorcari et al. 2015).

A study compared gene expression between NLC from purified PBMC of CLL patients with CD14 cells from healthy donors exposed to CLL culture ($CD14_{CLL}$) and CD14 cells from healthy donors cultured on healthy B-lymphocytes ($CD14_B$) (Bhattacharya et al. 2011). They found the gene expression profile (GEP) of NLCs to be closely similar to that of $CD14_{CLL}$ cells than to the GEP of $CD14_B$ cells (Bhattacharya et al. 2011). They also found that the antigen presenting pathway was the most significantly deregulated pathway, where the genes were mostly HLA class II genes and the CD74 gene. Also, the genes found dysregulated between NLCs and $CD14_{CLL}$ cells were FCGR2B, LYZ, HLA-DRA and CD74 (Bhattacharya et al. 2011).

In a study that compared CLL monocytes with monocytes from normal controls, where the CD14+ monocytes were highly purified, they identified 65 significantly upregulated genes and 48 downregulated

genes in the CLL monocytes compared to normal controls (Maffei et al. 2013). Of the upregulated genes, the involved pathways include those for Wnt signalling, VEGF signalling, angiogenesis and apoptosis (Maffei et al. 2013). The downregulated genes were involved in inflammation signalling, cytoskeletal regulation and oxidative stress response (Maffei et al. 2013). Specific genes involved in the CLL CD14+ monocytes that were upregulated, included RAP1GAP (reported to be involved in Fcγ-receptor and complement-receptor phagocytosis), ARHGEF12/LARG and LPAR6/P2Y5 which are involved in cell migration and Raf/ERK signalling (Maffei et al. 2013). Additionally, there was upregulated genes of toll-like receptor 4 (TLR4), Lipin-2 (LIP2), Lipin-3 (LIP3), phosphatidic acid (PA) and phosphatases (PAP). PLA2G4A was also upregulated (Maffei et al. 2013). Down-regulated genes in the CLL CD14+ monocytes were tubulins TUBB3 and TUBB2, CDC42EP3, chemokine (C-C motif) ligand 5 (CCL5) and PTGR2 (Maffei et al. 2013).

A study investigated the survival of CLL cells (by trypan blue exclusion) in cultures with anti-human CD62L (involved in controlling the traffic of T-lymphocytes) with untreated CLL PBMCs and performed microarray analysis on the monocytes/macrophages after 7 days of culture and found that the NLCs did not have statistically significant differentially expressed transcripts between sensitive and resistant patients (Burgess et al. 2016). When they compared their data with that from the study by Martinez et al (Martinez et al. 2006), they found that day 0 monocytes were similar and the NLCs they developed displayed an M2-like transcript profile (Burgess et al. 2016).

A previous study investigated the changes in gene expression by microarray in CLL cells after 14 days of co-culture with NLCs, as compared to CLL cells without co-culture (Burger et al. 2009b). The gene EGR2 was found to be among the top 10 genes to be significantly upregulated in co-cultured CLL cells (in 6 out of 9 paired samples). The other 9 genes included CCL4, TNFRSF17, EGR3, CCL3, PSAT1, MYCN, KIAA0101, KMO and FCRL5. In my study EGR2 was also significantly upregulated in CLL cells following 24 h co-culture with NLCs. The other 9 did not match with those of my study.

The study that compared the gene expression profiles of purified CD14 monocytes from CLL patients with those from normal controls, identified 65 upregulated and 48 downregulated genes (Maffei et al. 2013). Of the mentioned list, none had matched with my DGEA findings comparing NLC exposed and unexposed to CLL for 24 hours. The study did identify solute carrier family 25 (SLC25A17) to be upregulated, whereas my data identified solute carrier family 1 (SLC1A5) to be downregulated. The solute carrier families are a group of membrane transport proteins. The study used 5 sample pairs on whole human genome microarray, whereas I performed whole RNA sequencing using 6 sample pairs of NLC groups. It is likely

that the discrepancy between my study and the study mentioned is that a different method of analysis was used as well as a different control group was used. As mentioned earlier, the changes the study had identified is likely due to the heterogeneity of monocytes particularly in a heterogeneous disease of CLL patients. To solve this discrepancy, I would suggest performing an experiment using normal controls as the study used, with my two comparison groups and using whole RNA sequencing. RNA sequencing can detect higher percentage of differentially expressed genes than microarray. Increasing the number of sample pairs sent would be advantageous to provide a more accurate profile when predicting in vivo condition.

Comparing to the study that identified genes differentially expressed in M1 and M2 macrophages (Martinez et al. 2006), I was not able to have a suitable comparison with my NLC gene sets due to the low number of significantly expressed genes from 6 pairs of NLC groups. An increase in N number of NLC pairs for RNA-seq could be used to compare with gene subsets of this study in order to explore if NLCs are indeed M2 type of macrophages as well as to explore if there are any changes in the phenotype in the absence of CLL stimuli.

The Bioinformatics team compared the significantly upregulated genes among co-cultured CLL cells from my study to gene expression profile of CLL cells collected from the tissues by microarray (Herishanu et al. 2011). In their study, when peripheral blood (PB) CLL cells were compared with lymph nodes (LN) resident CLL cells, 151 differentially expressed genes were detected with at least 2-fold difference (false discovery rate, FDR <0.2). Of these, 133 were upregulated and 18 were down regulated (Herishanu et al. 2011). Between bone marrow (BM) and PB CLL samples, 26 genes were differentially expressed, in which 24 were upregulated and 2 were downregulated (Herishanu et al. 2011). Almost all the up-regulated genes in BM-derived CLL cells were also up-regulated in LN-derived CLL cells (Herishanu et al. 2011).

In comparison, the bioinformatics team found that 61 differentially expressed genes in co-cultured CLL cells from my study coincided with ranks of expression (See Gene Set Enrichment Analysis) based on “stat” values from DESeq2. These 61 genes were also found to be upregulated in LN CLL cells, but not PB CLL or BM CLL cells. This showed that the gene expression profile of CLL cells co-cultured with NLCs resemble that of LN CLL cells. Based on this observation, I selected 13 genes from a list of 63 genes for validation by RT-qPCR.

Validation of differentially expressed genes by RT-qPCR conformed changes detected by RNA-seq, in particular Myeloid Cell Leukaemia sequence 1 (MCL1, an apoptosis regulator which is a member of the

Bcl-2 family) (Pepper et al. 2008), Colony Stimulating Factor 1 (CSF1, produces cytokine that plays a role in survival, proliferation and differentiation of macrophages and monocytes) (Janowska-Wieczorek et al. 1991; Polk et al. 2016) and Guanylate Binding Protein 1 (GBP1, induced by interferon, the proteins are able to specifically bind to guanine nucleotides such as GMP, GDP and GTP) (Honkala, Tailor & Malhotra 2020).

Similarly, a study that showed that lenalidomide treated CLL patients identified 79 responded genes, of which 67 were upregulated included GBP1 (Aue et al. 2018). This study investigated the response of tumour microenvironment to lenalidomide through lymph node biopsy samples and microarray analysis. They found that IFN-y signalling pathway was of the most significantly overrepresented pathway. In my study, using RNA-seq data from CLL PBMC samples, GBP1 was among those significantly upregulated and IFN-y signalling pathway was among the highest predicted pathway involved.

5.6.4 A possible explanation to the findings from validating RNAseq DESeq2 list using RT-qPCR results:

Although both my study and the study by Burger et al (Burger et al. 2009b) found EGR2 to be upregulated in CLL cells after co-culture with NLCs, I was not able to validate by RT-qPCR because the primers available overlapped with the reading temperatures of primer dimers as well as produced a non-specific PCR product detected by agarose gel electrophoresis. Perhaps a better designed set of primers for EGR2 may be used to further validate the RNA-seq data.

In addition, both my study and the study by Boissard et al. (2016c) found CD28 to be upregulated in NLCs co-cultured with CLL cells, I was not able to validate this result as there were not enough cDNA samples to perform thorough optimisation and validation experiments. More NLCs collection is needed to confirm the findings in future.

Nonetheless, given that the majority of validated genes (6/7) were confirmed by RT-qPCR in more than 50% of samples, I was confident that the RNA-seq data was valid for the differential gene expression analysis.

5.6.5 Significantly Enriched Functional Pathways

Functional pathway analysis based on the differentially expressed genes was then performed, which revealed enriched set of genes involved in chemokine and cytokine signalling. REVIGO, a web server that summarizes and visualizes list of Gene ontology terms (Supek et al. 2011), identified that regulation of response to wounding and lymphocyte migration were the largest categories. This is not surprising as it is well known that CLL lymphocytes migrate into lymph nodes giving rise to the clinical feature of lymphadenopathy among CLL patients. It is also known that the tumour microenvironment exhibits features of chronic inflammation or response to wound healing, such as the differentiation of macrophages to M2 class, the production of CCL3 and CCL4, the release of IL-10, IL-6, the decreased pH, increased vasculature and remodelling to incorporate the involvement of various cell types (Krzyszczyk et al. 2018).

When comparing NLCcc with NLC using the same method described above, 18 enriched gene sets were identified including those for chemokine activity. This is also not surprising as one of the functions of macrophages are to move to the site of inflammation as a result of secreted chemokines and chemo attractants (Martinez et al. 2006). Given that only, 7 differentially expressed genes were detected, the predicted gene sets should be scrutinized. Perhaps a larger sample number of NLC would provide more detected differentially expressed genes and thus more accurate gene sets after GSEA.

A study investigating NLC from CLL patients with CD14 monocytes with CLL cells found 149 differentially expressed genes and 5 involved pathways (IPA) and 4 annotations (DAVID) (Bhattacharya et al. 2011). Due to the lower number of differentially expressed genes (n=7), the Bioinformatics team was not able to perform IPA and DAVID analysis.

5.6.6 Upstream Regulators and Pathways Involved

When feeding the 326 differentially expressed genes in co-cultured CLL cells (both up and downregulated) along with their fold-changes in log conversion (logFC) into IPA database of diseases and biological functions, it was found that the top categories of functions were of Cellular movement, Cell-cell signalling interaction (adhesion, binding), Inflammatory response, Free Radical Scavenging, Cellular Proliferation, shape change and cell death and viability. This is in agreement to what has been reported through numerous studies on CLL microenvironment (Kipps et al. 2017; Ten Hacken & Burger 2016).

Finally, Upstream Regulator analysis of the 326 differentially expressed genes in co-cultured CLL cells showed the top most enriched regulators included tumour necrosis factor (TNF) and interferon gamma (IFNγ). This was further evidenced by functional annotation using DAVID where major pathways involved were Toll-like receptor (TLR) signalling pathway, cytokine-cytokine receptor interactions and nuclear factor kappa B (NF-κB) signalling pathway. This is in agreement with numerous studies in literature investigating pathways involved in CLL (Arvaniti et al. 2011; Aue et al. 2018; Herishanu et al. 2011; Kipps et al. 2017; Muzio, Fonte & Caligaris-Cappio 2012). Through further DAVID KEGG pathway analysis, the pathways found to be relevant to CLL-NLC interaction included but not limited to, tumour necrosis factor (TNF) signalling pathway, Hypoxia-Inducible Factor-1 (HIF-1) signalling pathway, T cell receptor signalling pathway, MAPK signalling pathway, JAK-STAT signalling pathway and PI3K-AKT signalling pathway. In literature these pathways are also found to be involved (Ten Hacken & Burger 2016) as well as the basis of developing targeted drug therapy (e.g. PI3K inhibitor Idelalisib).

Activation of toll-like receptor (TLR) signalling pathway has been identified in CLL cells from the lymph node, which is consistent with the notion that CLL cells in the microenvironment behave differently from that in circulation (Dadashian et al. 2019). TLR pathway is involved in mediating immune surveillance and is known to promote pro-tumorigenic pathways (Ridnour et al. 2013). Depending on the type of TLR ligand binding, it produces pro-inflammatory cytokines (Spaner & Masellis 2007) that influence the immune response with T cell-mediated responses (via CD40), angiogenesis as well as initiate downstream response via NF-κB pathway (Spaner & Masellis 2007). The resulting effects include CLL proliferation, increased expression of adhesion molecules and CD40 (Spaner & Masellis 2007). This leads to pro-survival, proliferation and tissue homing of CLL cells.

JAK-STAT3 pathway consisting of Janus kinase (JAK) family of non-receptor kinase and signal transducer of activator of transcription (STAT) family of transcription factors are normally short and strictly regulated (Severin et al. 2019). In CLL there is aberrant activation which support survival, proliferation and metabolism of neoplastic cells (Severin et al. 2019). This pathway has also been implicated in CLL cells, its activation resulting in increased transcription of pro-survival and anti-apoptotic genes such as MCL-1 and BCL-2 (Severin et al. 2019). It has also been shown that the targeting of this pathway with inhibitors resulted in CLL-cell apoptosis (Severin et al. 2019).

Mitogen-activated protein kinase (MAPK) signalling pathway is a common event in pathogenesis of CLL (Shukla, Shukla & Joshi 2018). This pathway plays a fundamental role in the maintenance of basic cellular processes such as proliferation, differentiation, migration and inflammation (Shukla, Shukla & Joshi 2018).

In CLL, the level of MAPK activation is considered to link to the level of BCR signalling (Shukla, Shukla & Joshi 2018). In the microenvironment, molecules such as CD38, BCR and CXCR4 may modulate MAPK of proliferation centres (Shukla, Shukla & Joshi 2018). It was reported that an increased MAPK activation was seen in patients who displayed prognostic markers associated with poor disease outcomes (Shukla, Shukla & Joshi 2018). Novel molecularly targeted drugs such as ibrutinib, Idelalisib and fostamatinib show a suppressive effect on this pathway in CLL cells (Shukla, Shukla & Joshi 2018).

Activation of tumour necrosis factor (TNF) signalling pathway, particularly involving TNF receptor 1 (TNFR1), has been shown to activate NF-κB which promotes cell proliferation and survival of CLL cells (Dürr et al. 2018). It has also been shown that TNFR1 was highly expressed in CLL cells and its high expression in CLL patients has been associated with disease poor outcome (Dürr et al. 2018). High level expression of TNFR1 was also detected in proliferation centres of lymph nodes in patients with CLL (Dürr et al. 2018).

Hypoxia-inducible transcription factor (HIF) signalling, particularly with HIF protein 1α (HIF-1α), regulates the interaction between CLL cells and the microenvironment and is involved in a positive feedback loop that promotes cell survival and adaptation to hypoxic environment (Valsecchi et al. 2016). HIF-1α is found to be increased in CLL cells compared to non-malignant B and T cells in hypoxic conditions (Yosifov et al. 2020). It was shown that inhibiting this pathway impaired the interaction between CLL cells and its microenvironment (Valsecchi et al. 2016). HIF-signalling has also been implicated in vascular endothelial growth factor (VEGF) signalling that promotes angiogenesis (Shachar et al. 2012). Targeting this pathway could aid in preventing CLL cells from adapting and retuning the microenvironment.

In my study, it was observed that the most significant pathway enriched by the 326 differentially expressed genes of co-cultured CLL cells included NF-κB pathway. This is not unexpected, as NF-κB has been shown to be constitutively activated in CLL cells (Mansouri et al. 2016). NF-κB pathway has also been implicated as playing a central role in the pathology of CLL (Mansouri et al. 2016). Therefore, the result from my study provides further evidence that this gene expression data as measured by RNA-seq was consistent with what was published in the literature.

Furthermore, the genes that were found to be significantly upregulated in co-cultured CLL cells and in the top ranked pathways predicted by KEGG pathway analysis include Signal Transducer and Activator of Transcription 1 (STAT1), Secreted Phosphoprotein 1 (SPP1, also known as osteopontin) and Interleukin 6 (IL6).

The role of STAT1 has been well documented in CLL disease where it plays a role in the differentiation of CLL cells (Battle & Frank 2003). It has been shown that lenalidomide acts on STAT1 phosphorylation via interleukin 10 (IL-10) secretion, which leads to disruption of CLL-NLC interaction (Schulz et al. 2013).

IL6, a mediator of normal B cell differentiation and proliferation (Zhu et al. 2018), has also been documented in relation to CLL where it was shown to be secreted at high levels in bloodstream of CLL patients as well as correlated with poor prognosis (Zhu et al. 2018).

In contrast, the role of SPP1 (also known as osteopontin) in CLL is not well known. Only a handful studies have been performed and reported its overexpression in CLL cells in comparison to normal B cells (Dielschneider et al. 2016; Shukla 2013). One study showed that pharmacologically targeting lysosomes in CLL cells can be effective to lysosomal disruption leading to CLL cell apoptosis (Dielschneider et al. (2016). However, further studies are required to provide mechanistic insight into the role of SPP1 in CLL.

5.6.7 Conclusion

Collectively, the results from this chapter suggests that, there are numerous pathways involved in CLL-NLC interaction, that are supported by published studies in the literature. RNA sequencing is a valuable tool to identify such pathways, however, care must be taken when deriving conclusions from the data. In the cases of small changes, perhaps a sensitive (although more expensive) approach should be used to validate the changes biologically i.e. digital droplet PCR. In other cases, I have shown RT-qPCR is a useful efficient method to validate the changes detected by differential gene expression analysis (DGEA). Therefore, the pathways highlighted by the bioinformatics analysis from the RNA-seq data merit further investigations.

Numerous pathways have been identified that are well known in the research community of CLL such as NF-κB, PI3K, JAK-STAT3 and T-cell receptor signalling particularly on CD40L. The effect of NLCs on the gene expression of CLL cells shown from my study confirms that these pathways are indeed involved and may represent the mode of action of NLCs in CLL microenvironment *in vivo*. Pathways involving angiogenesis such as HIF-signalling pathway, however, have not been as intensively investigated as other pathways in CLL, and merits further study. The most significantly enriched pathway is the NF-κB Pathway as it is an integral player in the network of involved pathways. Additionally, identifying the genes STAT1, SPP1 and IL-6 suggests that they play additional roles in the interaction between CLL cells and NLCs.

6 General Discussion

In CLL microenvironment, one of the main components are the NLCs which provide pro-survival signals to the CLL cells (Burger et al. 2000). The NLCs appear to be a large oval adherent macrophages (Burger et al. 2000). NLCs which express CD163, was found in lymph node and spleen sections of CLL patients (Blonska, Agarwal & Vega 2015; Burger 2011a; Hanna et al. 2015; Ysebaert et al. 2010). The presence of NLCs may represent an unfavourable prognostic marker in patients with CLL, where the number of NLCs were positively correlated with beta 2 microglobulin (B2M) serum levels and SURVIVIN gene expression in CLL cells ex vivo (Filip et al., 2009 and 2013). It was also shown that a high density of CD68+ CD163+ NLCs at diagnosis was significantly correlated with unfavourable prognostic markers and to poor clinical outcomes in patients with DLBCL (Marchesi et al. 2015). A study investigating hepatocellular carcinoma showed a possible association between overexpression of CD163+ NLCs and worse patient outcome (Minami et al. 2018).

Although studies in this area of tumour microenvironment has been ongoing for the last two decades, exactly how NLCs protect CLL cells is still unclear. CLL remains an incurable disease and it is known that the microenvironment plays an important part in disease progression and the development of drug resistance. It becomes clear to me that more studies are required to comprehensively characterise the NLC development, in particular understanding the molecular mechanisms mediating the interaction between CLL cells and NLCs.

In my PhD study, I hypothesised that interactions between NLCs and CLL cells activate certain genes and pathways which are responsible for survival and drug resistance of CLL cells. To address this hypothesis, I attempted to first independently characterise NLCs developed *in vitro*. I then set up co-culture experiments and extracted RNA from the cultured CLL cells and NLCs using their respective counterparts cultured alone as controls, and identify the differentially expressed genes using NGS sequencing technology. Through the bioinformatics analysis, I identified a few molecules and pathways that are likely associated with the enhanced survival and resistance to apoptosis in CLL cells following interaction with NLCs.

6.1 Independent confirmation of development of NLCs from primary CLL PBMC cells

In the first part of my PhD study, I sought to optimise the culture conditions for developing NLCs *in vitro* by modifying the established cell culture techniques published in literature.

Previous studies have reported that various densities of CLL PBMCs were used for developing NLCs (Burger et al. 2000; Filip et al. 2009; Jia et al. 2014; Nishio et al. 2005; Polk et al. 2016). In my study, the use of a high cell density is found to be more favourable for NLC development and a cell density of 10 x 10^6/ml was an optimal concentration of CLL PBMC cells used to develop NLCs under the culture conditions used. Although, to truly assess the *in vivo* microenvironmental influences, bone marrow and lymph node samples would be ideal, I was only able to experiment on the available fresh PBMC. I next tried to independently confirm the morphology and immunophenotype of NLCs.

6.1.1 Morphology

The morphology of NLCs was first described as 'large oval adherent shape' by Burger et al. (2000). I investigated the morphological features of NLCs developed using a density of 10 x 10^6/ml CLL PBMC cultures throughout my study for consistency.

The morphology of NLCs was found to be more complex than that described in literature, particularly the cell shape and size were more dynamic than just becoming large oval adherent.

In addition, in order to distinguish the cellular components of the NLCs in development, I used MGG staining as detailed in results Chapter 1. Careful observations of morphology revealed that the NLCs appear not only as 'large oval adherent cells', but also display pleomorphism in appearance such as looking 'elongated', 'spindle-shaped' and 'clustered'. This detailed assessment of morphology of NLCs showed that the developmental of the NLCs is a very dynamic process, which was very much underappreciated previously.

6.1.2 Immunophenotype

To further confirm the immunophenotype of the NLCs, I performed immunofluorescent staining of the NLCs following morphologic identification. I investigated the several surface markers that were reported to be expressed by NLCs. In addition, the cellular localisation of these proteins has also been examined.

I confirmed that NLCs express CD68, CD163 and CD14, but not CD19 the CLL specific marker. CD163 expression was cytoplasmic and seen in all NLCs from all the CLL samples, whereas expression of CD68 and CD14 was variable and not as strong as CD163 although they were both detected. This suggests that CD163 is a better marker to identify NLCs in a research setting. My observation on the localisation and expression of the above markers for NLCs is largely in agreement with findings from others reported in the literature (Boissard et al. 2015a; Fiorcari et al. 2015; Marchesi et al. 2015). One study also showed that CD163 was a reliable marker for NLCs and has been used to investigate the link of NLCs with disease progression of CLL (Boissard et al. 2016a).

6.1.3 Biological function

It was known that NLCs provide pro-survival signals to CLL cells which protect the leukemic cells against spontaneous apoptosis, which I also confirmed in the co-culture experiments of my study.

I demonstrated that there was significant protection of CLL cells from spontaneous apoptosis following the first 24 h of co-culture when compared to CLL cells cultured alone. This was confirmed by apoptosis assays using flow cytometry with the reagents Annexin V and Propidium Iodide. It was also noted that NLC cultures which contained higher number of NLCs (observed by microscope) gave a greater protection to CLL cells. This was similarly shown in a study that found a positive correlation between number of NLCs counted and the viability of CLL cells (Boissard et al. 2016a).

I also investigated the levels of the T cell chemokines CCL3 and CCL4 in the supernatant of fresh CLL PBMC cultures in a time-course experiment and found that levels of CCL3 and CCL4 were increased over time, which was consistent with the findings of a previous study (Burger et al, 2009). In that study, authors also detected the increased levels of CCL3 and CCL4 in blood plasma from CLL patients who had adverse prognostic features (Burger et al, 2009), suggesting that by secreting these chemokines to attract T cells to the lymph node microenvironment CLL cells actively contribute to the development of CLL microenvironment. Due to time constraints, I did not perform correlation study of plasma levels of CCL3 and CCL4 from CLL patients with their clinical characteristics.

It is worth noting that I also observed interesting, previously unreported effects of the CLL cells on NLCs when in co-culture. I found that NLCs also displayed a healthy-looking appearance in co-culture with CLL cells when compared to their counterparts cultured alone. Although this was not thoroughly studied, the

presence of CLL cells appeared to be conducive to NLCs, implying that there is a two-way, mutual influence taking place between CLL cells and NLCs.

6.2 Wide variation in the NLC development between CLL samples

6.2.1 Variation in the magnitude of NLCs development

During the time period of developing the NLCs, I observed that not all the CLL samples had developed the similar number of NLCs, in fact some sample did not develop any NLCs. Some samples had less than 10 NLCs per field when viewed under light microscope (at 10 x magnification), whereas others had between 10-30 and in some cases more than 30. This finding was also reported by others (Filip et al. 2013a; Jia et al. 2014). Therefore, I confirmed that number of NLCs observed is variable from sample to sample, which makes it a challenge to reproduce the similar results using individual CLL samples.

6.2.2 Variation in the dynamic of NLC development

Most strikingly, I observed that the speed of NLC development were also variable from sample to sample. Whilst the changes in the shape and size were observed over the course of NLC development in the majority of NLC samples, these changes were not happening at the same rate. I observed changes in shape and size during NLC development under phase contrast microscope and confirmed these changes by MGG staining. Most other studies have reported that NLCs were developed following 14 days in culture, displaying a flattened adherent appearance (Burger et al. 2000; Gautam et al. 2016; Jia et al. 2014). My work largely confirmed this finding in many CLL samples I studied. However, I also noticed that there are many cases where mature, fully developed NLCs were seen as early as 8 days after culturing.

The observation of wide variation in development of NLCs between CLL samples led to the development of a unique NLC scoring system which assigns a number (from 0 to 3) to individual samples based on how well the CLL PBMC cells develop NLCs. This was done in order to determine whether the variation in developing NLCs may be correlated to the clinical features of the CLL samples used in the study.

6.2.3 Lack of correlation between NLC development and clinical features of CLL samples

To address the above question, I collected available clinical information of all the CLL samples used. However, I did not detect any statistically significant correlation of NLC development with gender, IGHV

mutational status, clinical staging, chromosomal abnormalities or treatment history. Therefore, exactly why there is such wide variation in generation of NLCs between CLL samples from individual patients remains unclear. Interestingly, one study reported that, in a 6-year follow-up, a longer survival rate in CLL patients who had a lower NLC count was observed, although this finding was not statistically significant (Filip et al, 2013). Therefore, whether the NLC number developed *in vitro* can be used to predict the clinical outcome of patients with CLL still remains to be seen.

6.3 Need for a cell line model of NLCs

Over the course of my PhD study, I encountered many technical difficulties in establishing optimal conditions to produce consistent results of developing NLCs using primary CLL PBMC samples. In particular, a continuous supply of fresh CLL PBMC samples poses a logistical challenge to me. Together with the variation in generating NLCs, it becomes clear to me that an alternative system to carry out NLC experiments needed to be explored.

6.3.1 Justification for selection of THP-1 cell line

In the next part of my PhD study, I attempted to determine if THP-1 cells can be developed as an *in-vitro* cell line model of NLCs. THP-1 cells derived from human monocytic leukemic cells and can be differentiated into macrophages and further polarised to M1 and M2 macrophages. This cell line has been commonly used for studies into behaviour of monocytes and macrophages (Tedesco et al. 2018). There are other cell lines which were also considered, such as U937, ML-2, HL-60 and Mono Mac 6 (Chanput, Peters & Wichers 2015). However, large number of studies have used THP-1 cells in preference to other cell lines (Aldo et al. 2013; Daigneault et al. 2010; Forrester et al. 2018; Park et al. 2007; Tedesco et al. 2018). It was soon evident that THP-1 cells were far more befitting to my requirements. First, comparing to the tissue resident monocyte-derived U937 cell line, THP-1 cells originated from blood monocytes and are more closely resembling to blood monocyte-derived NLCs (Chanput, Peters & Wichers 2015). Second, THP-1 cells is known to produce a phenotype of macrophage only with no expression of dendritic cell markers (Riddy et al. 2018). Finally, U937 cells do not display chemoattractant behaviour when using trans-well migration assay, whereas THP-1 cells (Riddy et al. 2018) and NLCs (Boissard et al. 2016b) share the similar chemoattractant property. Based on the above considerations, I chose THP-1 cells for my study.

An optimised density of 0.5 x 10^6/ml of THP-1 cells was used following a modified protocol to produce adherent macrophages (M0), which were further polarised to become M1 and M2 populations of macrophages using established protocol. M1 and M2 macrophages were confirmed by immunofluorescent microscopy using CD markers EGR2 and CD38, respectively.

6.3.2 Similarities of cell line model to primary NLCs

I then proceeded to compare the similarities and differences of this cell line model to primary NLCs in aspects of morphology, phenotype and biological functions.

The morphology of differentiated THP-1 cells largely matched those of NLCs. They exhibited the adherent macrophage property, as reported previously in other studies (Chimal-Ramirez et al. 2016; Genin et al. 2015). The phenotype of NLCs being of M2 subtype macrophages was replicated in differentiated THP-1 cells in which the expression of CD14 and CD163 as well as the elongated morphology were observed following polarisation to M2 subtype.

The NLCs were described as having predominantly M2 macrophage phenotype (Hanna et al, 2015; Marchesi et al, 2015, Ysebaert and Fournie, 2011; Ysebaert et al, 2010). I therefore induced the THP-1 cell-derived M0 macrophages to differentiate into M1 and M2 subtypes of macrophages and compared their relative contribution to the pro-survival effect towards CLL cells. My results showed that M2 macrophages conferred greater protection than M1 macrophages against spontaneous and fludarabine-induced cell death of CLL cells. Therefore, the cell line model using differentiated THP-1 cells can recapitulate the cytoprotective effect of NLCs on CLL cells.

6.3.3 Limitations of the cell line model

As with any model, there are limitations with the THP-1 cell line model which precludes it to completely replace primary NLCs. First, there were difficulties of using this model to verify the increased levels of CCL3 and CCL4 secreted by CLL cells when in co-culture with NLCs, as reported (Burger et al, 2009). This is due to the observations that the differentiated THP-1 cells alone spontaneously produce a high level of CCL3 and CCL4 as reported here in my study (Figure 4.10 in Section 4.4.4.3) and by others (Harrison et al. 2005; Mantovani et al. 2002). This makes it very difficult to measure the difference in the levels of the chemokines in the cultures of THP-1 cells with or without CLL cells.

Another limitation to this model was its inability to mimic the effect of NLCs on the levels of surface expression of IgM and IgD on CLL cells. It was reported that the expression levels of sIgM and sIgD of CLL cells were reduced when co-cultured with NLCs (Ten Hacken et al. 2016). However, the THP-1 cell-derived, polarised macrophages were not able to replicate this effect. This could be caused by addition of cytokine such as IL-4 that was used to induce polarisation of THP-1 cells to M2 macrophages. IL-4 has been shown to enhance the expression of sIgM in CLL cells (Aguilar-Hernandez et al. 2016). It has also been shown that small amounts of IL-4 are secreted by macrophages (La Flamme et al. 2012). Therefore, presence of exogenous IL-4 may have prevented the reduction in expression of sIgM and sIgD in CLL cells by the THP-1 cell-derived macrophages.

Therefore, it became clear that there are limitations to the use of cell line model as to how much it is truly representative of NLCs. Caution is thus required when interpreting the results generated from the use of cell line model and further extrapolating such interpretation to explain *in-vivo* events.

6.4 Comparison of global gene expression in CLL cells cultured with or without NLCs

Due to the limitations of the cell line model outlined above, in the final part of my PhD study I chose to use fresh CLL PBMCs samples to develop NLCs and apply cryopreserved autologous CLL cells for co-culture experiments and investigated at the level of gene expression the molecules and pathways involved in survival and resistance of CLL cells to therapy as a result of interaction between NLCs and CLL cells. Thus, my intention was to identify differentially expressed genes that could be targeted by future therapy to overcome resistance.

6.4.1 Identification of differentially expressed genes

I first sought to establish a comprehensive list of differentially expressed genes in primary CLL samples that were cultured with or without NLCs through RNA sequencing analysis. RNA samples were thus extracted from CLL cells cultured with NLCs for 24 h as well as cultured alone for the same time period and RNA sequencing was performed by a commercial biotechnology firm Novogene using RNA-seq technology. Bioinformatics analysis of the sequencing data was performed by Computational Biology Facility (CBF) of University of Liverpool. In total, 6 CLL samples were used to generate the RNA samples for sequencing. Out of 19,595 genes analysed, 326 genes were significantly differentially expressed among CLL cells in co-culture with NLCs in comparison with CLL cells cultured alone. Among the 326 differentially

expressed genes, 322 gene were upregulated in CLL cells co-cultured with NLCs. When compared to published comparative gene expression data from CLL cells isolated from lymph nodes versus peripheral blood (Herishanu et al. 2011), 61 out of 322 upregulated genes in our study were found in the list of the overly expressed genes (133 in total) in CLL cells from lymph nodes. Gene set enrichment analysis also produced a statistically significant positive enrichment of the two data sets, indicating that gene expression profile of CLL cells co-cultured with NLCs shared a high degree of similarity to that of CLL cells from the lymph nodes. Encouraged by the above results, I selected some of the 61 differentially expressed genes identified by RNA-seq for validation using RT-qPCR.

In the end, I managed to validate 9 genes for which RT-qPCR were optimised and performed on 14 CLL samples (with or without co-culture). Results from RT-qPCR largely confirmed the findings from RNA-seq analysis.

6.4.2 Molecules and pathways critically involved in the survival and resistance of CLL cells to therapy *in vivo*

Using the list of differentially expressed genes described above, I attempted to identify molecules and pathways critically involved in the survival and resistance of CLL cells to therapy *in vivo* through bioinformatics analysis. With the support from the CBF team of University of Liverpool, using the Ingenuity Pathway Analysis I was able to identify several significantly enriched upstream regulators, with the top most significantly enriched regulators including tumour necrosis factor (TNF) and interferon gamma (IFNγ). Using the identified upstream regulators, KEGG pathway analysis revealed several highly enriched signalling pathways involved in mediating the CLL-NLC interaction. The highest ranked pathway included the toll-like receptor (TLR), TNF, hypoxia-inducible factor (HIF) and NF-κB signalling pathways. NF-κB signalling pathway is known to be activated in the CLL cells that are localised within the lymph node microenvironment (Mansouri et al. 2016). The activation of NF-κB pathway leads to sustaining CLL proliferation and survival *in vivo*. My study therefore confirms the findings of NF-κB pathway involvement in survival signalling of CLL cells.

TLR signalling pathway is also known to be activated in CLL cells (Arvaniti et al. 2011; Dadashian et al. 2019; Muzio, Fonte & Caligaris-Cappio 2012), where it cooperates with BCR signalling to activate NF-κB pathway (Dadashian et al. 2019). My study is thus in agreement with this finding by implicating that TLR signalling pathway is strongly activated following NLC-CLL interaction.

Activation of TNF signalling pathway is known to play a role in CLL pathology (Dürr et al. 2018). Thus, it has been shown that the level of TNF receptor is increased in CLL cells (Dürr et al. 2018). Also, level of TNF-α is increased in CLL cells and high levels of TNF-α are indicative of aggressive disease states (Dürr et al. 2018). Activation of TNF signalling pathway can also activate NF-κB signalling pathway, contributing to the survival of CLL cells and their resistance to apoptosis (Dürr et al. 2018).

HIF signalling pathway has been reported to be activated in CLL cells residing in hypoxic tumour microenvironment where the upregulated HIF-1α regulates the interactions between CLL cells and the microenvironment, promoting cell survival and adapting to hypoxic environments (Valsecchi et al. 2016). However, in my knowledge there are not many studies reporting findings from experiments that were performed under hypoxic conditions in CLL, further investigation is warranted to investigate NLC-CLL interaction in a hypoxic culturing condition.

Further analysis also revealed some significantly enriched genes critically involved in these signalling pathways. They include STAT1, SPP1 and IL6.

It has been shown that STAT1 plays a role in the differentiation of CLL cells mediated by Byrostatin 1 (Battle & Frank 2003). Tyrosine phosphorylation of STAT1 promotes further maturation of CLL B cells leading to up-regulation of CD22 expression and IgM production (Battle & Frank 2003). It was also shown that lenalidomide treatment resulted in an increased level of the immunosuppressive cytokine IL-10 which was shown to induce apoptosis in CLL cells via STAT1 activation (Schulz et al. 2013). The activated STAT1 was shown to inhibit matrix metallopeptidase 9 (*MMP9*) expression in CLL cells, which is normally upregulated and important in cell migration and promote survival of CLL cells (Schulz et al. 2013).

IL6 is also a known mediator of B cell differentiation and proliferation (Zhu et al. 2018). High levels of IL-6 in CLL patients have been reported to be correlated with poor prognosis (Zhu et al. 2018).

The exact role of SPP1 (osteopontin) is not well known in the context of CLL. The role of osteopontin has been documented in a number of other cancers such as breast cancer, colorectal cancer and lung cancer (Shevde & Samant 2014) and disruption of the lysosomes has been shown to induce cell death in the cancer cells (Dielschneider et al. 2016). It was shown that SPP1 was overexpressed in CLL cells at the mRNA level as well as at protein level compared to normal B cells, but no difference between CLL patients with mutated IGHV and unmutated IGHV (Dielschneider et al. 2016). However, the clinical significance of this finding is not clear. It was suggested that in the sphingolipid pathway, the dephosphorylation of S1P by SPP1 (to produce sphingosine) makes CLL cells more sensitive to lysosome permeability (Dielschneider et

al. 2016). However, the exact mechanism of lysosome permeabilization leading to loss of mitochondrial potential in CLL cells is unknown (Dielschneider et al. 2016). It was speculated that the lysosome membrane oxidation can open the pore of the mitochondria which leads to cell death cascade (Dielschneider et al. 2016).

The role of SPP1 in survival of CLL cells following interaction with NLCs is still unclear, which requires further investigation.

6.5 Suggestions for future experiments

It is my view that the study of NLCs is still in its infancy, despite being researched for almost two decades. NLCs remain a key component of the CLL microenvironment. The interaction between NLCs and CLL cells in the microenvironment, to a large degree, resembles reciprocal interaction of cancer cells with the tumour microenvironments in general. It is still not yet known the exact mechanisms of how CLL cells are supported by NLCs. Further studies are required to not only understand better the underlying pathways that sustain a tumour microenvironment, but also help identify molecular targets for therapeutic intervention.

A pathway that was significantly activated following KEGG pathway analysis of the gene expression data from co-cultured CLL cells is the HIF signalling pathway. There are not many studies specifically looking at role of this pathway in mediating NLC-CLL interactions (Koczula et al. 2016; Yosifov et al. 2020). Considering that tumour microenvironment produces a hypoxic condition *in vivo* (Kim et al. 2009; Lyssiotis & Kimmelman 2017), it would be worth investigating of involvement of the HIF pathway in CLL-NLC interaction, ideally in a hypoxic condition. The protocols of creating hypoxic conditions using cobalt chloride ($CoCl_2$) solution or in Modular Incubator Chamber may be adapted when performing such experiments (Wu & Yotnda 2011). The pursuit of NLC study using CLL cells in a hypoxic environment would create a closer replica of environmental conditions *in vivo*. I hypothesize that in a hypoxic condition, there will be an enhanced development of NLCs as well as the greater protective effects on CLL cells. Since it has been shown that M2 macrophages are present more in hypoxic conditions (Bingle, Brown & Lewis 2002b; Petrova et al. 2018), more NLCs may develop in most CLL samples and protect the CLL from spontaneous apoptosis for a longer duration. A hypoxic condition experiment may uncover a trait of NLC interaction with CLL that would not have been so obvious in a standard non-hypoxic culture condition.

One of the upstream regulators that was also among the top "significantly enriched pathways" was SPP1 (osteopontin). Currently there are only two studies that investigated SPP1 in the CLL setting (Dielschneider et al. 2016; Shukla 2013). Since the understanding of the biological function of this gene in CLL is in its infancy, independent studies are required to first ascertain if findings from the two studies (Dielschneider et al. 2016; Shukla 2013) could be reproduced in CLL cells cultured with or without NLCs. If the pro-survival effect of SPP1 is confirmed, further experiments will be needed to provide definitive evidence of its function by manipulating gene expression (up or down regulation) and clear explanation on the mechanism of how SPP1 mediates its function. Finally, therapeutic potential of targeting SPP1 should be explored using pharmacological inhibitors.

Finally, a model system encompassing multiple components and stimuli relevant to an *in vivo* microenvironment has yet to be produced in a laboratory setting. The pursuit of such a model system can allow researchers to use such platform to perform cell death assay with drugs that target various components of the microenvironment, including CLL cells, NLCs, cancer associated stromal cells, in a hypoxic, vasculature environment. Current advances in this direction include development of cancer-on-a-chip models where microfluidic chips contain chambers for cell culture, which control fluid flow, oxygen diffusion, tissue mechanics and composition of cellular components (Asghar et al. 2015; Sleeboom et al. 2018; Wu & Swartz 2014). Although the *in vitro* models will not fully reproduce the microenvironment conditions *in vivo* and produce a truly representation of the responses from primary cells (Goodspeed et al. 2016), development of the *in vitro* system to mimic the *in vivo* conditions would enable researchers to gain an better understanding of an underlying pathology of a disease. This in turn will facilitate testing of the new drugs that target the molecules/pathways associated with survival and resistance to therapy. It is obvious that achieving such objectives will require the teamwork of bioengineering, cell culture specialists, computational biologists and histopathologists.

6.6 Conclusions

I independently confirmed many features of NLCs developed *in vitro* using primary CLL samples, but also produced an NLC scoring system based on the number and morphology of NLCs developed to reflect the wide variation in the development of NLCs between individual CLL samples. The NLCs indeed prolonged the survival of CLL cells as well as contributed to the increasedserum levels of CCL3 and CCL4. To determine if these effects can be reproduced using a cell line model, I showed that THP-1 cells can be used as a cell line model to mimic the pro-survival effect of NLCs and evaluated advantage and

disadvantage of the use of cell line model. Finally, I identified a list of differentially expressed genes involved in mediating the pro-survival effect of NLCs on CLL cells, some of which was validated using RT-qPCR techniques. Using contemporary bioinformatics tool, I analysed in depth the role of several molecules and pathways that are likely critically involved in the survival and resistance of CLL cells to therapy *in vivo,* and highlighted some molecules/pathways that could be therapeutically targeted to overcome therapy resistance in future.

References

Aguilar-Hernandez, M.M., Blunt, M.D., Dobson, R., Yeomans, A., Thirdborough, S., Larrayoz, M., Smith, L.D., Linley, A., Strefford, J.C., Davies, A., Johnson, P.M., Savelyeva, N., Cragg, M.S., Forconi, F., Packham, G., Stevenson, F.K. & Steele, A.J. (2016) 'IL-4 enhances expression and function of surface IgM in CLL cells', *Blood*, vol. 127, no. 24, pp. 3015-3025.

Al-Malti, A., Gribben, J.G. & Jia, L. (2012) 'HMGB1 Activates TLR9/RAGE Signalling Pathway and Sustains Chronic Lymphocytic Leukemic Cell in Vitro Survival', *Blood*, vol. 120, no. 21, pp. 3860-3860.

Aldo, P.B., Craveiro, V., Guller, S. & Mor, G. (2013) 'Effect of culture conditions on the phenotype of THP-1 monocyte cell line', *Am J Reprod Immunol*, vol. 70, no. 1, pp. 80-86.

Allavena, P., Piemonti, L., Longoni, D., Bernasconi, S., Stoppacciaro, A., Ruco, L. & Mantovani, A. (1998) 'IL-10 prevents the differentiation of monocytes to dendritic cells but promotes their maturation to macrophages', *Eur J Immunol*, vol. 28, no. 1, pp. 359-369.

Andersen, M.N., Al-Karradi, S.N., Kragstrup, T.W. & Hokland, M. (2016) 'Elimination of erroneous results in flow cytometry caused by antibody binding to Fc receptors on human monocytes and macrophages', *Cytometry A*, vol. 89, no. 11, pp. 1001-1009.

Arvaniti, E., Ntoufa, S., Papakonstantinou, N., Touloumenidou, T., Laoutaris, N., Anagnostopoulos, A., Lamnissou, K., Caligaris-Cappio, F., Stamatopoulos, K., Ghia, P., Muzio, M. & Belessi, C. (2011) 'Toll-like receptor signaling pathway in chronic lymphocytic leukemia: distinct gene expression profiles of potential pathogenic significance in specific subsets of patients', *Haematologica*, vol. 96, no. 11, pp. 1644-1652.

Asghar, W., El Assal, R., Shafiee, H., Pitteri, S., Paulmurugan, R. & Demirci, U. (2015) 'Engineering cancer microenvironments for in vitro 3-D tumor models', *Materials Today*, vol. 18, no. 10, pp. 539-553.

Aslam, R., Kim, M., Speck, E.R., Seetanah, A.C., Molinski, S., Freedman, J. & Semple, J.W. (2007) 'Platelet and red blood cell phagocytosis kinetics are differentially controlled by phosphatase activity within mononuclear cells', *Transfusion*, vol. 47, no. 11, pp. 2161-2168.

Aue, G., Sun, C., Liu, D., Park, J.H., Pittaluga, S., Tian, X., Lee, E., Soto, S., Valdez, J., Maric, I., Stetler-Stevenson, M., Yuan, C., Nakamura, Y., Muranski, P. & Wiestner, A. (2018) 'Activation of Th1 Immunity within the Tumor Microenvironment Is Associated with Clinical Response to Lenalidomide in Chronic Lymphocytic Leukemia', *J Immunol*, vol. 201, no. 7, pp. 1967-1974.

Azenabor, A.A., Cintron-Cuevas, J., Schmitt, H. & Bumah, V. (2011) 'Chlamydia trachomatis induces anti-inflammatory effect in human macrophages by attenuation of immune mediators in Jurkat T-cells', *Immunobiology*, vol. 216, no. 12, pp. 1248-1255.

Badoux, X., Bueso-Ramos, C., Harris, D., Li, P., Liu, Z., Burger, J., O'Brien, S., Ferrajoli, A., Keating, M.J. & Estrov, Z. (2011) 'Cross-talk between chronic lymphocytic leukemia cells and bone marrow endothelial cells: role of signal transducer and activator of transcription 3', *Human Pathology*, vol. 42, no. 12, pp. 1989-2000.

Bain, B.J., Bates, I., Laffan, M.A. & Lewis, S.M. (2012) *Dacie and Lewis Practical Hematology*, 11th edn, Churchill Livingstone.

Bakker, E., Qattan, M., Mutti, L., Demonacos, C. & Krstic-Demonacos, M. (2016) 'The role of microenvironment and immunity in drug response in leukemia', *Biochimica et Biophysica Acta (BBA) - Molecular Cell Research*, vol. 1863, no. 3, pp. 414-426.

Baliakas, P., Jeromin, S., Iskas, M., Puiggros, A., Plevova, K., Nguyen-Khac, F., Davis, Z., Rigolin, G.M., Visentin, A., Xochelli, A., Delgado, J., Baran-Marszak, F., Stalika, E., Abrisqueta, P., Durechova, K., Papaioannou, G., Eclache, V., Dimou, M., Iliakis, T., Collado, R., Doubek, M., Calasanz, M.J., Ruiz-

Xiville, N., Moreno, C., Jarosova, M., Leeksma, A.C., Panayiotidis, P., Podgornik, H., Cymbalista, F., Anagnostopoulos, A., Trentin, L., Stavroyianni, N., Davi, F., Ghia, P., Kater, A.P., Cuneo, A., Pospisilova, S., Espinet, B., Athanasiadou, A., Oscier, D., Haferlach, C., Stamatopoulos, K. & Eric, t.E.R.I.o.C.L.L. (2019) 'Cytogenetic complexity in chronic lymphocytic leukemia: definitions, associations, and clinical impact', *Blood*, vol. 133, no. 11, pp. 1205-1216.

Battle, T.E. & Frank, D.A. (2003) 'STAT1 mediates differentiation of chronic lymphocytic leukemia cells in response to Bryostatin 1', *Blood*, vol. 102, no. 8, pp. 3016-3024.

Bhattacharya, N., Diener, S., Idler, I.S., Rauen, J., Habe, S., Busch, H., Habermann, A., Zenz, T., Dohner, H., Stilgenbauer, S. & Mertens, D. (2011) 'Nurse-like cells show deregulated expression of genes involved in immunocompetence', *Br J Haematol*, vol. 154, no. 3, pp. 349-356.

Bingle, L., Brown, N.J. & Lewis, C.E. (2002a) 'The role of tumour-associated macrophages in tumour progression: implications for new anticancer therapies', *The Journal of Pathology*, vol. 196, no. 3, pp. 254-265.

Bingle, L., Brown, N.J. & Lewis, C.E. (2002b) 'The role of tumour-associated macrophages in tumour progression: implications for new anticancer therapies', *J Pathol*, vol. 196, no. 3, pp. 254-265.

Blombery, P., Birkinshaw, R.W., Nguyen, T., Gong, J.-n., Thompson, E.R., Xu, Z., Westerman, D.A., Czabotar, P.E., Dickinson, M., Huang, D.C.S., Seymour, J.F. & Roberts, A.W. (2019) 'Characterization of a novel venetoclax resistance mutation (BCL2 Phe104Ile) observed in follicular lymphoma', *British Journal of Haematology*, vol. 186, no. 6, pp. e188-e191.

Blonska, M., Agarwal, N.K. & Vega, F. (2015) 'Shaping of the tumor microenvironment: Stromal cells and vessels', *Semin Cancer Biol*, vol. 34, pp. 3-13.

Boissard, F., Fournie, J.J., Laurent, C., Poupot, M. & Ysebaert, L. (2015a) 'Nurse like cells: chronic lymphocytic leukemia associated macrophages', *Leuk Lymphoma*, vol. 56, no. 5, pp. 1570-1572.

Boissard, F., Fournie, J.J., Quillet-Mary, A., Ysebaert, L. & Poupot, M. (2015b) 'Nurse-like cells mediate ibrutinib resistance in chronic lymphocytic leukemia patients', *Blood Cancer J*, vol. 5, p. e355.

Boissard, F., Laurent, C., Ramsay, A.G., Quillet-Mary, A., Fournié, J.J., Poupot, M. & Ysebaert, L. (2016a) 'Nurse-like cells impact on disease progression in chronic lymphocytic leukemia', *Blood Cancer Journal*, vol. 6, no. 1, p. e381.

Boissard, F., Tosolini, M., Fournié, J.-J., Ligat1, L., Ysebaert, L., Quillet-Mary, A. & Poupot, M. (2016b) 'NLCs promote CLL survival through LFA3 CD2 interactions', *Oncotarget Advance Publications*.

Boissard, F., Tosolini, M., Ligat, L., Quillet-Mary, A., Lopez, F., Fournié, J.-J., Ysebaert, L. & Poupot, M. (2016c) 'Nurse-like cells promote CLL survival through LFA-3/CD2 interactions', *Oncotarget*.

Bojarczuk, K., Sasi, B.K., Gobessi, S., Innocenti, I., Pozzato, G., Laurenti, L. & Efremov, D.G. (2016) 'BCR signaling inhibitors differ in their ability to overcome Mcl-1-mediated resistance of CLL B cells to ABT-199', *Blood*, vol. 127, no. 25, pp. 3192-3201.

Bosch, F. & Dalla-Favera, R. (2019) 'Chronic lymphocytic leukaemia: from genetics to treatment', *Nat Rev Clin Oncol*.

Buggins, A.G. & Pepper, C.J. (2010) 'The role of Bcl-2 family proteins in chronic lymphocytic leukaemia', *Leuk Res*, vol. 34, no. 7, pp. 837-842.

Burger, J.A. (2011a) 'Nurture versus Nature: The Microenvironment in Chronic Lymphocytic Leukemia', *American Society of Hematology*, pp. 96-103.

Burger, J.A. (2011b) 'Nurture versus Nature: The Microenvironment in Chronic Lymphocytic Leukemia', *American Society of Hematology*.

Burger, J.A. & Chiorazzi, N. (2013) 'B cell receptor signaling in chronic lymphocytic leukemia', *Trends in Immunology*, vol. 34, no. 12, pp. 592-601.

Burger, J.A., Ghia, P., Rosenwald, A. & Caligaris-Cappio, F. (2009a) 'The microenvironment in mature B-cell malignancies: a target for new treatment strategies', *Blood*, vol. 114, no. 16, pp. 3367-3375.

Burger, J.A., Quiroga, M.P., Hartmann, E., Burkle, A., Wierda, W.G., Keating, M.J. & Rosenwald, A. (2009b) 'High-level expression of the T-cell chemokines CCL3 and CCL4 by chronic lymphocytic leukemia B cells in nurselike cell cocultures and after BCR stimulation', *Blood*, vol. 113, no. 13, pp. 3050-3058.

Burger, J.A., Tsukada, N., Burger, M., Zvaifler, N.J., Dell'Aquila, M. & Kipps, T.J. (2000) 'Blood-derived nurse-like cells protect chronic lymphocytic leukemia B cells from spontaneous apoptosis through stromal cell–derived factor-1', *Blood*, vol. 96, no. 8, pp. 2655-2663.

Burger, J.A. & Wiestner, A. (2018) 'Targeting B cell receptor signalling in cancer: preclinical and clinical advances', *Nat Rev Cancer*, vol. 18, no. 3, pp. 148-167.

Burger, M., Hartmann, T., Krome, M., Rawluk, J., Tamamura, H., Fujii, N., Kipps, T.J. & Burger, J.A. (2005) 'Small peptide inhibitors of the CXCR4 chemokine receptor (CD184) antagonize the activation, migration, and antiapoptotic responses of CXCL12 in chronic lymphocytic leukemia B cells', *Blood*, vol. 106, no. 5, pp. 1824-1830.

Burgess, A., Vigneron, S., Brioudes, E., Labbe, J.C., Lorca, T. & Castro, A. (2010) 'Loss of human Greatwall results in G2 arrest and multiple mitotic defects due to deregulation of the cyclin B-Cdc2/PP2A balance', *Proc Natl Acad Sci U S A*, vol. 107, no. 28, pp. 12564-12569.

Burgess, M., Ellis, J.J., Mapp, S., Mollee, P., Mazzieri, R., Mattarollo, S.R., Gill, D. & Saunders, N.A. (2016) 'Transcriptomic analysis of monocytes and macrophages derived from CLL patients which display differing abilities to respond to therapeutic antibody immune complexes', *Genom Data*, vol. 7, pp. 4-6.

Bustin, S.A., Benes, V., Garson, J.A., Hellemans, J., Huggett, J., Kubista, M., Mueller, R., Nolan, T., Pfaffl, M.W., Shipley, G.L., Vandesompele, J. & Wittwer, C.T. (2009) 'The MIQE guidelines: minimum information for publication of quantitative real-time PCR experiments', *Clin Chem*, vol. 55, no. 4, pp. 611-622.

Caligaris-Cappio, F., Bertilaccio, M.T.S. & Scielzo, C. (2014) 'How the microenvironment wires the natural history of chronic lymphocytic leukemia', *Semin Cancer Biol*, vol. 24, pp. 43-48.

Cang, S., Iragavarapu, C., Savooji, J., Song, Y. & Liu, D. (2015) 'ABT-199 (venetoclax) and BCL-2 inhibitors in clinical development', *Journal of hematology & oncology*, vol. 8, pp. 129-129.

Caras, I., Tucureanu, C., Lerescu, L., Pitica, R., Melinceanu, L., Neagu, S. & Salageanu, A. (2011) 'Influence of tumor cell culture supernatants on macrophage functional polarization: in vitro models of macrophage-tumor environment interaction', *Tumori*, vol. 97, no. 5, pp. 647-654.

Chanan-Khan, A.A., Chitta, K., Ersing, N., Paulus, A., Masood, A., Sher, T., Swaika, A., Wallace, P.K., Mashtare, T.L., Jr., Wilding, G., Lee, K., Czuczman, M.S., Borrello, I. & Bangia, N. (2011) 'Biological effects and clinical significance of lenalidomide-induced tumour flare reaction in patients with chronic lymphocytic leukaemia: in vivo evidence of immune activation and antitumour response', *Br J Haematol*, vol. 155, no. 4, pp. 457-467.

Chang, M.Y., Huang, D.Y., Ho, F.M., Huang, K.C. & Lin, W.W. (2012) 'PKC-dependent human monocyte adhesion requires AMPK and Syk activation', *PLoS One*, vol. 7, no. 7, p. e40999.

Chanput, W., Mes, J.J., Savelkoul, H.F. & Wichers, H.J. (2013) 'Characterization of polarized THP-1 macrophages and polarizing ability of LPS and food compounds', *Food Funct*, vol. 4, no. 2, pp. 266-276.

Chanput, W., Mes, J.J. & Wichers, H.J. (2014) 'THP-1 cell line: an in vitro cell model for immune modulation approach', *Int Immunopharmacol*, vol. 23, no. 1, pp. 37-45.

Chanput, W., Peters, V. & Wichers, H. (2015) THP-1 and U937 Cells, in K. Verhoeckx, P. Cotter, I. López-Expósito, C. Kleiveland, T. Lea, A. Mackie, T. Requena, D. Swiatecka & H. Wichers (eds), *The Impact of Food Bioactives on Health: in vitro and ex vivo models*, Springer International Publishing, Cham, pp. 147-159.

Cheson, B.D., Bennett, J.M., Rai, K.R., Grever, M.R., Kay, N.E., Schiffer, C.A., Oken, M.M., Keating, M.J., Boldt, D.H., Kempin, S.J. & et al. (1988) 'Guidelines for clinical protocols for chronic lymphocytic leukemia: recommendations of the National Cancer Institute-sponsored working group', *Am J Hematol*, vol. 29, no. 3, pp. 152-163.

Chimal-Ramirez, G.K., Espinoza-Sanchez, N.A., Chavez-Sanchez, L., Arriaga-Pizano, L. & Fuentes-Panana, E.M. (2016) 'Monocyte Differentiation towards Protumor Activity Does Not Correlate with M1 or M2 Phenotypes', *J Immunol Res*, vol. 2016, p. 6031486.

Choi, M.Y., Kashyap, M.K. & Kumar, D. (2016) 'The chronic lymphocytic leukemia microenvironment: Beyond the B-cell receptor', *Best Pract Res Clin Haematol*, vol. 29, no. 1, pp. 40-53.

Chronic lymphocytic leukaemia (CLL) statistics [Online], Cancer Research UK, Available from: http://www.cancerresearchuk.org/health-professional/cancer-statistics/statistics-by-cancer-type/leukaemia-cll#heading-Zero (Accessed: January 2019).

Chun, E.M., Park, Y.J., Kang, H.S., Cho, H.M., Jun, D.Y. & Kim, Y.H. (2001) 'Expression of the apolipoprotein C-II gene during myelomonocytic differentiation of human leukemic cells', *J Leukoc Biol*, vol. 69, no. 4, pp. 645-650.

Clancy, B. & Cauller, L.J. (1998) 'Reduction of background autofluorescence in brain sections following immersion in sodium borohydride', *J Neurosci Methods*, vol. 83, no. 2, pp. 97-102.

Collins, R.J., Verschuer, L.A., Harmon, B.V., Prentice, R.L., Pope, J.H. & Kerr, J.F.R. (1989) 'Spontaneous programmed death (apoptosis) of B-chronic lymphocytic leukaemia cells following their culture in vitro', *British Journal of Haematology*, vol. 71, no. 3, pp. 343-350.

Cols, M., Barra, C.M., He, B., Puga, I., Xu, W., Chiu, A., Tam, W., Knowles, D.M., Dillon, S.R., Leonard, J.P., Furman, R.R., Chen, K. & Cerutti, A. (2012) 'Stromal Endothelial Cells Establish a Bidirectional Crosstalk with Chronic Lymphocytic Leukemia Cells through the TNF-Related Factors BAFF, APRIL, and CD40L', *The Journal of Immunology*, vol. 188, no. 12, pp. 6071-6083.

Coscia, M., Pantaleoni, F., Riganti, C., Vitale, C., Rigoni, M., Peola, S., Castella, B., Foglietta, M., Griggio, V., Drandi, D., Ladetto, M., Bosia, A., Boccadoro, M. & Massaia, M. (2011) 'IGHV unmutated CLL B cells are more prone to spontaneous apoptosis and subject to environmental prosurvival signals than mutated CLL B cells', *Leukemia*, vol. 25, no. 5, pp. 828-837.

Crombie, J. & Davids, M.S. (2017) 'IGHV mutational status testing in chronic lymphocytic leukemia', *American journal of hematology*, vol. 92, no. 12, pp. 1393-1397.

Dadashian, E.L., McAuley, E.M., Liu, D., Shaffer, A.L., Young, R.M., Iyer, J.R., Kruhlak, M.J., Staudt, L.M., Wiestner, A. & Herman, S.E.M. (2019) 'TLR Signaling Is Activated in Lymph Node–Resident CLL Cells and Is Only Partially Inhibited by Ibrutinib', *Cancer Research*, vol. 79, no. 2, pp. 360-371.

Daigneault, M., Preston, J.A., Marriott, H.M., Whyte, M.K. & Dockrell, D.H. (2010) 'The identification of markers of macrophage differentiation in PMA-stimulated THP-1 cells and monocyte-derived macrophages', *PLoS One*, vol. 5, no. 1, p. e8668.

Davis, A.S., Richter, A., Becker, S., Moyer, J.E., Sandouk, A., Skinner, J. & Taubenberger, J.K. (2014) 'Characterizing and Diminishing Autofluorescence in Formalin-fixed Paraffin-embedded Human Respiratory Tissue', *J Histochem Cytochem*, vol. 62, no. 6, pp. 405-423.

Demchenko, A.P. (2013) 'Beyond annexin V: fluorescence response of cellular membranes to apoptosis', *Cytotechnology*, vol. 65, no. 2, pp. 157-172.

Dennis, G., Jr., Sherman, B.T., Hosack, D.A., Yang, J., Gao, W., Lane, H.C. & Lempicki, R.A. (2003) 'DAVID: Database for Annotation, Visualization, and Integrated Discovery', *Genome Biology*, vol. 4, no. 9, pp. R60-R60.

Depince-Berger, A.E., Aanei, C., Iobagiu, C., Jeraiby, M. & Lambert, C. (2016) 'New tools in cytometry', *Morphologie*, vol. 100, no. 331, pp. 199-209.

Dieffenbach, C.W., Lowe, T.M. & Dveksler, G.S. (1993) 'General concepts for PCR primer design', *PCR Methods Appl*, vol. 3, no. 3, pp. S30-37.

Dielschneider, R.F., Eisenstat, H., Mi, S., Curtis, J.M., Xiao, W., Johnston, J.B. & Gibson, S.B. (2016) 'Lysosomotropic agents selectively target chronic lymphocytic leukemia cells due to altered sphingolipid metabolism', *Leukemia*, vol. 30, no. 6, pp. 1290-1300.

Ding, W., Knox, T.R., Tschumper, R.C., Wu, W., Schwager, S.M., Boysen, J.C., Jelinek, D.F. & Kay, N.E. (2010) 'Platelet-derived growth factor (PDGF)–PDGF receptor interaction activates bone marrow–derived mesenchymal stromal cells derived from chronic lymphocytic leukemia: implications for an angiogenic switch', *Blood*, vol. 116, no. 16, pp. 2984-2993.

Dubois, N., Crompot, E., Meuleman, N., Bron, D., Lagneaux, L. & Stamatopoulos, B. (2020) 'Importance of Crosstalk Between Chronic Lymphocytic Leukemia Cells and the Stromal Microenvironment: Direct Contact, Soluble Factors, and Extracellular Vesicles', *Frontiers in Oncology*, vol. 10, no. 1422.

Dürr, C., Hanna, B.S., Schulz, A., Lucas, F., Zucknick, M., Benner, A., Clear, A., Ohl, S., Öztürk, S., Zenz, T., Stilgenbauer, S., Li-Weber, M., Krammer, P.H., Gribben, J.G., Lichter, P. & Seiffert, M. (2018) 'Tumor necrosis factor receptor signaling is a driver of chronic lymphocytic leukemia that can be therapeutically targeted by the flavonoid wogonin', *Haematologica*, vol. 103, no. 4, pp. 688-697.

Edwards, D.K., Sweeney, D.T., Ho, H., Eide, C.A., Rofelty, A., Agarwal, A., Liu, S.Q., Danilov, A.V., Lee, P., Chantry, D., McWeeney, S.K., Druker, B.J., Tyner, J.W., Tyner1, W., Spurgeon, S.E. & Loriaux, M.M. (2018) 'Targeting of colony-stimulating factor 1 receptor (CSF1R) in the CLL microenvironment yields antineoplastic activity in primary patient samples', *Oncotarget*, vol. 9, no. 37, pp. 24576-24589.

Eisenberg, E. & Levanon, E.Y. (2013) 'Human housekeeping genes, revisited', *Trends Genet*, vol. 29, no. 10, pp. 569-574.

Elías, E.E., Almejún, M.B., Colado, A., Cordini, G., Vergara-Rubio, M., Podaza, E., Risnik, D., Cabrejo, M., Fernández-Grecco, H., Bezares, R.F., Custidiano, M.D.R., Sánchez-Ávalos, J.C., Vicente, Á., Garate, G.M., Borge, M., Giordano, M. & Gamberale, R. (2018) 'Autologous T-cell activation fosters ABT-199 resistance in chronic lymphocytic leukemia: rationale for a combined therapy with SYK inhibitors and anti-CD20 monoclonal antibodies', *Haematologica*, vol. 103, no. 10, pp. e458-e461.

Fabbri, G. & Dalla-Favera, R. (2016) 'The molecular pathogenesis of chronic lymphocytic leukaemia', *Nature Reviews Cancer*, vol. 16, no. 3, pp. 145-162.

Filip, A.A., Cisel, B., Koczkodaj, D., Wasik-Szczepanek, E., Piersiak, T. & Dmoszynska, A. (2013a) 'Circulating microenvironment of CLL: are nurse-like cells related to tumor-associated macrophages?', *Blood Cells Mol Dis*, vol. 50, no. 4, pp. 263-270.

Filip, A.A., Ciseł, B., Koczkodaj, D., Wąsik-Szczepanek, E., Piersiak, T. & Dmoszyńska, A. (2013b) 'Circulating microenvironment of CLL: Are nurse-like cells related to tumor-associated macrophages?', *Blood Cells, Molecules, and Diseases*, vol. 50, no. 4, pp. 263-270.

Filip, A.A., Cisel, B. & Wasik-Szczepanek, E. (2015) 'Guilty bystanders: nurse-like cells as a model of microenvironmental support for leukemic lymphocytes', *Clin Exp Med*, vol. 15, no. 1, pp. 73-83.

Filip, A.A., Koczkodaj, D., Kubiatowski, T., Wasik-Szczepanek, E. & Dmoszynska, A. (2009) 'The Outgrowth of CLL Nurselike Cells in Vitro, and Its Relation to Clinical and Hematological Parameters', *Blood*, vol. 114, no. 22, pp. 2360-2360.

Fiorcari, S., Hacken, E.t., Burger, J.A., Maffei, R., Zucchini, P., Deaglio, S., Audrito, V., Grisendi, G., Marasca, R., Martinelli, S., Potenza, L. & Luppi, M. (2016) 'Ibrutinib modifies the function of monocyte/macrophage population in chronic lymphocytic leukemia', *Oncotarget*, vol. 7, no. 40, pp. 65968-65981.

Fiorcari, S., Martinelli, S., Bulgarelli, J., Audrito, V., Zucchini, P., Colaci, E., Potenza, L., Narni, F., Luppi, M., Deaglio, S., Marasca, R. & Maffei, R. (2015) 'Lenalidomide interferes with tumor-promoting

properties of nurse-like cells in chronic lymphocytic leukemia', *Haematologica*, vol. 100, no. 2, pp. 253-262.
Fitzpatrick, M. (2014) *Measuring cell fluorescence using ImageJ* [Online], Available from: https://www.mfitzp.com/article/measuring-cell-fluorescence-using-imagej/ (Accessed: September 2019).
Forrester, M.A., Wassall, H.J., Hall, L.S., Cao, H., Wilson, H.M., Barker, R.N. & Vickers, M.A. (2018) 'Similarities and differences in surface receptor expression by THP-1 monocytes and differentiated macrophages polarized using seven different conditioning regimens', *Cell Immunol*, vol. 332, pp. 58-76.
Friedman, D.R., Sibley, A.B., Owzar, K., Chaffee, K.G., Slager, S., Kay, N.E., Hanson, C.A., Ding, W., Shanafelt, T.D., Weinberg, J.B. & Wilcox, R.A. (2016) 'Relationship of blood monocytes with chronic lymphocytic leukemia aggressiveness and outcomes: a multi-institutional study', *Am J Hematol*, vol. 91, no. 7, pp. 687-691.
Furstenau, M., De Silva, N., Eichhorst, B. & Hallek, M. (2019) 'Minimal Residual Disease Assessment in CLL: Ready for Use in Clinical Routine?', *Hemasphere*, vol. 3, no. 5, p. e287.
Gautam, S., Fatehchand, K., Elavazhagan, S., Reader, B.F., Ren, L., Mo, X., Byrd, J.C., Tridandapani, S. & Butchar, J.P. (2016) 'Reprogramming Nurse-like Cells with Interferon gamma to Interrupt Chronic Lymphocytic Leukemia Cell Survival', *J Biol Chem*, vol. 291, no. 27, pp. 14356-14362.
Gazdar, A.F., Gao, B. & Minna, J.D. (2010) 'Lung cancer cell lines: Useless artifacts or invaluable tools for medical science?', *Lung Cancer*, vol. 68, no. 3, pp. 309-318.
Geisberger, R., Lamers, M. & Achatz, G. (2006) 'The riddle of the dual expression of IgM and IgD', *Immunology*, vol. 118, no. 4, pp. 429-437.
Genin, M., Clement, F., Fattaccioli, A., Raes, M. & Michiels, C. (2015) 'M1 and M2 macrophages derived from THP-1 cells differentially modulate the response of cancer cells to etoposide', *BMC Cancer*, vol. 15, p. 577.
Ghamlouch, H., Ouled-Haddou, H., Guyart, A., Regnier, A., Trudel, S., Claisse, J.F., Fuentes, V., Royer, B., Marolleau, J.P. & Gubler, B. (2014) 'Phorbol myristate acetate, but not CD40L, induces the differentiation of CLL B cells into Ab-secreting cells', *Immunol Cell Biol*, vol. 92, no. 7, pp. 591-604.
Ghosh, A.K., Secreto, C.R., Knox, T.R., Ding, W., Mukhopadhyay, D. & Kay, N.E. (2010) 'Circulating microvesicles in B-cell chronic lymphocytic leukemia can stimulate marrow stromal cells: implications for disease progression', *Blood*, vol. 115, no. 9, pp. 1755-1764.
Giannoni, P., Pietra, G., Travaini, G., Quarto, R., Shyti, G., Benelli, R., Ottaggio, L., Mingari, M.C., Zupo, S., Cutrona, G., Pierri, I., Balleari, E., Pattarozzi, A., Calvaruso, M., Tripodo, C., Ferrarini, M. & de Totero, D. (2014) 'Chronic lymphocytic leukemia nurse-like cells express hepatocyte growth factor receptor (c-MET) and indoleamine 2,3-dioxygenase and display features of immunosuppressive type 2 skewed macrophages', *Haematologica*, vol. 99, no. 6, pp. 1078-1087.
GmbH, P. (2015) 'Differentiation of M1- or M2-Macrophages from PBMC/Monocytes'.
Goodspeed, A., Heiser, L.M., Gray, J.W. & Costello, J.C. (2016) 'Tumor-Derived Cell Lines as Molecular Models of Cancer Pharmacogenomics', *Molecular cancer research : MCR*, vol. 14, no. 1, pp. 3-13.
Gordon, S. (2003) 'Alternative activation of macrophages', *Nat Rev Immunol*, vol. 3, no. 1, pp. 23-35.
Gordon, S. & Martinez, F.O. (2010) 'Alternative activation of macrophages: mechanism and functions', *Immunity*, vol. 32, no. 5, pp. 593-604.
Gu, B., Kaneko, T., Zaw, S.Y.M., Sone, P.P., Murano, H., Sueyama, Y., Zaw, Z.C.T. & Okiji, T. (2019) 'Macrophage populations show an M1-to-M2 transition in an experimental model of coronal pulp tissue engineering with mesenchymal stem cells', *Int Endod J*, vol. 52, no. 4, pp. 504-514.
Guo, B., Zhang, L., Chiorazzi, N. & Rothstein, T.L. (2016) 'IL-4 rescues surface IgM expression in chronic lymphocytic leukemia', *Blood*, vol. 128, no. 4, pp. 553-562.

Haimes, J. & Kelley, M. 'Demonstration of a ΔΔCq Calculation Method to Compute Relative Gene Expression from qPCR Data'.
Hallek, M. (2015) 'Chronic lymphocytic leukemia: 2015 Update on diagnosis, risk stratification, and treatment', *Am J Hematol*, vol. 90, no. 5, pp. 446-460.
Hallek, M. (2017) 'Chronic lymphocytic leukemia: 2017 update on diagnosis, risk stratification, and treatment', *Am J Hematol*, vol. 92, no. 9, pp. 946-965.
Hamilton, E., Pearce, L., Morgan, L., Robinson, S., Ware, V., Brennan, P., Thomas, N.S.B., Yallop, D., Devereux, S., Fegan, C., Buggins, A.G.S. & Pepper, C. (2012) 'Mimicking the tumour microenvironment: three different co-culture systems induce a similar phenotype but distinct proliferative signals in primary chronic lymphocytic leukaemia cells', *British Journal of Haematology*, vol. 158, no. 5, pp. 589-599.
Hanna, B.S., McClanahan, F., Yazdanparast, H., Zaborsky, N., Kalter, V., Rossner, P.M., Benner, A., Durr, C., Egle, A., Gribben, J.G., Lichter, P. & Seiffert, M. (2015) 'Depletion of CLL-associated patrolling monocytes and macrophages controls disease development and repairs immune dysfunction in vivo', *Leukemia*.
Harrison, L.M., van den Hoogen, C., van Haaften, W.C.E. & Tesh, V.L. (2005) 'Chemokine expression in the monocytic cell line THP-1 in response to purified shiga toxin 1 and/or lipopolysaccharides', *Infection and immunity*, vol. 73, no. 1, pp. 403-412.
Hartmann, E.M., Rudelius, M., Burger, J.A. & Rosenwald, A. (2016) 'CCL3 chemokine expression by chronic lymphocytic leukemia cells orchestrates the composition of the microenvironment in lymph node infiltrates', *Leuk Lymphoma*, vol. 57, no. 3, pp. 563-571.
Henze, A.T. & Mazzone, M. (2016) 'The impact of hypoxia on tumor-associated macrophages', *J Clin Invest*, vol. 126, no. 10, pp. 3672-3679.
Herant, M. & Dembo, M. (2010) 'Form and function in cell motility: from fibroblasts to keratocytes', *Biophys J*, vol. 98, no. 8, pp. 1408-1417.
Herishanu, Y., Perez-Galan, P., Liu, D., Biancotto, A., Pittaluga, S., Vire, B., Gibellini, F., Njuguna, N., Lee, E., Stennett, L., Raghavachari, N., Liu, P., McCoy, J.P., Raffeld, M., Stetler-Stevenson, M., Yuan, C., Sherry, R., Arthur, D.C., Maric, I., White, T., Marti, G.E., Munson, P., Wilson, W.H. & Wiestner, A. (2011) 'The lymph node microenvironment promotes B-cell receptor signaling, NF-kappaB activation, and tumor proliferation in chronic lymphocytic leukemia', *Blood*, vol. 117, no. 2, pp. 563-574.
Herling, C.D., Abedpour, N., Weiss, J., Schmitt, A., Jachimowicz, R.D., Merkel, O., Cartolano, M., Oberbeck, S., Mayer, P., Berg, V., Thomalla, D., Kutsch, N., Stiefelhagen, M., Cramer, P., Wendtner, C.M., Persigehl, T., Saleh, A., Altmüller, J., Nürnberg, P., Pallasch, C., Achter, V., Lang, U., Eichhorst, B., Castiglione, R., Schäfer, S.C., Büttner, R., Kreuzer, K.A., Reinhardt, H.C., Hallek, M., Frenzel, L.P. & Peifer, M. (2018) 'Clonal dynamics towards the development of venetoclax resistance in chronic lymphocytic leukemia', *Nat Commun*, vol. 9, no. 1, p. 727.
Hoffbrand, A.V., Moss, P.A.H. & Pettit, J.E. (eds) (2006) *Essential Haematology*, 5th edn, Blackwell Publishing.
Honkala, A.T., Tailor, D. & Malhotra, S.V. (2020) 'Guanylate-Binding Protein 1: An Emerging Target in Inflammation and Cancer', *Frontiers in Immunology*, vol. 10, no. 3139.
Hrdlickova, R., Toloue, M. & Tian, B. (2017) 'RNA-Seq methods for transcriptome analysis', *Wiley Interdisciplinary Reviews: RNA*, vol. 8, no. 1.
Hume, D.A. & Freeman, T.C. (2014) 'Transcriptomic analysis of mononuclear phagocyte differentiation and activation', *Immunological Reviews*, vol. 262, no. 1, pp. 74-84.
Italiani, P. & Boraschi, D. (2014) 'From Monocytes to M1/M2 Macrophages: Phenotypical vs. Functional Differentiation', *Front Immunol*, vol. 5, p. 514.

Jablonski, K.A., Amici, S.A., Webb, L.M., Ruiz-Rosado Jde, D., Popovich, P.G., Partida-Sanchez, S. & Guerau-de-Arellano, M. (2015) 'Novel Markers to Delineate Murine M1 and M2 Macrophages', *PLoS One*, vol. 10, no. 12, p. e0145342.

Janowska-Wieczorek, A., Belch, A.R., Jacobs, A., Bowen, D., Padua, R.A., Paietta, E. & Stanley, E.R. (1991) 'Increased circulating colony-stimulating factor-1 in patients with preleukemia, leukemia, and lymphoid malignancies', *Blood*, vol. 77, no. 8, pp. 1796-1803.

Jia, L., Clear, A., Liu, F.-T., Matthews, J., Uddin, N., McCarthy, A., Hoxha, E., Durance, C., Iqbal, S. & Gribben, J.G. (2014) 'Extracellular HMGB1 promotes differentiation of nurse-like cells in chronic lymphocytic leukemia', *Blood*, vol. 123, no. 11, pp. 1709-1719.

Jitschin, R., Braun, M., Qorraj, M., Saul, D., Le Blanc, K., Zenz, T. & Mougiakakos, D. (2015) 'Stromal cell–mediated glycolytic switch in CLL cells involves Notch-c-Myc signaling', *Blood*, vol. 125, no. 22, pp. 3432-3436.

Kang, M.H. & Reynolds, C.P. (2009) 'Bcl-2 Inhibitors: Targeting Mitochondrial Apoptotic Pathways in Cancer Therapy', *Clinical Cancer Research*, vol. 15, no. 4, pp. 1126-1132.

Kaur, G. & Dufour, J.M. (2012) 'Cell lines: Valuable tools or useless artifacts', *Spermatogenesis*, vol. 2, no. 1, pp. 1-5.

Kelly, P.N. & Strasser, A. (2011) 'The role of Bcl-2 and its pro-survival relatives in tumourigenesis and cancer therapy', *Cell death and differentiation*, vol. 18, no. 9, pp. 1414-1424.

Kern, C., Cornuel, J.-F.o., Billard, C., Tang, R., Rouillard, D., Stenou, V., Defrance, T., Ajchenbaum-Cymbalista, F., Simonin, P.-Y., Feldblum, S. & Kolb, J.-P. (2004) 'Involvement of BAFF and APRIL in the resistance to apoptosis of B-CLL through an autocrine pathway', *Blood*, vol. 103, no. 2, pp. 679-688.

Kim, Y., Lin, Q., Glazer, P.M. & Yun, Z. (2009) 'Hypoxic Tumor Microenvironment and Cancer Cell Differentiation', *Current molecular medicine*, vol. 9, no. 4, pp. 425-434.

Kipps, T.J., Stevenson, F.K., Wu, C.J., Croce, C.M., Packham, G., Wierda, W.G., O'Brien, S., Gribben, J. & Rai, K. (2017) 'Chronic lymphocytic leukaemia', *Nat Rev Dis Primers*, vol. 3, p. 16096.

Kitada, S., Zapata, J.M., Andreff, M. & Reed, J.C. (1999) 'Bryostatin and CD40-ligand enhance apoptosis resistance and induce expression of cell survival genes in B-cell chronic lymphocytic leukaemia', *British Journal of Haematology*, vol. 106, no. 4, pp. 995-1004.

Koczula, K.M., Ludwig, C., Hayden, R., Cronin, L., Pratt, G., Parry, H., Tennant, D., Drayson, M., Bunce, C.M., Khanim, F.L. & Gunther, U.L. (2016) 'Metabolic plasticity in CLL: adaptation to the hypoxic niche', *Leukemia*, vol. 30, no. 1, pp. 65-73.

Kohro, T., Tanaka, T., Murakami, T., Wada, Y., Aburatani, H., Hamakubo, T. & Kodama, T. (2004) 'A comparison of differences in the gene expression profiles of phorbol 12-myristate 13-acetate differentiated THP-1 cells and human monocyte-derived macrophage', *J Atheroscler Thromb*, vol. 11, no. 2, pp. 88-97.

Kotiah, S.D. (2019) *Chronic Lymphocytic Leukemia (CLL) Staging* [Online], Available from: https://emedicine.medscape.com/article/2006578-overview#a1 (Accessed: September 2019).

Kramer, A., Green, J., Pollard, J., Jr. & Tugendreich, S. (2014) 'Causal analysis approaches in Ingenuity Pathway Analysis', *Bioinformatics*, vol. 30, no. 4, pp. 523-530.

Krzyszczyk, P., Schloss, R., Palmer, A. & Berthiaume, F. (2018) 'The Role of Macrophages in Acute and Chronic Wound Healing and Interventions to Promote Pro-wound Healing Phenotypes', *Front Physiol*, vol. 9, p. 419.

Kukurba, K.R. & Montgomery, S.B. (2015) 'RNA Sequencing and Analysis', *Cold Spring Harb Protoc*, vol. 2015, no. 11, pp. 951-969.

Kurtova, A.V., Balakrishnan, K., Chen, R., Ding, W., Schnabl, S., Quiroga, M.P., Sivina, M., Wierda, W.G., Estrov, Z., Keating, M.J., Shehata, M., Jäger, U., Gandhi, V., Kay, N.E., Plunkett, W. & Burger, J.A. (2009) 'Diverse marrow stromal cells protect CLL cells from spontaneous and drug-induced

apoptosis: development of a reliable and reproducible system to assess stromal cell adhesion-mediated drug resistance', *Blood*, vol. 114, no. 20, pp. 4441-4450.
La Flamme, A.C., Kharkrang, M., Stone, S., Mirmoeini, S., Chuluundorj, D. & Kyle, R. (2012) 'Type II-activated murine macrophages produce IL-4', *PLoS One*, vol. 7, no. 10, p. e46989.
Lafarge, S.T., Hou, S., Pauls, S.D., Johnston, J.B., Gibson, S.B. & Marshall, A.J. (2015) 'Differential expression and function of CD27 in chronic lymphocytic leukemia cells expressing ZAP-70', *Leukemia Research*, vol. 39, no. 7, pp. 773-778.
Lagneaux, L., Delforge, A., Bron, D., De Bruyn, C. & Stryckmans, P. (1998) 'Chronic Lymphocytic Leukemic B Cells But Not Normal B Cells Are Rescued From Apoptosis by Contact With Normal Bone Marrow Stromal Cells', *Blood*, vol. 91, no. 7, pp. 2387-2396.
Lee, B.N., Gao, H., Cohen, E.N., Badoux, X., Wierda, W.G., Estrov, Z., Faderl, S.H., Keating, M.J., Ferrajoli, A. & Reuben, J.M. (2011) 'Treatment with lenalidomide modulates T-cell immunophenotype and cytokine production in patients with chronic lymphocytic leukemia', *Cancer*, vol. 117, no. 17, pp. 3999-4008.
Li, J. & Tibshirani, R. (2013) 'Finding consistent patterns: a nonparametric approach for identifying differential expression in RNA-Seq data', *Statistical methods in medical research*, vol. 22, no. 5, pp. 519-536.
Li Jia, A.C., Feng-Ting Liu, Janet Matthews, Nadiha Uddin, Aine McCarthy, Elena Hoxha, Catherine Durance, Sameena Iqbal, and John G. Gribben (2014) 'Extracellular HMGB1 promotes differentiation of nurse-like cells in chronic lymphocytic leukemia', *Blood*, vol. 123, no. 11, pp. 1709-1719.
Lichtman, M.A., Kipps, T.J., Seligsohn, U., Kaushansky, K. & Prchal, J.T. (2011a) *Chapter 67. Morphology of Monocytes and Macrophages*, 8 edn, McGraw-Hill Companies, Inc.
Lichtman, M.A., Kipps, T.J., Seligsohn, U., Kaushansky, K. & Prchal, J.T. (2011b) *Williams Manual of Hematology*, 8 edn, McGraw-Hill Companies, Inc.
Livak, K.J. & Schmittgen, T.D. (2001) 'Analysis of relative gene expression data using real-time quantitative PCR and the 2(-Delta Delta C(T)) Method', *Methods*, vol. 25, no. 4, pp. 402-408.
Love, M.I., Huber, W. & Anders, S. (2014) 'Moderated estimation of fold change and dispersion for RNA-seq data with DESeq2', *Genome Biology*, vol. 15, no. 12, p. 550.
Lutzny, G., Kocher, T., Schmidt-Supprian, M., Rudelius, M., Klein-Hitpass, L., Finch, Andrew J., Dürig, J., Wagner, M., Haferlach, C., Kohlmann, A., Schnittger, S., Seifert, M., Wanninger, S., Zaborsky, N., Oostendorp, R., Ruland, J., Leitges, M., Kuhnt, T., Schäfer, Y., Lampl, B., Peschel, C., Egle, A. & Ringshausen, I. (2013) 'Protein Kinase C-β-Dependent Activation of NF-κB in Stromal Cells Is Indispensable for the Survival of Chronic Lymphocytic Leukemia B Cells In Vivo', *Cancer Cell*, vol. 23, no. 1, pp. 77-92.
Lyssiotis, C.A. & Kimmelman, A.C. (2017) 'Metabolic Interactions in the Tumor Microenvironment', *Trends Cell Biol*, vol. 27, no. 11, pp. 863-875.
Maeß, M.B., Wittig, B., Cignarella, A. & Lorkowski, S. (2014) 'Reduced PMA enhances the responsiveness of transfected THP-1 macrophages to polarizing stimuli', *Journal of Immunological Methods*, vol. 402, no. 1, pp. 76-81.
Maffei, R., Bulgarelli, J., Fiorcari, S., Bertoncelli, L., Martinelli, S., Guarnotta, C., Castelli, I., Deaglio, S., Debbia, G., De Biasi, S., Bonacorsi, G., Zucchini, P., Narni, F., Tripodo, C., Luppi, M., Cossarizza, A. & Marasca, R. (2013) 'The monocytic population in chronic lymphocytic leukemia shows altered composition and deregulation of genes involved in phagocytosis and inflammation', *Haematologica*, vol. 98, no. 7, pp. 1115-1123.
Maki, G., Hayes, G.M., Naji, A., Tyler, T., Carosella, E.D., Rouas-Freiss, N. & Gregory, S.A. (2008) 'NK resistance of tumor cells from multiple myeloma and chronic lymphocytic leukemia patients: implication of HLA-G', *Leukemia*, vol. 22, no. 5, pp. 998-1006.

Mangolini, M. & Ringshausen, I. (2020) 'Bone Marrow Stromal Cells Drive Key Hallmarks of B Cell Malignancies', *Int J Mol Sci*, vol. 21, no. 4.

Mansouri, L., Papakonstantinou, N., Ntoufa, S., Stamatopoulos, K. & Rosenquist, R. (2016) 'NF-kappaB activation in chronic lymphocytic leukemia: A point of convergence of external triggers and intrinsic lesions', *Semin Cancer Biol*, vol. 39, pp. 40-48.

Mantovani, A., Marchesi, F., Malesci, A., Laghi, L. & Allavena, P. (2017) 'Tumour-associated macrophages as treatment targets in oncology', *Nat Rev Clin Oncol*, vol. 14, no. 7, pp. 399-416.

Mantovani, A., Sica, A., Sozzani, S., Allavena, P., Vecchi, A. & Locati, M. (2004) 'The chemokine system in diverse forms of macrophage activation and polarization', *Trends Immunol*, vol. 25, no. 12, pp. 677-686.

Mantovani, A., Sozzani, S., Locati, M., Allavena, P. & Sica, A. (2002) 'Macrophage polarization: TAMs as a paradigm for polarized m2 mononuclear phagocytes', *TRENDS in Immunology*, vol. 23, no. 11, pp. 549-555.

Marchesi, F., Cirillo, M., Bianchi, A., Gately, M., Olimpieri, O.M., Cerchiara, E., Renzi, D., Micera, A., Balzamino, B.O., Bonini, S., Onetti Muda, A. & Avvisati, G. (2015) 'High density of CD68+/CD163+ tumour-associated macrophages (M2-TAM) at diagnosis is significantly correlated to unfavorable prognostic factors and to poor clinical outcomes in patients with diffuse large B-cell lymphoma', *Hematological Oncology*, vol. 33, no. 2, pp. 110-112.

Marquez, M.-E., Hernández-Uzcátegui, O., Cornejo, A., Vargas, P. & Da Costa, O. (2015) 'Bone marrow stromal mesenchymal cells induce down regulation of CD20 expression on B-CLL: implications for rituximab resistance in CLL', *British Journal of Haematology*, vol. 169, no. 2, pp. 211-218.

Martinez, F.O., Gordon, S., Locati, M. & Mantovani, A. (2006) 'Transcriptional Profiling of the Human Monocyte-to-Macrophage Differentiation and Polarization: New Molecules and Patterns of Gene Expression', *The Journal of Immunology*, vol. 177, no. 10, pp. 7303-7311.

Masters, J.R. (2002) 'HeLa cells 50 years on: the good, the bad and the ugly', *Nat Rev Cancer*, vol. 2, no. 4, pp. 315-319.

McClanahan, F., Riches, J.C., Miller, S., Day, W.P., Kotsiou, E., Neuberg, D., Croce, C.M., Capasso, M. & Gribben, J.G. (2015) 'Mechanisms of PD-L1/PD-1–mediated CD8 T-cell dysfunction in the context of aging-related immune defects in the Eμ-TCL1 CLL mouse model', *Blood*, vol. 126, no. 2, pp. 212-221.

McCloy, R.A., Rogers, S., Caldon, C.E., Lorca, T., Castro, A. & Burgess, A. (2014) 'Partial inhibition of Cdk1 in G2 phase overrides the SAC and decouples mitotic events', *Cell Cycle*, vol. 13, no. 9, pp. 1400-1412.

McWhorter, F.Y., Wang, T., Nguyen, P., Chung, T. & Liu, W.F. (2013) 'Modulation of macrophage phenotype by cell shape', *Proc Natl Acad Sci U S A*, vol. 110, no. 43, pp. 17253-17258.

Mendez, M.G., Kojima, S.-I. & Goldman, R.D. (2010) 'Vimentin induces changes in cell shape, motility, and adhesion during the epithelial to mesenchymal transition', *FASEB journal : official publication of the Federation of American Societies for Experimental Biology*, vol. 24, no. 6, pp. 1838-1851.

Mendoza-Coronel, E. & Castanon-Arreola, M. (2016) 'Comparative evaluation of in vitro human macrophage models for mycobacterial infection study', *Pathogens and Disease*, vol. 74, no. 6.

Mills, C.D. (2015) 'Anatomy of a Discovery: M1 and M2 Macrophages', *Frontiers in Immunology*, vol. 6, no. 212.

Minami, K., Hiwatashi, K., Ueno, S., Sakoda, M., Iino, S., Okumura, H., Hashiguchi, M., Kawasaki, Y., Kurahara, H., Mataki, Y., Maemura, K., Shinchi, H. & Natsugoe, S. (2018) 'Prognostic significance of CD68, CD163 and Folate receptor-beta positive macrophages in hepatocellular carcinoma', *Exp Ther Med*, vol. 15, no. 5, pp. 4465-4476.

Mir, M.A., Rasool, H.J., Liu, D. & Patel, S.C. (2019) *Chronic Lymphocytic Leukemia* [Online], Available from: http://emedicine.medscape.com/article/199313-overview (Accessed: September 2019).

Mockridge, C.I., Potter, K.N., Wheatley, I., Neville, L.A., Packham, G. & Stevenson, F.K. (2007) 'Reversible anergy of sIgM-mediated signaling in the two subsets of CLL defined by VH-gene mutational status', *Blood*, vol. 109, no. 10, pp. 4424-4431.

Molica, S., Matutes, E., Tam, C. & Polliack, A. (2020) 'Ibrutinib in the treatment of chronic lymphocytic leukemia: 5 years on', *Hematological Oncology*, vol. 38, no. 2, pp. 129-136.

Murray, P.J., Allen, J.E., Biswas, S.K., Fisher, E.A., Gilroy, D.W., Goerdt, S., Gordon, S., Hamilton, J.A., Ivashkiv, L.B., Lawrence, T., Locati, M., Mantovani, A., Martinez, F.O., Mege, J.L., Mosser, D.M., Natoli, G., Saeij, J.P., Schultze, J.L., Shirey, K.A., Sica, A., Suttles, J., Udalova, I., van Ginderachter, J.A., Vogel, S.N. & Wynn, T.A. (2014) 'Macrophage activation and polarization: nomenclature and experimental guidelines', *Immunity*, vol. 41, no. 1, pp. 14-20.

Muzio, M., Fonte, E. & Caligaris-Cappio, F. (2012) 'Toll-like Receptors in Chronic Lymphocytic Leukemia', *Mediterranean journal of hematology and infectious diseases*, vol. 4, no. 1, pp. e2012055-e2012055.

Nabhan, C., Raca, G. & Wang, Y.L. (2015) 'Predicting Prognosis in Chronic Lymphocytic Leukemia in the Contemporary Era', *JAMA Oncol*, vol. 1, no. 7, pp. 965-974.

Nagelkerke, S.Q., Bruggeman, C.W., den Haan, J.M.M., Mul, E.P.J., van den Berg, T.K., van Bruggen, R. & Kuijpers, T.W. (2018) 'Red pulp macrophages in the human spleen are a distinct cell population with a unique expression of Fc-gamma receptors', *Blood Adv*, vol. 2, no. 8, pp. 941-953.

Nakayama, T., Okada, N., Yoshikawa, M., Asaka, D., Kuboki, A., Kojima, H., Tanaka, Y. & Haruna, S.I. (2018) 'Assessment of suitable reference genes for RT-qPCR studies in chronic rhinosinusitis', *Sci Rep*, vol. 8, no. 1, p. 1568.

Nakayama, Y., Yamaguchi, H., Einaga, N. & Esumi, M. (2016) 'Pitfalls of DNA Quantification Using DNA-Binding Fluorescent Dyes and Suggested Solutions', *PloS one*, vol. 11, no. 3, pp. e0150528-e0150528.

NCBI - Genome Reference Consortium Human Build 38 [Online], Available from: https://www.ncbi.nlm.nih.gov/assembly/GCF_000001405.26/ (Accessed: April 2020).

Neu, C., Sedlag, A., Bayer, C., Förster, S., Crauwels, P., Niess, J.-H., van Zandbergen, G., Frascaroli, G. & Riedel, C.U. (2013) 'CD14-Dependent Monocyte Isolation Enhances Phagocytosis of Listeria monocytogenes by Proinflammatory, GM-CSF-Derived Macrophages', *PLOS ONE*, vol. 8, no. 6, p. e66898.

Nguyen, T., Bhatti, A., Yang, S. & Nahavandi, S. (2016) 'RNA-Seq Count Data Modelling by Grey Relational Analysis and Nonparametric Gaussian Process', *PLOS ONE*, vol. 11, no. 10, p. e0164766.

Niemann, C.U., Herman, S.E., Maric, I., Gomez-Rodriguez, J., Biancotto, A., Chang, B.Y., Martyr, S., Stetler-Stevenson, M., Yuan, C.M., Calvo, K.R., Braylan, R.C., Valdez, J., Lee, Y.S., Wong, D.H., Jones, J., Sun, C., Marti, G.E., Farooqui, M.Z. & Wiestner, A. (2016) 'Disruption of in vivo Chronic Lymphocytic Leukemia Tumor-Microenvironment Interactions by Ibrutinib - Findings from an Investigator-Initiated Phase II Study', *Clin Cancer Res*, vol. 22, no. 7, pp. 1572-1582.

Nishio, M., Endo, T., Tsukada, N., Ohata, J., Kitada, S., Reed, J.C., Zvaifler, N.J. & Kipps, T.J. (2005) 'Nurselike cells express BAFF and APRIL, which can promote survival of chronic lymphocytic leukemia cells via a paracrine pathway distinct from that of SDF-1alpha', *Blood*, vol. 106, no. 3, pp. 1012-1020.

Nobuhiro Tsukada, J.A.B., Nathan J. Zvaifler, and Thomas J. Kipps (2002) 'Distinctive features of “nurselike” cells that differentiate in the context of chronic lymphocytic leukemia', *Blood*, vol. 99, no. 3, pp. 1030-1037.

Ozsolak, F. & Milos, P.M. (2011) 'RNA sequencing: advances, challenges and opportunities', *Nat Rev Genet*, vol. 12, no. 2, pp. 87-98.

Packham, G. & Stevenson, F. (2010) 'The role of the B-cell receptor in the pathogenesis of chronic lymphocytic leukaemia', *Semin Cancer Biol*, vol. 20, no. 6, pp. 391-399.
Parameswaran, N. & Patial, S. (2010) 'Tumor necrosis factor-α signaling in macrophages', *Crit Rev Eukaryot Gene Expr*, vol. 20, no. 2, pp. 87-103.
Park, E.K., Jung, H.S., Yang, H.I., Yoo, M.C., Kim, C. & Kim, K.S. (2007) 'Optimized THP-1 differentiation is required for the detection of responses to weak stimuli', *Inflamm Res*, vol. 56, no. 1, pp. 45-50.
Pedersen, I.M., Kitada, S., Leoni, L.M., Zapata, J.M., Karras, J.G., Tsukada, N., Kipps, T.J., Choi, Y.S., Bennett, F. & Reed, J.C. (2002) 'Protection of CLL B cells by a follicular dendritic cell line is dependent on induction of Mcl-1', *Blood*, vol. 100, no. 5, pp. 1795-1801.
Pekarsky, Y., Balatti, V. & Croce, C.M. (2018) 'BCL2 and miR-15/16: from gene discovery to treatment', *Cell Death & Differentiation*, vol. 25, no. 1, pp. 21-26.
Pepper, C., Lin, T.T., Pratt, G., Hewamana, S., Brennan, P., Hiller, L., Hills, R., Ward, R., Starczynski, J., Austen, B., Hooper, L., Stankovic, T. & Fegan, C. (2008) 'Mcl-1 expression has in vitro and in vivo significance in chronic lymphocytic leukemia and is associated with other poor prognostic markers', *Blood*, vol. 112, no. 9, pp. 3807-3817.
Petrova, V., Annicchiarico-Petruzzelli, M., Melino, G. & Amelio, I. (2018) 'The hypoxic tumour microenvironment', *Oncogenesis*, vol. 7, no. 1, p. 10.
Petty, A.J. & Yang, Y. (2019) 'Tumor-Associated Macrophages in Hematologic Malignancies: New Insights and Targeted Therapies', *Cells*, vol. 8, no. 12.
Polk, A., Lu, Y., Wang, T., Seymour, E., Bailey, N.G., Singer, J.W., Boonstra, P.S., Lim, M.S., Malek, S. & Wilcox, R.A. (2016) 'Colony-Stimulating Factor-1 Receptor Is Required for Nurse-like Cell Survival in Chronic Lymphocytic Leukemia', *Clin Cancer Res*, vol. 22, no. 24, pp. 6118-6128.
Pollard, J.W. (2004) 'Tumour-educated macrophages promote tumour progression and metastasis', *Nature Reviews Cancer*, vol. 4, no. 1, pp. 71-78.
Ponader, S., Chen, S.S., Buggy, J.J., Balakrishnan, K., Gandhi, V., Wierda, W.G., Keating, M.J., O'Brien, S., Chiorazzi, N. & Burger, J.A. (2012) 'The Bruton tyrosine kinase inhibitor PCI-32765 thwarts chronic lymphocytic leukemia cell survival and tissue homing in vitro and in vivo', *Blood*, vol. 119, no. 5, pp. 1182-1189.
Pontén, F., Jirström, K. & Uhlen, M. (2008) *The Human Protein Atlas—a tool for pathology* [Online], Available from: http://www.proteinatlas.org (Accessed: January 2020).
Provan, D., Baglin, T.P., Dokal, I. & Vos, J.d. (2015) *Oxford handbook of clinical haematology*, Fourth edition. edn, Oxford University Press, Oxford.
Qin, Z. (2012) 'The use of THP-1 cells as a model for mimicking the function and regulation of monocytes and macrophages in the vasculature', *Atherosclerosis*, vol. 221, no. 1, pp. 2-11.
'Quantification of Fluorescence Intensity of Labeled Human Mesenchymal Stem Cells and Cell Counting of Unlabeled Cells in Phase-Contrast Imaging: An Open-Source-Based Algorithm' (2010), *Tissue Engineering Part C: Methods*, vol. 16, no. 6, pp. 1277-1285.
Quintas-Cardama, A., Kantarjian, H.M. & Cortes, J.E. (2009) 'Mechanisms of primary and secondary resistance to imatinib in chronic myeloid leukemia', *Cancer Control*, vol. 16, no. 2, pp. 122-131.
Rai, K., Sawitsky, A., Cronkite, E., Chanana, A., Levy, R. & Pasternack, B. (1975) 'Clinical staging of chronic lymphocytic leukemia', *Blood*, vol. 46, no. 2, pp. 219-234.
Ramprasad, M.P., Terpstra, V., Kondratenko, N., Quehenberger, O. & Steinberg, D. (1996) 'Cell surface expression of mouse macrosialin and human CD68 and their role as macrophage receptors for oxidized low density lipoprotein', *Proceedings of the National Academy of Sciences*, vol. 93, no. 25, pp. 14833-14838.
Ramsay, A.G., Clear, A.J., Fatah, R. & Gribben, J.G. (2012) 'Multiple inhibitory ligands induce impaired T-cell immunologic synapse function in chronic lymphocytic leukemia that can be blocked with

lenalidomide: establishing a reversible immune evasion mechanism in human cancer', *Blood*, vol. 120, no. 7, pp. 1412-1421.

Ramsay, A.G., Johnson, A.J., Lee, A.M., Gorgün, G., Dieu, R.L., Blum, W., Byrd, J.C. & Gribben, J.G. (2008) 'Chronic lymphocytic leukemia T cells show impaired immunological synapse formation that can be reversed with an immunomodulating drug', *Journal of Clinical Investigation*, vol. 118, no. 7, pp. 2427-2437.

Rane, A.S., Rutkauskaite, J., deMello, A. & Stavrakis, S. (2017) 'High-Throughput Multi-parametric Imaging Flow Cytometry', *Chem*, vol. 3, no. 4, pp. 588-602.

Rassenti, L.Z., Jain, S., Keating, M.J., Wierda, W.G., Grever, M.R., Byrd, J.C., Kay, N.E., Brown, J.R., Gribben, J.G., Neuberg, D.S., He, F., Greaves, A.W., Rai, K.R. & Kipps, T.J. (2008) 'Relative value of ZAP-70, CD38, and immunoglobulin mutation status in predicting aggressive disease in chronic lymphocytic leukemia', *Blood*, vol. 112, no. 5, pp. 1923-1930.

Resta, R., Yamashita, Y. & Thompson, L.F. (1998) 'Ecto-enzyme and signaling functions of lymphocyte CD73', *Immunol Rev*, vol. 161, pp. 95-109.

Rickert, R.C. (2013) 'New insights into pre-BCR and BCR signalling with relevance to B cell malignancies', *Nat Rev Immunol*, vol. 13, no. 8, pp. 578-591.

Riddy, D.M., Goy, E., Delerive, P., Summers, R.J., Sexton, P.M. & Langmead, C.J. (2018) 'Comparative genotypic and phenotypic analysis of human peripheral blood monocytes and surrogate monocyte-like cell lines commonly used in metabolic disease research', *PLoS One*, vol. 13, no. 5, p. e0197177.

Ridnour, L.A., Cheng, R.Y., Switzer, C.H., Heinecke, J.L., Ambs, S., Glynn, S., Young, H.A., Trinchieri, G. & Wink, D.A. (2013) 'Molecular pathways: toll-like receptors in the tumor microenvironment--poor prognosis or new therapeutic opportunity', *Clin Cancer Res*, vol. 19, no. 6, pp. 1340-1346.

Rieger, A.M., Nelson, K.L., Konowalchuk, J.D. & Barreda, D.R. (2011) 'Modified annexin V/propidium iodide apoptosis assay for accurate assessment of cell death', *J Vis Exp*, no. 50.

Roberts, A.W., Davids, M.S., Pagel, J.M., Kahl, B.S., Puvvada, S.D., Gerecitano, J.F., Kipps, T.J., Anderson, M.A., Brown, J.R., Gressick, L., Wong, S., Dunbar, M., Zhu, M., Desai, M.B., Cerri, E., Heitner Enschede, S., Humerickhouse, R.A., Wierda, W.G. & Seymour, J.F. (2016) 'Targeting BCL2 with Venetoclax in Relapsed Chronic Lymphocytic Leukemia', *N Engl J Med*, vol. 374, no. 4, pp. 311-322.

Rosenwald , A., Alizadeh , A.A., Widhopf , G., Simon , R., Davis , R.E., Yu , X., Yang , L., Pickeral , O.K., Rassenti , L.Z., Powell , J., Botstein , D., Byrd , J.C., Grever , M.R., Cheson , B.D., Chiorazzi , N., Wilson , W.H., Kipps , T.J., Brown , P.O. & Staudt , L.M. (2001) 'Relation of Gene Expression Phenotype to Immunoglobulin Mutation Genotype in B Cell Chronic Lymphocytic Leukemia', *The Journal of Experimental Medicine*, vol. 194, no. 11, pp. 1639-1648.

Roszer, T. (2015) 'Understanding the Mysterious M2 Macrophage through Activation Markers and Effector Mechanisms', *Mediators Inflamm*, vol. 2015, p. 816460.

Rots, N.Y., Iavarone, A., Bromleigh, V. & Freedman, L.P. (1999) 'Induced differentiation of U937 cells by 1,25-dihydroxyvitamin D3 involves cell cycle arrest in G1 that is preceded by a transient proliferative burst and an increase in cyclin expression', *Blood*, vol. 93, no. 8, pp. 2721-2729.

Sanderson, M.J., Smith, I., Parker, I. & Bootman, M.D. (2014) 'Fluorescence microscopy', *Cold Spring Harb Protoc*, vol. 2014, no. 10, p. pdb top071795.

Schroeder, A., Mueller, O., Stocker, S., Salowsky, R., Leiber, M., Gassmann, M., Lightfoot, S., Menzel, W., Granzow, M. & Ragg, T. (2006) 'The RIN: an RNA integrity number for assigning integrity values to RNA measurements', *BMC Molecular Biology*, vol. 7, no. 1, p. 3.

Schulz, A., Durr, C., Zenz, T., Dohner, H., Stilgenbauer, S., Lichter, P. & Seiffert, M. (2013) 'Lenalidomide reduces survival of chronic lymphocytic leukemia cells in primary cocultures by altering the myeloid microenvironment', *Blood*, vol. 121, no. 13, pp. 2503-2511.

Schwende, H., Fitzke, E., Ambs, P. & Dieter, P. (1996) 'Differences in the state of differentiation of THP-1 cells induced by phorbol ester and 1,25-dihydroxyvitamin D3', *Journal of Leukocyte Biology*, vol. 59, pp. 555-561.

Serra, S., Vaisitti, T., Audrito, V., Bologna, C., Buonincontri, R., Chen, S.-S., Arruga, F., Brusa, D., Coscia, M., Jaksic, O., Inghirami, G., Rossi, D., Furman, R.R., Robson, S.C., Gaidano, G., Chiorazzi, N. & Deaglio, S. (2016) 'Adenosine signaling mediates hypoxic responses in the chronic lymphocytic leukemia microenvironment', *Blood Advances*, vol. 1, no. 1, pp. 47-61.

Severin, F., Frezzato, F., Visentin, A., Martini, V., Trimarco, V., Carraro, S., Tibaldi, E., Brunati, A.M., Piazza, F., Semenzato, G., Facco, M. & Trentin, L. (2019) 'In Chronic Lymphocytic Leukemia the JAK2/STAT3 Pathway Is Constitutively Activated and Its Inhibition Leads to CLL Cell Death Unaffected by the Protective Bone Marrow Microenvironment', *Cancers*, vol. 11, no. 12, p. 1939.

Shachar, I., Cohen, S., Marom, A. & Becker-Herman, S. (2012) 'Regulation of CLL survival by hypoxia-inducible factor and its target genes', *FEBS Letters*, vol. 586, no. 18, pp. 2906-2910.

Shevde, L.A. & Samant, R.S. (2014) 'Role of osteopontin in the pathophysiology of cancer', *Matrix Biology*, vol. 37, pp. 131-141.

Shukla, A. (2013) 'Stromal Tumor Microenvironment in Chronic Lymphocytic Leukemia: Regulation of Leukemic Progression', *Journal of Leukemia*, vol. 01, no. 02.

Shukla, A., Shukla, V. & Joshi, S.S. (2018) 'Regulation of MAPK signaling and implications in chronic lymphocytic leukemia', *Leukemia & Lymphoma*, vol. 59, no. 7, pp. 1565-1573.

Sica, A., Larghi, P., Mancino, A., Rubino, L., Porta, C., Totaro, M.G., Rimoldi, M., Biswas, S.K., Allavena, P. & Mantovani, A. (2008) 'Macrophage polarization in tumour progression', *Semin Cancer Biol*, vol. 18, no. 5, pp. 349-355.

Simbolo, M., Gottardi, M., Corbo, V., Fassan, M., Mafficini, A., Malpeli, G., Lawlor, R.T. & Scarpa, A. (2013) 'DNA Qualification Workflow for Next Generation Sequencing of Histopathological Samples', *PLOS ONE*, vol. 8, no. 6, p. e62692.

Sivina, M., Hartmann, E., Kipps, T.J., Rassenti, L., Krupnik, D., Lerner, S., LaPushin, R., Xiao, L., Huang, X., LillianWerner, Neuberg, D., Kantarjian, H., O'Brien, S., Wierda, W.G., Keating, M.J., Rosenwald, A. & Burger, J.A. (2011) 'CCL3 (MIP-1✓) plasma levels and the risk for disease progression in chronic lymphocytic leukemia', *Blood*, vol. 117, no. 5, pp. 1662-1669.

Sleeboom, J.J.F., Eslami Amirabadi, H., Nair, P., Sahlgren, C.M. & den Toonder, J.M.J. (2018) 'Metastasis in context: modeling the tumor microenvironment with cancer-on-a-chip approaches', *Disease Models & Mechanisms*, vol. 11, no. 3, p. dmm033100.

Solinas, G., Germano, G., Mantovani, A. & Allavena, P. (2009) 'Tumor-associated macrophages (TAM) as major players of the cancer-related inflammation', *J Leukoc Biol*, vol. 86, no. 5, pp. 1065-1073.

Souers, A.J., Leverson, J.D., Boghaert, E.R., Ackler, S.L., Catron, N.D., Chen, J., Dayton, B.D., Ding, H., Enschede, S.H., Fairbrother, W.J., Huang, D.C., Hymowitz, S.G., Jin, S., Khaw, S.L., Kovar, P.J., Lam, L.T., Lee, J., Maecker, H.L., Marsh, K.C., Mason, K.D., Mitten, M.J., Nimmer, P.M., Oleksijew, A., Park, C.H., Park, C.M., Phillips, D.C., Roberts, A.W., Sampath, D., Seymour, J.F., Smith, M.L., Sullivan, G.M., Tahir, S.K., Tse, C., Wendt, M.D., Xiao, Y., Xue, J.C., Zhang, H., Humerickhouse, R.A., Rosenberg, S.H. & Elmore, S.W. (2013) 'ABT-199, a potent and selective BCL-2 inhibitor, achieves antitumor activity while sparing platelets', *Nat Med*, vol. 19, no. 2, pp. 202-208.

Spaner, D.E. & Masellis, A. (2007) 'Toll-like receptor agonists in the treatment of chronic lymphocytic leukemia', *Leukemia*, vol. 21, no. 1, pp. 53-60.

Spano, A., Barni, S. & Sciola, L. (2013) 'PMA withdrawal in PMA-treated monocytic THP-1 cells and subsequent retinoic acid stimulation, modulate induction of apoptosis and appearance of dendritic cells', *Cell Proliferation*, vol. 46, no. 3, pp. 328-347.

Spencer, M., Yao-Borengasser, A., Unal, R., Rasouli, N., Gurley, C.M., Zhu, B., Peterson, C.A. & Kern, P.A. (2010) 'Adipose tissue macrophages in insulin-resistant subjects are associated with collagen VI

and fibrosis and demonstrate alternative activation', *American Journal of Physiology-Endocrinology and Metabolism*, vol. 299, no. 6, pp. E1016-E1027.
Stamatopoulos, B., Meuleman, N., De Bruyn, C., Pieters, K., Mineur, P., Le Roy, C., Saint-Georges, S., Varin-Blank, N., Cymbalista, F., Bron, D. & Lagneaux, L. (2012) 'AMD3100 disrupts the cross-talk between chronic lymphocytic leukemia cells and a mesenchymal stromal or nurse-like cell-based microenvironment: pre-clinical evidence for its association with chronic lymphocytic leukemia treatments', *Haematologica*, vol. 97, no. 4, pp. 608-615.
Stelzer G, Rosen R, Plaschkes I, Zimmerman S, Twik M, Fishilevich S, Iny Stein T, Nudel R, Lieder I, Mazor Y, Kaplan S, Dahary D, Warshawsky D, Guan - Golan Y, Kohn A, Rappaport N, M, S. & D, L. (2016) *GeneCards – the human gene database* [Online], Available from: www.genecards.org (Accessed: January 2020).
Stevenson, F.K., Krysov, S., Davies, A.J., Steele, A.J. & Packham, G. (2011) 'B-cell receptor signaling in chronic lymphocytic leukemia', *Blood*, vol. 118, no. 16, pp. 4313-4320.
Strefford, J.C., Foot, N.J., Chaplin, T., Neat, M.J., Oliver, R.T., Young, B.D. & Jones, L.K. (2001) 'The characterisation of the lymphoma cell line U937, using comparative genomic hybridisation and multi-plex FISH', *Cytogenet Cell Genet*, vol. 94, no. 1-2, pp. 9-14.
Supek, F., Bosnjak, M., Skunca, N. & Smuc, T. (2011) 'REVIGO summarizes and visualizes long lists of gene ontology terms', *PLoS One*, vol. 6, no. 7, p. e21800.
Takashiba, S., Van Dyke, T.E., Amar, S., Murayama, Y., Soskolne, A.W. & Shapira, L. (1999) 'Differentiation of monocytes to macrophages primes cells for lipopolysaccharide stimulation via accumulation of cytoplasmic nuclear factor kappaB', *Infect Immun*, vol. 67, no. 11, pp. 5573-5578.
Tan, H.Y., Wang, N., Li, S., Hong, M., Wang, X. & Feng, Y. (2016) 'The Reactive Oxygen Species in Macrophage Polarization: Reflecting Its Dual Role in Progression and Treatment of Human Diseases', *Oxid Med Cell Longev*, vol. 2016, p. 2795090.
Tavolaro, S., Peragine, N., Chiaretti, S., Ricciardi, M.R., Raponi, S., Messina, M., Santangelo, S., Marinelli, M., Di Maio, V., Mauro, F.R., Del Giudice, I., Foa, R. & Guarini, A. (2013) 'IgD cross-linking induces gene expression profiling changes and enhances apoptosis in chronic lymphocytic leukemia cells', *Leuk Res*, vol. 37, no. 4, pp. 455-462.
Tedesco, S., De Majo, F., Kim, J., Trenti, A., Trevisi, L., Fadini, G.P., Bolego, C., Zandstra, P.W., Cignarella, A. & Vitiello, L. (2018) 'Convenience versus Biological Significance: Are PMA-Differentiated THP-1 Cells a Reliable Substitute for Blood-Derived Macrophages When Studying in Vitro Polarization?', *Frontiers in Pharmacology*, vol. 9, no. 71.
Ten Hacken, E. & Burger, J.A. (2015) 'Microenvironment interactions and B-cell receptor signaling in Chronic Lymphocytic Leukemia: Implications for disease pathogenesis and treatment', *Biochim Biophys Acta*, vol. 1863, no. 3, pp. 401-413.
Ten Hacken, E. & Burger, J.A. (2016) 'Microenvironment interactions and B-cell receptor signaling in Chronic Lymphocytic Leukemia: Implications for disease pathogenesis and treatment', *Biochim Biophys Acta*, vol. 1863, no. 3, pp. 401-413.
Ten Hacken, E., Sivina, M., Kim, E., O'Brien, S., Wierda, W.G., Ferrajoli, A., Estrov, Z., Keating, M.J., Oellerich, T., Scielzo, C., Ghia, P., Caligaris-Cappio, F. & Burger, J.A. (2016) 'Functional Differences between IgM and IgD Signaling in Chronic Lymphocytic Leukemia', *J Immunol*, vol. 197, no. 6, pp. 2522-2531.
Thijssen, R., Slinger, E., Weller, K., Geest, C.R., Beaumont, T., van Oers, M.H., Kater, A.P. & Eldering, E. (2015) 'Resistance to ABT-199 induced by microenvironmental signals in chronic lymphocytic leukemia can be counteracted by CD20 antibodies or kinase inhibitors', *Haematologica*, vol. 100, no. 8, pp. e302-306.

Till, K.J., Pettitt, A.R. & Slupsky, J.R. (2015) 'Expression of functional sphingosine-1 phosphate receptor-1 is reduced by B cell receptor signaling and increased by inhibition of PI3 kinase δ but not SYK or BTK in chronic lymphocytic leukemia cells', *Journal of immunology (Baltimore, Md. : 1950)*, vol. 194, no. 5, pp. 2439-2446.

Tsai, C.-S., Lin, Y.-W., Huang, C.-Y., Shih, C.-M., Tsai, Y.-T., Tsao, N.-W., Lin, C.-S., Shih, C.-C., Jeng, H. & Lin, F.-Y. (2016) 'Thrombomodulin regulates monocye differentiation via PKCδ and ERK1/2 pathway in vitro and in atherosclerotic artery', *Scientific Reports*, vol. 6, no. 1, p. 38421.

Tsuchiya, S., Yamabe, M., Yamaguchi, Y., Kobayashi, Y., Konno, T. & Tada, K. (1980) 'Establishment and characterization of a human acute monocytic leukemia cell line (THP-1)', *International Journal of Cancer*, vol. 26, no. 2, pp. 171-176.

Tsukada, N., Burger, J.A., Zvaifler, N.J. & Kipps, T.J. (2002) 'Distinctive features of “nurselike” cells that differentiate in the context of chronic lymphocytic leukemia', *Blood*, vol. 99, pp. 1030-1037.

Turgut, B., Vural, O., Pala, F.S., Pamuk, G.E., Tabakcioglu, K., Demir, M., Ongoren, S., Soysal, T. & Algunes, C. (2007) '17p Deletion is associated with resistance of B-cell chronic lymphocytic leukemia cells to in vitro fludarabine-induced apoptosis', *Leuk Lymphoma*, vol. 48, no. 2, pp. 311-320.

Valsecchi, R., Coltella, N., Belloni, D., Ponente, M., Ten Hacken, E., Scielzo, C., Scarfò, L., Bertilaccio, M.T.S., Brambilla, P., Lenti, E., Martinelli Boneschi, F., Brendolan, A., Ferrero, E., Ferrarini, M., Ghia, P., Tonon, G., Ponzoni, M., Caligaris-Cappio, F. & Bernardi, R. (2016) 'HIF-1α regulates the interaction of chronic lymphocytic leukemia cells with the tumor microenvironment', *Blood*, vol. 127, no. 16, pp. 1987-1997.

van Kooten, C. & Banchereau, J. (2000) 'CD40-CD40 ligand', *Journal of Leukocyte Biology*, vol. 67, no. 1, pp. 2-17.

Vander Heiden, M.G., Cantley, L.C. & Thompson, C.B. (2009) 'Understanding the Warburg Effect: The Metabolic Requirements of Cell Proliferation', *Science (New York, N.Y.)*, vol. 324, no. 5930, pp. 1029-1033.

Vogler, M., Butterworth, M., Majid, A., Walewska, R.J., Sun, X.M., Dyer, M.J. & Cohen, G.M. (2009) 'Concurrent up-regulation of BCL-XL and BCL2A1 induces approximately 1000-fold resistance to ABT-737 in chronic lymphocytic leukemia', *Blood*, vol. 113, no. 18, pp. 4403-4413.

Wang, Z., Gerstein, M. & Snyder, M. (2009) 'RNA-Seq: a revolutionary tool for transcriptomics', *Nature Reviews Genetics*, vol. 10, p. 57.

Waters, J.C. (2009) 'Accuracy and precision in quantitative fluorescence microscopy', *The Journal of cell biology*, vol. 185, no. 7, pp. 1135-1148.

Witz, I.P. (2009) 'The Tumor Microenvironment: The Making of a Paradigm', *Cancer Microenvironment*, vol. 2, no. 1, pp. 9-17.

Wolf, J.B.W. (2013) 'Principles of transcriptome analysis and gene expression quantification: an RNA-seq tutorial', *Molecular Ecology Resources*, vol. 13, no. 4, pp. 559-572.

Woyach, J.A. & Johnson, A.J. (2015) 'Targeted therapies in CLL: mechanisms of resistance and strategies for management', *Blood*, vol. 126, no. 4, pp. 471-477.

Wu, D. & Yotnda, P. (2011) 'Induction and Testing of Hypoxia in Cell Culture', *Journal of Visualized Experiments : JoVE*, no. 54, p. 2899.

Wu, M. & Swartz, M.A. (2014) 'Modeling tumor microenvironments in vitro', *Journal of biomechanical engineering*, vol. 136, no. 2, pp. 021011-021011.

Yang, X., Yu, D.D., Yan, F., Jing, Y.Y., Han, Z.P., Sun, K., Liang, L., Hou, J. & Wei, L.X. (2015) 'The role of autophagy induced by tumor microenvironment in different cells and stages of cancer', *Cell Biosci*, vol. 5, p. 14.

Ye, J., Coulouris, G., Zaretskaya, I., Cutcutache, I., Rozen, S. & Madden, T.L. (2012) 'Primer-BLAST: a tool to design target-specific primers for polymerase chain reaction', *BMC bioinformatics*, vol. 13, pp. 134-134.

Yosifov, D.Y., Idler, I., Bhattacharya, N., Reichenzeller, M., Close, V., Ezerina, D., Scheffold, A., Jebaraj, B.M.C., Kugler, S., Bloehdorn, J., Bahlo, J., Robrecht, S., Eichhorst, B., Fischer, K., Weigel, A., Busch, H., Lichter, P., Dohner, H., Dick, T.P., Stilgenbauer, S. & Mertens, D. (2020) 'Oxidative stress as candidate therapeutic target to overcome microenvironmental protection of CLL', *Leukemia*, vol. 34, no. 1, pp. 115-127.

Ysebaert, L. & Fournie, J.J. (2011) 'Genomic and phenotypic characterization of nurse-like cells that promote drug resistance in chronic lymphocytic leukemia', *Leuk Lymphoma*, vol. 52, no. 7, pp. 1404-1406.

Ysebaert, L., Poupot, M., Sanchez-Ruiz, Y., Laurent, C., Laurent, G. & Fournié, J.-J. (2010) 'Chronic Lymphocytic Leukemia-Associated Macrophages: Not Just Nurse Cells', *Blood*, vol. 116, no. 21, pp. 46-46.

Zhang, S. & Kipps, T.J. (2014) 'The pathogenesis of chronic lymphocytic leukemia', *Annu Rev Pathol*, vol. 9, pp. 103-118.

Zhang, W., Trachootham, D., Liu, J., Chen, G., Pelicano, H., Garcia-Prieto, C., Lu, W., Burger, J.A., Croce, C.M., Plunkett, W., Keating, M.J. & Huang, P. (2012) 'Stromal control of cystine metabolism promotes cancer cell survival in chronic lymphocytic leukaemia', *Nature Cell Biology*, vol. 14, no. 3, pp. 276-286.

Zhang, X., Qi, R., Xian, X., Yang, F., Blackstein, M., Deng, X., Fan, J., Ross, C., Karasinska, J., Hayden, M.R. & Liu, G. (2008) 'Spontaneous Atherosclerosis in Aged Lipoprotein Lipase–Deficient Mice With Severe Hypertriglyceridemia on a Normal Chow Diet', *Circulation Research*, vol. 102, no. 2, pp. 250-256.

Zhang, Y., Choksi, S., Chen, K., Pobezinskaya, Y., Linnoila, I. & Liu, Z.G. (2013) 'ROS play a critical role in the differentiation of alternatively activated macrophages and the occurrence of tumor-associated macrophages', *Cell Res*, vol. 23, no. 7, pp. 898-914.

Zhu, F., McCaw, L., Spaner, D.E. & Gorczynski, R.M. (2018) 'Targeting the IL-17/IL-6 axis can alter growth of Chronic Lymphocytic Leukemia in vivo/in vitro', *Leuk Res*, vol. 66, pp. 28-38.

Zhuang, J., Laing, N., Oates, M., Lin, K., Johnson, G. & Pettitt, A.R. (2014) 'Selective IAP inhibition results in sensitization of unstimulated but not CD40-stimulated chronic lymphocytic leukaemia cells to TRAIL-induced apoptosis', *Pharmacol Res Perspect*, vol. 2, no. 6, p. e00081.

Zucchetto, A., Benedetti, D., Tripodo, C., Bomben, R., Dal Bo, M., Marconi, D., Bossi, F., Lorenzon, D., Degan, M., Rossi, F.M., Rossi, D., Bulian, P., Franco, V., Del Poeta, G., Deaglio, S., Gaidano, G., Tedesco, F., Malavasi, F. & Gattei, V. (2009) 'CD38/CD31, the CCL3 and CCL4 chemokines, and CD49d/vascular cell adhesion molecule-1 are interchained by sequential events sustaining chronic lymphocytic leukemia cell survival', *Cancer Res*, vol. 69, no. 9, pp. 4001-4009.

Zupo, S., Massara, R., Dono, M., Rossi, E., Malavasi, F., Cosulich, M.E. & Ferrarini, M. (2000) 'Apoptosis or plasma cell differentiation of CD38-positive B-chronic lymphocytic leukemia cells induced by cross-linking of surface IgM or IgD', *Blood*, vol. 95, no. 4, pp. 1199-1206.

7 Appendix

7.1 Clinical Data

Appendix Table 7.1 Clinical data on CLL Samples used in my study.

IGHV status refers to somatic mutations in IGHV gene of CLL cells compared to gene sequence of the nearest germ line. IGHV mutation rates of ≥2% difference from germline are considered mutated, while un-mutated disease has a <2% mutation rate (Crombie & Davids 2017). WBC, White Blood Cell (10^9/l); Absolute Lymphocyte Count (10^9/l); Absolute Monocyte Count (10^9/l); ritux, Rituximab; FCR, Fludarabine Chlorambucil and Rituximab; lenalid, lenalidomide; NA, not available.

Sample number	WBC	Absolute Lymphocyte Count	Absolute Monocyte Count	Drug Treatment	IGHV status	Chromosomal status	Age at Diagnosis	Age at collection of samples	Gender	Staging
3259	209	123.1	1.4	other	NA	NA	NA	70	Male	NA
3314	359.8	351.2	NA	NA	NA	17p- 13q-	NA	51	Male	C
3369	163.5	157	2.2	untreated	NA	13q-	37	39	Male	NA
3379	228.5	NA	NA	NA	NA	NA	69	70	Male	NA
3381	157.4	149.7	3.1	ritux, bendamustine	NA	normal	67	74	Female	NA
3385	56.5	53.1	0.6	ritux, bendamustine	unmutated	normal	70	76.9	Male	C
3436	144.3	137	2.2	untreated	NA	13q-	NA	72	Male	B
3460	80.5	73.7	2	ibrutinib	NA	17p-13q-	NA	51	Male	NA
3461	22.6	15.3	1.1	untreated	NA	NA	73	74	Male	A
3463	52.7	46.7	1.1	DIB4	NA	normal	67	76	Female	A
3464	224.9	220.8	2	CLL210 induction	NA	17p- 13q-	NA	68	Male	B

3465	32.1	29.7	0.3	ibrutinib	NA	17p-	NA	55	Male	C
3469	65.4	63.3	0.5	FCR	NA	normal	55	63	Male	C
3470	159.6	149.9	2.7	untreated	NA	13q-	77	97	Female	A
3471	23.6	21.7	0.5	ibrutinib	NA	17p-	NA	55	Male	C
3472	149.9	144.8	0.7	untreated	NA	13q-	75	77	Female	B
3481	21.3	16.5	0.6	ritux, bendamustine	unmutated	normal	70	78	Male	C
3482	61.8	56.5	0.6	untreated	NA	11q- 13q-	70	71	Male	B
3483	3.7	1.3	0.3	ibrutinib	NA	17p-	NA	56	Male	C
3484	212.2	208.2	2.2	untreated	unmutated	13q-	58	65	Male	B
3485	100.8	89.6	3.2	untreated	NA	NA	74	79	Female	A
3490	196.3	190.8	NA	untreated	NA	13q-	82	82	Male	C
3491	66.4	62.7	1.1	ritux, idelalisib	NA	11q- 13q-	NA	66	Male	C
3492	67.6	63.8	0.8	FCR	NA	11q-	NA	77	Male	A
3493	72.8	67.6	1.3	untreated	NA	13q-	62	68	Female	A
3494	111.1	108.6	1.2	ritux, idelalisib	unmutated	17p-, trisomy 12	NA	74	Male	C
3500	226.7	224.5	NA	venetoclax	NA	trisomy 12	67	76	Male	C
3502	196.3	194.3	NA	venetoclax	NA	trisomy 12	67	76	Male	C
3504	129.5	126.7	1.6	venetoclax	NA	trisomy 12	67	76	Male	C
3505	38.1	36.9	0.8	venetoclax	NA	trisomy 12	67	76	Male	C
3506	5.7	0.6	0.1	venetoclax	NA	trisomy 12	67	76	Male	C

3507	33	30.7	0.3	untreated	NA	NA	63	65	Female	A
3510	275.6	268.8	2.7	untreated	NA	13q-, trisomy 12	73	80	Male	C
3511	226	221.9	1	untreated	NA	13q-, trisomy 12	73	80	Male	C
3512	138.3	130.3	2.3	FCR, Ibrutinib	NA	13q-	NA	67	Male	C
3513	112.8	109.8	0.8	fcr	NA	11q-	NA	67	Male	C
3516	55.9	53.4	1.5	ibr	NA	11q-, 13q-	NA	66	Male	C
3519	39.3	30.1	1	ibr	NA	17p-, 13q-	NA	52	Male	NA
3520	51.2	44.2	1.1	untreated	mutated	17p- 13q-	75	77	Female	A
3522	79.7	76.7	0.6	ibr	NA	11q-, 13q-	NA	71	Male	C
3523	15.7	14.8	0.1	FCR	NA	13q-	NA	68	Male	C
3526	244	224.7	NA	NA	NA	trisomy 12	NA	74	Male	C
3527	98	95	1.1	untreated	mutated	normal	69	75	Female	C
3528	23.3	17.5	1.4	FCRM	NA	11q-	55	68	Male	A
3529	42.1	36.2	1	ibrutinib	NA	11q- 13q-	NA	59	Male	C
3530	243.2	234	1.4	untreated	unmutated	normal	56	56	Male	C
3536	7	3	0.7	dex, ofatumumab, lenalid	NA	17p-	76	80	Male	A
3537	9.7	1.8	1.2	venetoclax	NA	17p-	NA	52	Male	A
3538	20.8	16.1	0.8	untreated	NA	11q-	NA	66	male	C
3539	56.6	50.7	1	untreated	NA	13q-	93	94	Male	B
3542	45.8	40.6	0.9	FCRM	NA	11q-	55	68	Male	A

3544	13.5	0.4	2.3	venetoclax	NA	17p-		57	Male	A
3561	85.8	76.8	1.7	untreated	unmutated	11q-	30	38	Male	B
3564	63	58.7	0.8	ofatumumab, chloramb	NA	11q- 13q-	52	84	Male	C
3566	70.3	63	1.6	untreated	mutated	13q-	59	66	Male	C
3568	155.8	148.9	1.4	ofatumumab, chloramb, idelalisib	unmutated	normal	72	76	Male	C
3574	71	65		ritux and idelalisib	normal	trisomy 12	NA	86	Male	B
3576	47.5	43.9	0.5	fludarabine	mutated	NA	57	82	Female	C
3577	85.7	75.8	1.4	ibrutinib	NA	17p-	NA	55	Male	A
3579	162.8	159.4	2	bendamustine, ritux	NA	11q-, 13q-	NA	58	Male	C
3582	147.8	143.9	1.2	untreated	no clonal rearranged IGHV detected	normal	62	66	Male	A
3585	109.9	101.4	1.5	untreated	unmutated	11q-, 13q-	66	68	Male	A
3587	257.2	>200	5.3	untreated	mutated	13q-	54	55	Male	
3589	170.6	104.9	1	untreated	mutated	normal	69	76	Female	C
3599	63.9	59.2	0.9	untreated	NA	13q-	62	70	Female	A
3602	50.8	49.9	0.6	untreated	unmutated	11q-	NA	61	Male	C
3603	106.2	101.7	2.5	ofatumumab, chloramb, idelalisib	unmutated	normal	72	77	Male	B
3605	252.8	244	1.6	untreated	mutated	13q-	60	63	Male	B
3606	109.2	103.6	1.8	ofatumumab, chlor, idel	unmutated	13q-	58	67	Male	B

3607	254.2	247.7	2.2	untreated	mutated	normal	66	69	Male	B
3609	120.8	109	3.7	untreated	NA	normal	46	62	Male	B
3610	240.9	237.9	1	ibr, ritux	NA	normal	62	66	Male	A
3611	74.3	65.5	1.5	untreated	NA	11q- 13q-	88	89	Female	A
3612	59	54.3	1.7	untreated	mutated	13q-	79	81	Female	B
3613	147.8	145.5	1.2	untreated	mutated	normal	56	67	Female	A
3620	145.9	142.6	1.2	untreated	mutated	normal	69	76	Female	C
3621	70.2	60.6	2	ibrutinib	mutated	13q-	58	59	Female	B
3627	136.7	129.4	2	ibrutinib	unmutated	13q del	58	68	Male	C
3631	256.1	>200	4.7	ibrutinib	mutated	13q-	60	64	Male	B
3637	144.6	134.9	2.2	untreated	unmutated	11q-, 13q-	66	69	Male	A
3639	277.2	266.1	2.4	ofatumumab, chloramb	unmutated	normal	72	77	Male	C
3640	177.5	163.4	2.3	untreated	unmutated	13q- equivocal	78	82.9	Male	A
3642	129.4	122.8	1.3	ibrutinib	unmutated	normal	67	73	Male	C
3644	187.6	174.1	5.1	ibrutinib	unmutated	normal	72	77	Male	C
3645	264.1	258.8	1.5	untreated	unmutated	normal	68	72	male	C
3647	145.9	138.2	2.8	untreated	mutated IGHV2-21	normal	66	67	Female	A
3650	119.6	110	1.9	untreated	mutated	normal	63	70	Female	B
3674	116.1	108.7	1.5	untreated	mutated	normal	63	70	Female	B
3679	171.4	164.7	1.6	untreated	NA	13q-	53	54	male	C

3682	33.2	25.8	0.5	untreated	NA		71	74	female	A
3684	230.1	220.8	NA	untreated	mutated	13q-	75	84	male	A
3686	38.5	31.3	1	untreated	mutated	trisomy 12	70	71	female	A
3691	226.5	216.1	2.9	ibrutinib, ritux	unmutated	13q-, trisomy 12	65	69	female	NA
3694	119.8	99.3	NA	ibrutinib	NA	normal	55	66	Male	C
3696	125.4	116.8	1.7	untreated	NA	13q-	61	71	Female	NA
3697	113.7	96.2	2.3	ibrutinib, ritux	unmutated	13q-, trisomy 12	65	69	female	NA
3707	108.7	100.8	2.3	untreated	unmutated	13q- equivocal	78	83	Male	B

Appendix Table 7.2 Summary of Clinical features with context of treatment

		Untreated		Treated	
		Frequency	Percentage	Frequency	Percentage
Staging	A	17	42.5	8	19.5
	B	12	30.0	6	14.6
	C	11	27.5	27	65.9
NLC Score	0	2	4.8	1	2.2
	1	16	38.1	26	57.8
	2	11	26.2	7	15.6
	3	13	31.0	11	24.4

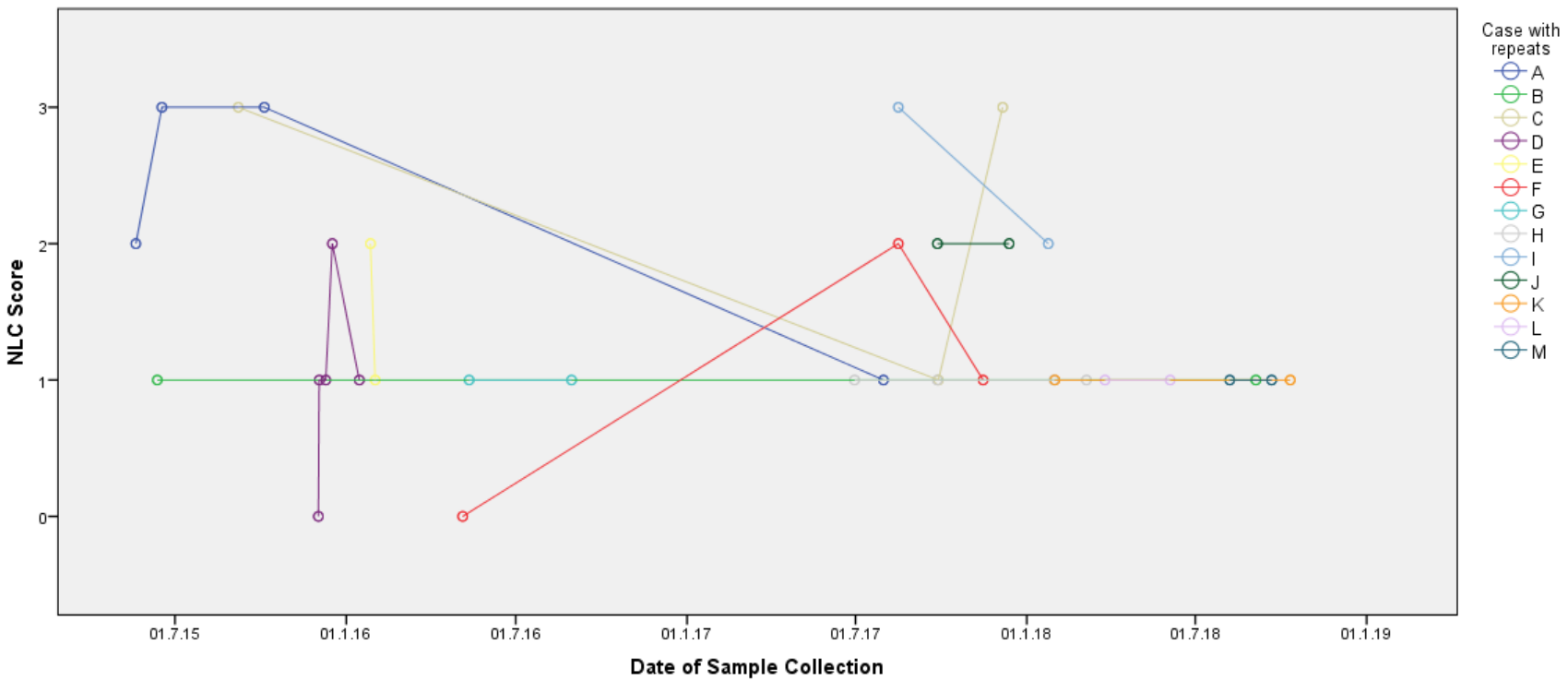

Appendix Figure 7.1 NLC score changes with time among patients with multiple re-bleeds.

Reorganising all samples collected into those from the same patients (A-M), the changes in NLC score (0-3) were plotted with the date in which the sample was taken. Image created using SPSS software.

7.2 Phenotyping NLCs using Flow Cytometry

Similar to analysis of cell purity, when the cells of interest are harvested, spun and washed with PBS at 300G at 4^{o}C, Fixation/Permeabilisation is done to allow antibodies to cross and bind to selected intracellular CD Markers. The cells are washed to remove excess debris with fixation/permeabilisation solution. After this, the cells are dehydrated so the size of the cells and overall pellet size is smaller.

Fluorochrome-conjugated antibodies are added at appropriate volume and incubated for at least 1 hour. The cells are washed thoroughly to remove the excess unbound antibodies. The remaining complexes are then sent for FACS analysis. Compensation using beads are used to allow well spread out peaks of each fluorochromes and an isotype control and test is done on each sample harvested.

Data Collection is performed using Attune software and Analysis is done by both Attune software and Flowing Software.

When analyzing, appropriate gating strategies are made to ensure that CLL cells (the majority) are identified and not selected seen in Appendix Figure 7.2. It is known that macrophages are bigger and more complex (higher granularity and vacuoles) so it is expected to see that their population would have a higher Forward Scatter. This was also observed in early literature pertaining to NLCs (Burger et al. 2000; Tsukada et al. 2002).

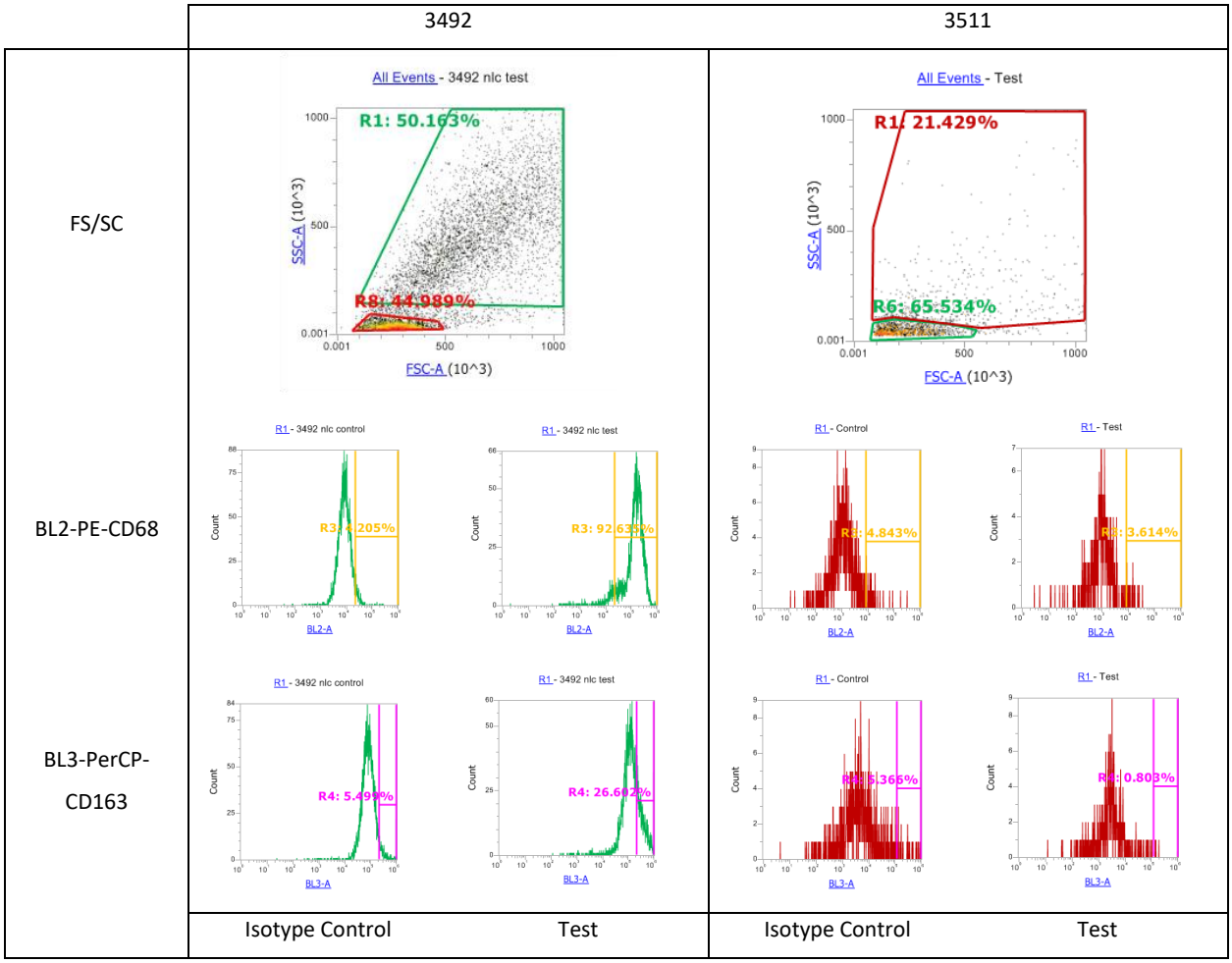

Appendix Figure 7.2 Phenotyping NLCs using Flow Cytometry. NLCs were harvested using cell scraping method (left) and Trypsin/EDTA (right)

Sample 3492 and 3511, when harvesting NLCs using a plate scraper (left), the gated region of NLCs is selected as R1 and the level of antibody is detected with the histograms comparing the test with isotype control. Image taken from Attune Flow Cytometry

7.3 RNA Sequencing

7.3.1 Library Preparation

RNA samples are sent in ice cold temperature following extraction from harvested cells and checked for eligible purity and quantity as per requirements of the outsourced sequencing company (Novogene).

The mRNA is enriched and fragmented, followed by reverse transcription to produce cDNA fragments from the mRNA template (Appendix Figure 7.3). Adapters are added to the ends to make it easier to perform cluster generation. This is known as Next Generation Sequencing (NGS) Library preparation.

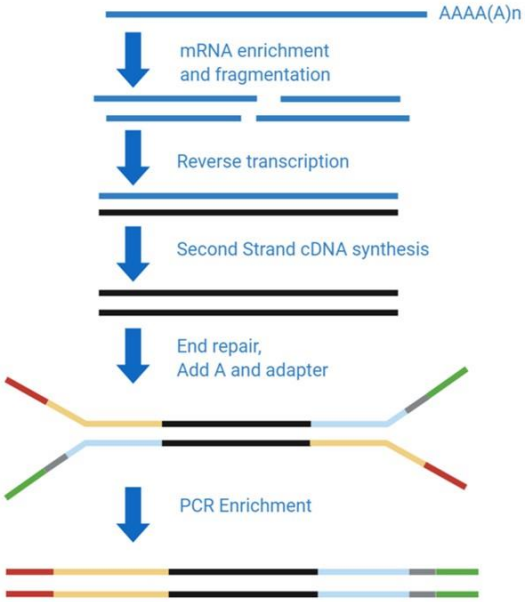

Appendix Figure 7.3 Diagram of New England Biolabs (NEB) library preparation of mRNA for RNAseq. Image adapted from Novogene report using BioRender online tools.

7.3.2 Cluster generation

This is where the fragments with adapters are added onto a glass slide with lanes (Appendix Figure 7.4). The lanes are coated with a lawn. Here, the lawn is composed of two types of oligos that are complimentary to one of the two ends of the DNA fragments. Polymerase action occurs to amplify the strands into millions.

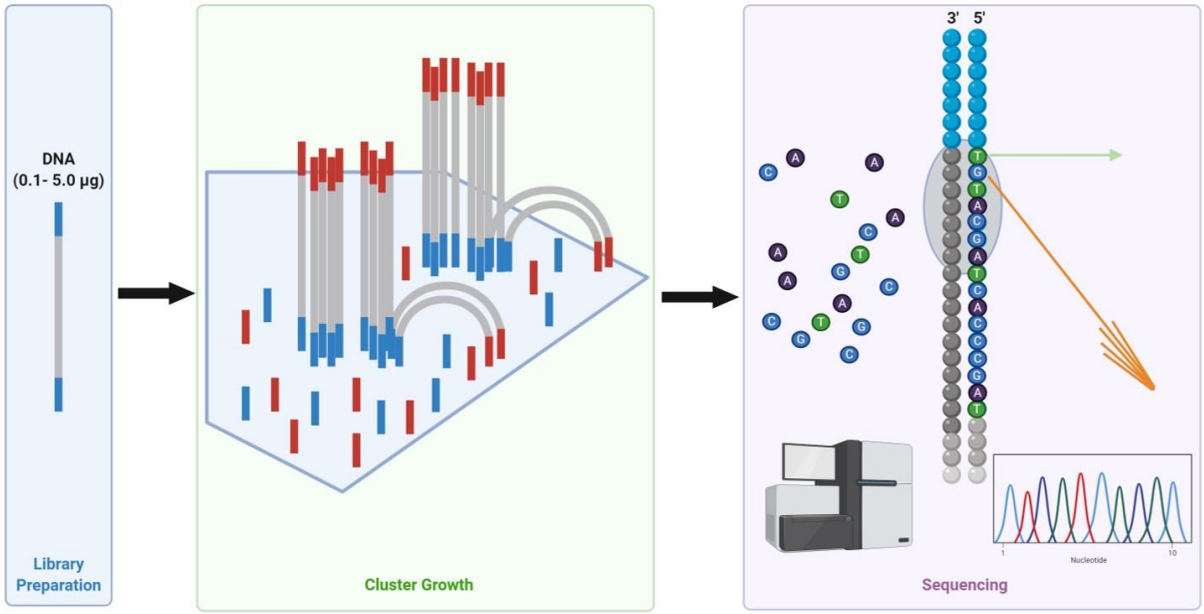

Appendix Figure 7.4 Steps of preparing DNA for sequencing. Image adapted from Novogene report using BioRender online tools.

7.3.3 Sequencing

Sequencing starts with the reading of the primer (Appendix Figure 7.4). Fluorescently tagged nucleotides then come and bind complement to the strand. On binding, the fluorescence is excited and detected by the machine. Forward and reverse reads occur to avoid ambiguous alignments.

The machine converts the signals detected into digital representations of the sequence and produces raw data as bam and FastQ files for data analysis (described in Appendix Figure 7.10).

7.4 Phases/ progression of Monocyte/macrophage differentiation observed

These observations are made on following cultures from the start of plating the PBMC from CLL patients.

1. **Well defined monocyte** seen with spherical/oval shape that is slightly larger than lymphocytes. Nucleus show chromatin pattern and cytoplasm appear grey. Granules appear as very fine specs in cytoplasm. Slight gap may be seen between monocyte and lymphocytes giving a sort of halo like appearance around the monocyte. Almost no pleomorphism
2. Monocytes appear **larger** now with more granules giving a darker denser appearance than other monocytes. Shape is still spherical/ oval. Some may show some fine fibrous extensions from well-defined cell membrane. Slight pleomorphism.
3. Shape of monocyte is altered giving an **elongated** look, where nucleus and cytoplasm is harder to distinguish under PC. Obvious pleomorphism is observed.
4. **Tail-like projections** are observed extending from the cytoplasm as if leaving a trail. This is seen on one pole of the cell giving a distinct head and tail appearance, suggestive of active motion of the cell. Cell membrane at tip of tail is not well defined.
5. Tail-like projections increase in number to give a **spindle shaped appearance**, where the nucleus appears to be in the middle and the tails are at separate ends extending or projecting outwards, giving a strong adherent appearance. Usually in close proximity with lymphocytes or other earlier monocytes. (monocytes in general appear very pleomorphic)
6. Monocytes may form **clusters** near less healthy (dead or dying lymphocytes), others may join. Mix of spherical/oval and elongated, tailed monocytes.
7. **Cluster may grow** consisting of more pleomorphic monocytes and lymphocytes.
8. Period of **plateau** where this not much difference in size, shape, density appearance of monocytes, clusters.
9. **Clusters reduce** in number, with darker looking cells yet not as granulated. Pleomorphism may be less. Most monocytes may appear smaller with occasional giant-sized monocytes
10. More dead/dying cells are observed where lymphocytes appear dark and shrunken if adhered and floating aggregate bodies. Number of both lymphocytes and monocytes seem reduced, predominantly the lymphocytes. **Mild apoptotic background** is observed where small particle bodies are seen, giving a darker background. Areas of dead cells appear as black opaque aggregates.
11. Tail like projectioned monocytes and occasional giant-sized monocytes remain unaltered in number, however, other forms appear reduced or nil. **Background appears more apoptotic**.

12. Under the **dark opaque dead aggregates** if washed, may show some early Phased monocytes. Overall number of monocytes is reduced.
13. Number of live cells in general is severely reduced leaving behind a **darkly apoptotic background with shrivelled and shrunken dying cells**. No visual color change in medium by naked eye.

7.5 Integrity of RNA

The integrity of RNA was analysed using Agilent Bioanalyzer by Novogene. Samples that achieve RIN ≥7.0 are acceptable and used for sequencing. Samples which do not meet the required RIN can undergo an additional step of purification by Novogene to raise the RIN to acceptable level.

The Agilent Bioanalyzer is based on microfluidics technology and is also capable of performing electrophoretic separations using capillary electrophoresis. The Bioanalyzer uses Lab-on-a-chip technology which have tiny channels analogous to capillary tubing, where the proteins or other analytes are subjected to an electric field, migrate along a separation channel and are picked up by the detector. These LabChip Kits are now a standard in RNA quality assessment and quantitation. Using electrophoresis-based techniques on micro-fabricated chips, RNA samples are separated and subsequently detected via laser induced fluorescence detection.

The machine can run small sample volumes, requiring short analysis time and is generally automated which improves accuracy, precision and productivity.

The software generates an electropherogram and gel-like image and displays results such as sample concentration and the ribosomal ratio. The electropherogram provides a detailed visual assessment of the quality of the RNA sample.

RNA degradation is a gradual process where there is a decrease in the 18S to 28S ribosomal band ratio and increase in the baseline signal between the two ribosomal peaks and the lower marker. The software automatically generates the ratio of the 18S to 28S ribosomal subunits. However, a further analysis using RNA Integrity Number (RIN) can adequately describe the sample integrity. The RIN considers the entire electrophoretic trace. The software algorithm for RIN allows for the classification of total RNA based on a numbering system from 1 to 10, with 1 being the most degraded profile and 10 being the most intact. RIN is generated based on a number of features such as: Peak height/position, Areas/Area ratio, Signal/Noise ratio, Max Min values, waviness of the curve etc (Schroeder et al. 2006). The total RNA ratio measures the fraction of the area covered by 18S and 28S compared to the total area under the curve (Schroeder et al. 2006). The height of 28S peak gives additional information on the state of degradation process where the 28S band vanishes faster than 18S during degradation (Schroeder et al. 2006). Accurate RIN values can be obtained when concentration values are above 50ng/ul. The RIN, however, cannot predict the usefulness of gene expression data without prior validation work (Schroeder et al. 2006). As seen in Appendix Figure 7.5, the sample has a distinct high 28S and 18S peak that contributes to most of the total area, giving a high RIN value of 9.9.

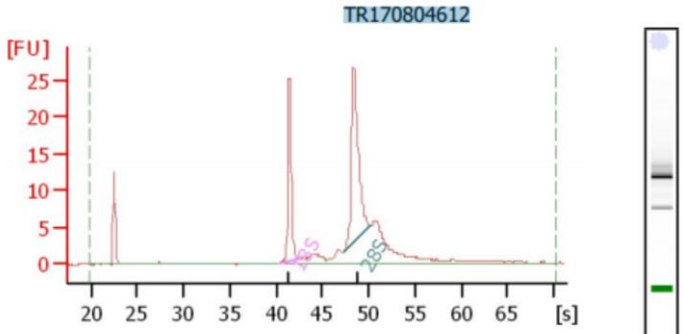

Overall Results for sample 1 : TR170804612

RNA Area:	133.4
RNA Concentration:	76 ng/µl
rRNA Ratio [28s / 18s]:	1.8
RNA Integrity Number (RIN):	9.9 (B.02.08)
Result Flagging Color:	
Result Flagging Label:	RIN: 9.90

Fragment table for sample 1 : TR170804612

Name	Start Time [s]	End Time [s]	Area	% of total Area
18S	40.42	42.45	24.5	18.3
28S	47.29	50.29	44.4	33.2

Appendix Figure 7.5 Bioanalyzer report of a sample with a high RIN value.

Bioanalyzer report of a sample sent for RNAseq. 18S (pink) seen as the middle peak and 28S (green) seen as the peak on the right. The sample was harvested and RNA was extracted as described in Methods. Bioanalyzer report was generated using outsourced Agilent machine by Novogene

7.6 Purification of sample

Some of the RNA extracted unfortunately do not meet the RIN requirements to perform the RNAseq and so an option of purification of RNA is offered. This technology combines the selective binding properties of a silica-based membrane with speed of microspin technology. First lyzed and homogenized in presence of denaturing guanidine-thiocyanate-containing buffer, which inactivates the RNases to ensure purification of intact RNA. Ethanol is used to provide appropriate binding conditions. The sample is applied into RNeasy Mini spin column, where the total RNA binds to the membrane and the contaminants are efficiently washed away. This procedure provides enrichment of mRNA since most RNAs <200 nucleotides (such as ribosomal RNA and translational RNA, which together comprises of 15-20% of total RNA) are selectively excluded. This was done solely by the outsourced agent Novogene. As seen in Appendix Figure 7.6, the sample 3679 CL had an initially low RIN value and undergone purification and as seen in Appendix Figure 7.7 the same sample then had an improved RIN value, acceptable for RNAseq experiment.

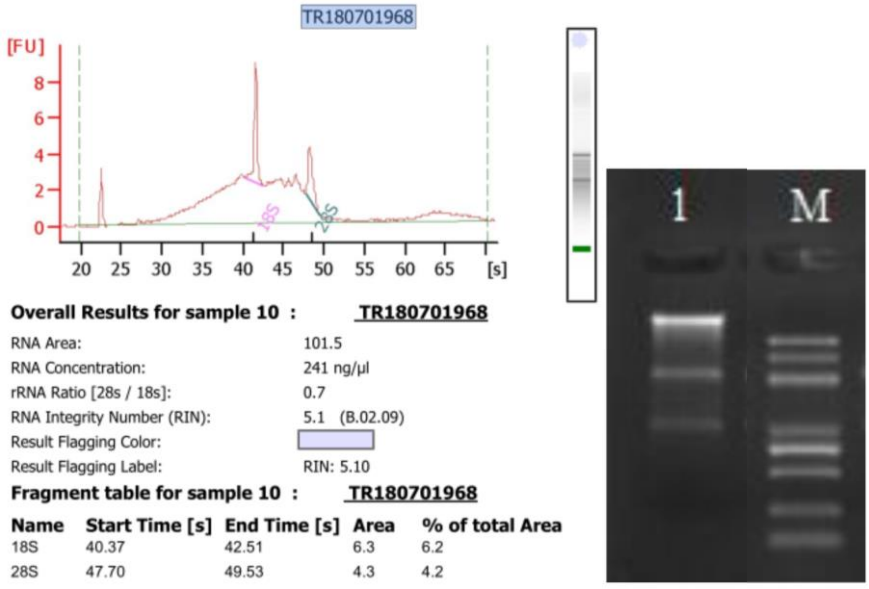

Appendix Figure 7.6 Bioanlayzer report and Agarose gel electrophoresis of RNA sample with low RIN value.

Bioanalyzer data (left) of Sample 3679 CL with low RIN number (5.1), Agarose gel electrophoresis (right) where the sample is in well #1 with the conditions of Gel Conc.: 1%, Voltage: 180v and Run Time of 16min. The sample was harvested and RNA was extracted as described in Methods. Bioanalyzer report was generated using outsourced Agilent machine by

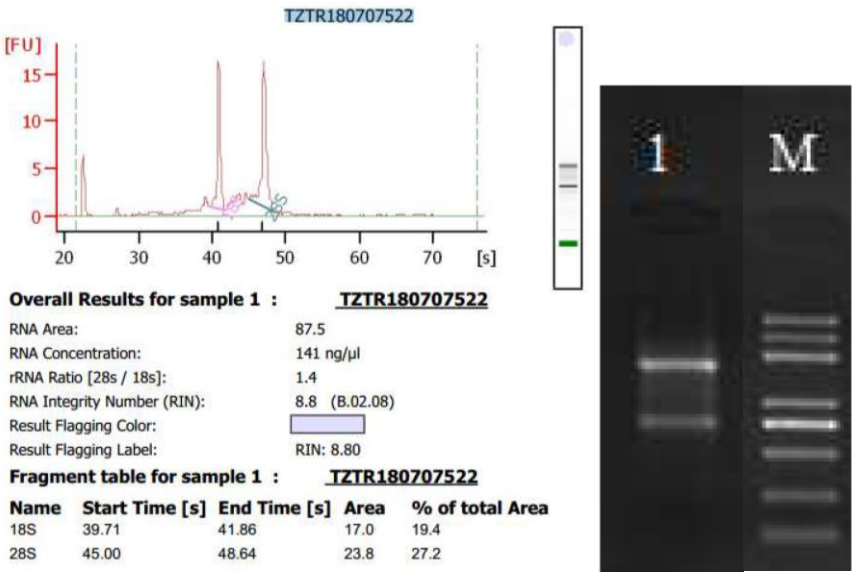

Appendix Figure 7.7 Bioanalyzer report and Agarose gel electrophoresis of an RNA sample following purification with a good RIN value.

Following purification of Sample 3679 CL, Bioanalyzer data (left) with encouraging RIN number (8.8), Agarose gel electrophoresis (right) where the sample is in well #1 with the conditions of Gel Conc.: 1%, Voltage: 180v and Run Time of 16min. The sample was harvested and RNA was extracted as described in Methods. Bioanalyzer report was generated using outsourced Agilent machine by Novogene.

7.7 Preliminary steps to confirm quality of cDNA and PCR primers

To confirm the quality of the cDNA, cDNA from CLL samples was first used to measure the expression of GAPDH using PCR primers by agarose gel electrophoresis. As shown in Appendix Figure 7.8, it showed that the old stock of GAPDH primer was not suitable as all the samples did not properly express GAPDH, but rather showed expression below the expected length. This suggested that new stock of GAPDH was imperative for subsequent experiments.

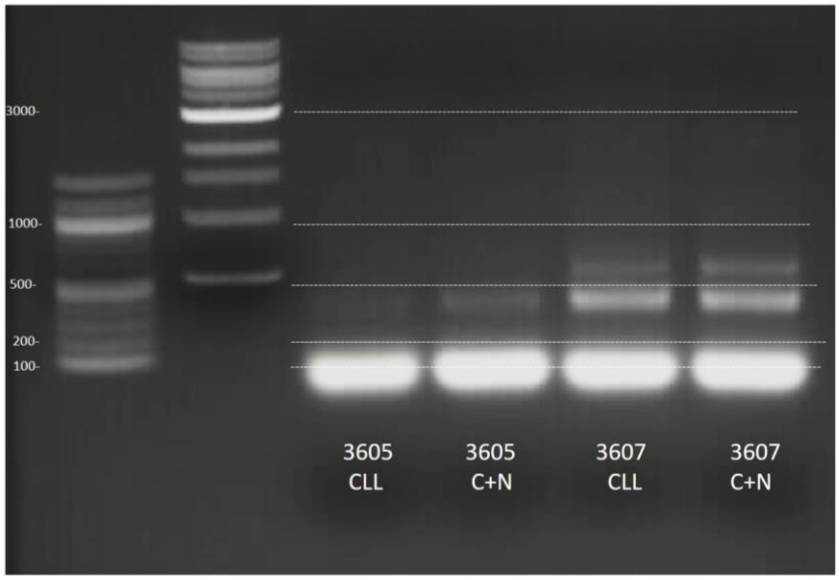

Appendix Figure 7.8 PCR gel run on four samples with an old stock of GAPDH

An old stock of GAPDH primers was used on 4 RNA samples (Wells #3-6). The Quick-Load Purple DNA ladders 100bp (Well #1) and 1kb (Well #2) were used to compare the bp. The agarose gel electrophoresis was performed as described in Methodology.

After ordering new GAPDH primers and preparing them (as described in Methodology 2.1.8.3), I repeated agarose gel electrophoresis and as seen in Appendix Figure 7.9, GAPDH was detected at the expected location at around 400bp. This suggested that this stock of GAPDH was suitable.

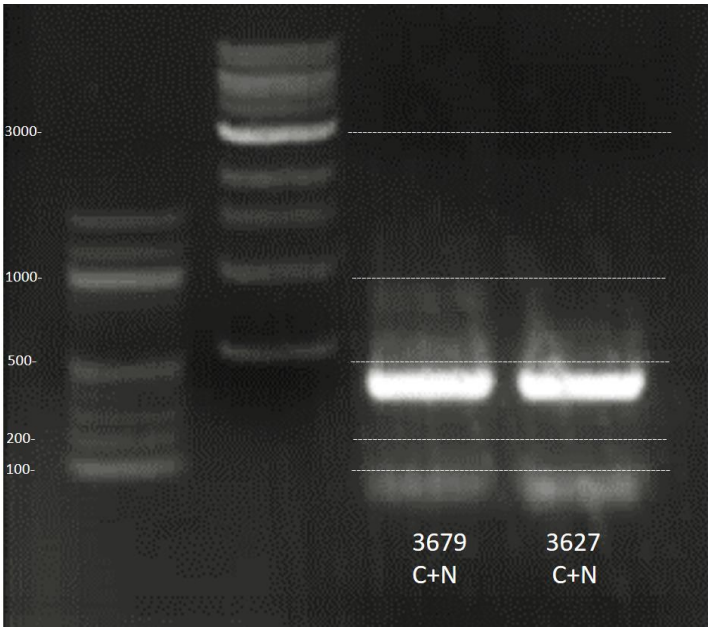

Appendix Figure 7.9 PCR gel run on two samples with a new stock of GAPDH primer

A new stock of GAPDH primers was used on 2 RNA samples (Wells #3-4). The Quick-Load Purple DNA ladders 100bp (Well #1) and 1kb (Well #2) were used to compare the bp. The agarose gel electrophoresis was performed as described in Methodology.

7.8 Quality Control

Briefly, as mentioned in Methods, the MultiQC report was generated from the FastQ files. As seen in Appendix Figure 7.10, the number of unique reads were more than duplicate reads as well as being quite high. This was indicative of good quality of the reads. Mean quality scores were produced based on Phred Score. It was found that the scores were all above 30 in the 'green zone' which was indicative of a pass. The average %GC content of reads was calculated, all the samples were around 51-54% which was considered a pass. Sequence duplication levels was represented and showed that the levels were all low thereby considered to be a pass. The percentage reads of T, C, A and G nucleotides were measured according to position (bp) and except for the first 10bp or so, the levels were all approximately 25%. As with every template the beginning would have oligo reads and so the initial part is expected to have a jagged graph. The remaining portion of the positions in the graph was flat line and excluding the first 10bp it was considered a pass. Two measurements that usually results in failure because they are very sensitive. Per-base sequence content and Per-sequence GC content. Per-base sequence content is common to show variation in the first 10 base pairs which was seen in our data as well.

A

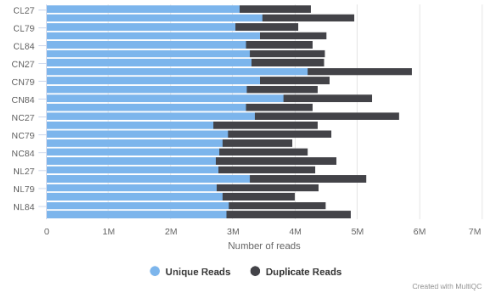

B

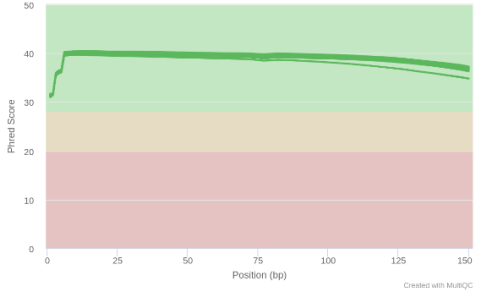

C

Sample Name	% GC	Sample Name	% GC
CL27	54%	NC27	52%
CL77	52%	NC77	52%
CL79	53%	NC79	53%
CL82	51%	NC82	52%
CL84	52%	NC84	54%
CL99	54%	NC99	52%
CN27	53%	NL27	52%
CN77	52%	NL77	54%
CN79	52%	NL79	54%
CN82	53%	NL82	53%
CN84	51%	NL84	53%
CN99	52%	NL99	53%

D

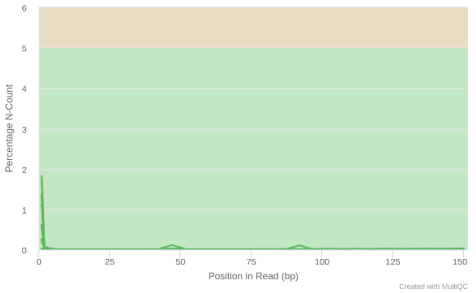

E

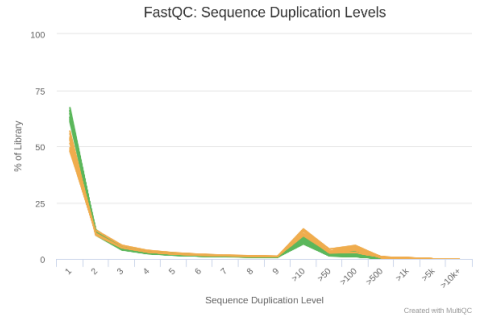

F

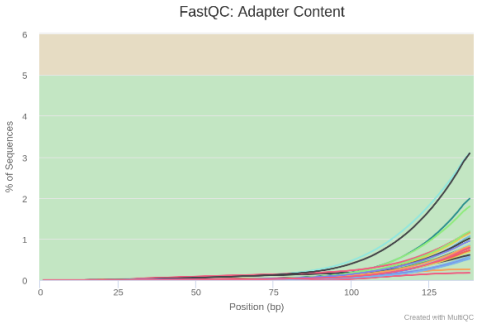

G

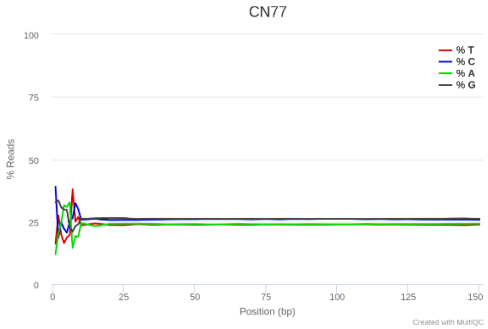

Appendix Figure 7.10 RNAseq MultiQC Report generated from FastQ files

MultiQC Report generated from FastQ files from RNAseq raw data. The report consists of Sequence Counts (**A**), Mean Quality Scores (**B**), Average %GC content (**C**), Per Base N Content (**D**), Sequence Duplication Levels (**E**), Adapter Content (**F**) and %Reads of T, C, A and G nucleotides measured according to position (**G**).

7.9 Differential Gene Expression List

Appendix Table 7.3 Differential Gene Expression Analysis of significantly upregulated genes in CLL samples

Differential Gene Expression of significantly upregulated genes in the comparison between CLL alone (CLL) with CLL cultured with NLC (CLLcc). The genes are listed according to their log2fold change among CLLcc where CLL alone is the control. All the genes are statistically significant with their pvalue and padj values mentioned. Highlighted are those that were also upregulated in the literature study mentioned (Herishanu et al. 2011).

Gene	log2FoldChange	lfcSE	stat	pvalue	padj	ExpressionLevelCLL	ExpressionLevelCLLcc
CHI3L1	6.626538	0.547598	12.10109	1.04E-33	8.23E-30	7.018133985	8.97364278
CCL13	6.623863635	0.762716	8.684575	3.80E-18	8.58E-15	3.741797174	6.108092264
CXCL9	6.472251527	1.002515	6.456016	1.07E-10	7.38E-08	4.007903563	5.975133685
SPARC	6.28328509	0.501492	12.52918	5.17E-36	8.17E-32	6.088225541	8.319318944
C1QA	5.605885135	0.542476	10.33389	4.95E-25	1.96E-21	7.053632523	9.382525933
ANKRD22	5.543077736	0.973897	5.691645	1.26E-08	4.42E-06	1.33334491	2.919537681
SLC1A2	5.463363463	0.875512	6.240193	4.37E-10	2.56E-07	2.432986191	3.930114202
C1QB	5.319892541	0.6103	8.716848	2.86E-18	7.53E-15	6.075224015	8.329537997
GPC4	5.251611677	0.75173	6.986033	2.83E-12	2.79E-09	5.128599786	6.593348076
APOE	5.111120844	0.480545	10.6361	2.02E-26	1.07E-22	9.055853644	11.18368727
KREMEN1	5.08319543	0.891993	5.698697	1.21E-08	4.33E-06	2.347373709	3.822795255
KAL1	5.036022762	0.946592	5.320162	1.04E-07	2.78E-05	1.989989525	3.16329548
CCL18	5.008110973	0.658317	7.607441	2.80E-14	4.91E-11	3.680027204	5.52084199
NUPR1	4.998388338	0.81886	6.104085	1.03E-09	5.83E-07	3.334462361	4.982100132
STAC	4.954662635	0.725022	6.833806	8.27E-12	7.26E-09	3.175955907	5.303174349

DCSTAMP	4.846985448	0.659995	7.343971	2.07E-13	2.52E-10	4.600787681	6.028399576
IGFBP6	4.735214774	1.063908	4.450775	8.56E-06	0.001165	2.604781652	3.848555095
AK4	4.729690626	0.837811	5.645296	1.65E-08	5.66E-06	2.255642297	3.640282549
SLITRK4	4.661927929	0.955611	4.878478	1.07E-06	0.000201	1.690721383	2.74645581
TSKU	4.610341963	0.643165	7.168209	7.60E-13	8.57E-10	3.836114315	5.436698925
ZBED2	4.609355576	0.79343	5.809403	6.27E-09	2.54E-06	1.959037927	3.701267881
UBD	4.594555212	0.798702	5.752525	8.79E-09	3.39E-06	2.500421617	4.336665778
PRRG1	4.535987405	0.93604	4.845931	1.26E-06	0.000226	2.020187683	3.057216291
ZBTB7C	4.53E+00	0.953224	4.756361	1.97E-06	0.000328	1.940282272	2.848593146
P2RY13	4.438806046	0.850559	5.218695	1.80E-07	4.31E-05	1.966519088	3.478319838
TRPV4	4.431821585	0.748424	5.921535	3.19E-09	1.57E-06	2.840077584	4.374728274
TNFAIP6	4.378211526	0.868035	5.04382	4.56E-07	9.48E-05	2.084370432	3.444422059
HJURP	4.353566596	0.820154	5.308228	1.11E-07	2.91E-05	1.163358911	2.400684275
HSD11B1	4.263068739	0.953851	4.469325	7.85E-06	0.001084	1.732209015	2.605374498
CD1B	4.261200749	0.90875	4.68908	2.74E-06	0.000442	1.482004733	2.613510067
GNG4	4.228534081	0.806909	5.240407	1.60E-07	3.89E-05	0.963593869	2.182950795
SUCNR1	4.183642328	0.792086	5.2818	1.28E-07	3.31E-05	2.906331676	4.158310801
LCNL1	4.156275291	0.959284	4.332684	1.47E-05	0.001711	2.182145481	3.201184587
GJB2	4.142628894	0.839569	4.934234	8.05E-07	0.000159	2.858312722	4.257472156
ALOX15B	4.090781412	0.938938	4.356818	1.32E-05	0.001604	2.30671985	3.621888841
CXCL10	4.089416869	1.013389	4.035385	5.45E-05	0.005156	2.638053066	4.17251983

CXCL12	4.079820404	1.021651	3.993359	6.51E-05	0.00588	1.55402758	2.826468618
SH3PXD2B	4.03504769	0.41138	9.808568	1.03E-22	3.27E-19	5.477802162	7.344849929
NPR1	4.030785297	1.061584	3.796952	0.000146	0.011287	2.332771802	3.387439989
CCL1	4.021500827	0.936356	4.294844	1.75E-05	0.001972	1.838320702	2.806584649
SERPING1	3.981529848	0.745435	5.341218	9.23E-08	2.60E-05	3.624071175	5.438191304
F3	3.939404622	0.840849	4.685033	2.80E-06	0.000447	3.15458496	4.125749821
KCNF1	3.914441753	0.899025	4.354097	1.34E-05	0.001611	2.051602963	2.984318707
TMTC1	3.894855418	0.882287	4.414498	1.01E-05	0.0013	1.868938318	3.043258983
BCAR1	3.823695239	0.7295	5.241528	1.59E-07	3.89E-05	3.17706564	4.363881608
IL6	3.820445498	0.923348	4.137599	3.51E-05	0.003465	1.607223176	2.916593341
LINC01010	3.802950694	0.846245	4.493912	6.99E-06	0.001004	2.920231489	3.797758229
SSPN	3.78830165	0.73605	5.146802	2.65E-07	5.98E-05	2.070894758	3.310948344
SEZ6L2	3.7552522	0.788793	4.76076	1.93E-06	0.000328	1.803568957	2.871153306
PTGES	3.72938821	0.824049	4.525689	6.02E-06	0.000872	1.72875144	2.847733269
SLC30A3	3.719924818	0.918314	4.050818	5.10E-05	0.004857	1.900486089	2.562603033
CCL8	3.717788937	0.695538	5.3452	9.03E-08	2.59E-05	3.134032515	4.630204181
C1QC	3.699102233	0.558358	6.624961	3.47E-11	2.74E-08	7.962435867	9.920848403
SULT1C2	3.694020337	0.891696	4.14269	3.43E-05	0.00341	1.844328993	2.599796633
RRM2	3.684022831	0.755041	4.879236	1.06E-06	0.000201	2.077368816	3.453782845
SHC4	3.680497755	0.977372	3.765707	0.000166	0.012259	1.487501245	2.390795804
NES	3.664349132	0.77722	4.714689	2.42E-06	0.000394	3.537111122	4.647522845

UNQ6494	3.652027398	1.075025	3.397156	0.000681	0.036708	1.008573869	1.941173679
SLC6A12	3.627039533	0.777236	4.666588	3.06E-06	0.000479	2.556788927	3.528327743
GPR85	3.601887213	1.049371	3.432424	0.000598	0.033628	0.814492825	1.526694072
KIAA1462	3.49309833	1.036551	3.369924	0.000752	0.039589	0.906553991	1.749111651
PROS1	3.470245452	0.88182	3.935321	8.31E-05	0.007172	1.767187088	2.841225116
MMP7	3.456616895	0.681633	5.071086	3.96E-07	8.44E-05	3.474453786	4.514641131
TMEM130	3.451263435	1.00128	3.446851	0.000567	0.032379	0.651995921	1.512203112
VNN1	3.431769903	0.53583	6.404581	1.51E-10	9.53E-08	3.723711811	5.049868843
COL6A3	3.407492601	0.714617	4.768277	1.86E-06	0.000323	2.129063163	3.409556138
KCNMA1	3.391712798	0.794424	4.269397	1.96E-05	0.002112	4.206601342	5.746010893
TFCP2L1	3.382286955	0.711103	4.756397	1.97E-06	0.000328	2.363376541	3.364466008
CLEC6A	3.354986484	0.940165	3.568508	0.000359	0.022684	1.396445349	2.126641153
ETV7	3.354168829	0.832662	4.028247	5.62E-05	0.005284	0.947260402	1.905024354
RP11-1008C21.1	3.353940458	0.811997	4.130486	3.62E-05	0.00353	1.404456006	2.387237331
RBP1	3.350847524	0.686901	4.878211	1.07E-06	0.000201	2.383067794	3.61545953
CLEC1A	3.303857379	0.977185	3.380993	0.000722	0.038413	1.340837097	2.047449498
UNC13A	3.303187894	0.942694	3.503986	0.000458	0.027321	1.915654819	2.976503112
DIRAS2	3.268983297	0.936438	3.490869	0.000481	0.028453	1.515874934	2.213049072
ACOX2	3.265349343	0.984634	3.316307	0.000912	0.045887	0.799834348	1.5833897
SLC28A3	3.239167139	0.647832	5.000009	5.73E-07	0.000118	3.219850144	4.259834449
STOX2	3.232196196	0.782185	4.132264	3.59E-05	0.003524	2.041684395	2.940638303

ALDH1A1	3.224246257	0.553085	5.829567	5.56E-09	2.31E-06	3.525088345	4.932737576
LILRB5	3.209866305	0.737627	4.351614	1.35E-05	0.001617	5.280097282	7.099933041
LOC101928716	3.206469862	0.767099	4.179997	2.92E-05	0.002952	2.237089859	3.007439665
TGM2	3.19071212	0.458486	6.959236	3.42E-12	3.18E-09	6.628500378	8.031114549
PIR	3.177872627	0.926577	3.429689	0.000604	0.033728	1.445906959	2.274696327
EGLN3	3.177700594	0.848007	3.747257	0.000179	0.012895	1.597394375	2.577946667
MKI67	3.165215913	0.574545	5.509086	3.61E-08	1.14E-05	3.909497173	5.826288065
RAI14	3.095768613	0.794785	3.895101	9.82E-05	0.008076	2.32760727	3.299609543
PGM5	3.075041485	0.847871	3.626779	0.000287	0.019108	1.438239416	2.384984401
C3	3.036073249	0.779399	3.895402	9.80E-05	0.008076	2.5428523	3.690269073
CD1E	2.965642577	0.839192	3.533927	0.000409	0.025165	1.201941975	2.08749124
ACE	2.959932995	0.50061	5.912648	3.37E-09	1.61E-06	5.285715512	6.765415501
STAC2	2.928547428	0.823014	3.558319	0.000373	0.023211	2.707554667	3.358691357
GPRC5B	2.926645251	0.849394	3.44557	0.00057	0.032379	1.25605411	1.932332848
TCN2	2.917771807	0.639284	4.564123	5.02E-06	0.00074	3.687374274	5.039426127
CCL24	2.882530445	0.762078	3.782462	0.000155	0.01185	4.754146721	6.486863487
C5orf20	2.877608007	0.67666	4.252667	2.11E-05	0.002224	3.380267591	4.727984181
FGD5	2.875595942	0.769633	3.736323	0.000187	0.013347	2.054799134	2.832587351
SLAMF8	2.868013916	0.378328	7.580769	3.44E-14	5.43E-11	6.616365029	8.102927884
LYZ	2.810718653	0.424889	6.615179	3.71E-11	2.79E-08	11.01941977	12.50647395
CCL7	2.805728662	0.625242	4.487429	7.21E-06	0.001017	3.154842062	4.496967665

GBP1	2.79436008	0.543899	5.137647	2.78E-07	6.15E-05	5.470164254	7.090013599
SPP1	2.788645231	0.344373	8.097737	5.60E-16	1.11E-12	8.054320427	9.224239119
USP2	2.779727582	0.796448	3.490158	0.000483	0.028453	2.808053936	3.526143712
MMP9	2.770866693	0.370179	7.485208	7.14E-14	9.40E-11	10.59207459	12.14787944
CLEC4E	2.767874458	0.508155	5.44691	5.13E-08	1.59E-05	3.53636976	4.776920727
SHOX2	2.766616748	0.828377	3.339803	0.000838	0.042858	1.844631378	2.604162233
TICRR	2.761454998	0.738661	3.738462	0.000185	0.013294	1.315315689	2.417409092
CSPG4	2.760948304	0.662223	4.169215	3.06E-05	0.003075	3.21514844	4.163186054
PKMYT1	2.759253811	0.76035	3.628928	0.000285	0.019049	1.704284485	2.746633491
BHLHE41	2.757111192	0.435531	6.330454	2.44E-10	1.49E-07	5.946217502	7.316384931
FAM213A	2.737070334	0.555965	4.923101	8.52E-07	0.000166	3.830178907	5.066674648
LOC101927029	2.726699572	0.784229	3.476919	0.000507	0.029564	1.592828889	2.449367305
TMEM119	2.726549108	0.815821	3.342092	0.000831	0.042644	4.044543288	5.39719044
PTPRF	2.724727353	0.744212	3.661223	0.000251	0.017165	2.530394599	3.753364658
MYOF	2.722972101	0.501278	5.432061	5.57E-08	1.68E-05	3.801199821	4.967605769
MT1G	2.720817084	0.649719	4.187682	2.82E-05	0.002872	2.30734131	3.139373622
PADI2	2.720103321	0.755537	3.600223	0.000318	0.020668	3.189776968	4.26230293
ACOT11	2.69E+00	0.811978	3.307069	0.000943	0.047127	1.803145581	2.675574747
MARCO	2.67898073	0.815608	3.284644	0.001021	0.049629	1.235895595	2.054373152
EBI3	2.659217679	0.632781	4.202429	2.64E-05	0.002726	2.061149028	3.0127506
SLCO5A1	2.653973418	0.77056	3.444212	0.000573	0.032426	1.357637485	2.548511567

CCL22	2.653022873	0.767905	3.454885	0.000551	0.031854	7.122369841	8.392779356
COL6A1	2.645220064	0.480097	5.509761	3.59E-08	1.14E-05	5.407021025	6.665951187
FBP1	2.642875468	0.396407	6.667074	2.61E-11	2.17E-08	6.207922368	7.547922296
ARNTL2	2.638560879	0.451181	5.848123	4.97E-09	2.12E-06	4.185195333	5.510800143
GPR84	2.615458358	0.498819	5.243296	1.58E-07	3.89E-05	4.562793111	5.923592934
CDC42EP1	2.584476285	0.503192	5.136161	2.80E-07	6.15E-05	3.850052746	5.047192383
CDA	2.511516789	0.494641	5.077451	3.83E-07	8.28E-05	3.795760363	4.905958734
LPAR1	2.489597482	0.430616	5.781482	7.40E-09	2.92E-06	4.309036284	5.61479244
FAM127C	2.484470805	0.649126	3.827411	0.000129	0.010279	2.703005591	3.527991494
CXCL5	2.471649939	0.509193	4.854052	1.21E-06	0.000221	7.815298248	9.353058605
TIFAB	2.470237877	0.738775	3.343694	0.000827	0.042537	2.946708582	3.905951445
MSR1	2.464043688	0.506729	4.862644	1.16E-06	0.000215	5.730586603	7.057665376
RTN1	2.459389725	0.452945	5.42977	5.64E-08	1.68E-05	4.814632831	6.13663653
FPR2	2.447902115	0.458717	5.336407	9.48E-08	2.63E-05	3.217218036	4.441548028
C2	2.429211788	0.376893	6.445369	1.15E-10	7.59E-08	5.077187028	6.383838821
MT1E	2.425969555	0.718355	3.377116	0.000733	0.038827	1.8587446	2.659906651
PTGDS	2.418592411	0.600898	4.024964	5.70E-05	0.005295	4.35620859	5.613856277
TIMP3	2.41150927	0.661106	3.647687	0.000265	0.017862	4.939966201	5.940408997
DSC2	2.400472724	0.501573	4.785886	1.70E-06	0.0003	3.794322575	5.037415027
TNFRSF9	2.398691656	0.50504	4.749513	2.04E-06	0.000336	5.043936003	6.340854187
TFPI	2.389388921	0.624174	3.828081	0.000129	0.010279	2.812443585	3.705247277

SAMD4A	2.385365493	0.557682	4.27729	1.89E-05	0.002061	4.374930783	5.57454348
TIE1	2.38341902	0.63878	3.731207	0.000191	0.013559	4.012050775	4.885536361
CSF1	2.37726335	0.415585	5.720284	1.06E-08	4.00E-06	7.404226384	8.565177123
ADAMDEC1	2.362678981	0.393012	6.011722	1.84E-09	1.00E-06	6.462885682	7.747883958
RTN4RL2	2.328651608	0.643397	3.619305	0.000295	0.019442	3.980305975	4.934984123
IL1RN	2.30478328	0.532014	4.332188	1.48E-05	0.001711	6.084326651	6.963612062
TGFA	2.294242964	0.415541	5.521096	3.37E-08	1.11E-05	3.52472785	4.693753884
LDHD	2.27964988	0.653997	3.485718	0.000491	0.028715	2.209035353	2.855411095
TSPAN15	2.264951581	0.397169	5.702733	1.18E-08	4.33E-06	4.1508152	5.208028694
A2M	2.262830322	0.528847	4.2788	1.88E-05	0.002061	4.8079415	5.815978803
CBX2	2.246039797	0.648436	3.46378	0.000533	0.030932	1.535814257	2.418783091
PHLDA3	2.216261722	0.493825	4.487948	7.19E-06	0.001017	5.681075852	6.862112308
MREG	2.202493167	0.413215	5.330141	9.81E-08	2.67E-05	5.513168253	6.584007332
GPR150	2.189617865	0.660511	3.315037	0.000916	0.045949	2.498785733	3.395116423
PPM1H	2.158482329	0.599986	3.597554	0.000321	0.020772	3.361673765	4.370781455
ZNF366	2.145760737	0.601813	3.565496	0.000363	0.022855	3.255714277	4.107759816
C17orf96	2.144970685	0.489167	4.384942	1.16E-05	0.001454	6.132419143	7.307959685
PLAU	2.144497271	0.501344	4.277493	1.89E-05	0.002061	5.4716579	6.75269536
ZNF618	2.137287136	0.566022	3.775982	0.000159	0.012104	3.10857692	4.086807059
TMEM176B	2.132997105	0.512796	4.159547	3.19E-05	0.003188	6.849769687	8.019348051
PLAUR	2.111031835	0.280184	7.53444	4.90E-14	7.04E-11	5.727854979	6.816071225

PDCD1LG2	2.098348	0.452356	4.638705	3.51E-06	0.000538	3.8515348	4.995069464
PRKCDBP	2.097546699	0.472707	4.437304	9.11E-06	0.001209	3.774291278	4.704240818
DST	2.096791802	0.404277	5.186523	2.14E-07	5.05E-05	3.403828787	4.445323266
LILRB4	2.090648151	0.317599	6.582658	4.62E-11	3.32E-08	7.023214378	8.143477734
SIGLEC15	2.079723103	0.596395	3.487154	0.000488	0.028667	3.34345732	4.138771974
STEAP3	2.077690072	0.538506	3.858248	0.000114	0.009204	5.676499042	6.949527809
C1S	2.073592619	0.418188	4.958522	7.10E-07	0.000142	5.032248321	6.16824813
IL4I1	2.0720521	0.627954	3.299687	0.000968	0.048231	6.753139574	8.018442978
CRTAM	2.058016668	0.397966	5.171334	2.32E-07	5.32E-05	3.421394275	4.447714953
E2F2	2.048348164	0.539164	3.799121	0.000145	0.011244	2.753861549	3.89767876
SERPINA1	2.03150396	0.378247	5.37084	7.84E-08	2.29E-05	5.710689004	6.969767601
GADD45G	2.031244364	0.518212	3.919716	8.87E-05	0.007489	3.401437528	4.369301519
SLC1A3	1.99517996	0.584703	3.412295	0.000644	0.035332	5.477782165	6.47126489
QPCT	1.991083695	0.410293	4.852838	1.22E-06	0.000221	3.666247963	4.746379519
APBA1	1.983135603	0.504194	3.933275	8.38E-05	0.007194	3.739169082	4.709318248
STAT1	1.981890105	0.356148	5.564791	2.62E-08	8.82E-06	9.495398091	10.74298069
SEMA3A	1.962978794	0.542346	3.619419	0.000295	0.019442	3.482740835	4.345685706
ADAMTS14	1.945162117	0.569193	3.417405	0.000632	0.034917	3.18210349	4.288981994
CECR6	1.931012046	0.432183	4.468046	7.89E-06	0.001084	3.721786856	4.637300096
LGALS3BP	1.925234014	0.441184	4.363785	1.28E-05	0.001565	6.019772323	7.189864882
OLR1	1.91422206	0.444873	4.30285	1.69E-05	0.001918	4.567127206	5.666832353

MSC	1.904327179	0.400119	4.759404	1.94E-06	0.000328	6.007669842	7.0151259
NHS	1.891086119	0.555742	3.402812	0.000667	0.03608	2.500424126	3.358133897
SDC4	1.886936549	0.322086	5.858485	4.67E-09	2.05E-06	5.598424331	6.622193422
FSCN1	1.884562399	0.410634	4.589399	4.45E-06	0.000675	6.268463806	7.283809482
SERPINE1	1.868627725	0.528946	3.532738	0.000411	0.02518	5.039959913	6.113502445
ICAM1	1.865175567	0.454343	4.105213	4.04E-05	0.003915	8.159556908	9.272797397
CRIM1	1.8595304	0.473016	3.931222	8.45E-05	0.007216	6.251741337	7.249421139
TTC7B	1.855936865	0.431351	4.302614	1.69E-05	0.001918	4.139051105	5.045587965
MMP14	1.85207004	0.426737	4.340078	1.42E-05	0.001679	9.851417816	10.85562218
QPRT	1.827217727	0.538365	3.394014	0.000689	0.037006	3.983546535	4.847414531
CLEC7A	1.8259118	0.26056	7.007655	2.42E-12	2.55E-09	6.787067164	7.813706321
PVRL2	1.816874544	0.308624	5.887023	3.93E-09	1.77E-06	6.284927503	7.29920649
SCN1B	1.804112598	0.503165	3.585529	0.000336	0.021426	3.546342209	4.373289918
GPR141	1.799936523	0.538271	3.343923	0.000826	0.042537	4.129112945	5.148662041
NRP1	1.770450064	0.350115	5.056769	4.26E-07	8.98E-05	7.602675168	8.637881655
LINC01094	1.769017525	0.50248	3.520573	0.000431	0.026061	3.700976562	4.633324057
CTSB	1.759837871	0.378671	4.647407	3.36E-06	0.000521	12.71276193	13.72257275
MAP1A	1.740909391	0.455333	3.82338	0.000132	0.010397	3.983916724	4.79438377
TMEM176A	1.737015584	0.517542	3.356283	0.00079	0.040913	5.345163698	6.30735233
G0S2	1.727882546	0.501464	3.445678	0.00057	0.032379	3.936498337	4.792955296
GBP4	1.721031323	0.473705	3.63313	0.00028	0.018821	8.127818706	9.398371407

IFIT3	1.717430495	0.386377	4.444957	8.79E-06	0.001177	5.78840605	6.885662806
EMILIN1	1.71319934	0.383255	4.470127	7.82E-06	0.001084	6.688811307	7.625877516
CR1	1.703994902	0.40333	4.22482	2.39E-05	0.002485	4.315474518	5.234952521
LRP3	1.697773835	0.445617	3.809943	0.000139	0.010869	4.533592527	5.353975101
RNF207	1.687143094	0.461491	3.655852	0.000256	0.017452	2.811595968	3.643489424
FXYD6	1.687080663	0.480339	3.512272	0.000444	0.026719	3.363256865	4.320780463
CISH	1.678065571	0.37905	4.427031	9.55E-06	0.001247	5.400595563	6.361826753
KIAA1522	1.671504444	0.416317	4.014978	5.95E-05	0.005463	4.73952298	5.587551326
PXDC1	1.666247472	0.374798	4.445724	8.76E-06	0.001177	5.087743736	6.00327779
CACNA1A	1.664383947	0.446551	3.727196	0.000194	0.013593	6.167550872	7.345509983
CYP2S1	1.663761947	0.426342	3.90241	9.52E-05	0.00796	4.48900512	5.367128626
MGST1	1.649673448	0.417058	3.955504	7.64E-05	0.006665	4.902050939	5.711915634
CLEC11A	1.648301024	0.4372	3.770128	0.000163	0.012244	4.168739036	5.028223137
SPSB1	1.646824213	0.441712	3.728277	0.000193	0.013593	4.647949985	5.438176002
PRR11	1.638520221	0.273176	5.998042	2.00E-09	1.05E-06	4.598553953	5.548284217
CD38	1.628108205	0.483855	3.364869	0.000766	0.040177	3.184110173	4.052285894
HK3	1.627280516	0.44568	3.65123	0.000261	0.017693	6.328672451	7.156113749
TUSC1	1.62E+00	4.76E-01	3.414283	0.00064	0.035197	3.688615425	4.503893379
LOC100132891	1.621025043	0.438862	3.6937	0.000221	0.015245	3.539717581	4.324697037
CDCP1	1.613470182	0.42803	3.769524	0.000164	0.012244	3.576578679	4.377385621
SOCS3	1.606208769	0.402692	3.988675	6.64E-05	0.005963	6.850228029	7.822685109

CD300LF	1.586723111	0.349081	4.545433	5.48E-06	0.000802	4.398984912	5.193485115
ME1	1.575592507	0.299892	5.253859	1.49E-07	3.79E-05	4.430867963	5.207767067
NCS1	1.567630826	0.356399	4.398523	1.09E-05	0.001377	5.083364237	5.887082715
VSIG4	1.552228188	0.455146	3.410397	0.000649	0.035374	5.800552769	6.689975459
LAMB2	1.541601983	0.467975	3.294198	0.000987	0.048875	4.010206668	4.715167414
DAPK1	1.529660386	0.407361	3.755047	0.000173	0.012674	7.410945644	8.287764988
DRAM1	1.523557209	0.305749	4.983037	6.26E-07	0.000127	7.843388471	8.737692116
IGSF6	1.494036504	0.401289	3.723095	0.000197	0.013755	6.017348311	6.85664924
ZNF697	1.481319249	0.286314	5.173766	2.29E-07	5.32E-05	4.701802982	5.494242723
SLC7A11	1.455268134	0.304145	4.784789	1.71E-06	0.0003	8.404588054	9.28026671
GAS2L1	1.454118799	0.402813	3.609913	0.000306	0.019993	5.761362354	6.511316796
TBC1D16	1.426997086	0.408325	3.494754	0.000474	0.028177	5.387439627	6.142566086
EGR2	1.421167023	0.358133	3.968266	7.24E-05	0.006353	7.715223942	8.502206279
RCN1	1.415075253	0.39148	3.614685	0.000301	0.01971	4.84984228	5.773138518
IL13RA1	1.413919314	0.302262	4.677791	2.90E-06	0.000458	7.214300426	8.044699452
IL8	1.412098876	0.354772	3.980305	6.88E-05	0.006074	8.800519427	9.688728538
GSN	1.379571635	0.323789	4.260711	2.04E-05	0.002175	6.667014682	7.413904327
CYP1B1	1.379508647	0.314961	4.37994	1.19E-05	0.001477	11.12625466	11.91698286
PSTPIP2	1.3751902	0.418523	3.285814	0.001017	0.049616	6.826314333	7.612555235
COL8A2	1.374888112	0.361421	3.804113	0.000142	0.011074	6.048610369	6.860703528
IRF1	1.372668205	0.324528	4.229737	2.34E-05	0.002447	9.271304747	10.31693483

NR1H3	1.360850229	0.335129	4.060675	4.89E-05	0.004684	6.782265023	7.545468109
TNFAIP2	1.341269991	0.40851	3.283324	0.001026	0.049709	8.418716987	9.143392848
SMOX	1.338071113	0.354951	3.769739	0.000163	0.012244	4.650555634	5.394482567
SOD2	1.337102015	0.338985	3.944433	8.00E-05	0.006942	9.622857587	10.41539699
NRIP3	1.327510857	0.389328	3.409747	0.00065	0.035374	4.412116485	5.048162113
SLC8A1	1.319245512	0.288364	4.574932	4.76E-06	0.00071	6.186571119	6.94467915
EMR2	1.318678174	0.223206	5.907896	3.47E-09	1.61E-06	5.492923793	6.22111072
PHLDA2	1.316825898	0.345439	3.812037	0.000138	0.010831	3.518929106	4.160671923
FTH1	1.314352465	0.296534	4.432386	9.32E-06	0.001227	12.42247851	13.17506191
WBP5	1.310263131	0.326826	4.009052	6.10E-05	0.005534	4.480915332	5.185931098
LRP12	1.308681837	0.296702	4.41076	1.03E-05	0.001312	5.237593393	5.956953544
CTSL	1.307064611	0.36769	3.554803	0.000378	0.023432	8.165076798	9.003925476
NFAM1	1.293022788	0.375897	3.43983	0.000582	0.032838	7.893941397	8.661703406
MRC1	1.286677548	0.320591	4.013461	5.98E-05	0.005463	7.63812517	8.41236587
PTAFR	1.282629734	0.299627	4.280756	1.86E-05	0.002061	8.696884507	9.473556166
SCD	1.279602037	0.371262	3.446625	0.000568	0.032379	8.094244092	8.904858601
FBXO6	1.252642656	0.336008	3.728019	0.000193	0.013593	6.222487869	6.975905348
VDR	1.252341943	0.351775	3.560063	0.000371	0.023149	6.334891336	7.077692429
PRRG4	1.250462185	0.336774	3.713055	0.000205	0.014249	4.283328343	5.05196881
GLRX	1.224291998	0.322556	3.795596	0.000147	0.011294	6.066187111	6.784797888
SORT1	1.192866223	0.274473	4.346026	1.39E-05	0.001646	5.61722794	6.273527354

WARS	1.174485949	0.349514	3.360341	0.000778	0.040583	9.895620744	10.7103906
CD4	1.142979836	0.317778	3.596783	0.000322	0.020772	8.357101769	9.016755566
GALNT6	1.141681455	0.267452	4.268736	1.97E-05	0.002112	5.760946748	6.463982597
VANGL1	1.141398977	0.311227	3.667411	0.000245	0.016827	3.758494531	4.394404335
APOL6	1.137911252	0.260124	4.374499	1.22E-05	0.001502	9.482012437	10.33195001
PARP9	1.134157438	0.264915	4.281219	1.86E-05	0.002061	8.64216067	9.439790228
ITGB2	1.101961942	0.273781	4.024974	5.70E-05	0.005295	9.787509346	10.45695783
FNDC3B	1.097825905	0.291397	3.767461	0.000165	0.012259	6.630309259	7.293599959
ARHGAP31	1.096869722	0.184199	5.954805	2.60E-09	1.33E-06	8.102767813	8.787197005
ACTN1	1.032773883	0.313724	3.291982	0.000995	0.048955	6.270576905	6.867922322
ARRDC4	1.028201506	0.256184	4.013524	5.98E-05	0.005463	6.034255799	6.623128108
PLD3	1.012249133	0.247666	4.087159	4.37E-05	0.004206	10.59298382	11.18672339
SGMS2	1.005630188	0.286347	3.511929	0.000445	0.026719	4.497613558	5.116981833
UBE2L6	1.00070244	0.259785	3.85204	0.000117	0.009392	8.597448871	9.330144786
TXN	0.97339544	0.289844	3.358343	0.000784	0.040743	4.616988131	5.156539
NFKBIA	0.971499409	0.274468	3.539571	0.000401	0.024729	9.086207819	9.775131437
IL15RA	0.951760798	0.28226	3.371926	0.000746	0.039434	5.951039122	6.637743017
EPSTI1	0.920621967	0.276221	3.332912	0.000859	0.043651	7.305540578	7.990038534
CDKN1A	0.917031452	0.207578	4.417774	9.97E-06	0.001291	9.086247563	9.674095561
OAS3	0.911452261	0.258666	3.523663	0.000426	0.025858	8.089851891	8.767542925
PLEK	0.909576196	0.241499	3.766371	0.000166	0.012259	9.049542707	9.60947955

SIRPA	0.896194474	0.264959	3.382387	0.000719	0.038347	9.224259594	9.762751504
DTX3L	0.89335188	0.209908	4.255916	2.08E-05	0.002207	10.03192658	10.65075862
MOB3B	0.889248009	0.260161	3.418065	0.000631	0.034917	5.103679081	5.653567799
CREG1	0.884129157	0.265135	3.334634	0.000854	0.043521	9.77881841	10.30289055
TRIM21	0.871340446	0.221963	3.92561	8.65E-05	0.007347	7.67616144	8.274978937
LAP3	0.869162439	0.235269	3.694342	0.00022	0.015245	6.640079525	7.221350461
SAMD9L	0.858141057	0.257549	3.331958	0.000862	0.04366	9.450360184	10.10564841
PANDAR	0.844434633	0.215836	3.912388	9.14E-05	0.007679	8.1406666	8.707774192
SQRDL	0.809132638	0.208456	3.881554	0.000104	0.008495	6.795210478	7.306393762
STX11	0.805145162	0.206669	3.895819	9.79E-05	0.008076	8.227171916	8.770137681
IFIH1	0.79526682	0.212194	3.747825	0.000178	0.012895	7.769123303	8.315472393
TAP1	0.793857952	0.22478	3.531713	0.000413	0.025181	10.10645246	10.72183956
NCF2	0.782352206	0.234875	3.330928	0.000866	0.043682	8.159922926	8.63589692
GBP3	0.766277835	0.232721	3.292689	0.000992	0.048955	6.569272518	7.105437543
PARP14	0.759049027	0.196615	3.860587	0.000113	0.009163	10.40799141	10.94856917
PLXNA1	0.743149699	0.197736	3.75829	0.000171	0.012569	8.397245163	8.882458581
S100A11	0.71940713	0.166106	4.331	1.48E-05	0.001711	7.331013641	7.766355143
MCL1	0.678802868	0.161914	4.192367	2.76E-05	0.002832	12.42520851	12.90463029
BPGM	0.675198951	0.169395	3.985942	6.72E-05	0.005969	6.869370351	7.341985072
PLOD1	0.66587457	0.185647	3.586782	0.000335	0.02141	6.352201592	6.776201013
GNS	0.651923791	0.142149	4.586207	4.51E-06	0.000679	10.20985295	10.61944687

CD59	0.63123875	0.1628	3.87738	0.000106	0.008597	9.246134461	9.663956475
PGD	6.23E-01	1.72E-01	3.625947	0.000288	0.019108	8.270082583	8.658090527
ACO1	0.579587026	0.176171	3.28992	0.001002	0.049162	6.461648692	6.820603187
PRCP	0.563449449	0.167492	3.36403	0.000768	0.040177	8.259459453	8.637617111
WDFY1	0.562897437	0.149968	3.753442	0.000174	0.012697	10.0799269	10.47454181
PKM	0.554604485	0.163931	3.383159	0.000717	0.038347	11.09969364	11.46298606
ATP6V1A	0.519134428	0.150471	3.450053	0.00056	0.032311	8.859468141	9.196640715
TAP2	0.50549182	0.144042	3.509336	0.000449	0.026879	10.31773321	10.68956285
PLIN3	0.497820508	0.138705	3.589047	0.000332	0.021311	8.473635063	8.805794073
ARHGAP17	0.458817886	0.128772	3.56302	0.000367	0.02298	8.866751019	9.193224248
NECAP2	0.407313225	0.118964	3.423827	0.000617	0.034343	9.135100424	9.413017019
ADAR	0.314667647	0.087922	3.578937	0.000345	0.021886	11.99512068	12.22772073
CDC42SE2	0.301087677	0.091309	3.297461	0.000976	0.048463	11.48281287	11.70869316

Appendix Table 7.4 Differential Gene Expression Analysis of significantly downregulated genes in CLL samples.

Differential Gene Expression of significantly downregulated genes in the comparison between CLL alone (CLL) with CLL cultured with NLC (CLLcc). The genes are listed according to their log2fold change among CLLcc where CLL alone is the control. All the genes are statistically significant with their pvalue and padj values mentioned.

Gene	log2FoldChange	lfcSE	stat	pvalue	padj	ExpressionLevelCLL	ExpressionLevelCLLcc
SLC12A9	-0.277864424	0.069714	-3.98576	6.73E-05	0.005969	9.832294893	9.62873565
ABHD16A	-0.400266298	0.121825	-3.29E+00	0.001018	0.049616	7.635560807	7.348312123
YPEL4	-0.859812745	0.250681	-3.4299	0.000604	0.033728	5.777184655	5.233534269
RN7SK	-1.211002739	0.355222	-3.41E+00	6.52E-04	0.035374	6.430653545	5.559862195

Appendix Table 7.5 Differential Gene Expression Analysis of significantly upregulated genes in NLC samples.

Differential Gene Expression of significantly upregulated genes in the comparison between NLC alone (NLC) with NLC cultured with CLL (NLCcc). The genes are listed according to their log2fold change among NLCcc where NLC alone is the control. All the genes are statistically significant with their pvalue and padj values mentioned.

Gene	log2FoldChange	lfcSE	stat	pvalue	padj	ExpressionLevelNLC	ExpressionLevelNLCcc
GLRA3	3.918075639	0.901167	4.35E+00	1.38E-05	0.044912	1.387227048	2.730208571
PPBP	3.175807416	0.636214	4.991726	5.98E-07	0.005863	4.312860313	6.851488588
CD28	2.619639645	5.21E-01	5.028325	4.95E-07	0.005863	7.156489894	8.83889896
CXCL1	2.062421425	4.79E-01	4.31E+00	1.63E-05	0.045677	7.216240319	8.879749244

Appendix Table 7.6 Differential Gene Expression Analysis of significantly downregulated genes in NLC samples.

Differential Gene Expression of significantly downregulated genes in the comparison between NLC alone (NLC) with NLC cultured with CLL (NLCcc). The genes are listed according to their log2fold change among NLCcc where NLC alone is the control. All the genes are statistically significant with their pvalue and padj values mentioned.

Gene	log2FoldChange	lfcSE	stat	pvalue	padj	ExpressionLevelNLC	ExpressionLevelNLCcc
SLC1A5	-0.775945044	1.77E-01	-4.38E+00	1.18E-05	0.044912	11.29980371	10.71055042
GATA4	-1.79E+01	3.744001	-4.77E+00	1.83E-06	0.011974	-1.249859707	-1.474156508
RP11-40F8.2	-1.91E+01	4.23E+00	-4.52E+00	6.32E-06	0.030963	-1.294469758	-1.415283878

7.10 Primer Designing

Appendix Table 7.7 Sequence of the primers used to validate DGEA of RNAseq data.

Genes of interest and their primer sequences, product lengths, genotype length, GC content and expected Tm. Genes are selected as described from DGEA.

Gene	Direction	Primer	Product length	Genotype length	GC content %	Temperature (salt adjusted)
CCL13	F	GCAGGTGTCCCCAGAAG	83	519	65	57.3
	R	CTGGACCCACTTCTCCTTT			53	57.5
CXCL9	F	AAGTGGGAGAAACAGGTCAG	131	1240	50	58.4
	R	GGTGAAGTGGTCTCTTATGTAGTC			46	63.6
NUPR1	F	TGAGACAGAGCTGGAGATGAG	90	426	52	61.2
	R	ATCCTGTCCTGGGTCCTC			61	58.4
CXCL12	F	TACAGATGCCCATGCCGAT	225	2264	52.6	60.5
	R	GTGGGTCTAGCGGAAAGTCC			60	62.5
EGLN3	F	GGCGTCTCCAAGCGACAC	246	19426	67	60.8
	R	GCAGGTGATGCAGCGACCAT			60	62.5
GBP1	F	GGGCGACTGATGGCGAAT	243	2963	61	58.4
	R	CTCGGTGTCCAGCAGAACTA			55	60.5
EBI3	F	GCTCCCTACGTGCTCAATGT	221	1580	55	60.5
	R	CCCTGACGCTTGTAACGGAT			55	60.5
CSF1	F	GCCATCAAGAGCCTCAGAG	119	>4119	58	59.5
	R	TGTGCGTCCAGCTTAGAATT			45	56.4
STEAP3	F	GGAGGGAGTTCAGCTTCGTT	124	8208	55	60.5
	R	GGCAGGTAGAACTTGTAGCGG			57	63.2
EGR2	F	CCTTTGACCAGATGAACGG	97	1489	53	57.5
	R	AAGCTGCTGGGATATGGG			56	56.3
MCL1	F	GTCTCGAGTGATGATCCATGTT	254	1006	45.5	60.1
	R	CATTCCTGATGCCACCTTCT			50	58.4
CXCL10	F	TGTACGCTGTACCTGCATCA	268	920	50	58.4
	R	CTGTGTGGTCCATCCTTGGAA			52.38	61.2
YPEL4	F	TCACCGCACTTACAGCTGTG	260	1003	55	60.5
	R	TCCCTTCCTTGTACTTCTGGC			52.38	61.2
GAPDH	F	TCACCATCTTCCAGGAGCGA	401	905	55	60.5
	R	GATGATGTTCTGGAGAGCCC			55	60.5

7.11 Reference Gene comparisons

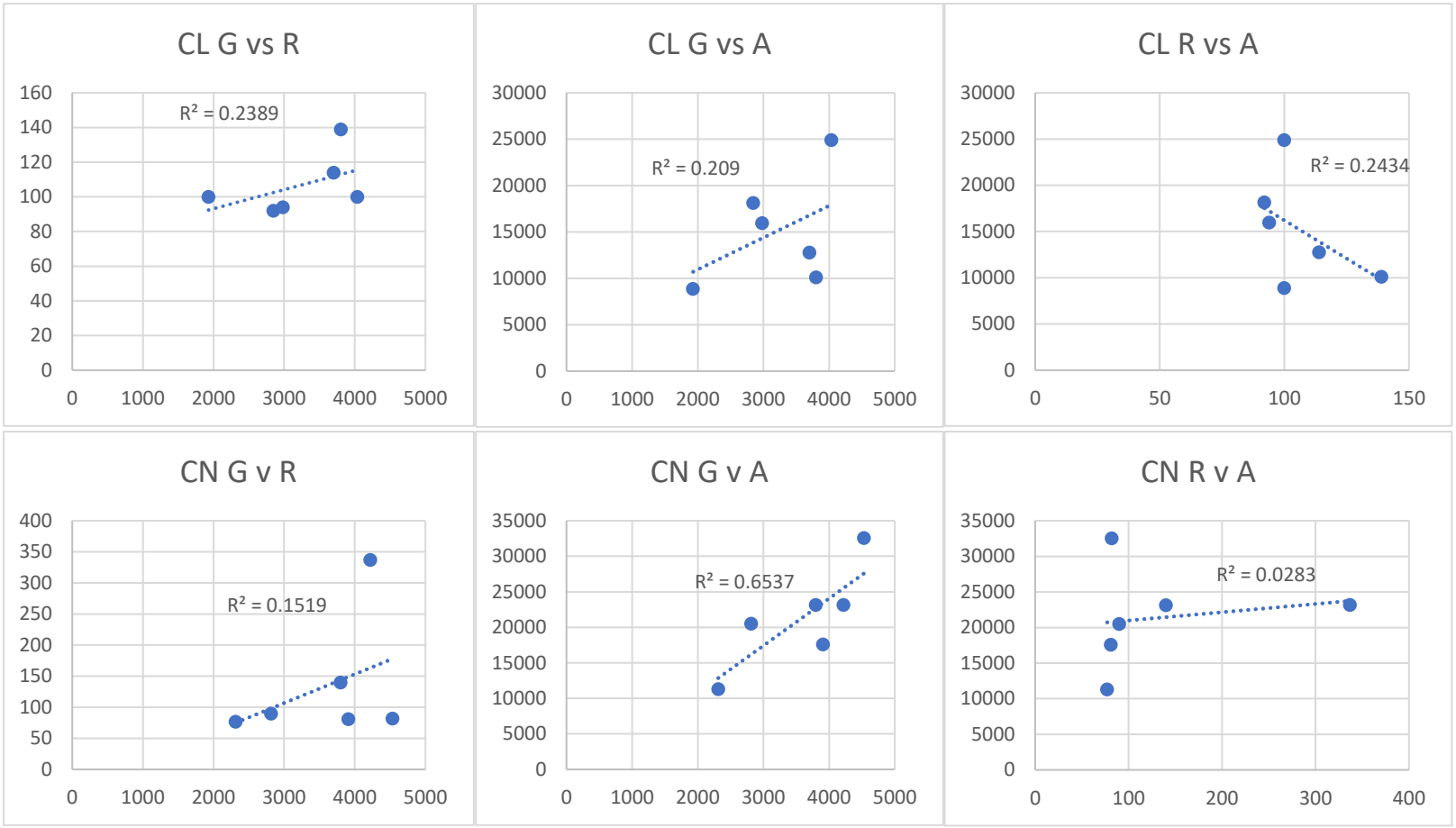

Appendix Figure 7.11 Linear correlation graphs to compare the housekeeping genes from DGEA.

Correlation between the reference genes GAPDH (G), RL27 (R) and Beta Actin (A) of samples from CLL cultured alone (CL) and CLL cultured with NLCs (CN).

7.12 Clinical Data analysis of the combined data

I attempted to analyse the samples based on their clinical data (See Appendix Table 7.1) to explain the findings and found that the majority of the samples were untreated (except for 2) and originating from different patients (except two). As seen in Appendix Table 7.8, a comparison between samples treated (with ibrutinib) and untreated of the same patient, shows an almost complete reversal in gene expression changes of each gene of interest.

Appendix Table 7.8 Comparison of gene expression changes between samples that were treated and untreated from the same case.

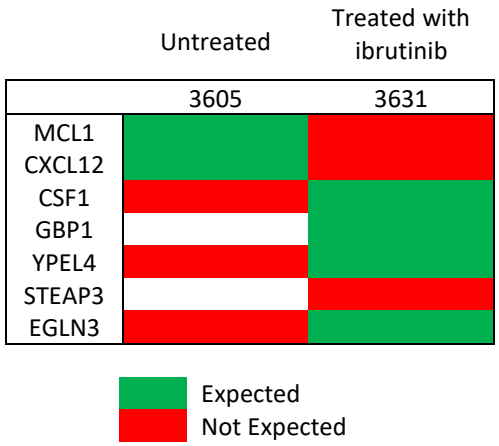

Comparison of gene expression changes from samples #3605 and #3631 which were derived from the same patient. Sample #3631 was collected after the patient was treated with ibrutinib for approximately one month. Changes that are in agreement by both RT-qPCR and DGEA of RNA-seq are in green and those that are not in agreement are in red. The gene expression changes are those from samples that are CLL alone and CLL in co-culture with NLCs. Gaps are indicated where qPCR data was not obtainable. These samples were not sent for RNA-seq.

It is possible to consider that based on this finding, that the treatment with ibrutinib in this patient may have caused a change in the direction of gene expression of these selected genes. However, further investigations are required.

Given that the reliability of the RNA-seq results were confirmed, I then proceeded with pathway analysis by the Bioinformatics team.

7.13 Other Pathways generated from DAVID KEGG analysis

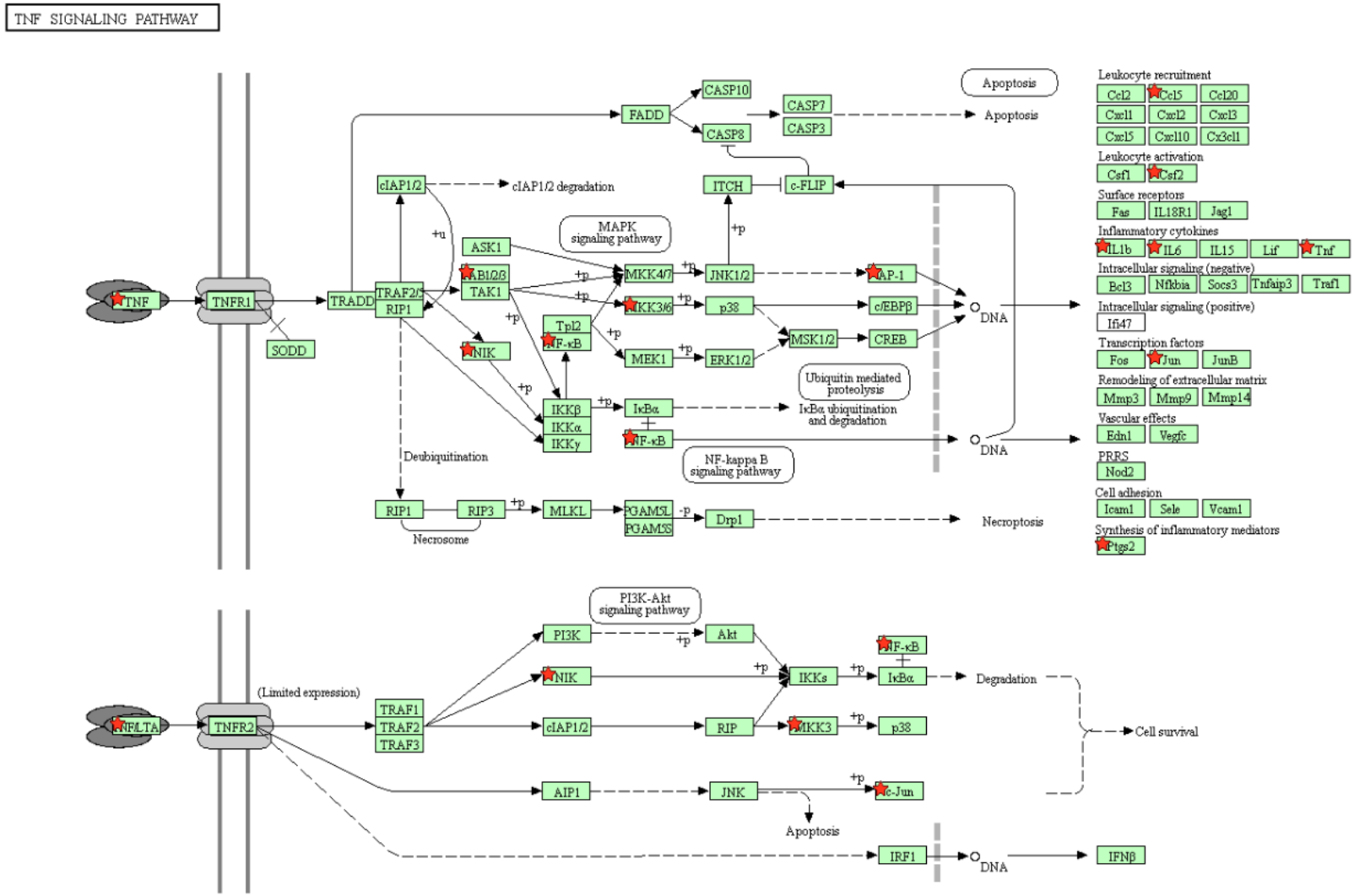

Appendix Figure 7.12 DAVID KEGG pathway analysis; mRNA targeted genes (red star) are involved in tumour necrosis factor (TNF) signalling pathway

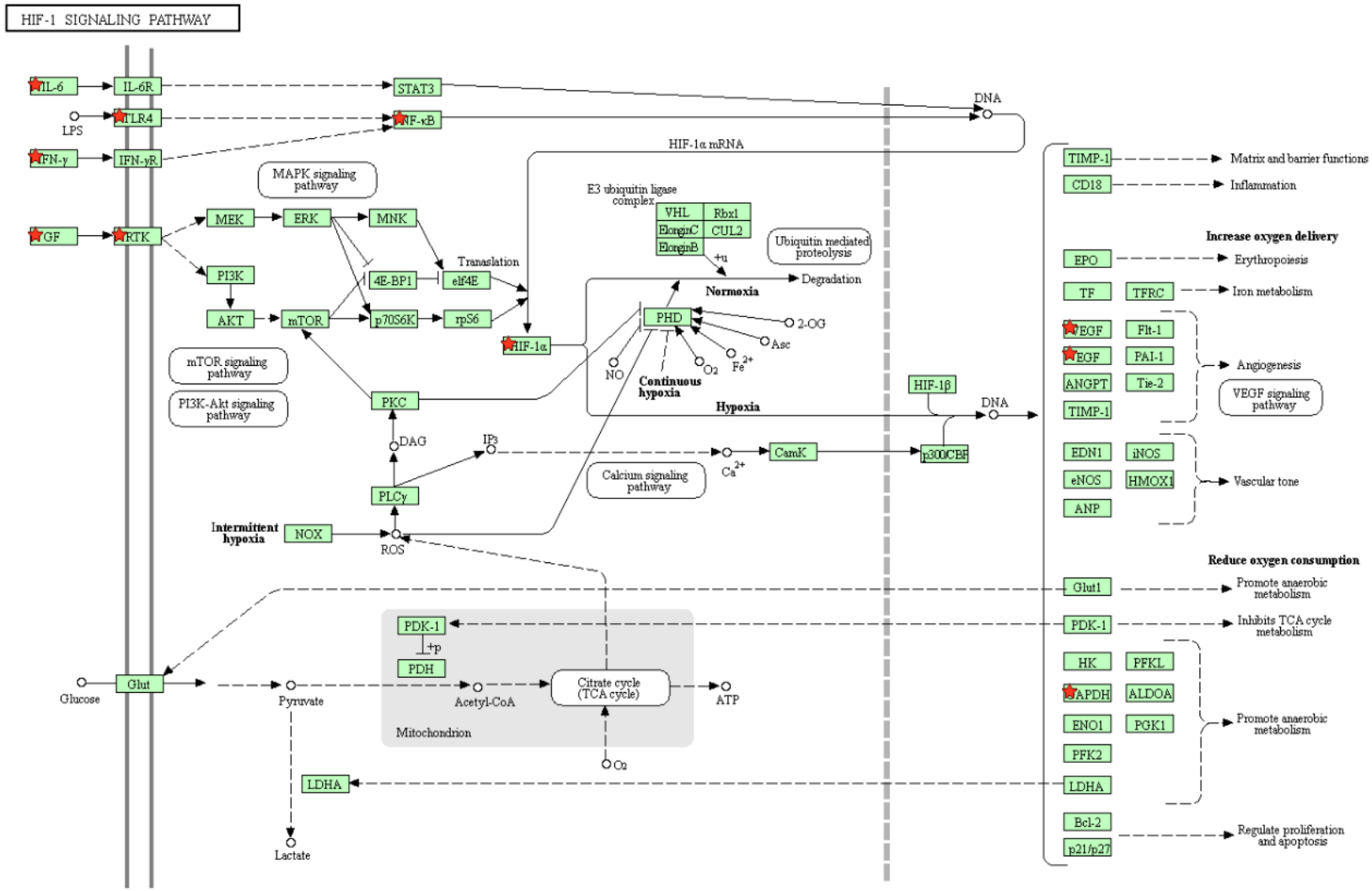

Appendix Figure 7.13 DAVID KEGG pathway analysis; mRNA targeted genes (red star) are involved in Hypoxia-Inducible factor-1 (HIF-1) signalling pathway

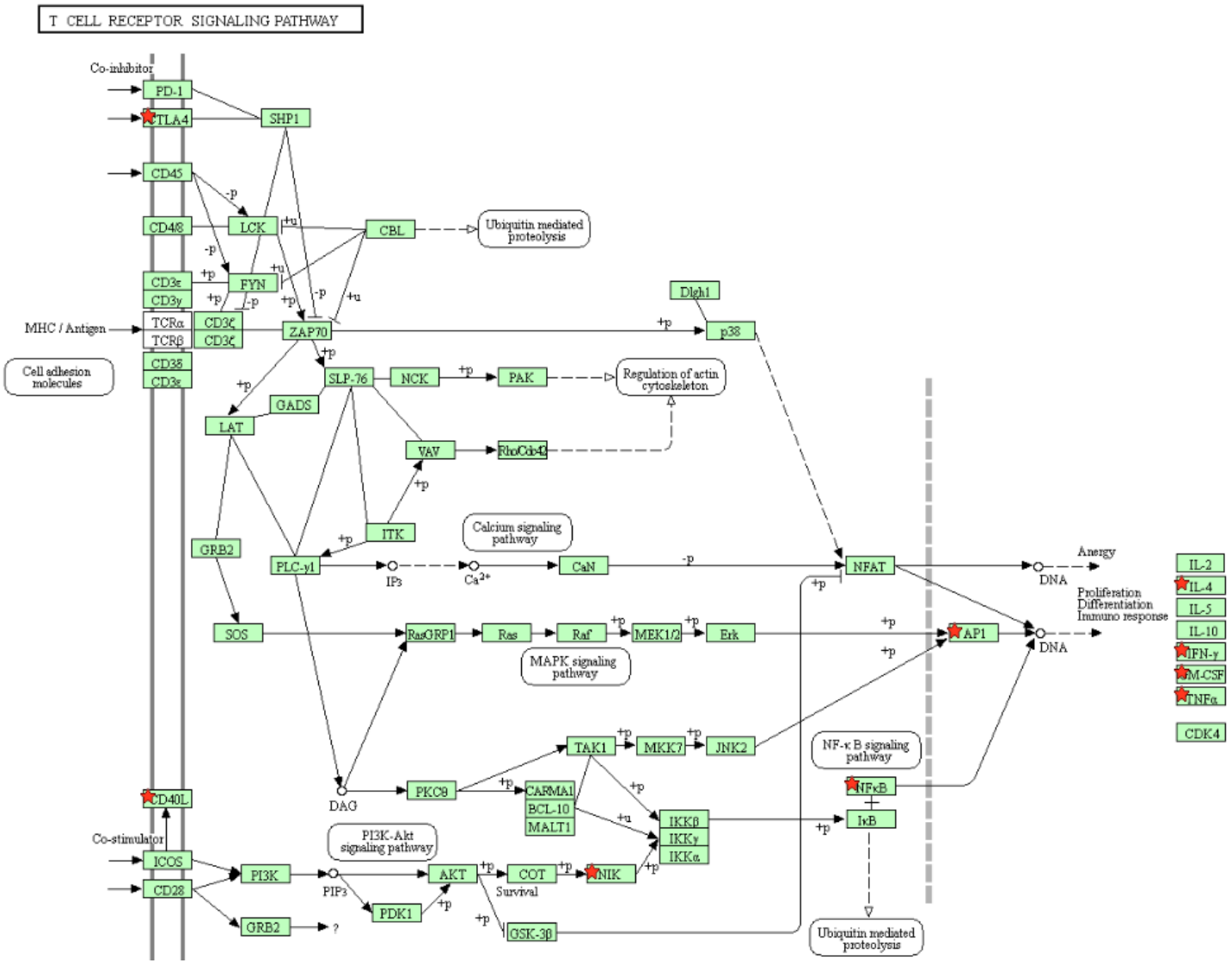

Appendix Figure 7.14 DAVID KEGG pathway analysis; mRNA targeted genes (red star) are involved in T cell receptor signalling pathway

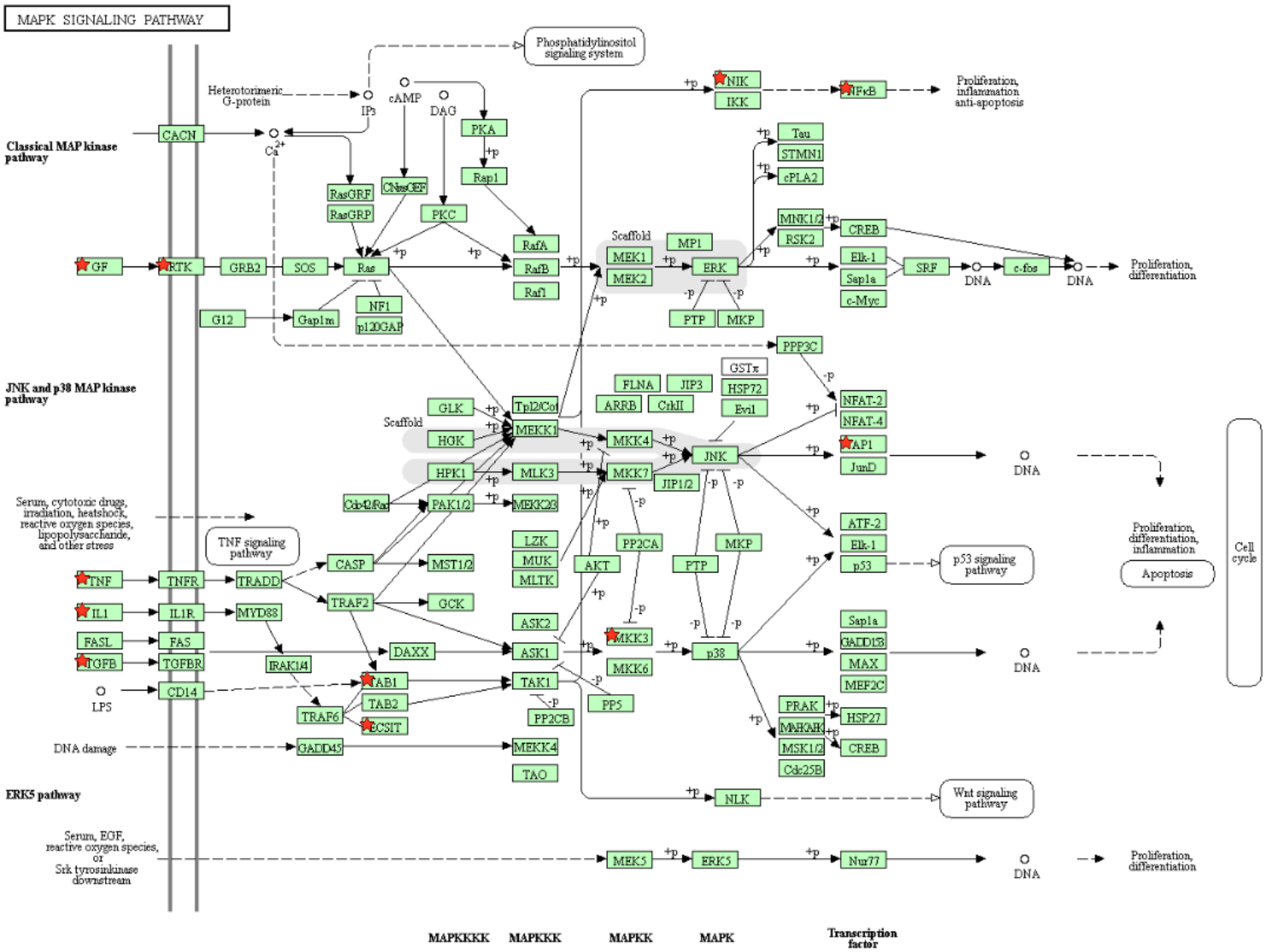

Appendix Figure 7.15 DAVID KEGG pathway analysis; mRNA targeted genes (red star) are involved in MAP kinase (MAPK) signalling pathway

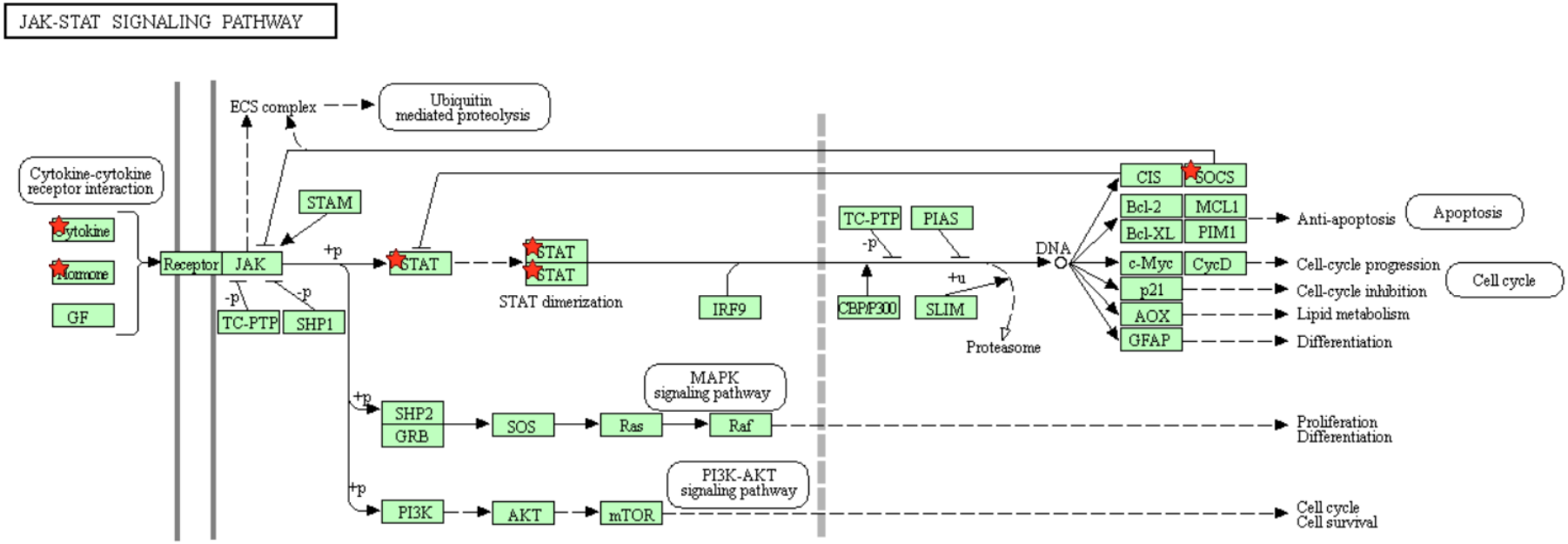

Appendix Figure 7.16 DAVID KEGG pathway analysis; mRNA targeted genes (red star) are involved in JAK-STAT signalling pathway.

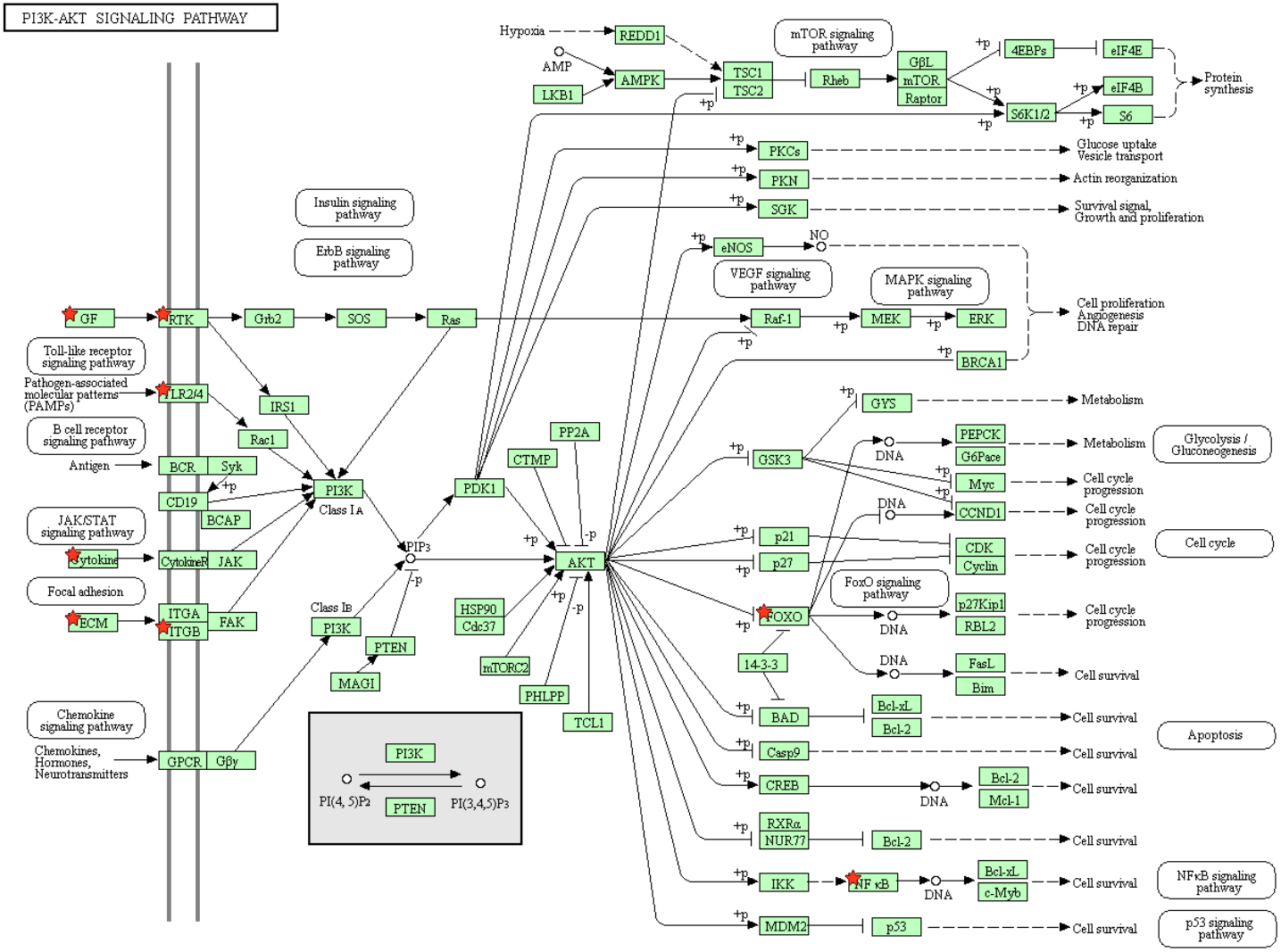

Appendix Figure 7.17 DAVID KEGG pathway analysis; mRNA targeted genes (red star) are involved in PI3 kinase- AKT (PI3K-AKT) signalling pathway

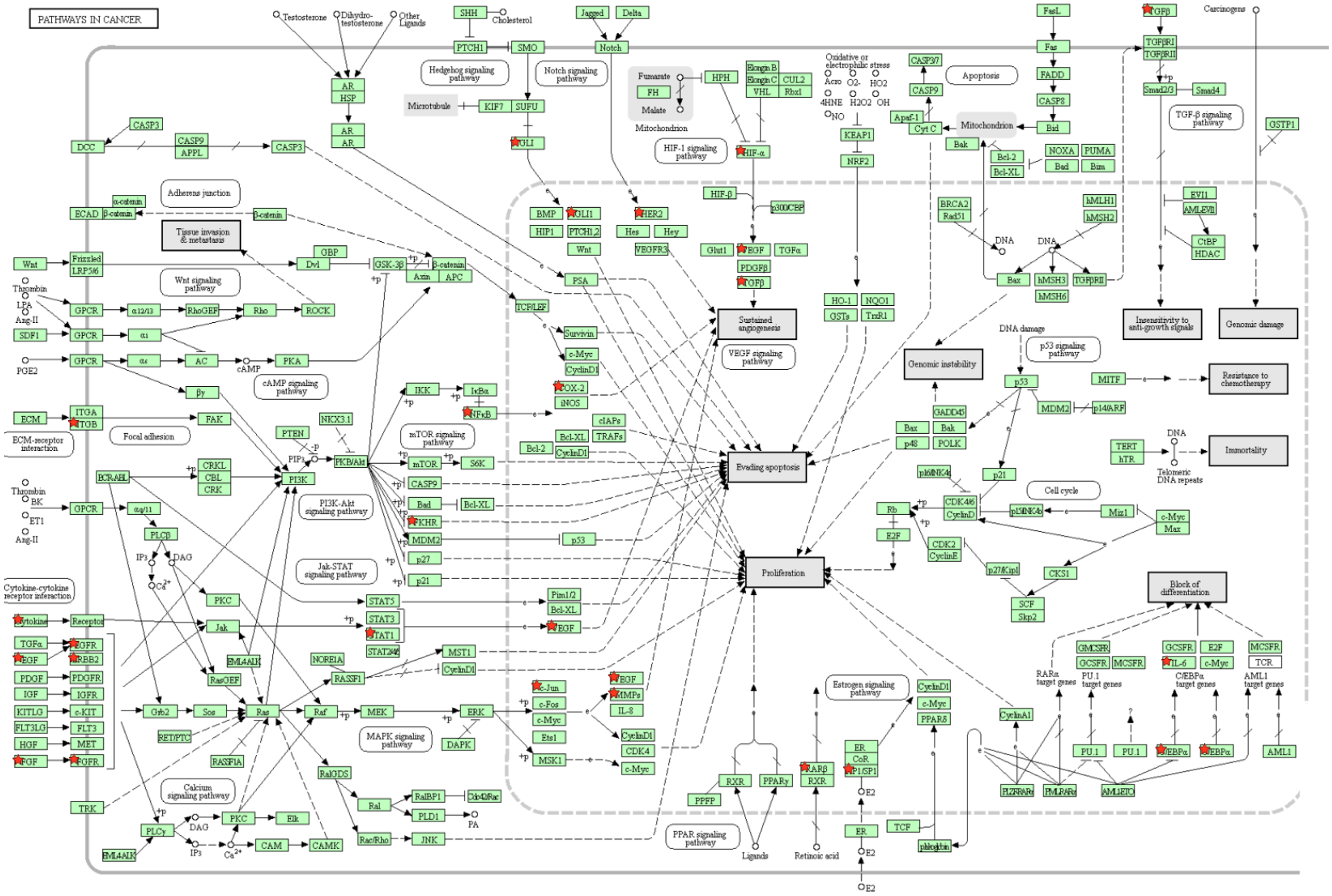

Appendix Figure 7.18 DAVID KEGG pathway analysis; mRNA targeted genes (red star) are involved known pathways in cancer

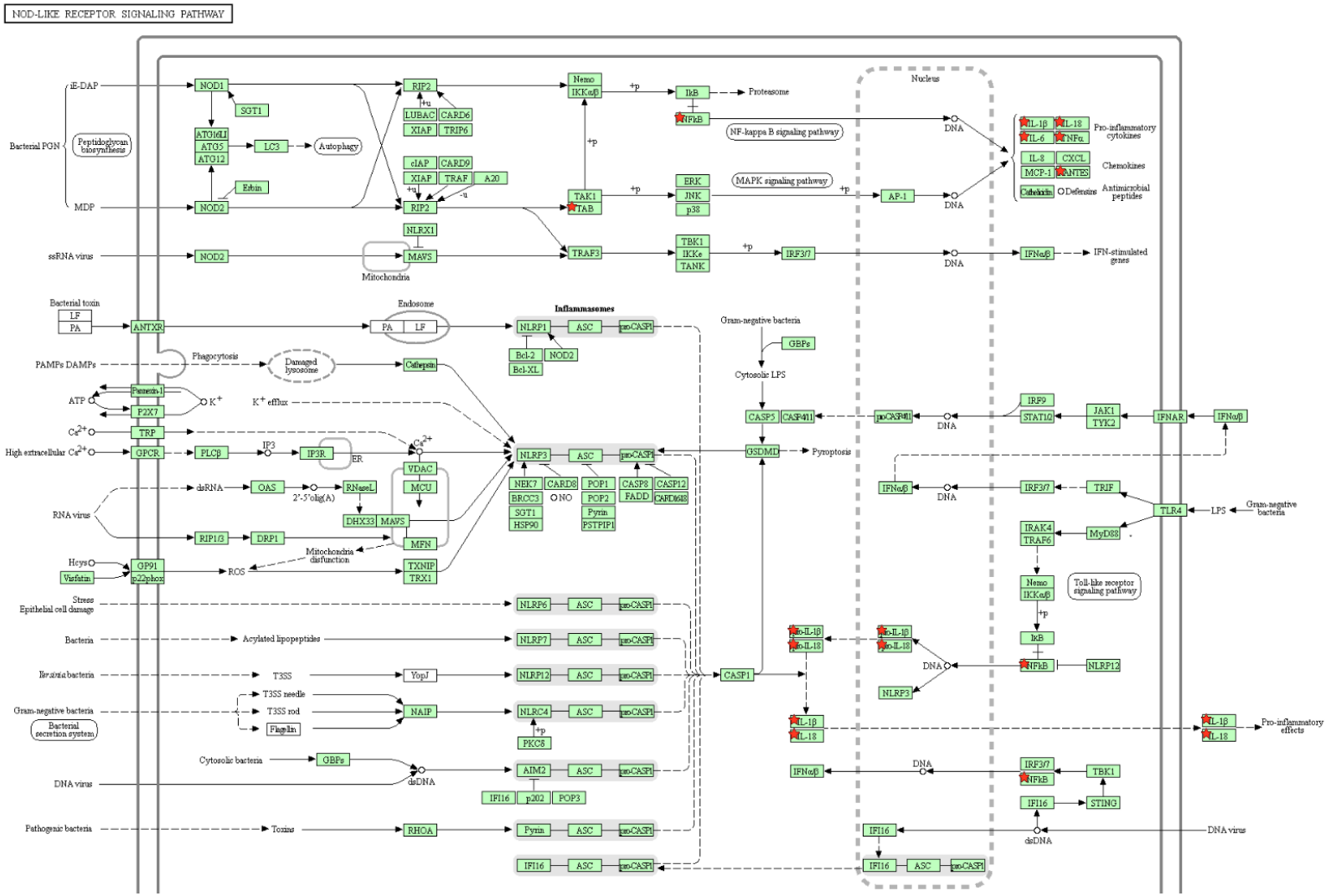

Appendix Figure 7.19 DAVID KEGG pathway analysis; mRNA targeted genes (red star) are involved in nucleotide-binding oligomerization domain-like (NOD-Like) receptor signalling pathway

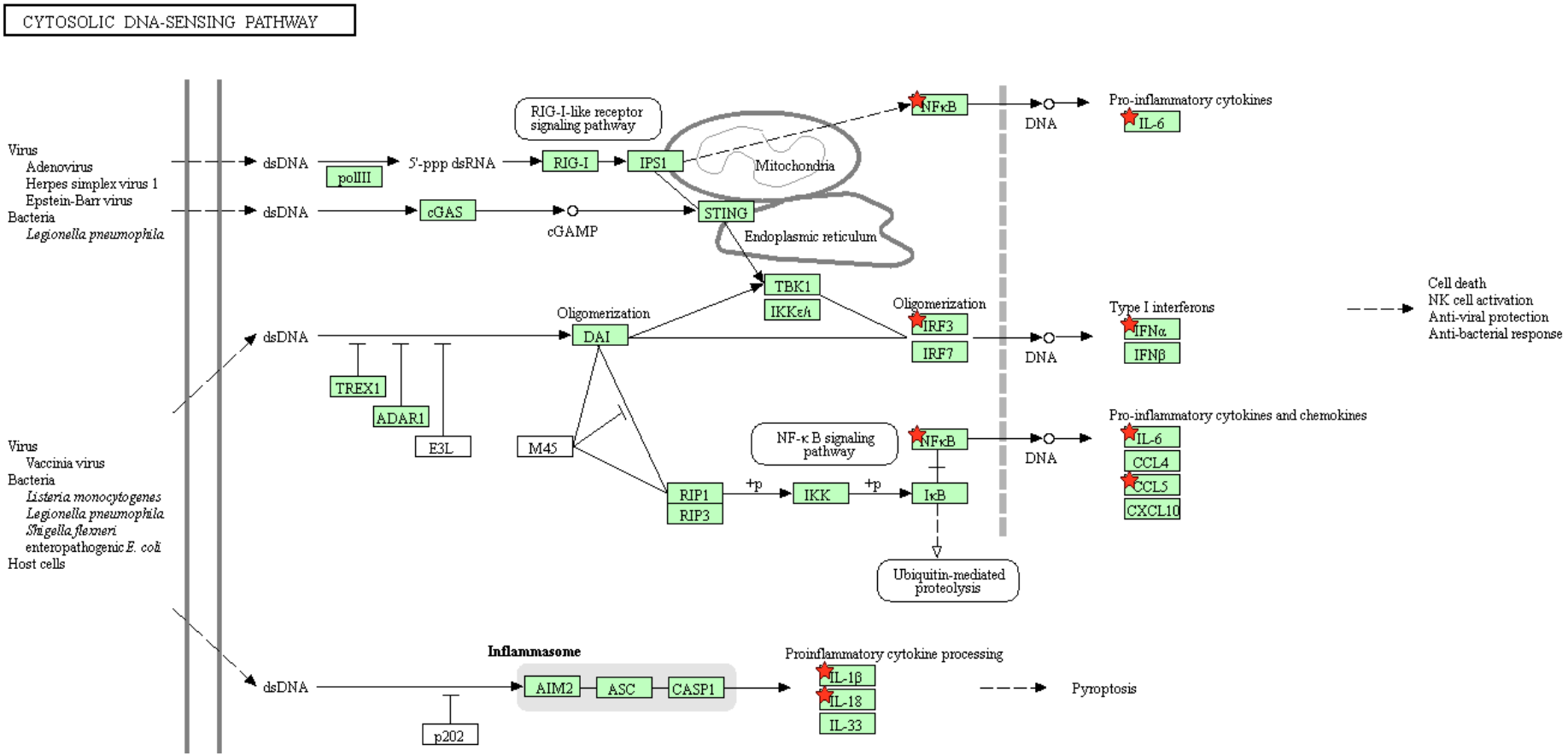

Appendix Figure 7.20 DAVID KEGG pathway analysis; mRNA targeted genes (red star) are involved in cytosolic DNA-sensing pathway

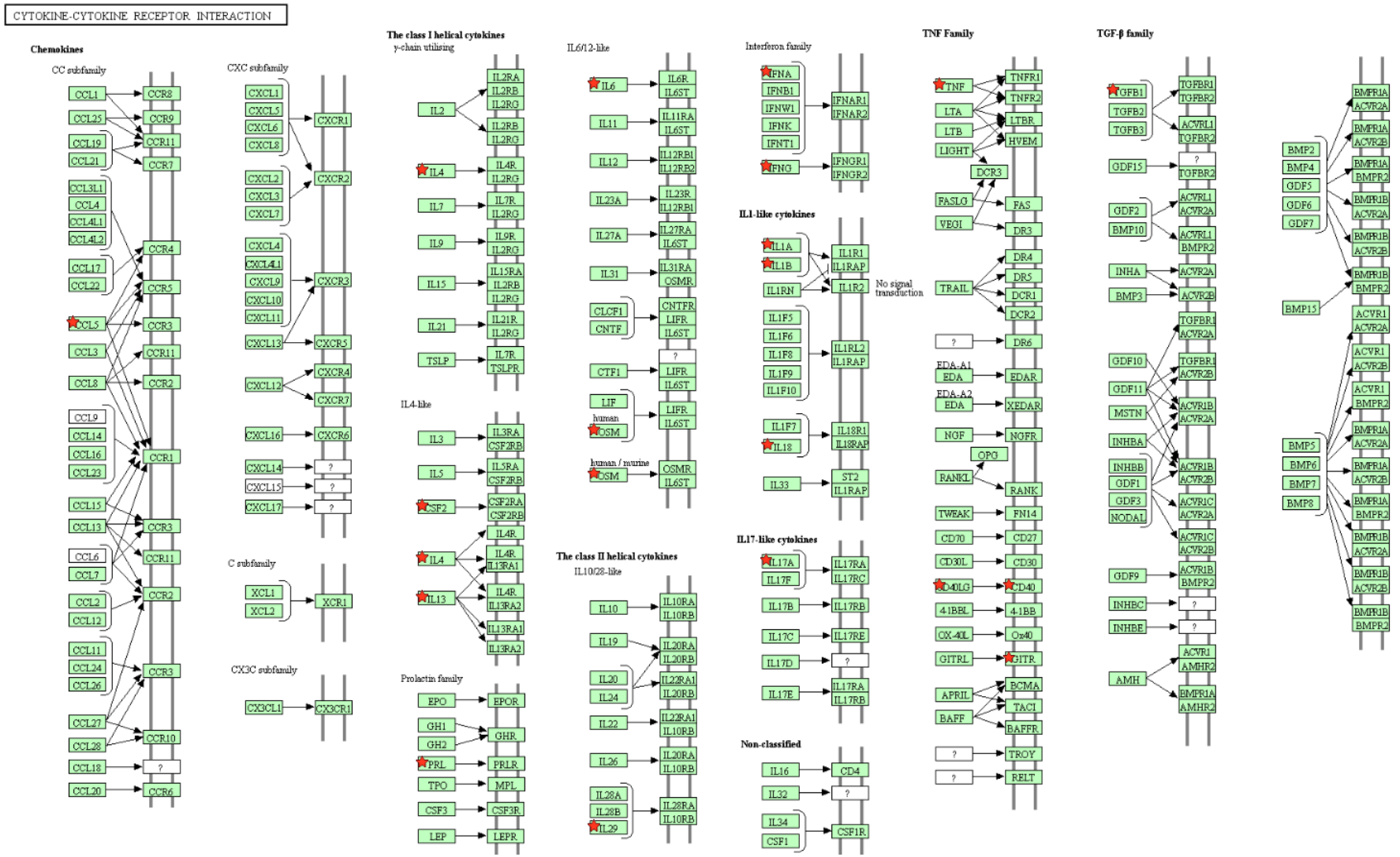

Appendix Figure 7.21 DAVID KEGG pathway analysis; mRNA targeted genes (red star) are involved in Cytokine-cytokine receptor interactions.

7.14 Protocols

7.14.1 PBMC and Plasma Separation

Into 50ml falcon tubes, pour Lymphoprep solution in a ratio of 2:1 ratio of blood to Lymphoprep. Blood sample is slowly poured on top of the lymphoprep making sure that blood doesn't disturb the layers. Centrifuge at 800RCF for 30 minutes where the brake setting is off.

Following centrifuge, carefully remove some of the plasma layer starting from the top most part using sterile Pasteur pipette.

Using a sterile Pasteur pipette, collect the dense cloud of mononuclear cells, careful not to disturb nor collect any of the other layers. Collect into a labelled falcon tube. Wash the collected later by filling the tube with RPMI up to 50ml. Centrifuge at 550RCF for 10 minutes with standard brake settings. Following centrifugation, remove the supernatant and resuspend the pellet with a known volume of 100% Fetal calf serum (FCS) media. Take a small diluted volume for cell counting.

Based on cell counting, take a known volume of fresh PBMC for primary cell culture experiments, the remainder is for storage in freezing conditions.

After cell counting, while in 4^{o}C ice cold temperature, add media containing DMSO in a drop wise fashion slowly, to ensure the final media contains 10% DMSO. Aliquot the sample in pre-labelled cryovials at 1ml each and immediately transfer to freezing storage (-80^{o}C and then -150^{o}C). The number of vials and location of such vials are recorded for future reference.

7.14.2 Cell Counting

7.14.2.1 Automated

CLL cells and cell lines were counted for experimental purposes using an automated cell counter (Nexcelom USA Cellometer™ Auto T4 cell counter), using disposable cell counting slide (Nexcelom Cat# CHT4/PD100/002), after mixing the cells 1:10 with a 0.1% Trypan blue dye solution in PBS. Errors in this method of counting are usually from introducing too high a concentration of cells into the machine.

Appendix Equation 7.1 was used to calculate the volume of cell suspension required to obtain desired cell density for each experiment as indicated.

Appendix Equation 7.1 Calculating concentration of desired suspension from current suspension

$$V_1C_1=V_2C_2$$

Where V_1= volume of current suspension, C_1= concentration of current suspension, V_2= volume of desired suspension and C_2= concentration of desired suspension.

Eg. If the Volume of the current suspension is 3ml with a concentration of $15x10^6$/ml, the desired concentration is $10x10^6$/ml what is the volume required to be resuspended?

$$3x15=V_2x10$$

$$V_2=4.5ml$$

7.14.2.2 Neubauer Chamber

The Neubauer chamber, a hemocytometer, is a counting-chamber device that was designed to count blood cells. It consists of a thick glass microscope slide with indentations that make up a chamber. Within the chamber are perpendicular lines (Appendix Figure 7.22) that are of known distance and depth. Cells are counted within the gridlines and subsequently the number of cells can be counted within a specific volume, thereby calculating the concentration in the original solution overall.

The chamber and cover slip are first cleaned with 70% ethanol, the cover slip is placed on the counting area and pressed down until rainbow spectrum waves are seen. A diluted known volume of cells (up to 20ul) stained with trypan blue is added into the chamber under the cover slip. The chamber is then placed under the microscope and focused to the desired counting region. CLL cells are counted within the four large squares. Using Appendix Equation 7.2, the concentration of cells in suspension can be found.

Errors are common in this method due to pipetting errors, statistical errors, chamber volume errors, and errors from volume of sample introduced into the chamber. Regardless, the Neubauer chamber remains the most widely used cell counting method in the world.

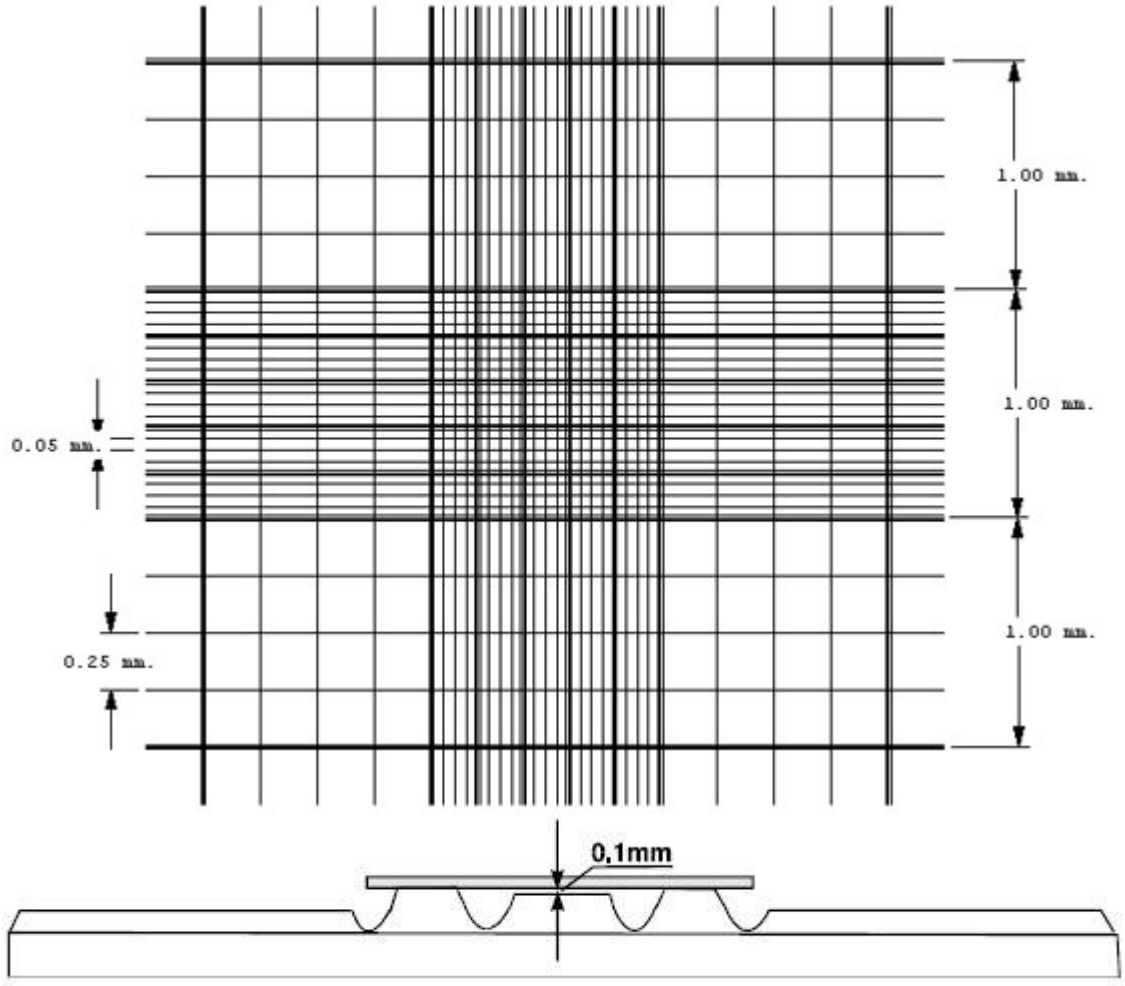

Appendix Figure 7.22 Schematic of counting fields of Neubauer Counting Chamber seen from above (top) and side (bottom)

To calculate the number of viable cells/mL:

Take the average cell count from each of the sets of 16 corner squares.

Multiply by 10,000 (10^4).

Multiply by dilution factor.

The final value is the number of viable cells/mL in the original cell suspension.

Appendix Equation 7.2 Concentration of cells in original mixture

$$\text{Cells in suspension} \times 10^4/\text{mL} = \frac{\text{Number of cells counted} \times \text{Dilution Factor}}{\text{Number of large squares counted}}$$

Example:

If the cell counts for each of the 16 squares were 50, 40, 45, 52 and dilution factor of 5 the average cell count would be:

(50 + 40 + 45 +52) ÷ 4 = 46.75

46.75 x 10^4

46.75 x 5 = 233.75x10^4 live cells/mL in original cell suspension

7.14.3 Calibrating and adding a scale bar using ImageJ software

The pictures were captured using phase contrast microscope at 20x objective lens, Light microscope with 40x objective lens or Light microscope 100x objective lens. In order to provide a scale, an image of a section of a Neubauer Chamber grid is also captured at the same magnification of objective lens using the same microscope. Using the ImageJ software, the known distance on the grid is calibrated to the number of pixels in the image. Once this is set, the other images can therefore have the same scale (ie. Number of pixels equate to a known distance). The scale is then added using tools of ImageJ software. Scale for IF images was pre-calibrated using IF microscope software.

7.14.4 Viability assay using FACS Attune

FITC Annexin V, Propidium Iodide, (BD Pharmingen 556420), (BD Pharmingen 556463)

Annexin Binding Buffer preparation:

(From Data Sheet) 10x Binding Buffer: 0.1M Hepes (pH7.4), 1.4M NaCl, 25mM $CaCl_2$

1x Binding buffer is therefore: 10mM Hepes (pH7.4), 140mM NaCl, 2.5mM $CaCl_2$

For 500ml stock:

5ml of 1M Hepes Stock

14ml of 5M NaCl stock

1.25ml of 1M CaCl2 stock

Then add 479.75ml of distilled H20, mix well, then filter with 0.45um through syringe.

1. Wash with cold PBS and re-suspend cells in 1x Binding buffer at concentration of 1x10^6/ml volume of 100ul.
2. Add 2.5µl of FITC Annexin V, incubate for 8 minutes at RT
3. Add 5µl of PI (concentration of 50µg/ml), incubate for further 2 minutes.
4. Add up to 400ul of Binding Buffer and analyze by flow cytometry within 1 hour

7.14.5 Immunofluorescence Microscopy

7.14.5.1 Coverslip Preparation

Sterilize by cleaning with absolute ethanol, dry in hood for 10-30mins (May use UV light for 10mins).

7.14.5.2 Grow the cells

Place the coverslips in culture plate for adding cells in medium. Gently press on coverslips with pipette tip to remove air bubbles to avoid cells from growing under the coverslip.

Once ready, drain the medium, gently wash with PBS, drain the PBS (leave some behind). Transfer the coverslips to a sterile platform. Place damp cloth near the plate to provide humidity and avoid quick drying.

7.14.5.3 Fixation/Permeabilization

Fixation using 4% Paraformaldehyde for 10mins, then Permeabilisation with 0.5%Triton X (in PBS) for 10mins in room temperature.

7.14.5.4 Removing Autofluorescence

Prepare 0.1% sodium borohydride ($NaBH_4$) (in PBS). CAUTION: Hydrogen gas is produced, FLAMMABLE

Prepare 0.2g powder $NaBH_4$ and dissolve in 20ml of PBS to make 0.1% in Fume cupboard.

Place plate on ice and add the $NaBH_4$ approx. 250-400ml in each well. There will be bubble formations, so this needs to be replaced after 5mins. Do twice. (5mins, replace, 5mins)

When completed, wash properly 3x with PBS.

7.14.5.5 Blocking

Leaving behind some PBS from last wash, lift the coverslips, drain from the side on tissue. If possible, wipe the surface of the coverslip NOT with cells.

Drop approx. 100ul of blocking solution (1%BSA in PBS) on parafilm. Place coverslip face down on the drop. Leave for 30mins room temperature. This step can be prolonged. Additional step of using TruStain Fc blocker can be used in the same manner.

7.14.5.6 Incubate with Antibody

Remove blocking buffer by holding at angle over fibre-free paper or tissue. No need to wash with PBS.

Dilute antibody to 1.0-10ug/ml in blocking buffer, Add 100ul onto parafilm and place coverslip face down on it. Incubate at room temperature for 30mins in humidified chamber. Remove antibody by lifting coverslip off it, wash with PBS 3x 5mins each wash.

If more than one antibody, (secondary antibody) then block with Serum of that species (eg. Donkey Serum) as before, then repeat procedure using secondary antibody (prepare dilution in Donkey serum). Incubate for 30mins at room temperature in humidified chamber. Remove antibody by lifting coverslip off it, wash with PBS 3x 5mins each wash.

7.14.5.7 Incubate with DAPI/Hoechst stain

Prepare DAPI/Hoechst stain (with staining buffer) in covered Eppendorf tube (100ul per coverslip).

Place a drop on parafilm. Transfer coverslip face down on the drop. Incubate for 5mins at room temperature in humidified chamber. Remove excess stain by lifting coverslip off it, wash with staining buffer 3x 5mins each wash.

Make sure to let the coverslip dry as much as possible before mounting.

7.14.5.8 Preparation for Microscopy

Take a clean slide. Add 10ul of mounting medium. Invert coverslip and apply onto that.

Remove excess mounting media with fiber-free paper. Allow to solidify for a few hours (overnight is best). Avoid touching the coverslip as this would alter the volume of medium underneath and introduce air bubbles.

Seal the edges of coverslip with nail polish. Allow to dry for 3mins. Keep slides in dark (cover with aluminium foil) and in $4^{o}C$ till microscopy.

At the time of microscopy, observe in dark room. Using Q-tip, dip in distilled water and gently wipe the surface of the coverslip (exposed part) in circular outward motion to remove dust.

7.14.5.9 Microscopy

Prepare machine: switch on camera, laser, microscope and computer. Open ImageJ Microscopy Software. Adjust magnification at 40x. Locate, focus and identify cells using DAPI at LOW exposure. This will avoid excess spill over onto Green

7.14.6 Optimizing IF protocol

As shown in Appendix Figure 7.23 using PMA differentiated THP1 cell line, it seemed there was clear spill-over of Hoechst 33342 (blue) over to green, with co-expression of both antibodies in same location giving an orange colour. In addition to that, there wasn't any difference in intensity of either colours with their respective isotype controls. Even their unstained counterpart showed expression in both the antibody colours. The level of expressions of the antibodies were quite weak despite using low dilution.

The use of secondary antibodies was advised and the experiment was repeated. The results (Appendix Figure 7.24) showed that there was a greater intensity seen at greater dilutions, however the problem of auto fluorescence, spill over and nonspecific binding persisted.

The use of Fc-receptor blocker reagent was suggested to reduce non-specific binding, the reason was that the monocyte-lineage cells are essentially immune cells that express Fc-receptors for antigen binding (Andersen et al. 2016; Forrester et al. 2018). By blocking these Fc sites, this reduces or eliminates the chances of false positive detection. As seen in Appendix Figure 7.25, despite using the Fc-receptor blocker, there was still non-specific binding as well as auto-fluorescence.

To tackle the auto-fluorescence, 0.1% Sodium Borohydride was used based on literature recommendations (Clancy & Cauller 1998; Davis et al. 2014). The results (Appendix Figure 7.26) showed a decrease in auto fluorescence however there was still nonspecific binding.

The presence of non-specific binding was resolved using an additional blocking step using donkey serum (of same species as secondary antibody) and as seen in Appendix Figure 7.27, it showed further reduction in nonspecific binding.

Despite optimising secondary antibody and performing stains on primary cells, there was still too much spill-over of blue (Hoechst 33342) onto green, despite using greater dilution of Hoechst 33342 of 1:20,000 Appendix Figure 7.28)

It was then suggested to use DAPI as alternative to Hoechst 33341 as a nuclear stain. Using different concentrations, (Appendix Figure 7.29), it was found that DAPI was indeed stained much better and clear staining of nucleus was achieved even at a dilution of 1:10,000. In addition, the duration of exposure to DAPI was compared at 2 minutes versus 20 minutes and it was found that there was less spill-over at short exposure time.

Using the previous adjustments, the final protocol was used and there was minimal spill-over from blue to green.

Using the optimised conditions to remove auto-fluorescence, non-specific binding (by using 0.1% $NaBH_4$ and Fc-receptor blocker and DAPI respectively) and DAPI for nuclear staining, I then proceeded to perform IF on primary cells.

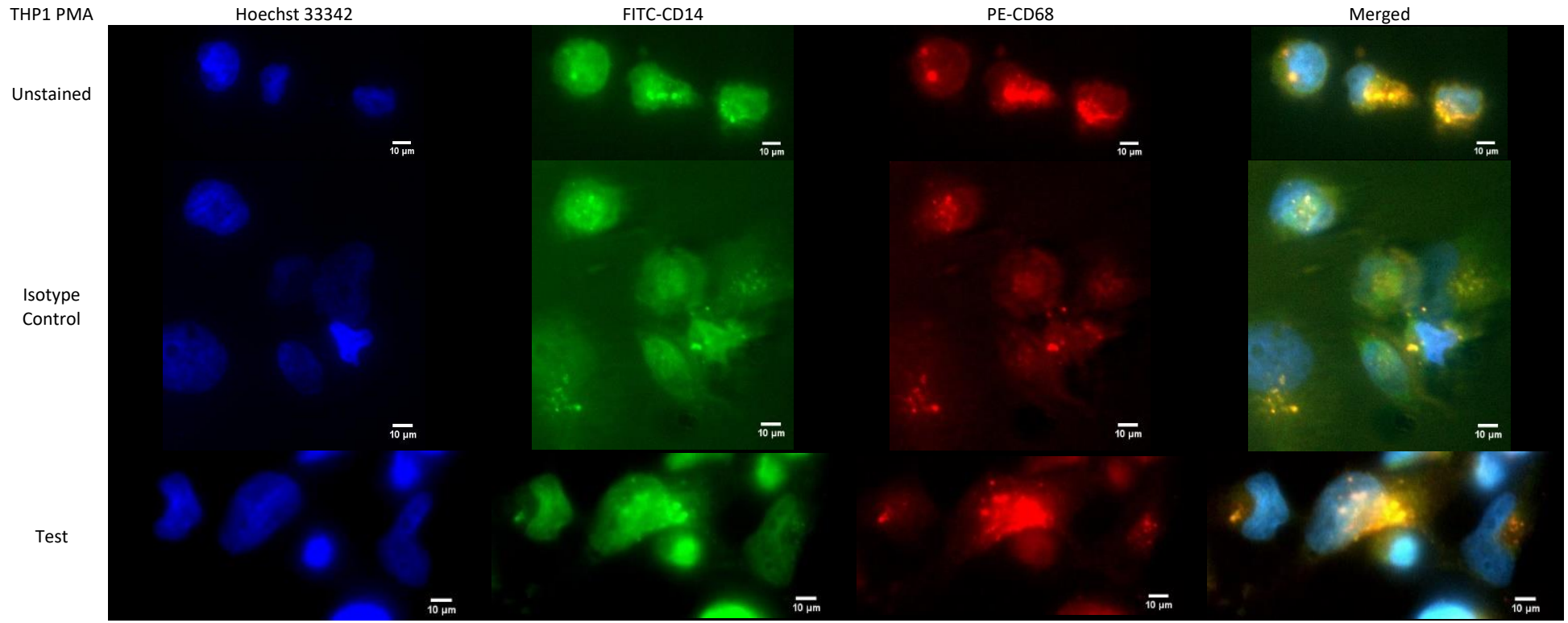

Appendix Figure 7.23 Initial IF staining showed auto-fluorescence, non-specific fluorescence and spill-overs of nuclear stain.

Immunofluorescence staining of PMA differentiated THP1 cell line to test out fluorescent conjugated anti CD14 (green), anti CD68 (red) and counterstained with Hoechst 33342 (blue)nuclear staining. THP-1 cells were PMA differentiated for 24-48 hr as described, fixed, stained with fluorochrome-conjugated antibodies as described, counterstained with nuclear stain as described and viewed under fluorescence microscope in the dark. Corresponding Isotype controls were used for each antibody. Images were prepared using ImageJ software.

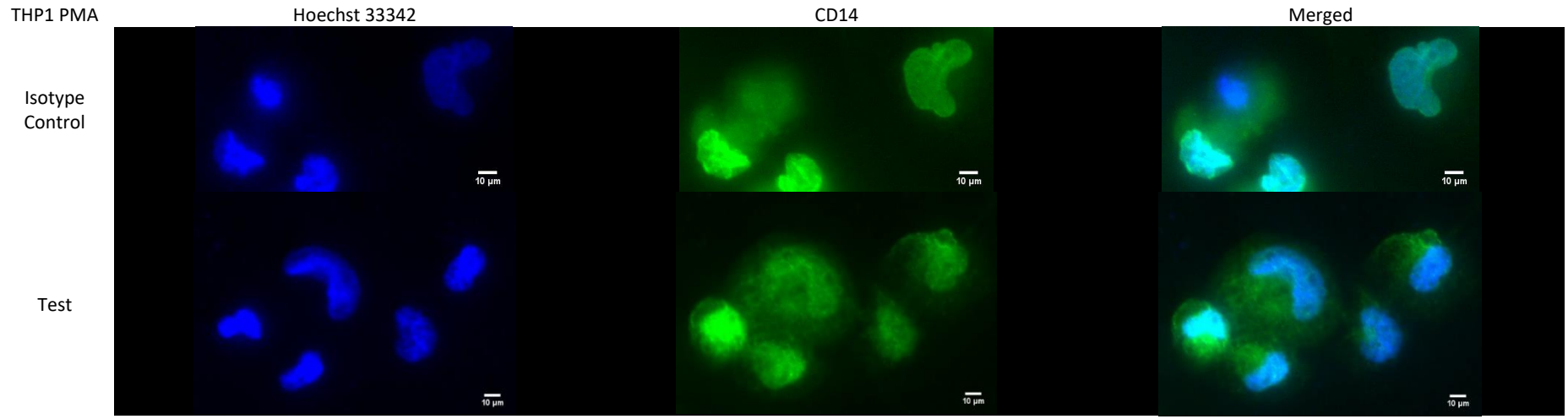

Appendix Figure 7.24 Use of secondary antibodies improved the IF staining.

Immunofluorescence staining using chemically differentiated THP1 cell line with anti-CD14 and secondary antibody (green), counterstained with Hoechst 33342 nuclear stain (blue). THP-1 cells were PMA differentiated for 24-48 hr as described, fixed, stained with primary and secondary antibodies as described, counterstained with nuclear stain as described and viewed under fluorescence microscope in the dark. Corresponding Isotype controls were used for each primary antibody. Images were prepared using ImageJ software.

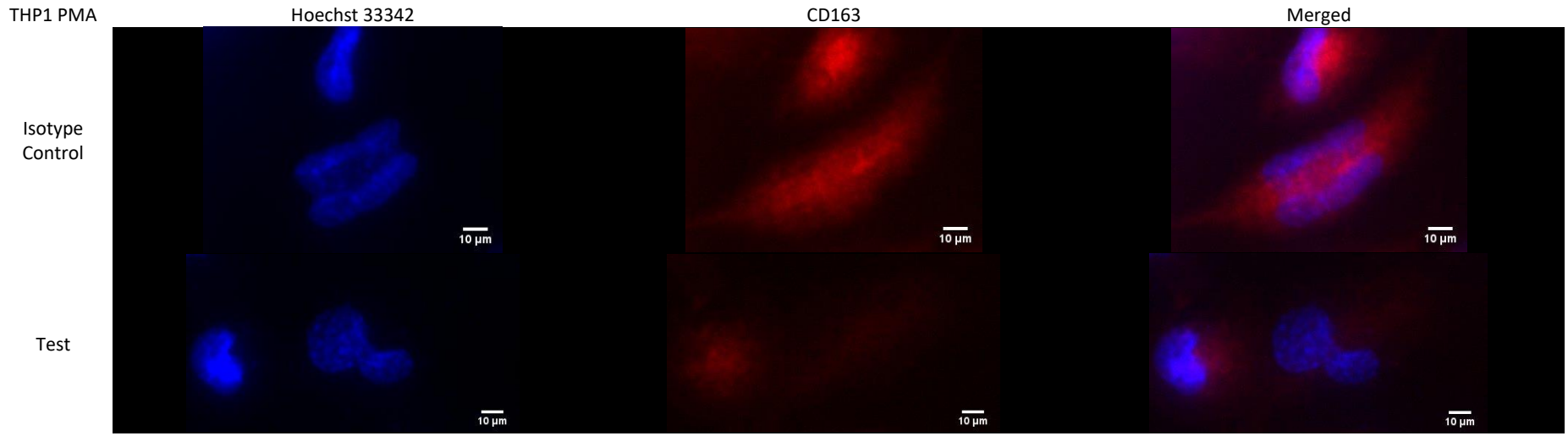

Appendix Figure 7.25 Use of Fc-receptor blocker reduced non-significant fluorescence.

Immunofluorescence staining using chemically differentiated THP1 cell line with anti-CD163 and secondary antibody (red), counterstained with Hoechst 33342 nuclear stain (blue). Fc-receptor blocker was used. THP-1 cells were PMA differentiated for 24-48 hr as described, fixed, stained with primary and secondary antibodies as described, counterstained with nuclear stain as described and viewed under fluorescence microscope in the dark. Corresponding Isotype controls were used for each primary antibody. Images were prepared using ImageJ software.

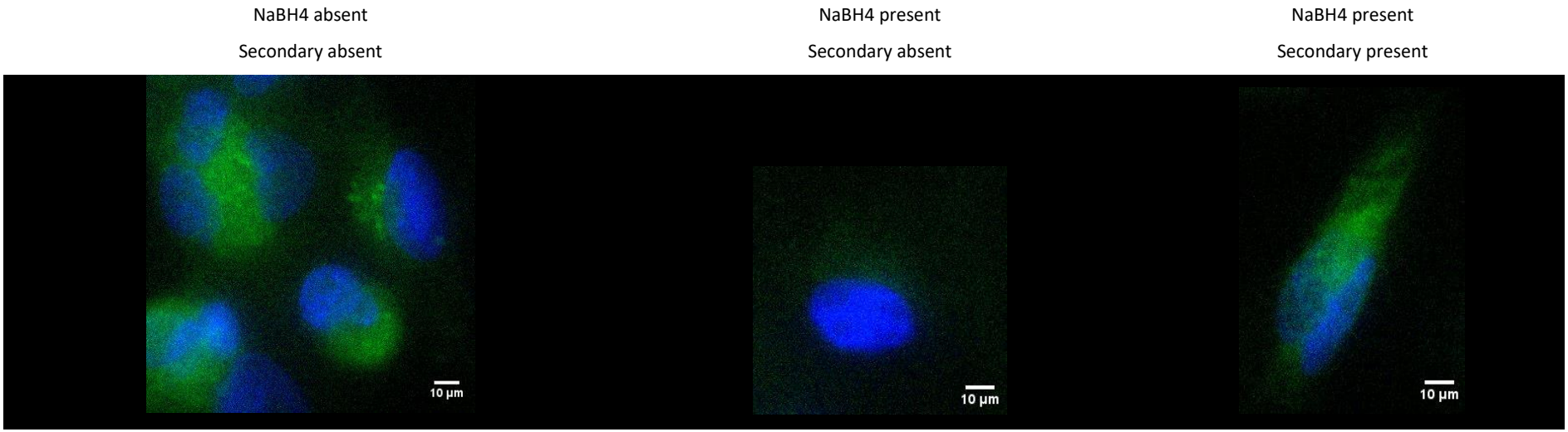

Appendix Figure 7.26 Auto-fluorescence was removed using 0.1% sodium borohydride.

Immunofluorescence staining using chemically differentiated THP1 cell line under green light merged with blue, without any primary antibody but with secondary antibody (green), counterstained with Hoechst 33342 nuclear stain (blue). Here Fc-receptor Blocker was used. 0.1% Sodium Borohydride incubation was introduced and compared with those not incubated. Secondary antibody was either absent or present as indicated. THP-1 cells were PMA differentiated for 24-48 hr as described, fixed, stained with secondary antibodies as described, counterstained with nuclear stain as described and viewed under fluorescence microscope in the dark. Images were prepared using ImageJ software.

Hoechst 33342 CD14 Merged

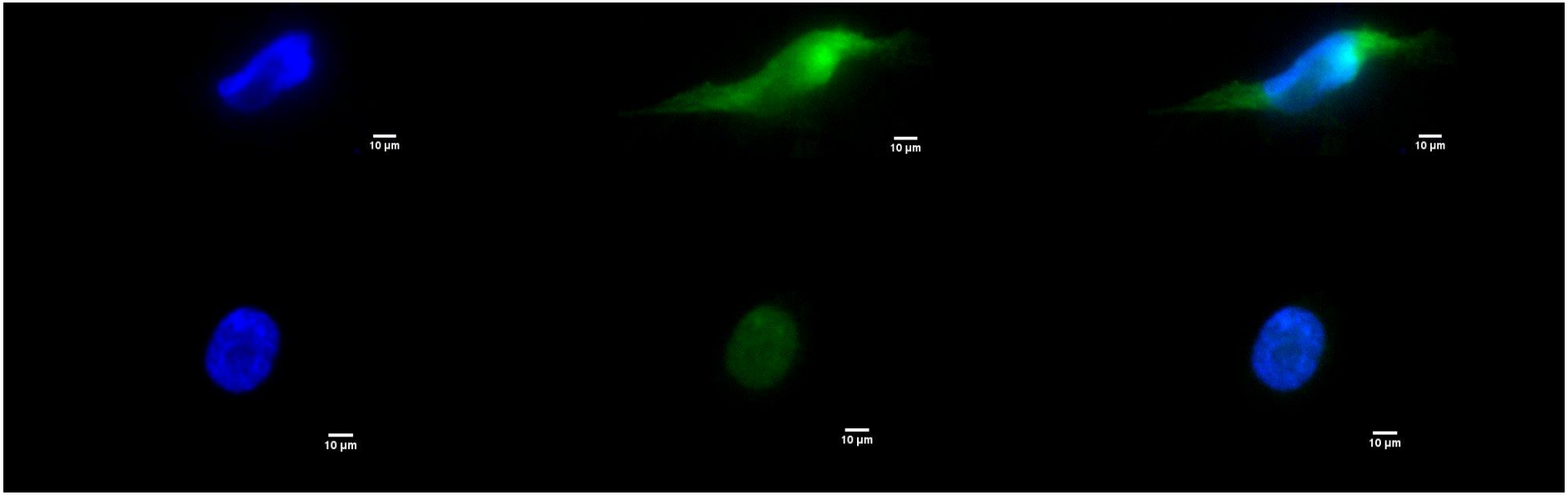

Appendix Figure 7.27 The combined used of Fc-receptor blocker and Donkey serum reduced non-specific fluorescence.

Immunofluorescence staining using chemically differentiated THP1 cell line with anti-CD14 and secondary antibody (green), counterstained with Hoechst 33342 nuclear stain (blue). Here 0.1% sodium borohydride, Fc-receptor Blocker and donkey serum blocking step was used. THP-1 cells were PMA differentiated for 24-48 hr as described, fixed, stained with primary and secondary antibodies as described, counterstained with nuclear stain as described and viewed under fluorescence microscope in the dark. Images were prepared using ImageJ software.

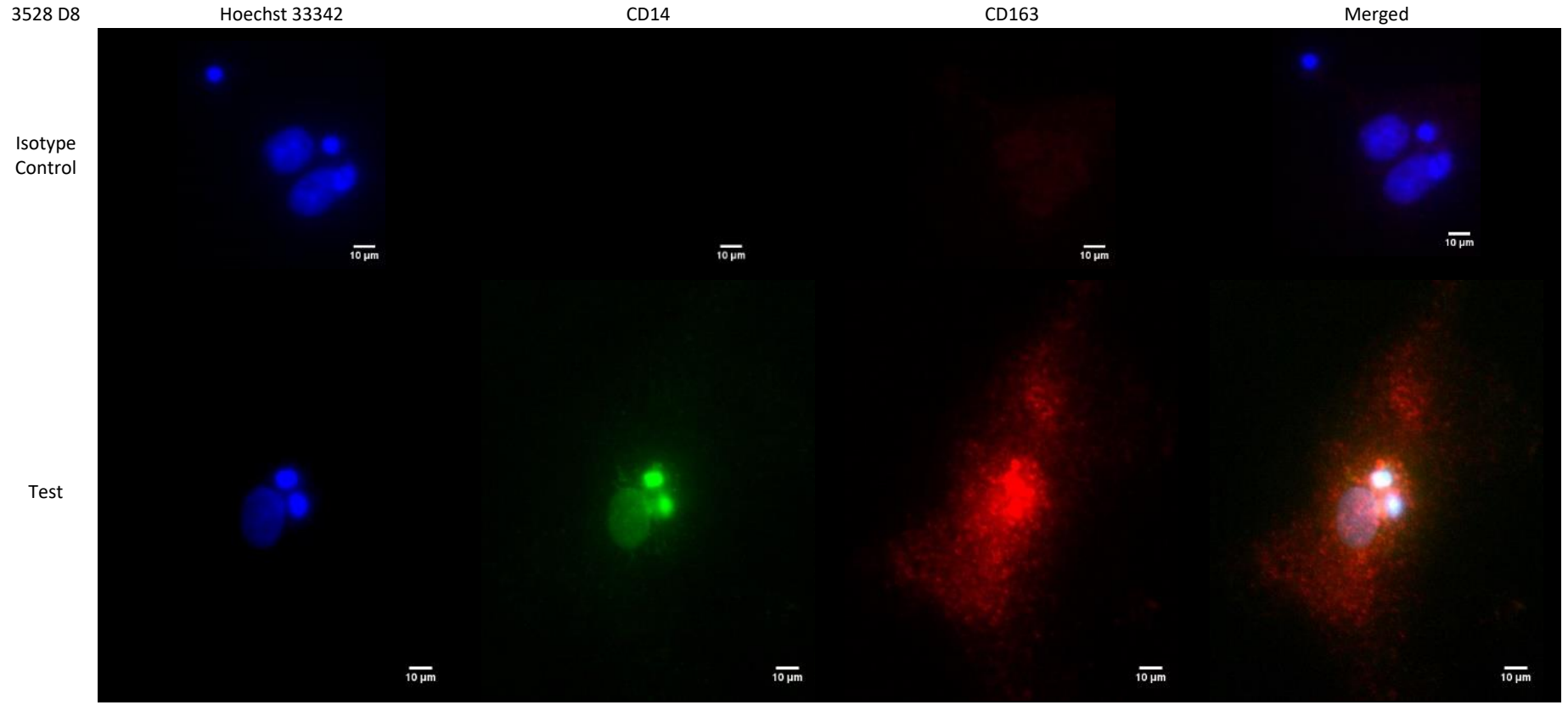

Appendix Figure 7.28 Spill-over was still seen using Hoechst 33342 nuclear stain.

Immunofluorescence staining using sample 3528 at day 8, with anti-CD14 (green), anti-CD163 (red) and counterstained with Hoechst 33342 nuclear stain (blue). Here 0.1% sodium borohydride, Fc-receptor Blocker and donkey serum blocking step was used. Fresh PBMC were cultured as described till Day 8, fixed, stained with primary and secondary antibodies as described, counterstained with nuclear stain as described and viewed under fluorescence microscope in the dark. Corresponding Isotype controls were used for each primary antibody. Images were prepared using ImageJ software.

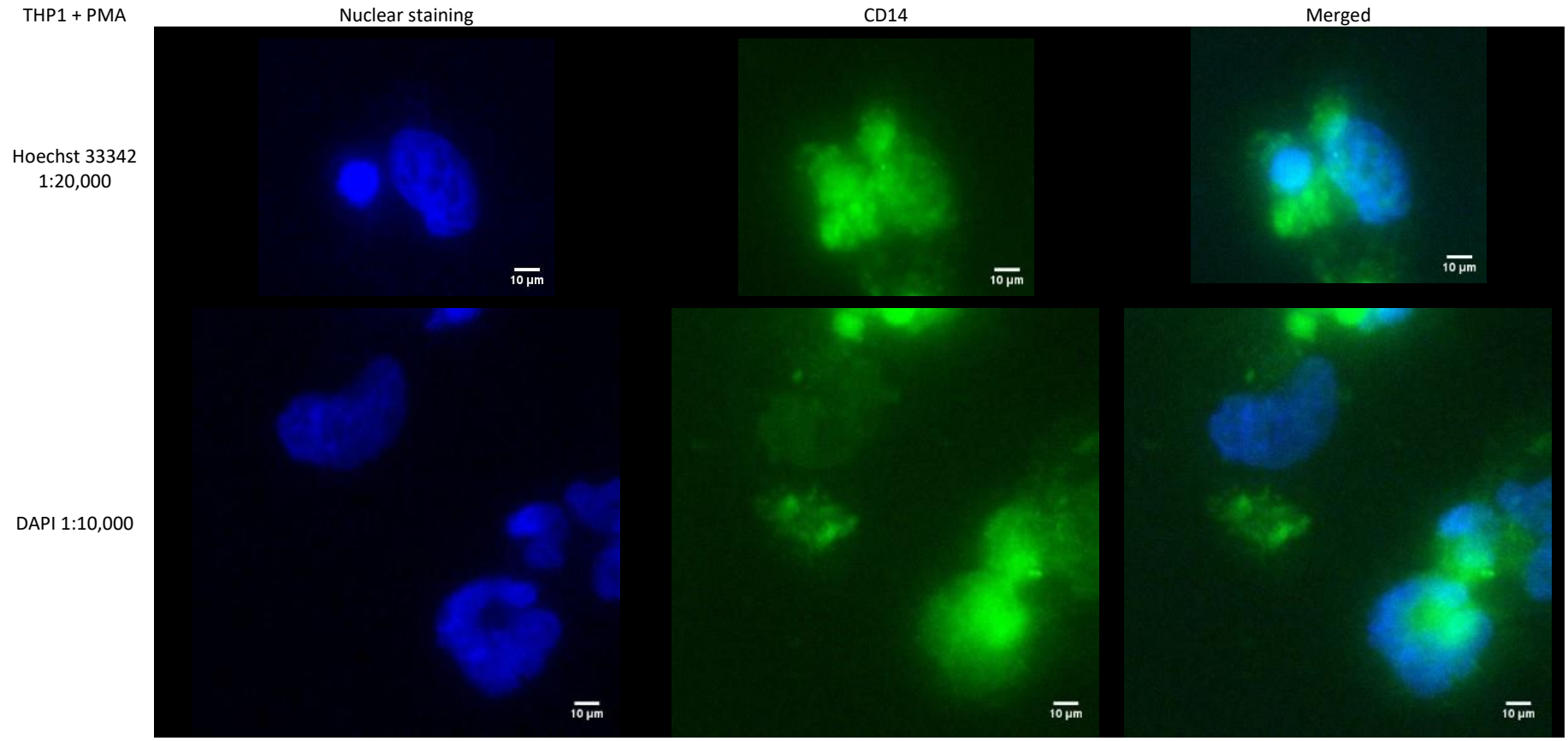

Appendix Figure 7.29 Use of DAPI nuclear staining significantly reduced the spill-over and still efficiently fluoresced at diluted concentrations.

Immunofluorescence staining using chemically differentiated THP1 cell line with anti-CD14 and secondary antibody (green), counterstained with either Hoechst 33342 or DAPI nuclear stain (blue). Here 0.1% sodium borohydride, Fc-receptor Blocker and donkey serum blocking step was used. THP-1 cells were PMA differentiated for 24-48 hr as described, fixed, stained with primary and secondary antibodies as described, counterstained with nuclear stain as described and viewed under fluorescence microscope in the dark. Images were prepared using ImageJ software.

7.14.7 Reagent preparation for THP-1 cell line experiments

IL-4 stock of 10ng/ul. In order to achieve 20-30 ng/ml, take 1 vial and add either 2ul of stock (20ng/ml) or 3ul of stock (30ng/ml).

IFNγ stock of 1000ng/ul (100ul). Aliquoted into 5ul of 20ng/ul). In order to achieve 20ng/ml, take 1ul and add into 1ml of cells.

LPS stock of 500ng/ml (500pg/ul) where each vial has 1ul. To achieve 10pg/ml, on the day of experiment, add 49ul of media to the 1ul to make 10pg/ul, then take 1ul of that and add into 1ml of cell mixture.

7.14.8 ELISA

Materials Needed:

- Buffers
    - Wash buffer: 1x PBS, 0.05% Tween-20 (or Thermo Fisher ELISA Wash Buffer Powder, Cat No. 00-0400)
    - Stop Solution: 1M H3PO4 (recommended or 2N H2SO4
- Pipettes
- Refrigerator & frost-free -20oC freezer
- 96-well plate (Corning Costar 9018 or NUNC MaxicorpTM)
- 96-well ELISA plate reader (microplate spectrophotometer
- ELISA plate washer (highly recommended)

Time Requirements

- 1 overnight incubation
- 4.5 hour incubations
- 1 hour washing and analysing samples

Experimental Procedure

1. Coat ELISA plate with 100 µL/well of capture antibody in 1X Coating Buffer. Seal the plate and incubate overnight at 4°C.
2. Aspirate wells and wash 3 times with >250 µL/well Wash Buffer. Allowing time for soaking (~ 1 minute) during each wash step increases the effectiveness of the washes. Blot plate on absorbent paper to remove any residual buffer.
3. Dilute 1 part 5X ELISA/ELISPOT Diluent with 4 parts DI water. Block wells with 200 µL/well of 1X ELISA/ELISPOT Diluent. Incubate at room temperature for 1 hour.
4. Optional: Aspirate and wash at least once with Wash Buffer.
5. Using 1X ELISA/ELISPOT Diluent, dilute standards to prepare the top concentration of the standard. Add 100 µL/well of top standard concentration to the appropriate wells. Perform 2-fold serial dilutions of the top standards to make the standard curve for a total of 8 points. Add 100 µL/well of your samples to the appropriate wells. Seal the plate and incubate at room temperature for 2 hours (or overnight at 4°C for maximal sensitivity).

6. Aspirate/wash as in step 2. Repeat for a total of 3-5 washes.
7. Add 100 µL/well of detection antibody diluted in 1X ELISA/ELISPOT Diluent. Seal the plate and incubate at room temperature for 1 hour.
8. Aspirate/wash as in step 2. Repeat for a total of 3-5 washes.
9. Add 100 µL/well of Avidin-HRP diluted in 1X ELISA/ELISPOT Diluent. Seal the plate and incubate at room temperature for 30 minutes.
10. Aspirate and wash as in step 2. In this wash step, soak wells in Wash Buffer for 1 to 2 minutes prior to aspiration. Repeat for a total of 5-7 washes.
11. Add 100 µL/well of 1X TMB Solution to each well. Incubate plate at room temperature for 15 minutes.
12. Add 50 µL of Stop Solution to each well.
13. Read plate at 450 nm. If wavelength subtraction is available, subtract the values of 570 nm from those of 450 nm and analyze data.

7.14.8.1 Grid Outline for CCL3 CCL4 for 3605, 3606 and 3607 with cell line or with primary cocultures and alone

Appendix Table 7.9 An example of Grid Outline for measuring CCL3 and CCL4 using ELISA

Duplicates are prepared for each. Standards are prepared as instructed (Std); Supernatant from freshly prepared THP-1, M0, M1 and M2 cell line cultures; Supernatant from Samples (3605, 3607, 3606, 3605 and 3607) were used as either cultured alone, with M0, with M1, with M2; Supernatant of primary samples from fresh PBMC of Days 4, 5, 6, 7 and 8; Supernatant from co-culture experiments of 3607 and 3605 from the 3 conditions; Supernatant from co-cultures after CLL samples were removed; Control wells containing only RPMI and diluent used for the samples.

Std1	Std1	3605	3605	3605 M0	3605 M0	3607	3607	3607 M0	3607 M0	3607 D6	3607 D6
Std2	Std2	3605 M1	3605 M1	3605 M2	3605 M2	3607 M1	3607 M1	3607 M2	3607 M2	3607 D8	3607 D8
Std3	Std3	3606	3606	3606 M0	3606 M0	M2 3605	M2 3605	M0 3606	M0 3606	3607 CC CLL	3607 CC CLL
Std4	Std4	3606 M1	3606 M1	3606 M2	3606 M2	M1 3606	M1 3606	M2 3606	M2 3606	3607 CC NLC	3607 CC NLC
Std5	Std5	M0 3605	M0 3605	M1 3605	M1 3605	M0 3607	M0 3607	M1 3607	M1 3607	3607 CC C+N	3607 CC C+N
Std6	Std6	M1	M1	M2	M2	M2 3607	M2 3607	3605 d5	3605 d5	3605 CC CLL	3605 CC CLL
Std7	Std7	THP-1	THP-1	M0	M0	3605 d7	3605 d7	3605 d8	3605 d8	3605 CC NLC	3605 CC NLC
Std 8	Std8	diluent	Diluent	RPMI	RPMI	3606 d4	3606 d4	3606 d6	3606 d6	3605 CC C+N	3605 CC C+N

7.14.8.2 Grid Outline of Primary Cells time course experiment

Appendix Table 7.10 An example of Grid outline of measuring CCL3 and CCL4 on Primary Cells in time course

Duplicates are prepared for each. Standards are prepared as instructed (Std); Supernatant from Samples (3561, 3577, 3621, 3627, 3609, 3585, 3510, 3589, 3492, 3564, 3493, 3523, 3507, 3612, 3530, 3483, 3512, 3484, 3491 and 3599) from fresh PBMC of Days 4-14; Control wells containing only RPMI and diluent used for the samples.

STD1	STD1	3561 D4	3561 D4	3577 D4	3577 D4	3621 D4	3621 D4	3627 D4	3627 D4	3609 D4	3609 D4
STD2	STD2	3561 D10	3561 D10	3577 D10	3577 D10	3621 D8	3621 D8	3627 D8	3627 D8	3585 D5	3585 D5
STD3	STD3	3510 D5	3510 D5	3492 D6	3492 D6	3564 D6	3564 D6	3523 D6	3523 D6	3507 D6	3507 D6
STD4	STD4	3589 D5	3589 D5	3492 D10	3492 D10	3564 D9	3564 D9	3523 D9	3523 D9	3507 D10	3507 D10
STD5	STD5	3529 D5	3529 D5	3492 D13	3492 D13	3493 D7	3493 D7	3612 D8	3612 D8	3507 D13	3507 D13
STD6	STD6	3530 D6	3530 D6	3483 D7	3483 D7	3512 D8	3512 D8	3484 D9	3484 D9	3491 D7	3491 D7
STD7	STD7	3530 D8	3530 D8	3483 D11	3483 D11	3512 D14	3512 D14	3484 D12	3484 D12	3491 D9	3491 D9
STD8	STD8	Diluent	Diluent	RPMI	RPMI	3599 D9	3599 D9	3484 D14	3484 D14	3491 D13	3491 D13

7.14.8.3 Grid outline of Cell line coculture time course

Appendix Table 7.11 An example of Grid outline to measure CCL3 and CCL4 using Cell lines with Sandwich ELISA method

Duplicates are prepared for each. Standards are prepared as instructed (Std); Supernatant from Samples (3587, 3379 and 2916) were used as either cultured alone, with M0, with M1, with M2; Each culture mixture is taken on Days 1, 2 and 3; Supernatant from M0, M1 and M2 cultured alone at day 1, 2 and 3; Control wells containing only RPMI and diluent used for the samples.

Std1	Std1	3587 Day 1	3587 Day 1	3587+ M0 Day 1	3587+ M0 Day 1	3587+ M1 Day 1	3587+ M1 Day 1	3587+ M2 Day 1	3587+ M2 Day 1	M0 Day1	M0 Day1
Std2	Std2	3587 Day 2	3587 Day 2	3587+ M0 Day 2	3587+ M0 Day 2	3587+ M1 Day 2	3587+ M1 Day 2	3587+ M2 Day 2	3587+ M2 Day 2	M0 Day 2	M0 Day 2
Std3	Std3	3587 Day 3	3587 Day 3	3587+ M0 Day 3	3587+ M0 Day 3	3587+ M1 Day 3	3587+ M1 Day 3	3587+ M2 Day 3	3587+ M2 Day 3	M0 Day 3	M0 Day 3
Std4	Std4	3379 Day 1	3379 Day 1	3379+ M0 Day 1	3379+ M0 Day 1	3379+ M1 Day 1	3379+ M1 Day 1	3379+ M2 Day 1	3379+ M2 Day 1	M1 Day1	M1 Day1
Std5	Std5	3379 Day 2	3379 Day 2	3379+ M0 Day 2	3379+ M0 Day 2	3379+ M1 Day 2	3379+ M1 Day 2	3379+ M2 Day 2	3379+ M2 Day 2	M1 Day 2	M1 Day 2
Std6	Std6	3379 Day 3	3379 Day 3	3379+ M0 Day 3	3379+ M0 Day 3	3379+ M1 Day 3	3379+ M1 Day 3	3379+ M2 Day 3	3379+ M2 Day 3	M1 Day 3	M1 Day 3
Std7	Std7	2916 Day 1	2916 Day 1	2916+ M0 Day 1	2916+ M0 Day 1	2916+ M1 Day 1	2916+ M1 Day 1	2916+ M2 Day 1	2916+ M2 Day 1	BLANK	BLANK
Std 8	Std8	diluent	Diluent	RPMI	RPMI	M2 Day 1	M2 Day 1	M2 Day 2	M2 Day 2	M2 Day 3	M2 Day 3

7.14.9 Homogenising samples using QiaShredder – purple columns

1. Thaw samples if frozen
2. Spin to get all of the sample down to the bottom
3. Label columns – number them and keep a list of what the numbers correspond to!
4. Add a maximum of 700uL to each column
5. This can be done in the UV hood, or at the bench but if at the bench be careful not to contaminate – the RNA is very delicate and easily contaminated! So: obtain sample from tube using filter tip – open lid, take up sample and then close. Open cap from column add sample and close quickly – try not to pick up the columns as its quicker to do it from the stand
6. Spin the samples for 2 mins at maximum speed
7. The flow through is then used for the RNeasy protocol

7.14.10 RNeasy Protocol

1. Label RNeasy spin columns with the corresponding numbers you used for the QiaShredder
2. Add the same volume of 70% ethanol as you did of RLT buffer (ie 350uL or 600uL)
3. Mix well by pipetting
4. Following RNeasy steps
5. Use nanodrop to quantify RNA
6. You need 1ug of RNA for to convert to cDNA
7. This then needs to be made up to constant volume for each sample = 12.5Ul

7.14.11 RNA extraction using RNeasy mini kit (Qiagen)

1. Clean the hood with 10%bleach and 70% ethanol and turn on UV light for at least 30min to get read off RNAs.
2. Prepare RLT buffer under the hood according the final volume you want (for each 1ml RLT + 10πl β-mercaptoethanol)
3. Add 700 µl of RLT buffer to lysis cells, mix by pipetting than transfer into labelled Q1Ashredder column for homogenizing, Spin for 2min at 14000g.
4. Add 700 µl of 70% ethanol to the sample, mix and transfer 700 µl of the mix to a new labelled RNeasy spin column, centrifuge for 30sec at ≥8000 x *g,* discard the flow-through, add the remaining lysis cells from the main sample to the same RNeasy column and repeat the spin, discard to maximize the RNA yield.
5. Add 350 µl Buffer RW1 to the RNeasy spin column. Close the lid gently, and centrifuge for 30sec at ≥8000 x *g*. Discard the flow-through.
6. (on-column DNase digestion) calculate the mount needed of DNase I stock, each sample column will take 10 µl DNase I stock to 70 µl buffer RDD. So, for 2 samples>> 22 µl DNase+154 buffer RDD>> give 176µl from which we add 80µl to each sample
7. Add DNase I incubation mix (80 µl) directly to RNeasy column membrane, and place on benchtop for 15 min.
8. Add 350 µl Buffer RW1 to the RNeasy spin column. Centrifuge for 30sec at ≥8000 x *g*. Discard the flow-through.
9. Add 500 µl Buffer RPE to the RNeasy spin column. Centrifuge for 30sec at ≥8000 x *g*. Discard the flow-through.
10. Add 500 µl Buffer RPE to the RNeasy spin column, centrifuge for 2min at ≥8000 x *g* to wash the spin column membrane.
11. Place the RNeasy spin column in a new 2 ml collection tube (supplied), and discard the old collection tube with the flow-through. Centrifuge at full speed for 1 min to dry the membrane.
12. Place the RNeasy spin column in a new 1.5 ml collection tube (supplied). Add 50 µl RNase-free water directly to the spin column membrane, incubate for 5min and centrifuge for 1 min at ≥8000 x *g* to elute the RNA. Put the samples on ice.
13. Add 2µl of the sample into labelled Eppendorf to measure RNA concentration using Nanodrop.

7.14.12 Nanodrop measurement

Blank with 1µl RNase-free water and measure RNA by adding 1µl of the sample into the reader.

(260/280) represent RNA & DNA purity.

(260/230) represent DNA purity.

Both should be between (1.8 - 2.1)

RNA calculation: Concentration X dilution factor X 40 (Constant) = ? ng/µl

?/1000 = ? µg/µl in total

if the expected RNA yield is >30 µg, repeat last step using another 30–50 µl RNase free water, or using the eluate (if high RNA concentration is required). Reuse the collection tube from last step.

Freeze down samples at -80°C. to obtain 1µg for RT we divided 1000/?ng

7.14.13 Reverse transcription protocol (RT)

Reagents:

dNTP 10mM

Oligo (dT) 15 primers (Promega UK, C1101)

RNase inhibitor (Promega UK, N2511)

Superscript III (Invitrogen UK, 18080-044)

Procedure:

- To a labelled RNase-free tube, add:

Oligo (dT) 15 primers (0.5µg/µl)	1.0 µl
dNTPs (10 mM)	1.0 µl
Total mRNA	1µg (up to 9.5 µl)
RNase free H2O	variable (final volume 20 µl)

Heat at 70°C for 5 mins, then cool on ice for 5 mins.

5x Reaction buffer	4.0 µl
DTT (0.1M)	1.0 µl
Superscript III	1.0 µl
RNase inhibitor (40u/µl)	1.0 µl
Total	20 µl

- Heat tubes on heating block for 50°C for 60 min and then 95°C for 5 min. Store cDNA samples at -20°C freezer.

7.14.14 Polymerase Chain Reaction (PCR)

Reaction mix (20µl)

One-Taq 2Xmm (#M0486S)	10 µl
20 µM Forward primer	(1 µl of 100 µM primer + 4 µl free RNA water, mix and then take 1 µl)
20 µM Reverse primer	(1 µl of 100 µM primer + 4 µl free RNA water, mix and then take 1 µl)
cDNA	1.0 µl
Free RNA water	7 µl

PCR programme (GAPDH)

Stage 1	95°c for 2 min
Stage 2	95°c for 30 sec
	56°c for 30 sec (annealing)
	72°c for 1 min
	(Repeated for 35 cycles)
Stage 3	72°c for 5 min
Stage 4	4°c indefinitely

7.14.15 Agarose gel electrophoresis

Materials

Agarose (ULTRAPURE)

1X TBE (Tris-Borate electrophoresis buffer) (1L= 20ml 50XTBE + 980ml dH2O)

Midori Green Advance DNA Stain

Procedure

1. For a 1 % gel, add 0.5 g agarose to 50 ml 1x TBE. (for 1.5% gel, add 0.75g to 50ml)
2. Heat the solution in the microwave to dissolve the agarose. Let it cool down (~5min) and 5 µl of Midori Green Advance DNA Stain to the dissolved agarose and mix.
3. Prepare the gel assembling box, pour the melted agarose and place the comb on the top.
4. Allow the gel to solidify (about 20 minutes); then carefully remove the comb and tape, transfer the gel to the electrophoresis box. Make sure that the comb is nearest to the black electrode (cathode), as the DNA migrates towards the red electrode (anode).
5. Top up the box 1X TAE buffer, make sure it covers the gel.
6. Load the gel with 8µl of Ladder and 20µl samples.
7. Electrophorese at 110 V for 25 minutes.
8. View the gel against a white light box or bright surface.

Quick-Load Purple 100bp DNA Ladder

Size range: 100 bp to 1,517 bp

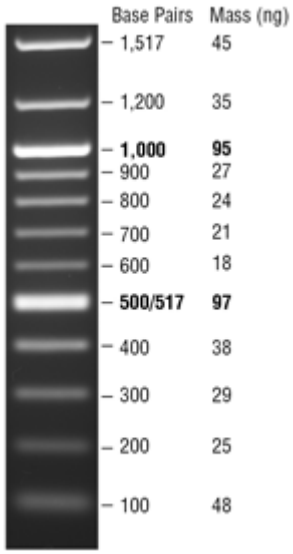

Quick-Load Purple 1kb DNA Ladder

Size range: 500 bp to 10 kb

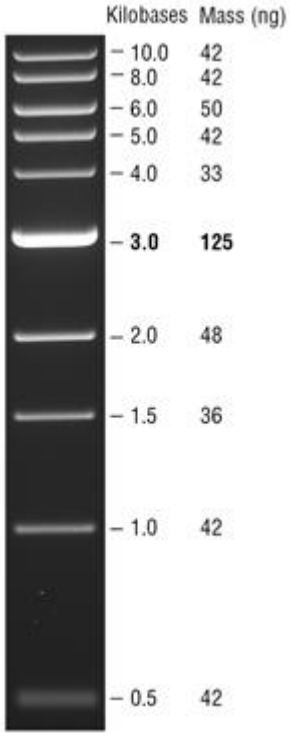

Problem solving

Problem	Solution(s)
Gel doesn't solidify	1) Not enough agarose added. 2) Not heated enough to dissolve the agarose.
Collapsed wells	Gel wasn't cool when the comb was removed
Skinny gel or irregular gel	Agarose leaked past the dams. Put the dams in securely.
Well too small (sample won't fit in the well)	Agarose leaked past the dams. Put the dams in securely.
Gel runs too slowly	50X TAE not diluted correctly
Gel runs too quickly	Little or no 50X TAE added to electorphoresis buffer.
Only the ladder is visible under UV light	1) Poor DNA purification (e.g., minipreps). 2) Sample leaked out of the well.
No bands appear under UV light	1) No ethidium bromide was added. 2) Samples leaked out of the well.
Fuzzy bands	1) Agarose wasn't dissolved completely 2) Too much DNA 3) Particulates in the sample

7.14.16 Protocol for Resuspending PCR Primers

7.14.16.1 Materials

- Molecular Grade H_2O
- Primers (dry)
- Sterile Microcentrifuge Tubes

7.14.16.2 Method

Primers are often shipped and received in a lyophilized state. First create a master 100× stock (for each primer and then dilute it to a 10× working stock.

This reduces the number of freeze/thaw cycles that the master primer stock goes through and reduces the chances of contaminating the primary source for the primer.

Spin Down Tubes

Primers should always be spun down before opening the tube for the first time. The pellet can often come dislodged during shipping and may be in the cap!

Master stock, 100 µM

100 µM = X moles lyophilized primer + (X × 10 µl molecular grade H_2O)

To determine the amount of H_2O to add to the lyophilized primer simply multiply the number of nmol of primer in the tube by 10 and that will be the amount of H_2O to add to make a 100 µM primer stock.

For example, if there are 38.2 nmol of primer then by adding 382 µl of H_2O, a 100 µM primer stock is created.

The original primer tubes are often used for this 100 µM stock.

Master stock primers newly suspended in H_2O should be allowed to sit at room temperature for 10 minutes before they are used for working stock dilutions. Mix well before making working stock dilutions.

Mix the solution by vortexing to reconstitute the primers. Store primer stocks at -20°C.

Working stock, 10 µM

Dilute the primer master stock in a sterile microcentrifuge tube 1:10 with molecular grade H_2O.

You should never use the stock primers directly into a PCR because they are so concentrated. Working from one tube is also a bad idea. It only takes a bit of contamination to creep in to the tube and you will have to re-order the primers again.

Therefore, it is best practise to create working solutions that are of lower concentrations. The concentration of choice for the working primer solution is totally user-determined. The most common concentration for a working primer solution is 10 µM.

To make a 10 µM working primer solution, follow these steps: (1 in 10 dilution)

1 Add 10 µL of primer stock solution to an RNase- and DNAse-free tube.

2 Add 90 µL of PCR-grade water.

3 Mix by vortexing.

Aliquot and store working primer solutions at -20°C. Avoid excessive freeze-thawing of working primers.

Thaw SYBR Green Mix and Water PCR grade.

While thawing:

1. Dilute cDNA (1+4) in H_2O
2. Work out total volume of diluted cDNA needed.

   Total reactions = 8(primers) x2(duplicates)= 16 reactions

   In each reaction you need 2 ul of diluted cDNA.

   So… total vol of diluted working stock of cDNA is 16x2=32ul

   7ul of Master stock of cDNA + 28ul of H2O= 35ul of working stock cDNA
3. Dilute stock of primers from Master stock of 100mM to 10mM in H_2O (1ul Primer + 9ul H_2O)= 10ul working stock of primer.

   Then add 0.8-1ul of diluted primers to each tube

Seal and spin in centrifuge.

Run in PCR machine. It will take about 1hr 45mins

7.14.17 Protocol for RT-qPCR

7.14.17.1 Preparation of Primers

1. Dilute cDNA

   1+4 (H_2O)

2. Work out total volume of diluted cDNA needed

   Total reactions = 8 x 2 = 16

   In each reaction 2ul of diluted cDNA needed

   Therefore, Total volume of diluted cDNA = 16 x 2 = 32 ul

   7ul original cDNA + 28ul of H_2O = 35ul (enough for 32ul of reactions)

3. Dilute Stock Primers (100pmol) to 10 pmol in H_2O

   1ul of primer + 9ul of H_2O

   Then add 0.8-1ul of diluted primer in each tube

7.14.17.2 qPCR Programming for Light Cycler 480

Name	**Cycles**	**Analysis Model**
Preincubation	1	None
Amplification	45	Quantification
Melting	1	Melting Curve
Cooling	1	None

Preincubation				
None	95°C	x10min	RamptT.	4.4C/s
Amplification				
None	95°C	x15s	RamptT.	4.4C/s
None	58°C	x20s	RamptT.	2.2C/s
None	72°C	x20s	RamptT.	4.4C/s
Single	81°C	x10s	RamptT.	4.4C/s
Melting				
None	95°C	x1s	RamptT.	4.4C/s
None	65°C	x10s	RamptT.	2.2C/s
Continuous	97°C	acquisition 4-5/per °C		0.14C/s
Cooling				
None	40°C	Hold 10s		2.2C/s

7.14.17.3 Grid Outline for qPCR for Primer Optimizing

Appendix Table 7.12 An example of Grid outline of optimising qPCR for selected primers

Duplicates were done for each sample; cDNA from a control sample was used for all coloured wells; Primers (CXCL12, EGLN3, GBP1, EBI3, MCL1, CXCL10, YPEL4 and GAPDH) were used in combination with the control sample or alone in PCR water (+ Water); Control of only water was used to detect contamination.

	1	2	3	4	5	6	7	8	9	10	11	12
A	CXCL12	CXCL12		EGLN3	EGLN3		GBP1	GBP1		EBI3	EBI3	
B	+ WATER	+ WATER		+ WATER	+ WATER		+ WATER	+ WATER		+ WATER	+ WATER	
C												
D	MCL1	MCL1		CXCL10	CXCL10		YPEL4	YPEL4				
E	+ WATER	+ WATER		+ WATER	+ WATER		+ WATER	+ WATER				
F												
G	GAPDH	GAPDH										
H	+ WATER	+ WATER									Only WATER	Only WATER

Appendix Table 7.13 An example of Grid outline to optimize the qPCR reading temperature for selected Primers

Duplicates were done for each sample; cDNA from a control sample was used for all coloured wells; Primers (CCL13, CXCL9, NUPR1, CSF1, STEAP3, EGR2 and GAPDH) were used in combination with the control sample or alone in PCR water (+ Water); Control of only water was used to detect contamination.

	1	2	3	4	5	6	7	8	9	10	11	12
A	CCL13	CCL13		CXCL9	CXCL9		NUPR1	NUPR1		CSF1	CSF1	
B	+ WATER	+ WATER		+ WATER	+ WATER		+ WATER	+ WATER		+ WATER	+ WATER	
C												
D	STEAP3	STEAP3		EGR2	EGR2							
E	+ WATER	+ WATER		+ WATER	+ WATER							
F												
G	GAPDH	GAPDH										
H	+ WATER	+ WATER									Only WATER	Only WATER

7.14.17.4 Grid Outline for qPCR after optimizing

Appendix Table 7.14 An example of Grid outline to perform optimized qPCR on cDNA samples for each Primers of Interest

Triplicate wells were done for each sample; cDNA from a sample (3599, 3627, 3682, 3577, 3679, 3684, 3620, 3637, 3645, 3686, 3605, 3607, 3621 and 3631) was used for all coloured wells as CLL cultured alone (CL) or CLL cultured with NLCs (CN); A selected control sample was used; Single primer and GAPDH were used in combination with the samples; Control of primer with water was used.

	1	2	3	4	5	6	7	8	9	10	11	12
A	3599 CL	3599 CL	3599 CL	3627 CL	3627 CL	3627 CL	3682 CL	3682 CL	3682 CL	3577 CL	3577 CL	3577 CL
B	3599 CN	3599 CN	3599 CN	3627 CN	3627 CN	3627 CN	3682 CN	3682 CN	3682 CN	3577 CN	3577 CN	3577 CN
C	3679 CL	3679 CL	3679 CL	3684 CL	3684 CL	3684 CL	3620 CL	3620 CL	3620 CL	3637 CL	3637 CL	3637 CL
D	3679 CN	3679 CN	3679 CN	3684 CN	3684 CN	3684 CN	3620 CN	3620 CN	3620 CN	3637 CN	3637 CN	3637 CN
E	3645 CL	3645 CL	3645 CL	3686 CL	3686 CL	3686 CL	3605 CL	3605 CL	3605 CL	3607 CL	3607 CL	3607 CL
F	3645 CN	3645 CN	3645 CN	3686 CN	3686 CN	3686 CN	3605 CN	3605 CN	3605 CN	3607 CN	3607 CN	3607 CN
G	Blank	Blank	Blank	Control cell	Control cell	Control cell	3621 CL	3621 CL	3621 CL	3631 CL	3631 CL	3631 CL
H	H2O (GAPDH)	H2O (GAPDH)	H2O (GAPDH)	H2O (PRIMER)	H2O (PRIMER)	H2O (PRIMER)	3621 CN	3621 CN	3621 CN	3631 CN	3631 CN	3631 CN